

TEC-0056

AD-A282 927



Technology Requirements for Minefield Detection from Space

Thomas Anderson
Alan Poirier

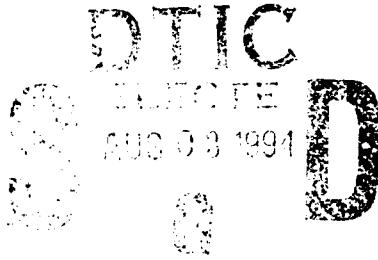
The Futures Group
80 Glastonbury Boulevard
Glastonbury, CT 06033-4409

April 1994

94

Approved for public release; distribution is unlimited.

U.S. Army Corps of Engineers
Topographic Engineering Center
7701 Telegraph Road
Alexandria, Virginia 22315-3864



94-24428

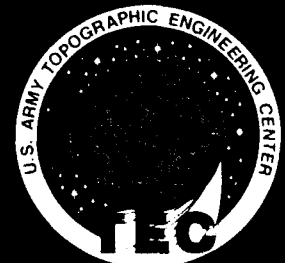


US Army Corps
of Engineers
Topographic
Engineering Center

T

E

C



**Best
Available
Copy**

**Destroy this report when no longer needed.
Do not return it to the originator.**

The findings in this report are not to be construed as an official Department of the Army position unless so designated by other authorized documents.

The citation in this report of trade names of commercially available products does not constitute official endorsement or approval of the use of such products.

DISCLAIMER NOTICE



THIS DOCUMENT IS BEST QUALITY AVAILABLE. THE COPY FURNISHED TO DTIC CONTAINED A SIGNIFICANT NUMBER OF COLOR PAGES WHICH DO NOT REPRODUCE LEGIBLY ON BLACK AND WHITE MICROFICHE.

REPORT DOCUMENTATION PAGE

Form Approved
OMB No 0704-0188

Public reporting burden for this collection of information is estimated to average 1 hour per response, including the time for reviewing instructions, searching existing data sources, gathering and maintaining the data needed, and completing and reviewing the collection of information. Send comments regarding this burden estimate or any other aspect of this collection of information, including suggestions for reducing this burden, to Washington Headquarters Services, Directorate for Information Operations and Reports, 1215 Jefferson Davis Highway, Suite 1204, Arlington, VA 22202-4302, and to the Office of Management and Budget, Paperwork Reduction Project (0704-0188), Washington, DC 20503.

1. AGENCY USE ONLY (Leave blank)	2. REPORT DATE April 1994	3. REPORT TYPE AND DATES COVERED Final Apr. 1992 - Apr. 1994
---	-------------------------------------	--

4. TITLE AND SUBTITLE Technology Requirements for Minefield Detection from Space	5. FUNDING NUMBERS DACA76-92-C-0030
--	---

6. AUTHOR(S) Thomas Anderson Alan Poirier	
---	--

7. PERFORMING ORGANIZATION NAME(S) AND ADDRESS(ES) The Futures Group 80 Glastonbury Boulevard Glastonbury, CT 06033-4409	8. PERFORMING ORGANIZATION REPORT NUMBER
--	---

9. SPONSORING / MONITORING AGENCY NAME(S) AND ADDRESS(ES) U.S. Army Topographic Engineering Center Alexandria, VA 22315-3864	10. SPONSORING / MONITORING AGENCY REPORT NUMBER TEC-0056
---	---

11. SUPPLEMENTARY NOTES

12a. DISTRIBUTION / AVAILABILITY STATEMENT Approved for public release; distribution is unlimited.	12b. DISTRIBUTION CODE
--	-------------------------------

13. ABSTRACT (Maximum 200 words) An analysis of the technology requirements for minefield detection from space has produced a design for a space based sensor that can be used to detect anti-armor minefields. The project produced some minefield reflectance measurements to support the tactical requirements analysis. The project final report describes some potential signature phenomenology based upon several aircraft flights over an Army test range. The flights were planned to collect reflectance data with a multispectral sensor over the test minefield at Twenty-nine Palms, California. The final report describes the tactical minefield problem as experienced in five hypothetical future battlefield scenarios. The tactical requirements for a space based minefield detection satellite are derived from the battlefield scenarios and a design is suggested for a low cost tactical imaging satellite that satisfies that stated requirements.

14. SUBJECT TERMS Minefields, Space, Anti-armor, LEO Satellite, Multispectral	15. NUMBER OF PAGES i38
	16. PRICE CODE

17. SECURITY CLASSIFICATION OF REPORT UNCLASSIFIED	18. SECURITY CLASSIFICATION OF THIS PAGE UNCLASSIFIED	19. SECURITY CLASSIFICATION OF ABSTRACT UNCLASSIFIED	20. LIMITATION OF ABSTRACT UNLIMITED
--	---	--	--

CONTENTS

List of Tables and Figures	v
List of Acronyms	vii
Executive Summary	ix
1. Anti-Armor Minefield Threat	1
1.1 Current Threat	1
1.2 Future Satellite Sensors	4
1.3 Expert Interviews	5
2. Battlefield Scenarios	7
2.1 U.S. Army TRADOC Scenario Gists	7
2.2 Future Battlefield Scenarios and Terrain Features	7
3. Optical Tests for Minefield Detection	39
3.1 Background	39
3.2 Optical Signature Measurements (Twentynine Palms)	40
3.3 Aircraft Validation	42
3.4 Minefield Aging Study (University of Arizona)	67
4. Minefield Imaging Satellite — Parametric Analysis	77
4.1 Satellite Orbital Constraints	77
4.2 Satellite Launch Vehicles	89
4.3 Signature Bands, Detector Materials	90
4.4 Ground Resolution and Target Signature	93
4.5 Field of Regard, Field of View, Pointing Resolution	101
4.6 Camera	102
4.7 Downlink Data Rates	106
4.8 Downlink Opportunities	108
5. Satellite Specifications and Design	119
5.1 Satellite Basing and Configuration	119
5.2 Telescope Configuration	122
5.3 Optical Platform	123
5.4 Link Budget	124
5.5 Earth Station	126
Bibliography	127
Appendix A. Hughes SBRC Report	
Appendix B. University of Arizona Report	

LIST OF TABLES

Table 2.2.1.	Tactical Operation (Korea)	15
Table 2.2.2.	Tactical Operation (Kuwait)	22
Table 2.2.3.	Tactical Operation (Balkan)	26
Table 2.2.4.	Tactical Operation (Cuba)	33
Table 2.2.5.	Tactical Operation (Philippines)	38
Table 4.1.1.	Satellite Orbital Characteristics	75
Table 4.1.2.	Density of Air by Altitude	84
Table 4.4.1.	Resolution Required for Interpretation Tasks	93
Table 4.8.1.	Forward Service Data Budget	113
Table 4.8.2.	Forward Service Link Budget	114
Table 4.8.3.	Return Service Link Budget	116
Table 4.8.4.	Return Service K-Band Antenna Requirements	116
Table 5.1.	Wide Area Search Tactical Satellite	120
Table 5.2.	Medium Resolution Tactical Satellite	120
Table 5.4.1.	Return Service Power and Gain Requirements	125
Table 5.4.2.	Effective Data Transmission Times	125

LIST OF FIGURES

Figure 2.2.1.	Battlefield Tactical Requirements	8
Figure 2.2.1.1.	LANDSAT MSS Image of Korea	11
Figure 2.2.1.2.	Korea Monthly Average Cloud Cover	13
Figure 2.2.2.1.	LANDSAT MSS Image of Kuwait	19
Figure 2.2.2.2.	Kuwait Monthly Average Cloud Cover	21
Figure 2.2.3.1.	Map of Macedonia	24
Figure 2.2.4.1.	LANDSAT MSS Image of Bayamo — Manzanillo, Cuba	29
Figure 2.2.4.2.	Cuba Monthly Average Cloud Cover	31
Figure 2.2.5.1.	LANDSAT MSS Image of Olongapo, Philippines	35
Figure 2.2.5.2.	Philippines Monthly Average Cloud Cover	37
Figure 3.1.1.	WIS Design	39
Figure 3.2.1.	Ostrich Site Minefield Layout	41
Figure 3.2.2.	Ostrich Site Ground Truth Measurements	42
Figure 3.3.1.a.	Project Ostrich Site: Reflectance Data (Bands 8, 15, 25)	43
Figure 3.3.1.b.	Project Ostrich Site: Reflectance Data (Bands 35, 45, 58)	45
Figure 3.3.2.	WIS Spectrometer Overflight Path	47
Figure 3.3.3.	Cleghorn Pass: Reflectance Data	49
Figure 3.3.4.	Narrowband Subtraction Operations on WIS Data	53
Figure 3.3.5.	Wideband Subtraction Operations on WIS Data	55
Figure 3.3.6.	Band Ratios Operation on WIS Data	57
Figure 3.3.7.	Feature Spectrum (Tarp and Jeep)	61
Figure 3.3.8.	Ground Truth Reflectance Data	63
Figure 3.3.9.	Feature Spectrum (Hill and Trench)	65
Figure 3.4.1.	Arizona Test Setup and Camera Response	67
Figure 3.4.2.	Plumbicon Camera Reflectance Measurements	69
Figure 3.4.3.	Plumbicon Camera Reflectance Measurements	71

Figure 3.4.4.	Plumbicon Camera Reflectance Measurements	73
Figure 3.4.5.	Plumbicon Camera Reflectance Measurements	75
Figure 4.2.1.	Pegasus Payload Capacity	90
Figure 4.3.1.	Solar Energy Reflected from Earth	91
Figure 4.3.2.	Quantum Efficiency of Detector Materials	92
Figure 4.4.1.	Aperture Diameter and Ground-Based Resolution Relationship	95
Figure 4.4.2.	Aperture Diameter and Ground-Based Resolution Limitation	96
Figure 4.4.3.	Focal Length and Ground-Based Resolution	97
Figure 4.4.4.	Rayleigh Distribution of Irradiance.	98
Figure 4.4.5.	Minefield Trench Layout.	99
Figure 4.4.6.	Multispectral Detection	99
Figure 4.4.7.	Linear Feature Across Pixel Array	100
Figure 4.6.1.	Solar Energy Incident on the Earth	102
Figure 4.6.2.	Kodak CCD Saturation Time	104
Figure 4.8.1.	Data Download Geometry	109
Figure 4.8.2.	Velocity Over Earth at Perigee	109
Figure 4.8.3.	Tracking and Data Relay Satellite System	111
Figure 4.8.4.	TDRS Forward and Return Service Frequency Plan	112
Figure 4.8.5.	Typical User Spacecraft G/T Versus Achievable Data Rate Forward Services	112
Figure 4.8.6.	Required Received Power at TDRS versus ADR: Return Services	113
Figure 4.8.7.	Forward Service Link	114
Figure 4.8.8.	Return Service Link	115
Figure 4.8.9.	TDRS Lower Coverage Zone Geometry	117
Figure 4.8.10.	TDRS Lower Coverage Zone	117
Figure 5.1.	Satellite Telescope	121
Figure 5.2.	Satellite Component Layout	121
Figure 5.2.1.	Cassegrain Telescope Configuration	122
Figure 5.2.2.	Triple-Folded Telescope	123
Figure 5.3.1.	Figure of Merit for Optical Components	124

Accession For	
NTIS CRA&I	<input checked="" type="checkbox"/>
DTIC TAB	<input type="checkbox"/>
Unannounced	<input type="checkbox"/>
Justification	
By	
Distribution /	
Availability Codes	
Dist	Avail and/or Special
A-1	

LIST OF ACRONYMS

ARIDPCM	Adaptive Recursive Interpolated Differential Pulse Code Modulation
ARPA	Advanced Research Projects Agency
ASAT	Anti-Satellite Satellite
ASEAN	Association of South East Asian Nations
BDA	Battle Damage Assessment
BER	Bit-Error Rate
BIL	Band Interleaved by Line
BSQ	Band Sequential
CAMEO	Collaboration on Advanced Multispectral Earth Observation
CAMEX	Computer-Assisted Map Exercises
CCD	Charge-Coupled Device
CIO	Central Imagery Office
DCT	Discrete Cosine Transform
DIA	Defense Intelligence Agency
DISA	Defense Information Security Agency
DMZ	Demilitarized Zone
DSNET	Defense Department Global Network
EIRP	Effective Isotropic Radiated Power
ELINT	Electronic Intelligence
FPA	Focal Plane Array
GBR	Ground-Based Resolution
GIF	Graphics Interchange Format
GIS	Geographic Information System
GOB	Ground Order of Battle
GPS	Global Positioning Systems
HUMINT	Human Intelligence
IOL	Inter-Orbit Link
IR	Infrared
ITU	International Telecommunication Union
JPEG	Joint Photographic Experts Group
JSTARS	Joint Surveillance and Target Attack RADAR System
LANDSAT	Land Satellite
LEO	Low Earth Orbit
MTISat	Multispectral Tactical Imaging Satellite
MIL STD	Military Standards
MSS	Multi-Spectral Scanner
NATO	North Atlantic Treaty Organization
NITFS	National Imagery Transmission Format Standard
OOB	Order of Battle
OSC	Optical Sciences Center
RADAR	Radio Detection and Ranging
RF	Radio Frequency
SAMs	Surface-to-Air Missiles
SBRC	Santa Barbara Research Center
SIDS	Secondary Imagery Dissemination System
SMC	Space and Missile Systems Center

SN	Space Network
SPOT	Satellite Pour l'Observation de la Terre
SWC-TRAC	Scenario and Wargaming Center of the TRADOC Analysis Center
TACSAT	Tactical Satellite
TACWAR	Tactical Warfare
TBM	Tactical Ballistic Missile
TDRS	Tracking and Data Relay Satellite
TIFF	Tagged Image File Format
TRADOC	Training and Doctrine Command
TRS	Theater Level Resolution
UAV	Unmanned Aerial Vehicle
USATEC	United States Army Topographic Engineering Center
USMC	U.S. Marine Corps
VIC	Vector-in-Commander
WAM	Wide Area Mine
WIS	Wedge Imaging Spectrometer

EXECUTIVE SUMMARY

In U.S. Army military operations today, forward obstacles such as anti-armor minefields are discovered by cavalry, with reconnaissance units leading the way. The purpose of this study is to describe the measurable signature phenomena of anti-armor minefields and determine the feasibility of detecting these minefields from space. A low-cost, light-weight multispectral tactical imaging satellite (MTISat) under the control of a tactical commander at brigade or division level could be called upon to provide early detection of potential minefields, thus maximizing the commander's breaching options and minimizing restrictions on mobility. The following conclusions refer to a hypothetical low earth orbit (LEO) imaging satellite:

Signature Phenomena Conclusions

- Buried anti-armor minefields (soil disturbances) can be detected from space under certain conditions
- The signature phenomenology of buried minefields is inadequately understood to design an imaging satellite specifically for detecting anti-armor minefields
- Individual mines, sparsely distributed in a buried anti-armor minefield can probably not be detected from space

Spacecraft Technology Conclusions

- A tactical imaging satellite can be constructed and launched for \$20 million
- 1994 technology can support a mission with the following profile:
 - Launched and operational within 72 hours
 - 6-month orbital lifetime
 - Daily revisit
 - Multispectral imaging (3-4 bands) from .4 to 1.1 microns
 - 20+ images per pass, near real time data
 - 1.5 5.0 meter ground-based resolution (GBR)
 - Wide area search sensor (10 x 15) km @ 7.0 meter GBR
 - High resolution sensor (3 x 4.5) km @ 1.5 meter GBR

Tactical Capabilities

- Satellite is under control of tactical commander
- Satellite is disposable after six-month lifetime
- Image product is at SECRET level
- Image ephemeris data is at SECRET level
- Image quality will support navigation, route planning, mission planning, and target search operations
- Image resolution will support target detection
- Image resolution may support target classification
- Image resolution will not support target identification
- Image resolution will not support battle damage assessment

Any specialized scientific imaging package launched to support a military operation would provide intelligence data to support far more than minefield detection missions. A light-weight LEO imaging satellite would support a variety of operations including mapping, order of battle, battle damage assessment, and mission planning.

The MTISat is designed for tactical reconnaissance and would be tasked as any other tactical reconnaissance asset. The tactical user would be the first priority user of this satellite. The imagery product would be transmitted to a secondary imagery dissemination system (SIDS) and displayed on any standardized tactical analyst workstation.

PREFACE

This report was prepared under Contract DACA76-92-C-0030 for the U.S. Army Topographic Engineering Center, Alexandria, Virginia 22315-3864 by The Futures Group, Glastonbury, Connecticut 06033-4409. The Contracting Officer's Representative is Mr. Tim Evans.

1. ANTI-ARMOR MINEFIELD THREAT

1.1 Current Threat

The primary purpose of this study is to ascertain the capability of a hypothetical tactical battlefield imaging satellite to assist in the detection, identification, and delineation of a mechanically emplaced anti-armor minefield. Any tactical battlefield satellite would necessarily have a number of missions, only one of which is the detection of minefields. The battlefield imaging satellite must be available to assist in the low-intensity conflict environment as well as during large-scale armored engagements. Although low-intensity or even peacekeeping operations are not generally thought of as requiring anti-armor minefield detection, there is ample evidence of the worldwide proliferation of anti-armor mine capabilities, and all future U.S. engagements will require tactics capable of operating in this environment.

It is impossible to forecast the likelihood of encountering mechanically emplaced anti-armor minefields in likely future U.S. engagements, as compared with other types of anti-armor minefields using scatterable mines. Although many countries have the equipment to construct mechanically emplaced linear minefields, there is great uncertainty about the proliferation speed of scatterable mine capabilities. A number of countries now have the capability to manufacture scatterable mines, and Western counterproliferation strategy has not had a strong deterrent effect. A rapid transition from the mechanically emplaced minefield to scatterable mines is expected due to the time saving, cost saving, and labor saving advantages of the scatterable mine.

Role of Minefield

A thorough understanding of the difficulty in detecting anti-armor minefields requires an understanding of the role of the minefield in modern warfare and how that role affects the U.S. ability to complete a military mission. It is inherently easier to build and field sophisticated anti-armor mines than it is to detect them, and this imbalance is unlikely to change in the foreseeable future. Mines are also very inexpensive compared with their targets. The combination of low cost and high lethality makes the anti-armor mine a particularly attractive option for many countries.

Minefield detection is only the first step in countermine operations; however, it is necessarily the first step. There is occasional confusion about detecting mines and detecting minefields. It is possible to detect minefields without detecting individual mines because an anti-armor minefield is only useful when it is large enough to slow down an armored advance. A small minefield is a nuisance and can easily be bypassed. A well-built anti-armor minefield must be breached.

The success of modern armored operations requires high mobility. Minefields slow the movement of armored forces and can force the armored unit into paths more easily defensible. The timely detection of a minefield allows the tactical commander to choose alternate routes or to minimize the time to breach the field by engineers. Unfortunately, even today most minefields are detected when they are stumbled onto. Attempts to advance through a minefield have usually resulted in disastrous consequences.

The usual objective of a minefield is to deny immediate access to the area being protected. Another use of mines is the nuisance role where mines are used as a "booby trap." In this instance, the role of the mines is temporary disruption of movement rather than area denial. During the Vietnam War, the role of anti-vehicular mines was primarily nuisance. This is not to imply that this is a minor problem because nuisance mines were frequently used to stop a convoy which was then attacked by small arms fire. Anti-armor mines are distinguished from anti-personnel mines primarily by the amount of explosives used. The objective of the anti-armor mine is to disable an armored vehicle or, for that matter, any vehicle. The objective of the anti-personnel mine is to injure personnel. To achieve these objectives, the density of mines in an anti-armor minefield is much lower than the density of mines in an anti-personnel minefield. The combination of large mine size, large minefield size, and low mine density is the uniquely distinctive signature of a mechanically emplaced anti-armor minefield.

Anti-armor mines laid on the surface of the ground are difficult to detect from an armored vehicle that is operated buttoned up or when maneuvering in crop areas or at night. Buried minefields may be easier to detect under certain conditions, even those that have been in place for some time. If the area ground cover has been sufficiently disturbed in the process of creating the minefield, then the disturbed ground can be used to infer a minefield. The study of minefield signature phenomenology is based on detecting the presence of disturbed soil over an area large enough to be a minefield.

Mine Types

Nuisance mines are emplaced in small quantities such that detection requires the signature of the mine itself. In contrast, a minefield is an area denial device that must occupy a significant portion of the area to be effective, and detection of the minefield does not require detection of the individual mines. There are three different types of area denial minefields: (1) engineer emplaced minefield, (2) scatterable minefield, and (3) smart mine. This study concentrates on the engineer emplaced minefield; however, the data may apply to certain types of scatterable mines that create extensive soil disturbances.

Scatterable mines can be emplaced by aircraft, ground vehicles, or artillery. Two features of the scatterable minefield are important from the detection point of view: the randomness of the location of the mines, and the speed with which a minefield can be created. An engineer emplaced minefield takes an hour or more to create and is usually distinguished by the spacing of the rows and the spacing of the mines. The spacing is optimized to impede the movement of vehicles, which results in a regularity that can be of assistance in detecting and delineating the minefield.

From the point of view of creator of the minefield, the scatterable minefield is the more desirable type and may be the way minefield technology is evolving. A number of countries are fabricating scatterable mines and the vehicles to deploy them, and it is possible that the ability to detect an engineer emplaced minefield may decrease in importance with time. At the present time, there is a huge international stockpile of older anti-armor mines that could be used in future conflicts.

The scatterable mine creates a special problem for satellite detection because of the speed with which a minefield can be deployed. Satellite revisit times are generally measured in hours, and a revisit time of 12 hours is a frequently mentioned goal. If an opponent can emplace a minefield in minutes, then only continuous observation of the area will ensure timely detection of the minefield. To achieve continuous observation of an area using LEO satellites requires a large constellation and is incompatible with the concept of a low-cost tactical system.

Smart mines are defined here as robotic devices such as the U.S. wide area mine (WAM). The concept for the U.S. WAM is based on combining a mobile device with a sophisticated sensor, thereby bringing the mine to the target rather than waiting for the target to pass by. The U.S. WAM is capable of a kill out to 100 meters from its stationary position. The mine has the capability of recognizing the signature of enemy vehicles and has the ability to deploy out to 100 meters. This means that a small number of smart mines have the capability of denying a large area to an enemy. Smart mines are also difficult to detect by satellite because they have an inherently low profile. To detect an area protected by a smart mine probably requires the detection of the mine itself.

At the present time it is not known to what extent foreign capability for smart mines has evolved, and therefore what problems they are likely to present to U.S. forces. The smart mine, however, is probably much more difficult to detect using a satellite than an engineer emplaced anti-armor minefield.

The Minefield Signature

The two ways to lay an engineer emplaced anti-armor minefield are with mechanical minelaying vehicles or by hand. The mines can be placed on the surface of the ground or can be buried. Mines laid on the ground are easily detectable by dismounted troops in the daylight but are difficult to see from a buttoned-up tank or infantry fighting vehicle in the daylight and are practically impossible to see at night under any circumstances.

An additional problem arises when mines are used in the snow or in crop areas where the mine is hidden from view by the foliage. Another advantage of using surface mines is the ability to pick up the mines and reuse them in another area. Buried mines can be dug up and reused; however, it is a much more difficult and dangerous job.

Mechanically emplaced buried mines may be easier to detect than hand-buried mines. The machinery generally used for emplacing a buried mine creates a continuous trench. A plow blade opens the earth to a distance of 6-10 inches, and a mechanical conveyer drops a mine in the open trench every 3-5 meters. The mine is armed in the conveyer. The trench is then covered over by a plow blade. From the detection point of view, a strip of earth is uncovered to a depth of 10 inches and a width of 0.5-1.0 meters. Even in desert areas the disturbed soil is immediately evident and remains so for a period of time.

When a minefield is dug by hand the trench is replaced by a series of mounds. The earth that is removed generally occupies a larger volume than the undisturbed soil, and the soil displaced by the mine must either be raked into the adjoining soil or mounded over it. If the ground is leveled when burying the mines, in a few days there is a depression caused by the settling of the soil, especially after a rainstorm. Mechanically emplaced minefields have the same settling problem with displaced soil.

Another feature of some of the new anti-armor mines is the ability to arm the mine using a radio frequency (RF) signal. Some mines can even be armed and disarmed by radio. This gives the user of the mines a major tactical advantage in that he can operate in the minefield at will yet deny access when necessary. Remotely armed mines can be buried or placed on the ground.

In field experiments, an attempt was made to understand the phenomenology of the disturbed soil that creates the visual signature evident to a ground observer. The phenomenon may be related to the differential moisture content of the disturbed soil with a resulting change in reflectance.

Another possibility is the preferential (or nonpreferential) plant growth or presence of decayed plant material in or near the minefield trench. In older trenches, the pattern of windblown debris will be interrupted by the depressions or elevation changes across the trench. In any event, the presence of a distinctive visual signature in recently disturbed soil has become the premise for minefield sensor analysis and subsequent design.

The minefield signature probably has multiple causes and is likely to be dependent on both climatic and seasonal conditions; therefore, a sensor capable of detecting disturbed soil probably had to replicate, to a certain extent, the spectral sensitivity of the human eye. This phenomenon is not well understood but was well documented during the SkyLab experiments. Astronauts were often able to discern details on the earth from SkyLab that were not visible in the photographs taken from space. This phenomenon was particularly evident in low-angle photographs where there was significant red absorption due to long pathlengths or moisture in the air. A sensor that could replicate the sensitivity of the human eye to color might have a greater chance of detecting the presence of recently disturbed soil. Any increased spectral information will come at the cost of increased data bandwidth. These potentially large data files must either be analyzed onboard the satellite or transmitted back to the ground station.

In addition to the unique spectral signature of the minefield, there are a number of other considerations that determine the probability of detecting a minefield from space. Many areas of the earth cannot easily be imaged due to the presence of cloud cover. This is universally true of tropical areas where extensive cloud cover exists, especially in the morning. In Europe during the winter months there is often extensive cloud cover near the ground. Fortunately in arid areas where armor units are more likely to be used, cloud cover is less of a problem; however, even here extensive cloud cover may exist for days, such as occurred during Desert Storm.

Minefields, unlike most other imaged objects, do not cast significant shadows; thus, the signature is less sensitive to illumination at a specific time of day than for detection of other objects such as armored columns. Time of day is important, however, when imaging in tropical areas because of the presence of cloud cover in the mornings. Early morning and late afternoon viewing conditions may be limited by the low angle of the sun with respect to the earth. Nighttime viewing is generally inadequate even with low light level image intensification.

1.2 Future Satellite Sensors

U.S. Air Force

The U.S. Air Force Space Command is planning to sponsor a Tactical Satellite Study in 1994 through the Space and Missile Systems Center (SMC) to research innovative space-based architectures for small tactical satellites (TACSATs) that provide direct support to warfighters. The study will document the requirements for small tactical imaging satellites for each of the U.S. military services, assess current systems capabilities to meet those needs, and document shortfalls.

ARPA

The Advanced Research Projects Agency (ARPA) project, Collaboration on Advanced Multispectral Earth Observation (CAMEO), is designed to demonstrate a multipurpose imaging satellite design for both military and civilian user communities. The two primary goals of the program are to demonstrate technology that meets the needs of two communities (dual-use), and to advance the concept of small satellites as a low-cost supplement to existing surveillance or environmental

monitoring systems. An additional objective of CAMEO is to demonstrate new payload and direct downlink concepts.

CAMEO missions will include wide area surveillance for the DoD, climate research, and environmental monitoring for civilian customers.

The CAMEO optical sensor will be multispectral covering the .4 to 5.0 micron spectrum with up to 30 discrete bands. The ground-based resolution is expected to be 5-10 meters with search areas 10-50 kilometers square.¹

Commercial

Recent changes in U.S. Government policy on imaging surveillance satellites will permit U.S. commercial firms to sell 1 meter resolution satellite images to commercial clients. Under the new concept of operations, U.S. firms can build and launch imaging satellite sensors that can obtain up to 1 meter resolution images, on a for-profit basis. The concept allows the government limited control over the satellite system to protect U.S. national security. The satellite downlink transmission can be encoded to protect commercial clients, but the encryption code must be available to the government. In addition, the U.S. Government has the right to examine records of images that have been taken by the satellite, to prevent misuse by foreign agencies or terrorists. Commercial satellite firms see this as an opportunity to offer a remote sensing on demand service, and the associated technological capability is not considered militarily sensitive considering recent advances in electronic imaging technology. If launched, these systems will provide image resolution 5 times better than the next planned Satellite Pour l'Observation de la Terre (SPOT) mission.²

1.3 Expert Interviews

Interviews with tactical experts have been conducted to identify user needs for the MTISat reconnaissance satellite. Experts from the Training and Doctrine Command (TRADOC) Scenario and Wargaming Center, the TRADOC Engineering Center Mobility Branch, and the U.S. Army Armor Center Intelligence Division have been consulted for assistance in defining the requirements. The interview process is not designed to arrive at a consensus on requirements, but rather to collect a comprehensive set of expert opinions on the subject of tactical uses for an imaging satellite under control of the tactical commander.

Some experts were interviewed in person, and others were asked to comment on hypothetical battlefield scenarios. The feedback from these interviews has been incorporated into the tactical scenarios (Section 2) and in the following general comments:

- Forward obstacles such as minefields are discovered by cavalry today, and are usually discovered by accident rather than detected prior to entry into the area.
- Intelligence requirements for U.S. Army Engineers continues to be a low priority topic, since any valuable intelligence sources or tasking will usually be directed toward determining the changing order of battle on the ground.

¹"Proceedings of the International Society for Optical Engineering," *Small Satellite Technology & Applications-3*, Montpetit & Prieur, Spar Aerospace Ltd., Quebec, Canada, April 1993.

²*New York Times*, March 11, 1994.

- The increased emphasis on scatterable mines is due to several factors. First, smaller armies have less labor available, and hence the scatterable mine is a low drain on personnel resources. Second, scatterable mines come in many types and can be delivered very quickly.
- Surveillance sensors today must support operations other than warfare.
- Many tactical users are still constrained by the "size of the pipe" (communications data receive rate) available to them in the field, so that they cannot receive large digital images very often if at all.
- Tactical users would like to know what priority would be assigned to their tasking for imagery, and would prefer to get a SECRET classification level product which does not have to be sanitized for distribution.
- A small surveillance satellite can be cued by other sources, that is, radio detection and ranging (RADAR), electronic intelligence (ELINT), and human intelligence (HUMINT) and can be used to cue other sensors or assets such as unmanned aerial vehicles (UAVs), and HUMINT for improved reconnaissance results.

2. BATTLEFIELD SCENARIOS

2.1 U.S. Army TRADOC Scenario Gists

The U.S. Army TRADOC has developed a series of standard scenarios for combat development purposes. These scenarios are produced and maintained by the Scenario and Wargaming Center of the TRADOC Analysis Center (SWC-TRAC) at Fort Leavenworth, Kansas. TRAC publishes a report called *Scenario Gists* containing abstracts of the battlefield scenarios, describing the purpose, scope, and sponsor of each scenario. The complete battlefield scenarios are classified, since they describe U.S. force structure, tactics, and battle doctrine.³

A comprehensive battlefield scenario can be used to test almost any new approach to the battle space including doctrine, tactics, weapon systems, force structures, and command and control. The scenarios are gamed on specific software models including tactical warfare (TACWAR), vector-in-commander (VIC), computer-assisted map exercises (CAMEX), and other customized models that provide the gaming dynamics of the battle.

Scenarios are designed as a starting point for a battlefield study, and can be modified for any specific battlefield application, including minefield detection and clearing.

2.2 Future Battlefield Scenarios and Terrain Features

The Futures Group has constructed five battlefield scenarios for a better understanding of the problem of detecting and delineating anti-armor minefields in near-term potential conflicts. The five scenarios are designed to match the concept and resolution of the Theater Level Resolution (TRS) Scenario Gists from the TRADOC Analysis Center.⁴ The future battlefield scenarios describe the terrain features affecting armored operations, with emphasis on minefield detection and breaching requirements, rather than the force attrition dynamics of any particular battle.

The scenarios are designed to represent the comprehensive range of operations and locations where U.S. Army armored forces may be engaged in the 1990s, from full-scale marine invasions to operations where U.S. involvement is strictly limited in scope. Each scenario contains an abstract, a road-to-war narrative, a terrain features description, a description of battle phases, and a description of tactical intelligence requirements such as minefield detection.

The tactical battlefield scenarios are used to help establish the satellite sensor technical requirements through a process of establishing intelligence requirements and evaluating satellite tradeoffs, as depicted in Figure 2.2.1.

³"Proceedings of the International Society for Optical Engineering," *Small Satellite Technology & Applications-3*, Montpetit & Prieur, Spar Aerospace Ltd., Quebec, Canada, April 1993.

⁴*Scenario Gists*, TRADOC Analysis Center, Fort Leavenworth, Kansas, August 1993.

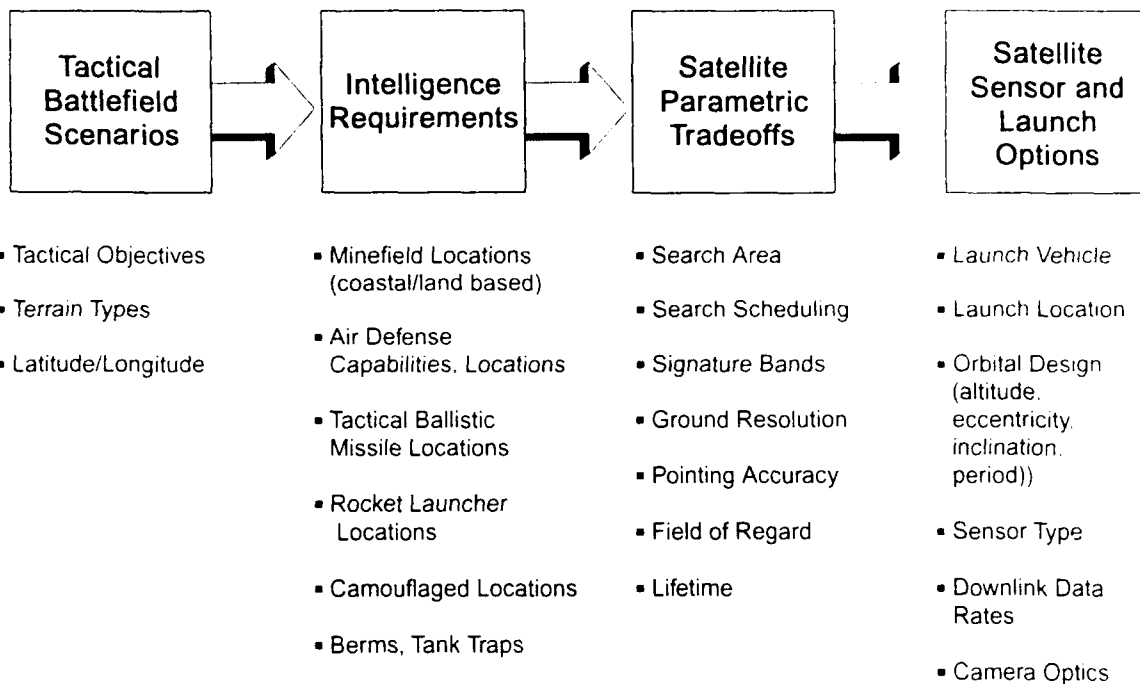


Figure 2.2.1. Battlefield Tactical Requirements Determine Satellite Design Specifications

The Futures Group scenarios share some characteristics with the following TRADOC scenarios:

<u>The Futures Group Scenarios</u>	<u>Related TRADOC Scenario</u>
2.2.1 South Korea, North Korea	Northeast Asia TRS 1.0
2.2.2 Desert Storm II	Southwest Asia TRS 1.0
2.2.3 Balkan Conflict	High Resolution Scenario 35.0
2.2.4 Cuban Revolution	Atlantic Command 1.0, HKS 33.0
2.2.5 Philippines 1997	PACOM 1.0

2.2.1. South Korea, North Korea

Abstract

This scenario is based on a postulated conflict between North Korea and South Korea resulting from a preemptive air attack by South Korea on North Korea's nuclear weapon facilities. U.S. Army armored forces are deployed to retake control of the northern sections of South Korea.

Road-to-War

In September 1995, intelligence reports indicate that North Korea is assembling nuclear weapons, and at the same time has placed its forces on alert. On October 3, 1995, South Korea launches a preemptive air attack inflicting severe damage on the nuclear assembly facility, effectively disabling it. North Korea retaliates by launching a major combined arms offensive across the demilitarized zone (DMZ) north of Seoul.

To avoid tipping off the North Koreans of their intentions, South Korea does not increase its force readiness until the preemptive strike is under way. North Korea, however, has anticipated the strike and is able to launch a prepared major armored offensive across the DMZ. At the same time, North Korea activates agents in Seoul, Taegu, and Kwangju denouncing South Korea's blatant attack against the "peace loving Democratic People's Republic of Korea." The resulting civil unrest forces a decision to keep six of the nineteen South Korean infantry divisions in reserve to control anticipated rioting in the major cities. North Korean agents are also able to attack South Korean airfields and disrupt the early-warning defense radars of South Korea, allowing successful attacks by North Korea's SU-25 ground attack jets. North Korean agents are able to assassinate a significant number of senior South Korean military officers and government officials, thus adding to the confusion.

North Korea has overrun the DMZ on a 70 km front centered on the road from Monson to Seoul. The North Korean Navy moves 15 of its 24 diesel electric boats and 120 of its 170 torpedo boats into the waters adjacent to Inch'on, thus preventing the U.S. Navy from evacuating U.S. civilians and other Western personnel from Seoul.

North Korea is able to overrun Seoul, Yongjungpo, and Inch'on on the third day of its offensive. In the process, North Korea is able to capture large numbers of U.S. and South Korean Hawk surface-to-air missiles batteries that it uses to help defend the captured cities. The North Koreans also capture 8,500 U.S. military and civilian personnel; 2,500 other Western personnel; and 1,800 Japanese citizens.

The South Korean Army is able to form a defensive line running west from Wonju to the coast. At the same time, the South Korean Air Force is able to regain the initiative with the assistance of U.S. carrier jets, and within eight days it dominates the sky to 70 km north of the DMZ. The U.S. decides to commit the 1st Marine Division along with two U.S. Army mechanized and one armored brigade in the defense of South Korea.

The armored engagement would consist of a combined U.S. and South Korean armored offensive through the North Korean defensive line with the objective of retaking Seoul and the other northern cities of South Korea. The North Koreans have moved the bulk of their armor into the defense of the line as well as much of their air defense guns and surface-to-air missiles (SAMs). After five weeks of heavy fighting, South Korean forces are unable to gain the offensive. The captured Hawks and SAMs used by the North Korean Army prevent the use of South Korean anti-armor helicopters and A-10s. The North Koreans have built extensive engineer emplaced anti-armor minefields utilizing Soviet mechanized minelayers.

North Korea anticipates a U.S. Marine Corps (USMC) amphibious assault at Inch'on and has heavily mined both Inch'on harbor and the anticipated beach landing sites. The USMC amphibious assault is therefore based on a landing in the coastal area west of Suwon (south of Seoul). To ensure a

successful operation, the breakout at Wonju must take place very rapidly. The lead is therefore assigned to the U.S. Army armored and mechanized brigades because of their superior mobility.

Korea Scenario Terrain Features

The area of concern is the region south of Seoul, centered on the city of Suwon, a heavily populated area. The defensive line is presumed to run west to east to Yongin then to Inch'on and Yonju with the line then running northeasterly toward the DMZ. The terrain in the vicinity of Suwon is devoted to paddy farming. Elevations are less than 500 meters (474 meter hill west of Kunp'ojabg), and the terrain is heavily farmed.

The photograph on the following page (Figure 2.2.1.1) is derived from the land satellite (LANDSAT) Multi-Spectral Scanner (MSS). It is a black and white image created from band 4 of the MSS, which covers the 0.8-1.1 micron (near-infrared [IR]) band at a ground resolution of approximately 80 meters per pixel.

There are a number of streams running north to south, and the Hanguang River, a major tributary, is on the easterly border of the area of concern. The swampy areas which would inhibit armor are small in area and can be bypassed easily. During the springtime and during periods of heavy rains, armor operations could be constrained.

The USMC amphibious operations will be severely constrained by the large areas of mud flats in the coastal area near Hugok. There is a navigable channel with exit points at Wonsan and a railroad that runs along the coast.

There are a large number of small villages between Suwon and Yongdungpo. These villages are frequently within 2-4 km of each other. The distance between Yongdungpo and Suwon is approximately 30 km. Route 1 is a major highway between Suwon and Seoul, running north and south through the resort area of Anyang-ni. There is an airfield just south of the city of Suwon.

Seoul sits on the north bank of the Hanguang River opposite the city of Yongdungpo. The river forms a natural barrier to an attack from the south. During the Korean conflict, the USMC 1st Division was able to dislodge the North Koreans from the city but only by doing immense damage to most of the buildings in the city. Given the extensive buildup in the city of Seoul since, a comparable operation would result in unthinkable damage.

Phases of the Battle

The minefield detection and clearing operations would follow a four-phase campaign for U.S. forces in the Korea scenario:

- Phase 1: Locate enemy, assess minefield threat, and prepare for battle
- Phase 2: Execute air war deep fires to weaken the enemy force
- Phase 3: Marine landing and decisive armored battle
- Phase 4: Force reconstitution and peacekeeping operations

Phase 1: North Korean military activities would have been carefully monitored prior to the invasion by South Korean airborne reconnaissance units and with U.S. reconnaissance assets. The U.S. reconnaissance assets, however, would have emphasized the discovery of force size, disposition, and

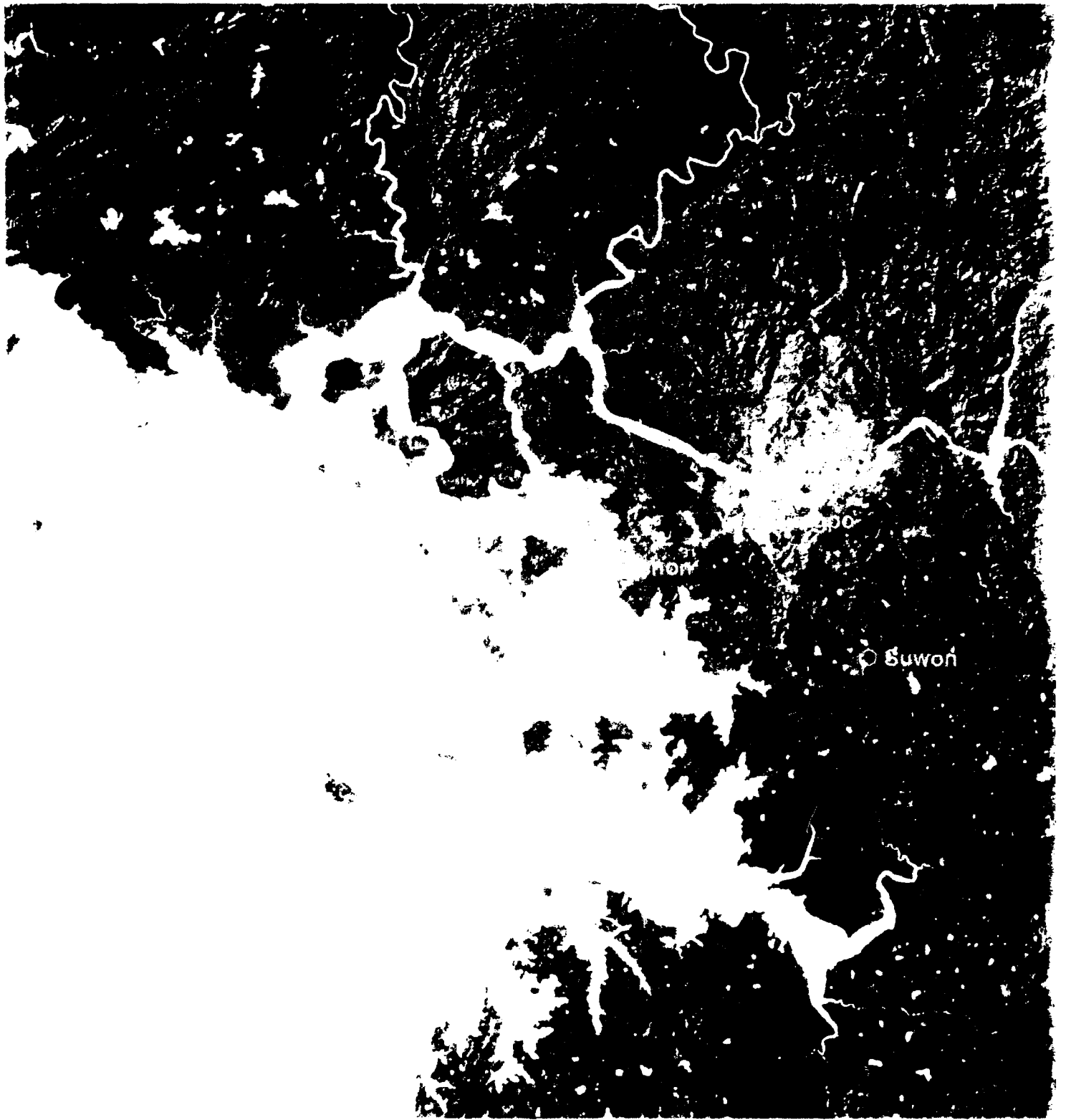
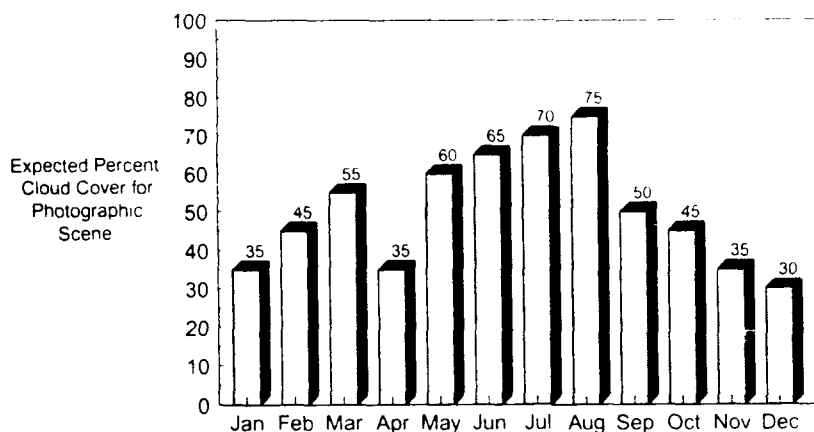


Figure 1. The Han River Basin, Korea

intentions, rather than minefield-laying operations. In addition, cloud coverage over this part of Korea is significant for much of the year, thereby limiting availability of good, quality photographic coverage.

The following graphic (Figure 2.2.1.2) shows cloud cover as percentage of total scene, for a series of LANDSAT scenes recorded from 1972 to 1989. A total of 123 LANDSAT scenes were recorded over the location for this Korea scenario, centered around 37.30 north latitude and 127.00 east longitude. For much of the year, this part of Korea has greater than 50 percent probability of cloud cover, complicating minefield detection by standard photographic means.



Source: LANDSAT scene database

Figure 2.2.1.2. Korea Monthly Average Cloud Cover

Phase 2: Prior to the USMC forces going ashore, there would be an air war campaign to establish air superiority, deny North Korean communications lines, and reduce enemy forces on the ground. Most primary photographic intelligence assets would be utilized to support the deep strikes, with activities such as minefield detection given a much lower priority level. Units preparing for the upcoming beach assault and ground campaign would use maps to identify potential areas where minefield clearing engineers might become engaged. Limited overhead photographic intelligence would be available to indicate where to search for minefields.

Phase 3: The third phase of the U.S. campaign is the Marine landing and the subsequent armored battle. Most photographic intelligence data would be available to support the tactical commander on the ground, but minefield detection and delineation would continue to have a low priority. The photographic imaging assets would be used to identify and evaluate safe beach landing zones.

Phase 4: During force reconstitution and peacekeeping operations, the cooperation of the defeated enemy force could be used to identify, delineate, and clear minefields. As part of the peace settlement, limited North Korean mine-laying plans would be provided to U.S. and South Korean forces for clearing. The clearing of minefields would now have a very high priority, with U.S. national and theater assets being employed to locate and delineate minefields. Limited military and civilian casualties would continue as a result of the clearing operations.

Tactical Satellite Surveillance Requirements

There are four primary intelligence support operations in the Korea scenario:

- Select Amphibious Landing Zones
- Minefield Locations (coastal and inland), X, Tank Traps
- Locate Mobile Targets (Tactical Ballistic Missiles, Rocket Launchers, Hawk Batteries)
- Terrain Evaluation
- Discover Camouflaged Locations

Select Amphibious Landing Zones

The selection of safe landing zones would require a determination of many characteristics of the amphibious environment. For landing safety, an assessment of sea surface roughness (wave height) would be required, since amphibious landing vessels have different operating envelopes for sea state. Locations of reefs, sandbars, and other obstacles would also be required. The detection of coastal mines in or near landing zones would require a wide area search. Prior to the amphibian landing, the identification of terrain and cultural landmarks may be needed as navigation aides.

Minefield Locations

The minefield locating abilities of a small satellite imaging sensor would be limited by the size of the image area, and by the resolution of the image. Once cued where to search, the satellite would record an image, and ground-based photo interpreters would look for extended areas of disturbed soil or minefield-laying vehicles or tank traps. The wide area search capability and high resolution would both be strong requirements.

Locate Mobile Targets

The problem of locating small, highly mobile targets would be impossible for a visible band lightweight imaging satellite to solve alone. The satellite sensor would have to be cued to know where to record images within a large field of regard. The sensor cueing could come from ELINT, HUMINT, or a RADAR platform such as the Joint Surveillance and Target Attack RADAR System (JSTARS). The JSTARS sensor has proved useful in Operation Desert Storm to vector U.S. armored forces and attack aircraft toward moving armored columns. The contacts from JSTARS fused with an image from a cued small satellite sensor may provide locations for high mobility transient targets that neither sensor alone could determine. As part of the highly mobile targets problem, locating air defense capabilities may also require cueing of the imaging satellite by ELINT or other sensors. The cued sensor would be able to manage smaller search areas at higher resolution.

Terrain Evaluation

If this Korea scenario were to take place during heavy spring rains, armored mobility could be limited. For decisive armored mobility throughout the campaign, the capacity of the terrain to permit vehicle movement must be known. The imaging satellite can be used to assist with route selection and terrain evaluation. If the tactical imaging satellite can cover the same bands as the French SPOT system, the tactical images can be compared to archived SPOT data for improved terrain analysis and mapping.

Discover Camouflaged Locations

A low resolution satellite image of a camouflaged location would not be likely to discover the location unless the sensor has multiple bands, and the camouflage reflectance is significantly different from the background reflectance in at least one band. The image would only detect reflected sunlight, and would be unable to penetrate vegetation cover as a RADAR image can. A multispectral image would be required to detect camouflage locations but the resolution can be less demanding since the image would attempt to discover the presence of camouflage material, rather than identifying specific weapon systems hidden by the material.

Table 2.2.1. TACTICAL OPERATION

Imagery Requirement	Minefield Locations	Locate Mobile Targets	Discover Camouflaged Locations	Terrain Evaluation	Select Amphibious Landing Sites
Orbital Lifetime	180 days	180 days	180 days	180 days	20 days
Timeliness	6 hrs	1 hour	6 hrs	8 hrs	2 hrs
Overflight Frequency	daily (Sun-Synchronous)	daily (Sun-S)	daily (Sun-S)	daily	daily (Sun-S)
Signature Bands	panchromatic	panchromatic	multispectral	3 bands in the 0.4-1.1 micron range	panchromatic
Resolution (m)	1 m	1 m	5 m	5 m	5 m
# of Images/Pass	4 sites	10 images	3+	2 images	3+
Image Area (km x km)	10 x 10 km	2 x 2 km	10 x 10 km	20 x 20 km	20 x 20 km
Pointing Accuracy (% of scene)	20% (1000 m)	10% (200 m)	20% (1000 m)	10% (2000 m)	10% (2000 m)

2.2.2 Desert Storm II

Abstract

A series of events increase Middle East tensions from 1994 to 1998, leading to U.S. involvement in a battle to retake Kuwait City, Kuwait.

Road-to-War

In 1994, Iraq attacks Syria over a water rights dispute. The Syrians prevail with the assistance of Iraqi Kurds. In a peace treaty, Iraq agrees to give up rights to Kurdistan, defined as the area north of the 36th parallel and particularly a line from Tuz Khurmatu through Kirkuk-Al Mawsil to Ayn Zalah. The Kurds cooperate with Turkey, to prevent cross-border attacks by Kurds into Turkey.

In 1995, Iran continues to promote unrest in Basra among the Shiite population. Iraq is experiencing severe internal economic difficulties, and when it attempts to put down rioting in Basra and marshy areas north of Basra, Iran intervenes. Iran captures and is able to hold an area of southern Iraq extending from Al Kut west and south to Al Hillah and including all of Basra.

Baghdad's area of influence is reduced to 40 percent of its 1991 population and its fighting forces are reduced by 20 percent by the defection of southern forces.

From 1995 to 1998, Iran increases its power by cementing its relationship with Azerbaijan. Iran purchases oilfield equipment and agricultural supplies from Azerbaijan. Sales of Iranian oil including oil from the areas captured from Iraq allow Iran to upgrade its military capability dramatically. Iran is able to purchase advanced military equipment from Russia and missiles from China. Iran plays Russia off China successfully due to the poor state of the Russian economy.

In September 1998, to cover the costs of massive purchases of military equipment, and with the solid control of southern Iraq, Iran invades Kuwait in an attempt to take the Kuwaiti oilfields. Iran assures Western powers that it intends to maintain the flow of oil from Kuwait at current market prices. Saudi Arabia, fearing for its own security, asks for support from the U.S. and the Arab League with the goal of retaking Kuwait and restoring the monarchy.

In a move known to U.S. forces but not to other states in the gulf region, Kuwait has taken a step to protect its own oilfields. The routes leading into the most important oilfields have been mined by the Kuwaitis themselves. They have employed RF-switchable mines that can be disarmed by remote control for access to the area. A system of anti-vehicle and anti-personnel mines has been buried around many of the strategically vital oilfields in Kuwait. The Kuwaiti armed forces maintain records of the exact mine locations with a sophisticated Geographic Information System (GIS), and are able to lead oilfield service workers into and out of the minefields using differential Global Positioning Systems (GPS) and equipped vehicles, or by switching off a minefield for access to the area.

Iranian forces take Kuwait City, but have lost several tanks and personnel carriers while negotiating the mined Kuwaiti oilfields. Iran, having learned from its own past mistakes and understanding what happened to Iraq in Desert Storm, fortifies a line along the border with Saudi Arabia. The fortifications consist of armor in depth as well as anti-armor barricades. Modern SAMs purchased from Russia and China back up the fortifications to prevent a repeat of the highly successful U.S. air war in Desert Storm.

Iran also moves the new anti-ship cruise missiles it purchased from China to reinforce the straights of Hormoz. Iran threatens to sink any U.S. or Western warship attempting to transit the straights of Hormoz.

In October 1998, the U.S. forms a coalition force with Egypt and Saudi Arabia. Iran has prevailed on Russia to use its veto in the United Nations to deny the U.S. a mandate in the Security Council. The U.S. supplies two armored brigades, one mechanized division, one light infantry division, and a Marine expeditionary brigade. Egypt supplies two mechanized divisions and Saudi Arabia supplies five mechanized brigades. The U.S. is unable to get its carrier task forces in close enough for support, and the allies must rely on the U.S. and Saudi Air Force for close air support at the beginning of the operation, until the Iranian missile threat is reduced.

The Iranians defend Kuwait City with eight mechanized divisions and three light infantry divisions located in Kuwait City. The Iranian engineers lay large quantities of anti-armor mines in depth, using previously purchased Soviet automated minelayers. U.S. forces conduct several amphibious landings and an armored assault into Kuwait from Saudi Arabia. The scenario ends with an Iranian withdrawal from Kuwait City.

Desert Storm II Terrain Features

The area of concern is the area north of Al Jahrah from the coast at Bahran west to Mutriba (see Figure 2.2.2.1. LANDSAT Multi-Spectral Scanner Image — Kuwait City, Kuwait). Recapturing the pipelines in the vicinity of Al Jahrah is crucial to the success of the operation. The Iranians are presumed to hold the island of Bubiyan, as well as the pumping station.

The area is desert terrain with extremely high summer daytime temperatures. The terrain is flat and consists of gravel and sand. The area is one of the primary oilfields in Kuwait just west of the primary battle zone of Desert Storm. There is only one paved road in the area, which follows the pipeline and dozens of gravel roads through the whole area.

Phases of the Battle

The minefield detection aspects of this scenario are profoundly different for two reasons; first, the escalation in hostilities would be monitored by U.S. intelligence operations for a long period so that there is a good opportunity to detect minefield-laying operations. The minefield-laying operations would be favorably observable in the desert terrain. Second, since hostilities have been going strong for several years in these areas, minefield locations would have been recorded over time, and some may become lost in the shifting sands or forgotten as territory changes hands. The battle scenario would consist of four phases:

- Phase 1: Monitoring enemy movements
- Phase 2: Aerial reconnaissance and assault preparation
- Phase 3: Armored battle
- Phase 4: Force reconstitution and peacekeeping

Phase 1: The first phase of the U.S. action is the monitoring of enemy movements over the past several years as tensions have risen. The locations of likely minefields and known minefields have been recorded, and the Kuwaiti Government has provided the exact location of its own minefields to U.S. forces. The accurate locations of these minefields would be entered into the Defense Intelligence Agency (DIA) order of battle (OOB) databases as they are identified.

Cloud coverage is not expected to inhibit the collection of photographic intelligence over Kuwait during this scenario. A total of 102 LANDSAT scenes were recorded over the location for this Desert Storm II scenario, centered on 29.20 north latitude and 47.55 east longitude in Kuwait. A series of LANDSAT scenes from 1972 to 1992 show the probability of cloud cover over Kuwait. For several months of the year, this part of the Middle East has greater than 50 percent probability of cloud cover, complicating minefield detection by standard photographic means. In the summer months, cloud cover is almost nonexistent over Kuwait City (Figure 2.2.2.2).

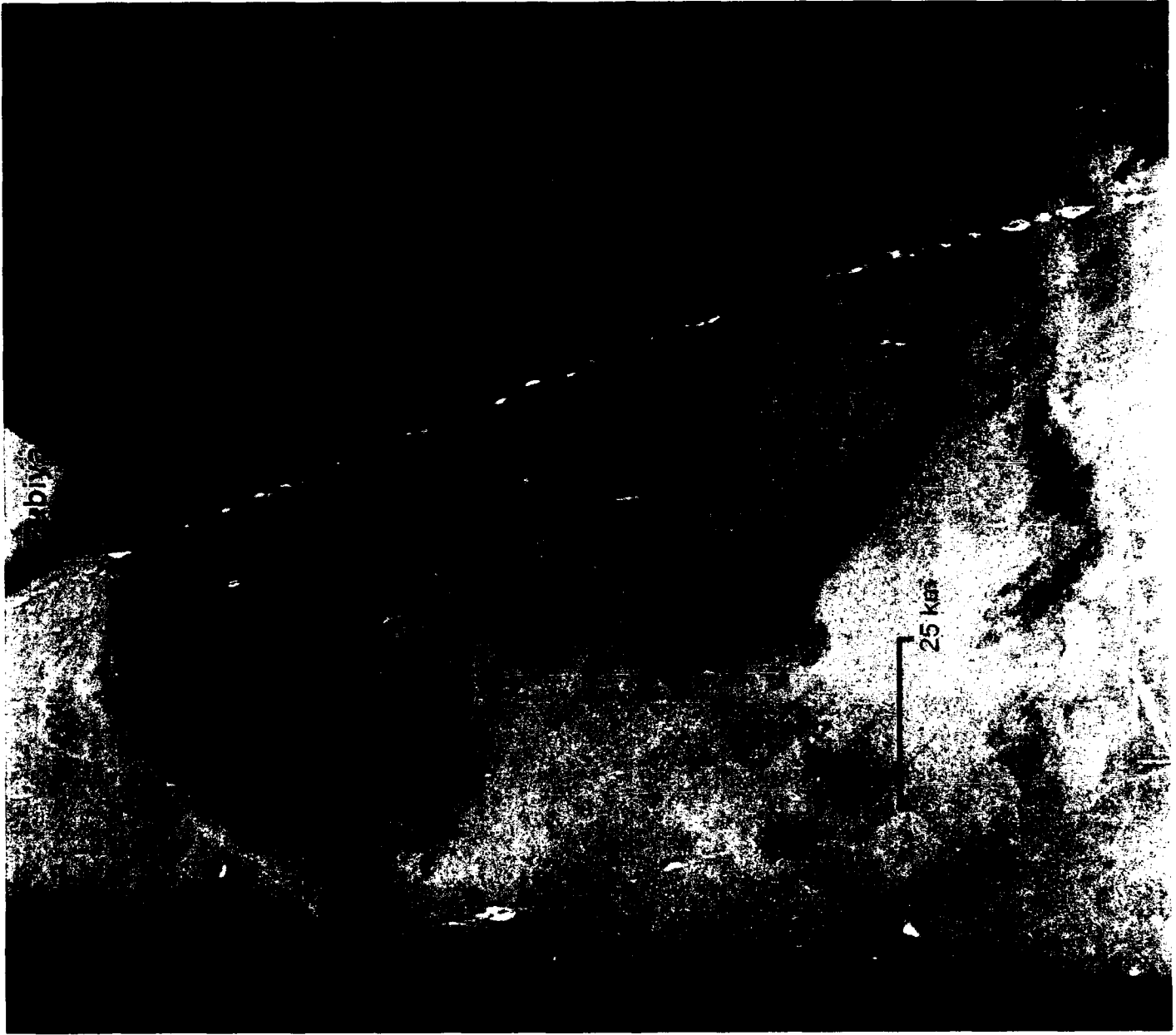
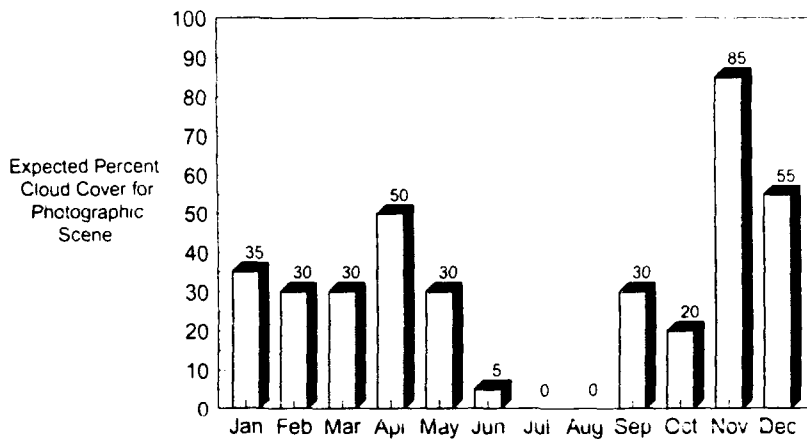


Figure 2.2.2.1. LANDSAT MSS Image of Kuwait



Source: LANDSAT scene database

Figure 2.2.2.2. Kuwait Monthly Average Cloud Cover

Phase 2: U.S. forces must begin to intervene around Kuwait City before the Iranian forces become more heavily fortified or better entrenched. While waiting for the air campaign to remove the Iranian mobile missiles near the straight of Hormoz, USMC forces in a Saudi port prepare for a Marine invasion onto Bubiyan Island. U.S. intelligence assets are primarily used to locate missiles around the straight of Hormoz, but limited high altitude aircraft reconnaissance assets are available for the monitoring of Iranian mine-laying operations around Kuwait City. Also, to prepare for the amphibious landings onto Bubiyan Island, USMC air power is used to reduce the strength of the Iranian forces. Aerial reconnaissance assets are used to accurately image Bubiyan Island to detect Iranian forces. These images are made available to Army Engineers for minefield detection operations and to USMC forces planning the amphibious landing.

Phase 3: Once the U.S. forces have entered Kuwait, minefields will be breached as they are discovered and as tactical requirements dictate.

Phase 4: After the battle, during force reconstitution and peacekeeping operations, the cooperation of the defeated Iranian force could be used to identify, delineate, and clear minefields. As part of the peace settlement, some Iranian minefield engineering plans would be provided to U.S. and coalition forces for clearing. The clearing of minefields would now have a very high priority, with U.S. national and theatre assets being employed to locate and delineate minefields. Nevertheless, limited military and civilian casualties would continue until the clearing operations are complete.

Tactical Satellite Surveillance Requirements

There are three primary intelligence support operations in the Desert Storm II scenario:

- Locate and Delineate Anti-armor Minefields
- Locate Mobile Targets (SAMs and TBMs)
- Selecting Sites for Amphibious Landing on Bubiyan

Locate and Delineate Minefields

Although some areas of Kuwait are mined by the Kuwaitis themselves, the Iranian forces also build a few minefields using Russian-designed mechanical minelayers. The search areas are limited, but the image resolution requirements are strict because the minefields are expected to be short. They

will have to be delineated, and if short enough, they can be bypassed and may not have to be breached.

Locate Mobile Targets

The Iranian forces are operating Anti-air SAMs and Surface-to-Surface Missiles from the Iranian coast on the strait of Hormoz. The satellite imaging sensor can sometimes be cued by ELINT intercepts of SAM activity. Search areas are 10 km x 10 km, with many images along the Iranian coast taken each day. Multiple bands may be needed to assist with locating targets in different terrain types.

Select Amphibious Landing Sites

During Phase 3 of the scenario, an amphibious landing onto Bubiyan Island is planned. Many of the potential landing sites are expected to be mined; thus, high resolution images are required to detect mines with high contrast to the water. The resolution requirement can be traded off for small search areas, since sandbar obstructions may limit the landing site options to a few miles of coastline.

Table 2.2.2. TACTICAL OPERATION

Imagery Requirement	Locate and Delineate Minefields	Locate Mobile Targets	Select Amphibious Landing Sites
Orbital Lifetime	80 days	180 days	10 days
Timeliness	8 hrs	2 hrs	24 hrs
Overflight Frequency	daily	daily	daily (Sun-S)
Signature Bands	panchromatic	3 bands in the 0.4-1.1 micron range	panchromatic
Resolution (m)	1 m	2 m	1 m
# of Images/Pass	6+	10+ images	10+
Image Area (km x km)	2 x 2 km	10 x 10 km	4 x 4 km
Pointing Accuracy (% of scene)	10% (200 m)	10% (1000 m)	10% (400 m)

2.2.3 Balkan Conflict

Abstract

In 1995, United Nations sanctions and the threat of North Atlantic Treaty Organization (NATO) intervention have caused the Serbs to abandon the siege and bombardment of Sarajevo. Having consented to international community demands to cease ethnic cleansing, the Serbs have turned southward and have gained military control of large areas with Croatian and Muslim populations.

A new Serbian thrust into Kicevo has pulled European forces into position around the former Yugoslavia to defend various national interests. U.S. forces are brought in under NATO control after a U.N. request to prevent further Serbian advances.

Road-to-War

In 1995, open hostility continues between the different ethnic populations of Serbia and Bosnia. Ethnic Albanians in Kicevo resist harassment by Serbian forces. Ethnic cleansing in Kicevo is expanding, and the resident Albanian population reacts with civil unrest. Serbian troops are killed and several Serbian politicians are injured by bombs. Albania provides clandestine support to dissidents in Kicevo. Civil war starts in Montenegro, with Albania providing clandestine military support to ethnic Albanians.

Serbia increases the number of troops in Kicevo and moves in heavy armor causing Albania to invade from the west, primarily with light infantry. The Serbs and the Albanians hold their ground with tanks and artillery.

Greek troops move into Macedonia ostensibly to protect the indigenous Greek population from Albanians. Turkey abstains from the NATO action, while threatening to introduce Turkish forces into Macedonia.

The U.N. brokers a cease-fire to be policed by NATO troops in conjunction with Russia. Germany and France move troops into the western border with Albania, and Russians move troops into eastern areas along the Serbian border. U.S. and British armored troops occupy southern Kicevo and parts of Macedonia. NATO troops are constantly harassed by local partisan bands, both Serbian and Albanian, and must be prepared to defend themselves if the warring factions decide to resume the civil war. As U.S. and British forces push back the Serbs, they must dismantle minefields built by several of the warring parties, who used mine-laying equipment of the former Yugoslav Army.

Balkan Conflict Terrain Features

The area of concern is centered on the city of Skopje, Macedonia (see Macedonia map — Figure 2.2.3.1). The mission of U.S. forces is to detect and deter the movement of Albanian troops through Macedonia into southern Kicevo. There is a major highway between Tirane in Albania and Skopje in Macedonia. U.S. and British forces would be tasked to prevent the movement of Albanian troops through this area.

U.S. and British forces would be required to patrol the roads from Skopje west to Tetovo (Route 26) and then south to Kicevo and then to Ohrid on the Greek border. The road from Tetovo follows an agricultural valley 2-3 km in width. The mountains to the west of Tetovo are imposing with peaks of over 2,500 meters (Sapka 2,747 meters).

There are several ski areas in the vicinity of Tetovo and Kicevo attesting to the severity of the winters. Most of the population live in small valley towns and derive their income from farming or forestry.

Two secondary roads traverse the mountains and could be used to move troops and supplies from Albania. One road starts in Tetovo, goes through Prizren, and then traverses the Kara-Nikola pass at 2,050 meters. A second road from Gostivar passes through numerous small mountain villages before connecting with a major thoroughfare to Albania. These roads are probably impassible in the winter.



Figure 2.2.3.1. Map of Macedonia

The area is mountainous and heavily forested with scattered villages. Most of the area west of Skopje is over 1,000 meters elevation. The forest is primarily evergreen, and the terrain is similar to the mountains of northern New England. Armored forces are primarily confined to the roads, although there are some extensive pastured areas. Skopje itself lies in a valley that is heavily farmed.

Weather conditions in the winter and spring can result in long periods of extensive cloud cover. Light infantry troops can traverse the area without using major roads; however, movement is restricted to the roadways in winter.

The two main cities in the area are Tetovo and Gostivar. Tetovo has a population of 165,000 (includes surrounding area) and Gostivar has a population of 110,000. Skopje has a population of approximately 300,000.

Commercial deliveries into Skopje are normally carried over land through Thessaloniki, Greece — a distance of approximately 200 km. Thessaloniki is a major seaport, and armored forces would probably be brought to Skopje by way of Thessaloniki.

When Macedonia was under Yugoslavian control, Skopje was a major military town with an airfield and an armored division of the Yugoslav Army stationed there.

Phases of the Battle

The battlefield scenario consists of three phases. The terrain is so mountainous that anti-armor minefields will only be expected in a limited number of areas, primarily around roads, mountain passes, and through farmland. Minefield detection is expected to merit a low priority for this scenario, since U.S. forces are primarily used to defend a line rather than to take territory.

Phase 1: Monitoring Serbian, Albanian, and Greek advances

Phase 2: Limited NATO air strikes

Phase 3: De-escalation and U.S. force withdrawal

Phase 1: U.S. intelligence-collecting assets are stretched thin attempting to determine the accurate OOB in this scenario with so many belligerent parties. The Serbs have the largest and most threatening force and are therefore monitored most closely. Photographic reconnaissance assets are primarily utilized for an accurate OOB assessment, with very low priority given to minefield detection.

The LANDSAT imagery scene database contains an insufficient number of scenes to estimate the probability of cloud cover over Skopje at any given time of the year.

Phase 2: During Phase 2 of the Balkan Conflict, NATO aircraft are used to maintain air superiority, monitor changes in the Ground Order of Battle (GOB), and conduct limited strikes on Serbian forces around Kicevo. On the ground, U.S. forces primarily rely on HUMINT sources to identify nearby minefields, which have been created by Serbs and Albanians. The suspected locations of minefields are recorded in a GIS database, since some minefields may be expected to migrate over several freeze and thaw cycles.

Phase 3: After several months, Serbian and other forces have left the area and U.S. ground forces are beginning to withdraw. The HUMINT sources among the local population are enlisted for a comprehensive minefield detection and clearing operation.

Tactical Satellite Surveillance Requirements

There are two primary intelligence support operations in the Balkan scenario:

- Monitor Movement of Albanian, Greek, and Serbian forces
- Battle Damage Assessment (BDA)

Monitor Movement of Forces

The monitoring of changes in the GOB will primarily require accurate, high-resolution coverage of highways since the local terrain inhibits the movement of forces by other routes. The high-speed avenues of approach include from Skopje west to Tetovo (Route 26) and then south to Kicevo and then to Ohrid on the Greek border. The search areas are narrow but numerous, and the resolution requirement to identify vehicles is 1 meter.

Battle Damage Assessment

A requirement for BDA exists to determine the effectiveness of NATO strikes and to detect strikes among the belligerent. The two types of BDA mandate two sets of BDA requirements on the imaging sensor. First, the NATO strike locations are accurately known, and BDA reconnaissance would be used to very accurately assess the effectiveness of the weapon on the target. This weapon assessment demands extremely high resolution, as high as 1 foot or less. The second BDA requirement is to locate strike zones among the belligerent, which can be done in this part of the world by looking for smoke from fires. The second type of BDA therefore requires a wide search at lower resolution.

Table 2.2.3. TACTICAL OPERATION

Imagery Requirement	Monitor Force Movements	BDA — Weapon Assessment	BDA — Low Resolution
Orbital Lifetime	180 days	180 days	180 days
Timeliness	4 hrs	2 hrs	2 hrs
Overflight Frequency	daily	daily	daily
Signature Bands	panchromatic	panchromatic	panchromatic
Resolution (m)	1 m	< 1 m	2 m
# of Images/Pass	10+	20+ images	4+
Image Area (km x km)	2 x 2 km	1 x 1 km	10 x 10 km
Pointing Accuracy (% of scene)	10% (200 m)	10% (100 m)	20% (2000 m)

2.2.4 Cuban Revolution

Abstract

Fidel Castro's death and a nascent civil war create instability and armed conflict throughout Cuba. The U.S. responds with USMC amphibious forces to protect U.S. personnel at Guantanamo Bay, Cuba, and to provide limited assistance to the anti-government Cuban forces.

Road-to-War

In 1996 Fidel Castro is killed in a helicopter accident; however, it is widely believed within Cuba that the cause of the crash was sabotage. Raul Castro assumes the leadership role after promising reforms to the ruling council, but internal instabilities cause civil war to break out within a few weeks of Castro's death. The opposition starts to solidify around Colonel Felix Ortiz, a moderate leftist. Colonel Ortiz, a Soviet educated professional soldier is a veteran of Cuba's involvement in Angola, South Yemen, and Ethiopia. He is a protege of General Arnaldo Ochoa Sanchez. General Ochoa and four other military officers were executed by Castro in July 1989 for alleged drug dealings; the executions were widely believed to be tied to General Ortiz's popularity among Angolan war veterans.

Cuban exiles in Miami attempt to aid the anti-government faction fighting in the Sierra Maestra mountains of southern Cuba. The exiles are able to supply small arms and cash to the anti-government forces; however, they are unable to counter the heavy armored capabilities of the government. In addition, Colonel Ortiz does not support many of the goals of the Miami exiles and his leftist ideas frighten them. The Cuban Government with the aid of a number of former Sandinista volunteers appears to be gaining militarily on the insurgents, primarily because of their access to aircraft, armor, and artillery. The anti-government forces have been reduced to fighting a guerrilla operation and must appeal to the U.S. for support. The U.S. agrees to help since it has evidence that the Colombian drug cartel is funneling money from its cocaine sales to senior Cuban military officers. In turn, the Cuban Government requests assistance from Russia and other former Soviet republics; their request is denied.

The U.S. has evacuated all dependent personnel from Guantanamo Bay and introduced a Marine amphibious brigade to back up the defense of the installation. A U.S. Navy carrier task force with a second USMC amphibious brigade has moved into the Santaren channel, and the 82nd Airborne Division has been placed in a heightened state of readiness.

The U.S. initiates an airdrop of supplies to the anti-government forces; however, the difficulty of accurate airdrop landing points from high altitude reduces the effectiveness of the resupply effort to the insurgents in the Sierra Maestra mountains, just outside of Bayamo. A decision is made to deploy U.S. forces to protect the insurgents by setting up a defense line between Manzanillo on the west coast of Cuba, and Holguin. Units of the 82nd Airborne will jump into Contramaestra until the Marines arrive from Guantanamo Bay. The USMC amphibious brigade at Guantanamo moves westward toward Palma Soriano to establish the defense from Manzanillo to Holguin.

Once the Cuban Government forces learn of the U.S. intervention, they begin mining routes from Guantanamo to Bayamo with remaining Soviet automated mine-laying equipment to slow the U.S. advance. Although these old Soviet mines are not the most effective available today, they are all that remain in the Cuban Government inventory. Cuban Government forces begin to change sides in the conflict, and the insurgents eventually form a new government with popular support.

Cuban Revolution Terrain Features

The Cuban scenario takes place over a distance of approximately 250 km from east to west and 150 km north and south (see Figure 2.2.4.1). The USMC amphibious brigade must move north and west of the base (U.S. Naval Station Guantanamo Bay, Cuba). USMC forces must move north through the city of Guantanamo (approximately 15 km) and then westward through the town of La Maya, north of Santiago de Cuba. From Santiago de Cuba, the Marines must move north and west through San Luis to Palma Soriano, Contramaestre, and then to Bayamo.

The area from Guantanamo to Santiago de Cuba is primarily grasslands and forest with an airport at Santiago de Cuba. It might be possible to bypass the town of Santiago de Cuba by staying to the north, heading directly to Bayamo. The bypass will be preferable if the airfield at Santiago de Cuba does not have to be attacked. There are sugar plantations to the north of Santiago de Cuba around St. Luis. In the region of Palma Soriano the land is primarily devoted to coffee plantations. From Contramaestre to Bayamo, the terrain is partly forested with extensive open grasslands and small farms. The land between the coastal town of Manzanillo and Bayamo (approximately 100 km) is flat with numerous large farms around the towns of Yara and Mabay. There is an airport at Bayamo.

The lowlands northwest of Bayamo are swampy and crossed by numerous streams. The road from Bayamo to Holguin crosses swampy farmland and continues into the more hilly terrain toward Holguin. Cuban Government armored forces moving south would approach Bayamo from the northeast through Holguin. Securing Bayamo would be the key to preventing the Cuban forces from mounting a successful assault on the anti-government forces in the Sierra Maestra Mountains.

Phases of the Battle

The Cuban revolution scenario has four phases:

- Phase 1: Monitor situation as the revolution begins
- Phase 2: Determine tactical requirements to reinforce the insurgents; Marine reinforcement landings at Guantanamo
- Phase 3: Finalize attack plans; USMC advance from Guantanamo and establishment of line from Manzanillo to Holguin
- Phase 4: U.S. force withdrawal

Phase 1: While monitoring the onset of the revolution, the intelligence assets will be primarily utilized to determine GOB and to identify the strategic position and intent of both sides. The quality of aerial or satellite observation of the area of concern would be highly dependent on the weather, time of day, and season. The high humidity in this tropical climate often includes extensive cloud cover during certain times of the year. The graphic in Figure 2.2.4.2 shows cloud cover as a percentage of total scene, for a series of LANDSAT scenes recorded from 1973 to 1992. A total of 83 LANDSAT scenes were recorded over the location for this Cuban revolution scenario, centered on 20.12 north latitude and 076.40 west longitude.

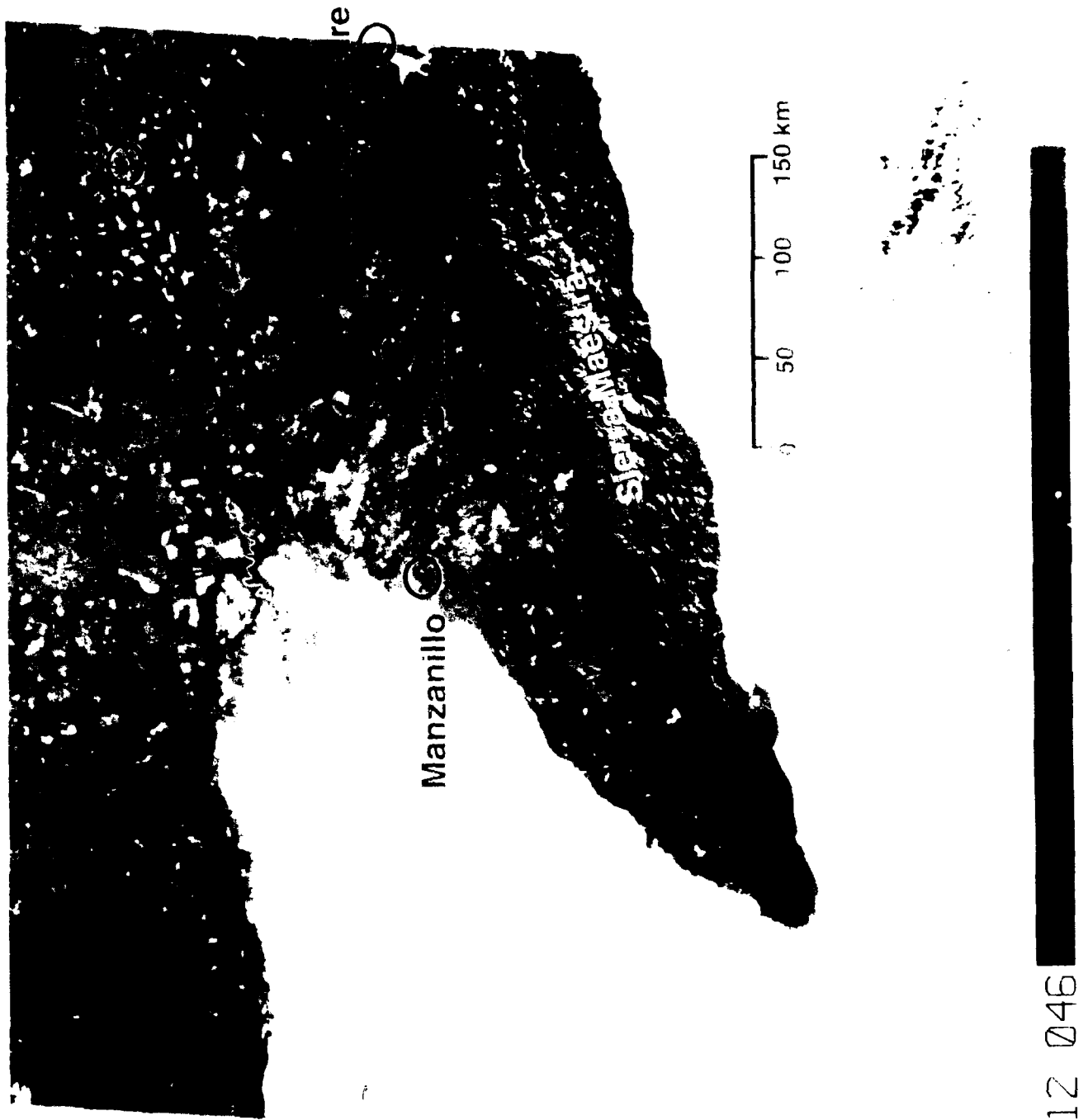
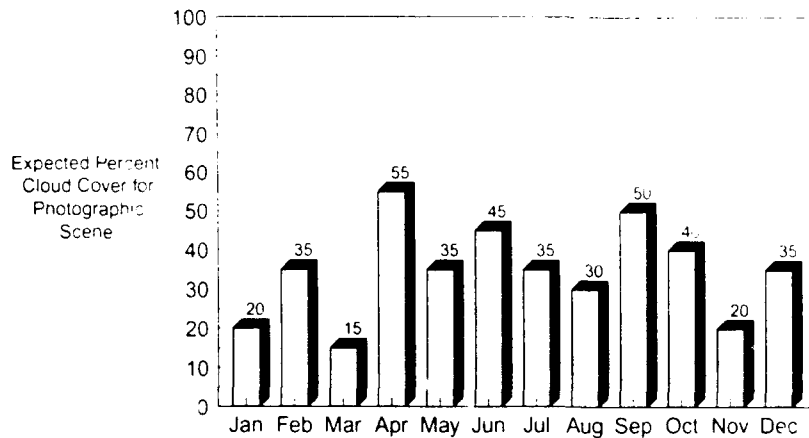


Figure 2.2.4 1. LANDSAT MSS Image of Bayamo — Manzanillo, Cuba



Source: LANDSAT scene database

Figure 2.2.4.2. Cuba Monthly Average Cloud Cover

Phase 2: Once the USMC has decided to assist the insurgents, intelligence collection would continue to focus on an exacting assessment of their needs, since a U.S. role on the ground has not been defined. The USMC advance from Guantanamo to Bayamo will be logistically supported through facilities around Guantanamo Bay. Prior to the Marine advance, numerous U.S. reconnaissance aircraft have been moved into southern Florida enabling extensive, continuous photographic coverage of the entire island of Cuba. Under these continuous monitoring conditions, any daytime efforts by Cuban Government forces to employ automated mine-laying equipment would probably be detected. The routes that U.S. forces expect to use to get to Bayamo are expected to be mined with nuisance mines. Aerial reconnaissance units based in Florida can be cued by HUMINT sources in southern Cuba. The surveillance assets will be used to establish order of battle estimates and survey the condition of roads from Guantanamo to Bayamo for the planned defense by USMC armored units. Marine forces from Guantanamo will be moved toward Bayamo by truck and by rail. Ideally, the Marine Commander at Guantanamo must evaluate the road and rail conditions from Guantanamo to Bayamo at least 8 hours prior to departure.

Phase 3: During the buildup of the USMC forces at Guantanamo Bay, reconnaissance assets will be used to monitor the condition of roads, rails, and bridges throughout the expected operating area from Guantanamo to Bayamo. The Marine Commander may decide to split his convoys at San Luis to send some armor directly north toward Holguin. Activity around airfields near Bayamo and Santiago de Cuba will be closely monitored. Throughout the advance of USMC forces, reconnaissance units will be tasked to search for evidence of minefields, air defense capabilities, missile and rocket launchers, and any camouflaged locations of Cuban Government forces. Anti-armor minefields are expected to be on the road from Bayamo to Holguin. These minefields are designed to halt the U.S. advance for an attack on U.S. forces by Cuban Government artillery units in the hills north of Bayamo.

Phase 4: During U.S. force withdrawal, defectors from the Cuban Army and local inhabitants assist with the delineation for the local clearing of nuisance mines.

Tactical Satellite Surveillance Requirements

There are four intelligence support operations for a tactical imaging satellite within the Cuban scenario. The first use of the tactical imaging satellite in the Cuban scenario is to help identify clear drop zones to airlift supplies to the anti-government forces, and later to identify safe drop zones for lightly armored units of the 82nd Airborne.

- Drop Zones to Resupply Anti-Government Forces
- Drop Zones for 82nd Airborne
- Monitoring Rail, Road, and Bridge Condition
- Locating Anti-Armor Minefields and Artillery

Drop Zones to Resupply Anti-Government Forces

In selecting drop zones for the resupply effort, the objective is to land the supplies (light arms and food) close to a road where they can be collected easily by the anti-government forces. The terrain does not have to be level, but the image scene must be large enough that the image clearly shows roadways, and the roadways can be correlated to current maps. The image resolution for qualifying drop zones is approximately 10 meters, with a search area of at least 10 km x 10 km. The satellite must be able to collect several images on each daily pass to afford the earliest image collection when cloud cover is at a minimum. The satellite lifetime requirement is very short for this site selection image collection mission.

Drop Zones for 82nd Airborne

The selection of drop zones for the lightly armored units of the 82nd Airborne is more restrictive than for the resupply operation to the anti-government forces. The drop zone will have to be flat enough, large enough, and dry enough for large aircraft to touch down momentarily. The 82nd Airborne will use a margin of safety in selecting several potential drop sites.

Monitoring Ra., Road, and Bridge Condition

Beyond the early days of the operation, other requirements for the tactical imaging satellite(s) are to provide daily coverage to supplement the photography collected by aircraft. The sensor must be available for the duration of the operation until U.S. forces have established the defensive line from Manzanillo to Holguin, which may take as long as several months. The required resolution for checking the condition of roads and bridges is approximately 2 meters, but the satellite would not be expected to provide continuous imagery coverage over the entire 250 km from Guantanamo to Bayamo. Much of that 250 km path would be covered by aerial reconnaissance units, especially UAVs. The satellite would be tasked to provide coverage over areas where reconnaissance aircraft are threatened by air defense units of the Cuban Government forces. In this "gap filler" role, the pointing accuracy of the satellite sensor optics can be matched to the accuracy of the maps used to identify features of interest, 500 meters for World Vector Shoreline maps. An acceptable search swath size would be 4 km x 4 km.

Locating Anti-Armor Minefields and Artillery

The secondary tasking for the satellite is to search for minefields and artillery near the road north of Bayamo, toward Holguin. The sensor image size requirements can probably be relaxed, since there are a limited number of good potential locations for artillery that can strike positions along the road. The availability of multiple image reflectance bands may help to identify camouflaged

units; therefore, in addition to the panchromatic signature band, some coverage from 2-4 microns would be desirable. A high resolution image would be preferred to prevent the misidentification of commercial vehicles as artillery pieces.

Table 2.2.4. TACTICAL OPERATION

Imagery Requirement	Identify Drop Zones for Resupply	Drop Zones for 82nd Airborne Forces	Rail, Road, Bridge Condition	Anti-armor Minefields and Artillery
Orbital Lifetime	7 days	14 days	120 days	180 days
Timeliness	48 hrs	24 hrs	6 hrs	6 hrs
Overflight Frequency	daily (Sun-Synchronous)	daily (Sun-S)	daily (Sun-S)	daily (Sun-S)
Signature Bands	panchromatic	panchromatic	panchromatic	panchromatic + near IR
Resolution (m)	10 m	2 m	2 m	1 m
# of Images/Pass	4 sites	4 sites	8+	6+
Image Area (km x km)	10 x 10 km	4 x 4 km	4 x 4 km	2 x 2 km
Pointing Accuracy (% of scene)	20% (1 km)	10% (400 m)	25% (500 m)	10% (200 m)

2.2.5. Philippines 1997

Abstract

In 1995, territorial and regional conflicts in Asia are grounds for a restored presence of U.S. military forces in the Philippines. After negotiations with the Philippine Government, the U.S. has resumed limited naval operations from Subic Bay and is reconstituting small-scale flight operations from the former Clark Field Air Force Base. A USMC armored brigade has been deployed to protect these poorly secured bases from guerrilla attack.

Road-to-War

Throughout the mid-1990s, tensions have increased between several neighboring southeast Asian states, many of whom are now suitably armed to stage military incursions into each other's territory to settle disputes. Vietnam and Cambodia have continued to violate each other's territory since the Vietnamese-backed Khmer Rouge Government was disbanded in Cambodia. In addition, territorial disputes between Vietnam and China have brought both sides near armed conflict several times in recent years. By 1995, the Asian nations that make up the treaty organization Association of South East Asian Nations (ASEAN) have become alarmed at the level of re-armament of Vietnam, especially since Vietnam has been operating two submarines out of Cahm Ran Bay, which can threaten shipping channels far beyond Vietnam's borders.

At the request of the ASEAN treaty organization, the U.S. Navy and Air Force have been invited back into the Philippines with the full backing of the Philippine Government. The U.S. Navy has resumed small-scale operational patrols from Subic Bay, and a limited number of U.S. Air Force reconnaissance aircraft have set up operations at Clark Field. The hastily organized re-establishments, at both Subic and Clark are protected by a USMC armored brigade which was deployed from Camp Pendleton. The primary role of the USMC brigade is to provide security and defense against the Philippine guerrilla movement which has become more powerful after the U.S. left the bases in 1992, especially since the Philippine economy has not enjoyed the growth seen in so many other Southeast Asian nations throughout the past decade.

The guerrilla movement is poorly funded, but has been able to establish highly mobile and well camouflaged artillery positions in the hills around Subic and Clark. The USMC brigade is aware that the guerrillas can set up minefields in the swampy areas cutting off the reconnaissance units of Clark from the more heavily protected Naval Base at Subic Bay. In addition, the guerrillas have a limited supply of modern scatterable mines for use along the road from Subic to Clark.

Philippines 1997 Terrain Features

The area of concern for this scenario is the area immediately surrounding Subic Naval Base (Olongapo) and the area in the vicinity of Clark Air Base (Angeles) (see Figure 2.2.5.1). The primary concern is ensuring the roads between Subic Naval Base and Clark are protected and kept free of mines. There was an airfield maintained by the U.S. Navy at Subic Bay.

Olongapo is a city of over 50,000 population, located at the northern end of the Bataan peninsula in Subic Bay, which meets the South China Sea. Clark Field is approximately 80 km northeast of Subic Bay and 110 km north of Manila.

The Marines going from Subic Bay to Clark can follow Route 7 going west to the town of Dinalpihan, a distance of 25 km. The road follows a 500 foot elevation valley and is surrounded by mountains with peaks of 4,000-5,000 feet. There is one 8,209 foot peak just north of the highway. For the first 15 km the road goes through scrub woods and brush to the town of Culo. From Culo to Dinalpihan, the road goes through a series of small villages with populations of 3,000 or fewer.

At Dinalpihan there are a number of alternate ways to go north to Clark. The roads are all secondary roads and pass through small villages. The landscape consists primarily of rice paddy farms and is very low and swampy with primary drainage through Manila Bay.

To the east of Clark, the country is densely populated, primarily small villages with populations of fewer than 3,000. To the west of Clark is an imposing range of mountains dominated by Mount Pinatubo (8 km west), a 1,745 meter elevation active volcano. The eruption of Mount Pinatubo was the primary reason that the U.S. abandoned Clark Airbase. The vegetation in the vicinity of Clark Field is primarily tropical grassland. The nearest town is Angeles, approximately 7 km southeast of Clark Field.

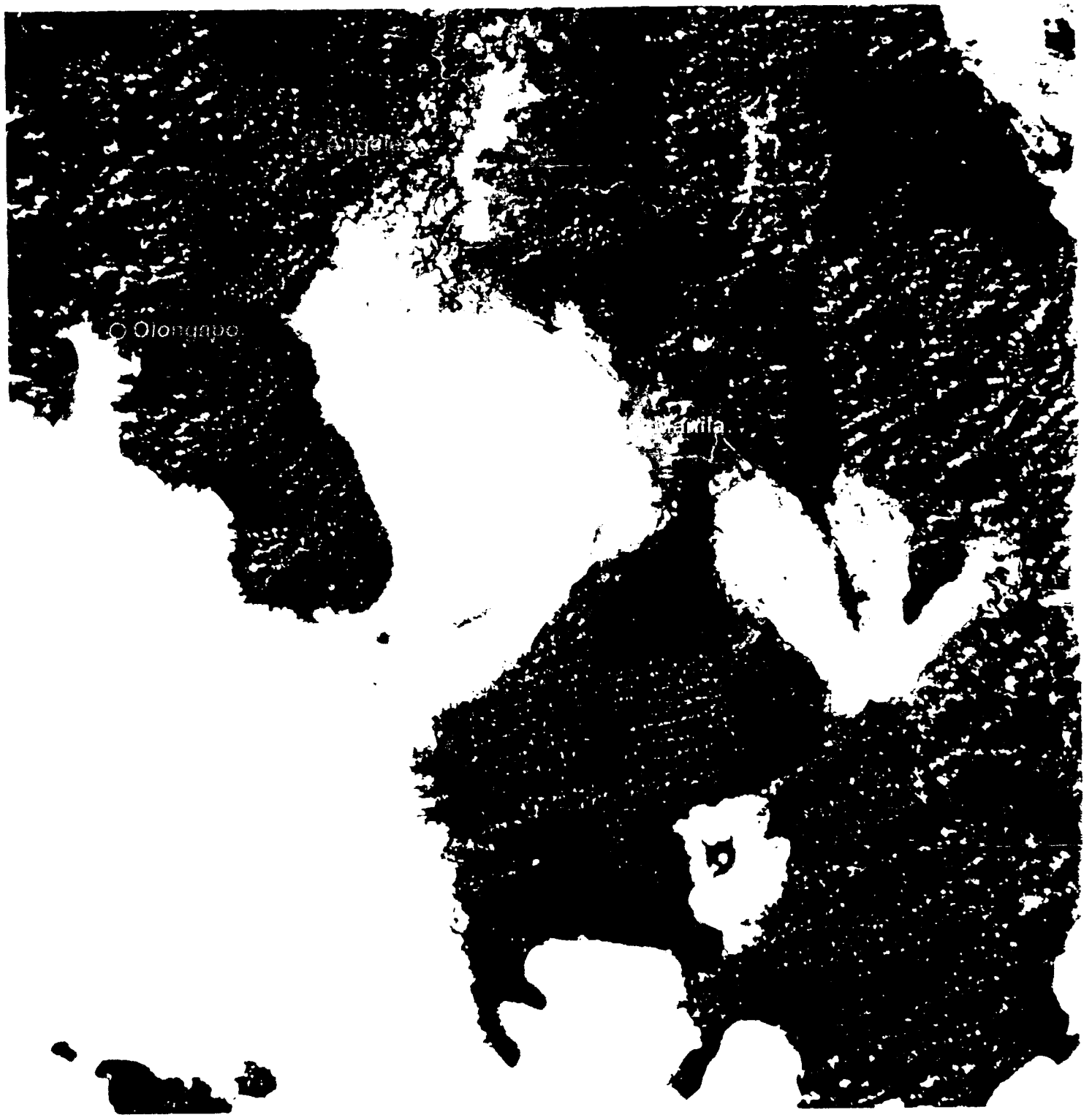


Figure 2.2.1. LANDSAT MSS Image of Olongapo - Philippines

Phases of the Battle

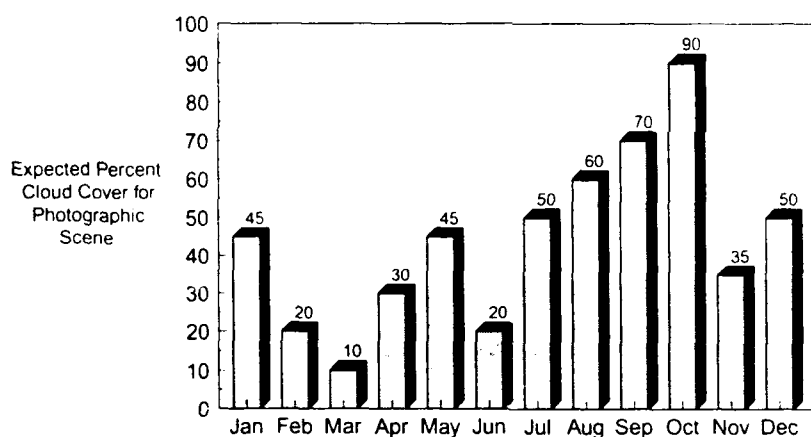
The Philippines 1997 scenario can be divided into two phases: the first phase is prior to the U.S. landing and re-establishment of Subic Bay Naval operations, and the second phase is maintaining control over the road from Subic to Clark.

Phase 1: Preparation for operations from Subic and Clark Field

Phase 2: Maintaining lines of communication from Subic to Clark Field

Phase 1: U.S. advisors and other pre-positioned units would be on the ground weeks or months before Subic or Clark could be re-opened for U.S. operations. These early forces would include reconnaissance units to assess the threat against the planned U.S. operations at Subic and Clark. The expected resistance of guerrilla forces gives mine detecting and clearing a high priority. Ground forces can be assisted by aerial reconnaissance that can operate safely, since the guerrillas have no means to threaten high altitude aircraft.

Figure 2.2.5.2 shows cloud cover as a percentage of total scene, for a series of LANDSAT scenes recorded from 1972 to 1992. A total of 36 LANDSAT scenes were recorded over the location for this Philippines 1997 scenario, centered on 14.50 north latitude and 120.20 east longitude.



Source: LANDSAT scene database

Figure 2.2.5.2. Philippines Monthly Average Cloud Cover

Phase 2: Since the guerrilla forces would be primarily interested in attrition of U.S. forces and morale, they would utilize nuisance and scatterable type mines, rather than laying extensive anti-armor minefields to slow the advance of U.S. forces.

Tactical Satellite Surveillance Requirements

There are two primary intelligence support operations in the Philippines scenario:

- Minefield Detection
- Monitor Road Condition between Clark and Subic Bay

Minefield Detection

As previously stated, no mechanically emplaced minelayers are expected during this scenario, but small scatterable and nuisance mines are expected.

Monitor Roads between Clark and Subic

This scenario is unique since the U.S. forces have a significant advantage on the ground from the start of hostilities and will have many HUMINT sources to help cue photographic sensors. The highway monitoring operation will therefore be limited to taking daily photographs of sections that are not easily accessible by observers on the ground.

Table 2.2.5. TACTICAL OPERATION

Imagery Requirement	Minefield Detection	Roadway Monitoring
Orbital Lifetime	180 days	180 days
Timeliness	8 hrs	6 hrs
Overflight Frequency	daily	daily
Signature Bands	panchromatic	panchromatic
Resolution (m)	< 1 m	2 m
# of Images/Pass	4 images	10+
Image Area (km x km)	1 x 1 km	10 x 10 km
Pointing Accuracy (% of scene)	10% (100 m)	20% (2000 m)

3. OPTICAL TESTS FOR MINEFIELD DETECTION

As part of the Phase 2 SBIR study, The Futures Group has subcontracted with several organizations to collect reflectance data over simulated minefields. Hughes Santa Barbara Research Center (SBRC) collected hyperspectral reflectance data over the simulated minefield on the Marine Corps Training Base at Twentynine Palms, California. The hyperspectral reflectance data collection corp training experiment is designed to simulate a single daily overpass of a lightweight imaging satellite. The University of Arizona conducted a minefield aging experiment on a simulated minefield at its Optical Sciences Center building in Tucson, Arizona.

3.1 Background

Hughes Santa Barbara Research Center

On December 21, 1992, at the Twentynine Palms test site, a hyperspectral imaging sensor built by SBRC was flown over the simulated minefield (Ostrich site). The SBRC reflectance measurement instrument is called a Wedge Imaging Spectrometer (WIS), and though it is based on a focal plane array, it was operated as a pushbroom sensor over the Ostrich site covering the .4-1.0 micron band. The WIS design employs a tapered filter material deposit to divide the .4-1.0 band into 64 discrete spectral channels, each channel spaced 10 nanometers apart. Figure 3.1.1 shows the WIS design.

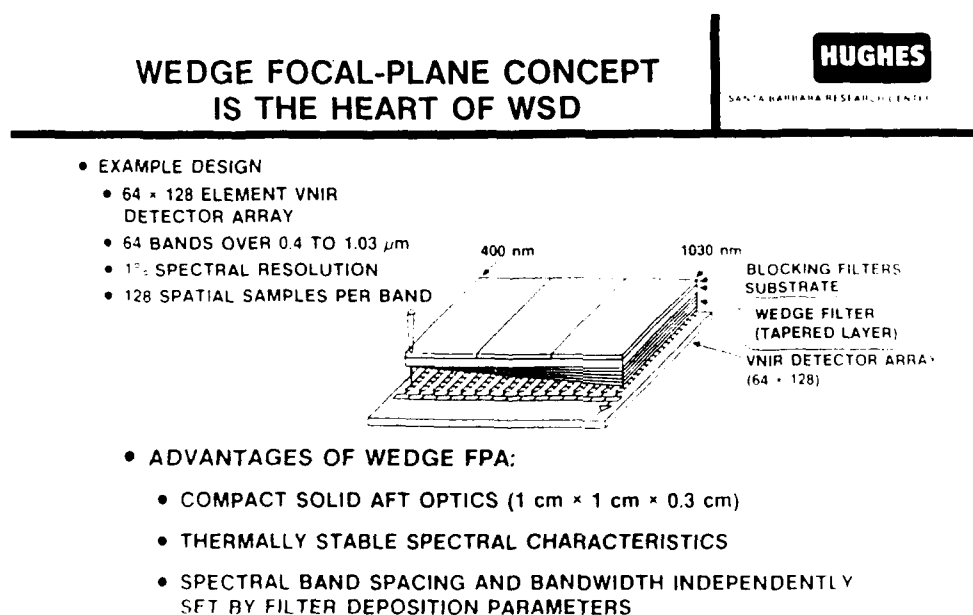


Figure 3.1.1. WIS Design

The lens used was a 35 mm focal length custom triplet. The WIS digital data output is 16 bits per word with 11 bits active, uncalibrated and recorded on 9-track tape. The data as recorded must be manipulated to convert to either a band-sequential (BSQ) format or band interleaved by line (BIL) format.

In the minefield overflight experiment, the WIS is mounted inside a Saberliner 40 jet aircraft, with the optics mounted over an open hatch. The aircraft altitude and flight speed are chosen to simulate a 1/2 meter ground-based resolution and to collect properly registered image data over all 64 bands. In addition to the project Ostrich data, the WIS was also flown over Cleghorn Pass.

University of Arizona Optical Sciences Center (OSC)

The University of Arizona was contracted to take measurements of simulated minefield signatures at the Ostrich site and on University of Arizona property in Tucson, Arizona. The measurement program for the project Ostrich site was hampered by logistical and equipment problems. As a result, the University of Arizona was unable to collect reflectance signature data at Twentynine Palms. A separate signature measurement program was undertaken in the desert at Tucson on University property near the OSC. The Tucson tests were designed as a minefield "aging study" to measure changes in the reflectance of recently turned soil over time. The objective was to determine if recently overturned soil has different reflectance properties than undisturbed soil. The Tucson test plan follows:

- Construct a trench (simulated minelaying) in undisturbed soil
- Place a thermal surrogate mine 6-10 inches beneath the soil
- Immediately rebury the trench with overturned soil
- Measure soil reflectance as function of time-of-day
- Take measurements over a period of time (several weeks)

3.2 Optical Signature Measurements (Twentynine Palms)

Ground truth reflectance measurements were taken on the ground at the Ostrich site in December 1992. The minefield site included both buried and surface mines in furrows over 100 meters in length. The Ostrich site layout is shown in Figure 3.2.1.

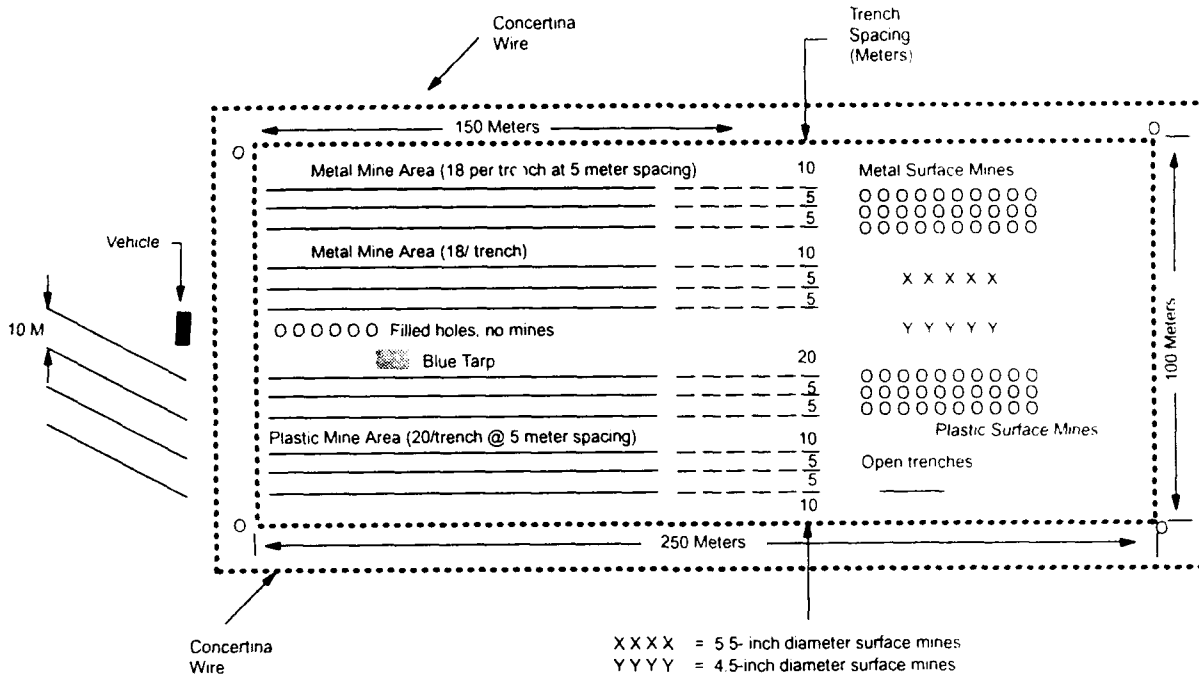


Figure 3.2.1. Ostrich Site Minefield Layout

The simulated minefield contains thermal surrogate mines, both plastic and metal varieties, as shown in the figure. The minefield was modified with a fresh trench and marked for this experiment prior to the data collection flights. A fresh trench was constructed inside the minefield area, using a leased "ditch witch" machine. The trench consists of two 10 meter perpendicular sections, which meet to form a "T", about 10 meters inside the minefield. A blue tarpaulin was placed within the minefield as a marker and source for ground truth reflectance measurements.

The U.S. Army Corps of Engineers used a radiometer manufactured by Environmental Research Corporation to record ground truth reflectance data at the Ostrich site. The radiometer instrument is sensitive between 350 and 2,500 nm wavelength and reads radiance directly. The ground truth measurements taken over the Ostrich site are shown in Figure 3.2.2.

Twentynine Palms, CA

21-Dec-92

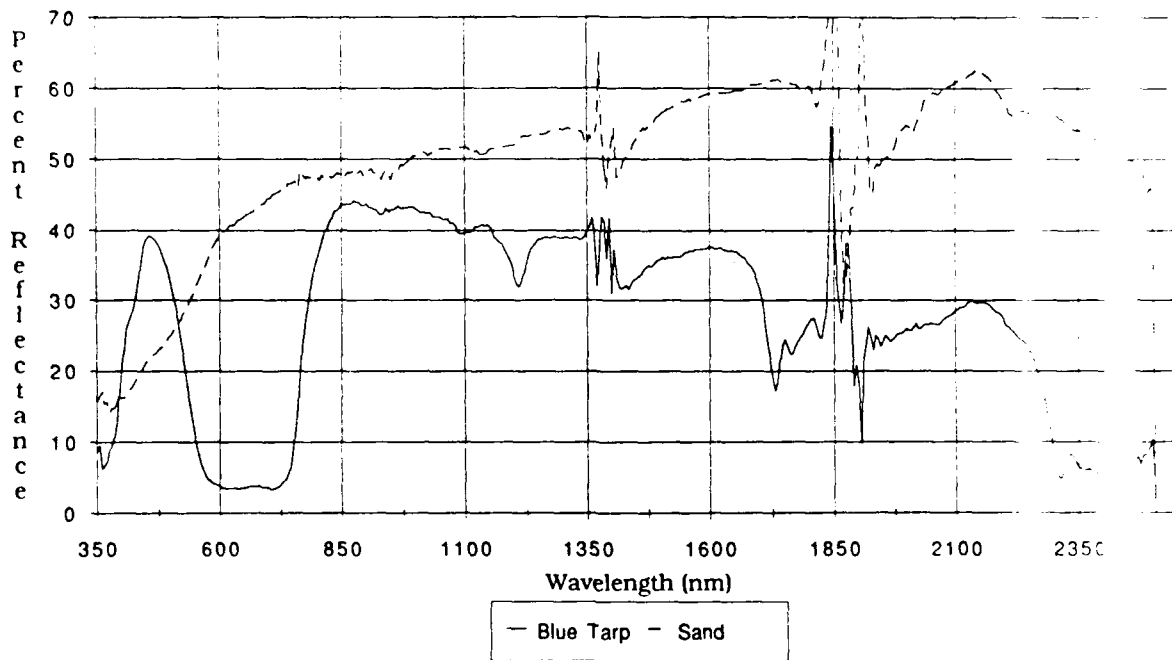


Figure 3.2.2. Ostrich Site Ground Truth Measurements

Other types of measurements were attempted but a series of unfortunate and unforeseen events including equipment failure and relentless rain (unusual for the Twentynine Palms area) conspired to reduce the comprehensiveness of the measurement program on the ground.

3.3 Aircraft Validation

The Hughes WIS sensor was flown over the Ostrich site to validate measurements taken on the ground. In Figures 3.3.1.a and 3.3.1.b, several bands of WIS image data have been converted into 8-bit tagged image file format (TIFF)-formatted files to demonstrate the reflectance differences for these sample bands. Prominent features such as the vehicles can clearly be seen across every band, while the blue tarp can be seen best against the contrasting desert sand in the bands where the tarp absorbs reflected sunlight but the surrounding desert is strongly reflective. Figure 3.3.2 shows the flight path of the Hughes Saberliner with the WIS spectrometer over the minefield at the Ostrich site. The dashed line shows the approximate area of the minefield covered by the WIS images. Several bands of WIS image data are shown for comparison.

On an additional flight, WIS data were recorded over Cleghorn Pass, California. Some of the Cleghorn Pass images are shown in Figure 3.3.3.

Hughes Wedge Imaging Spectrometer
Twentynine Palms, Ca. December 1992

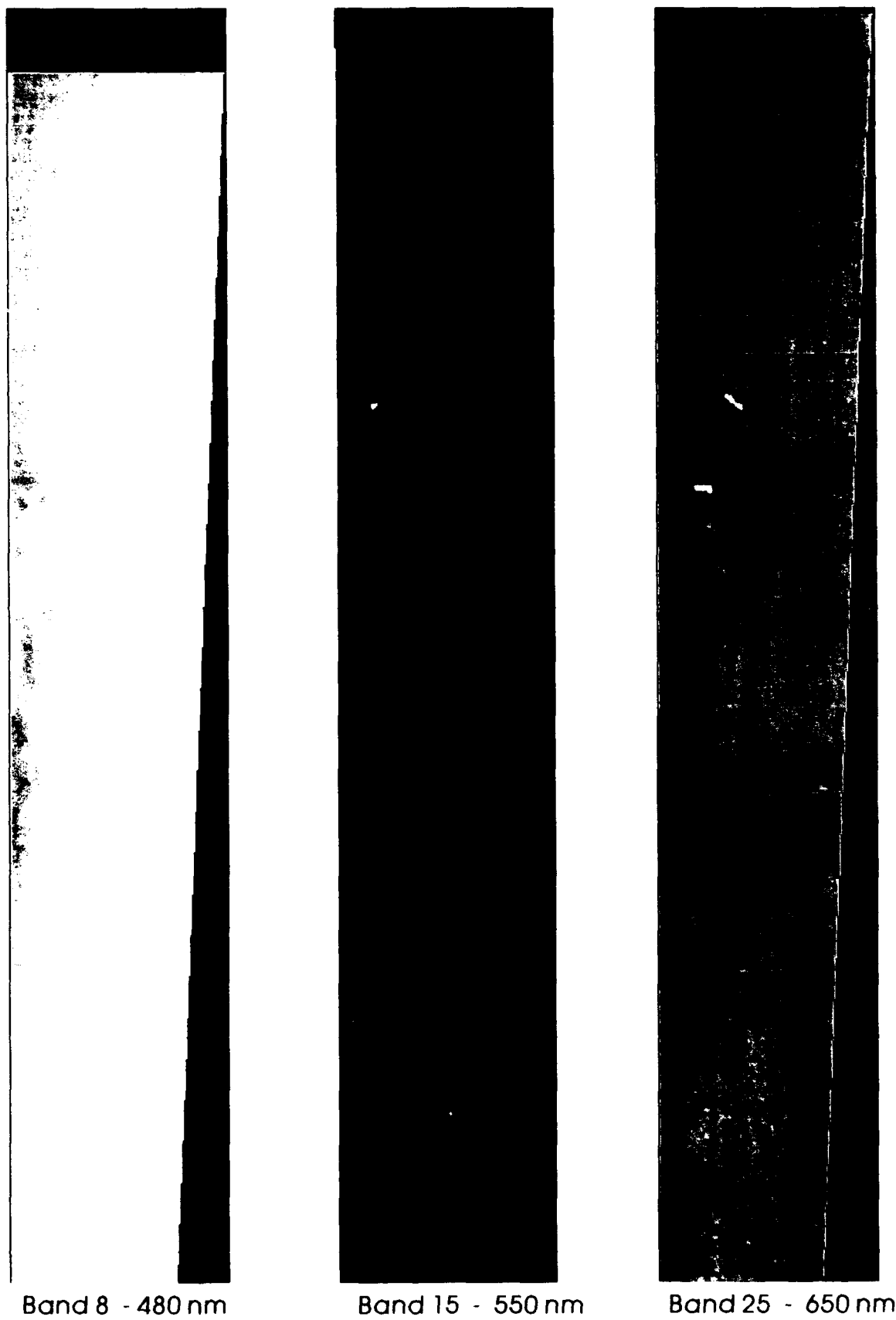
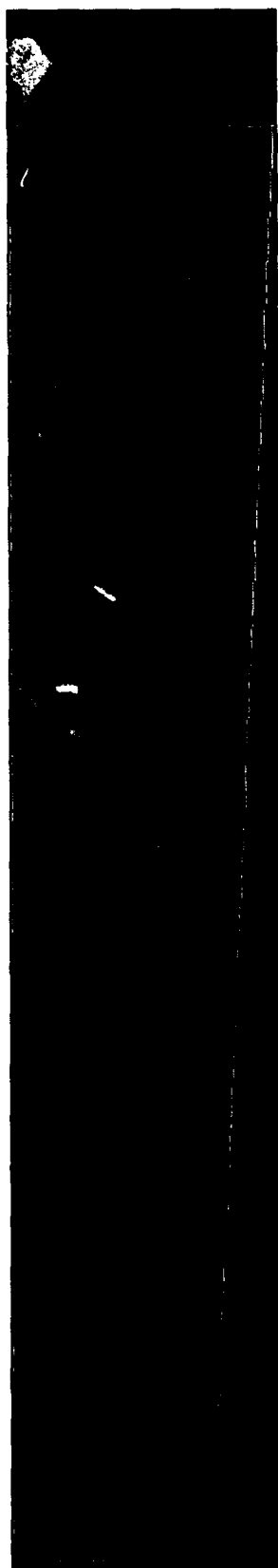
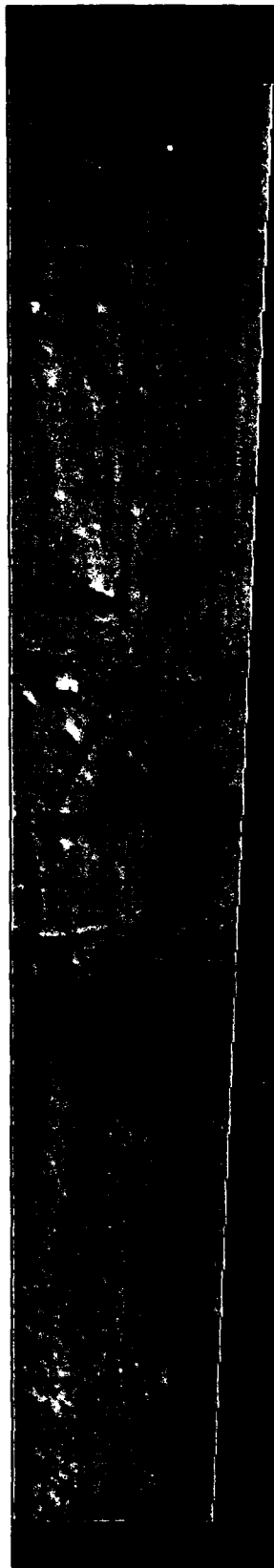


Figure 3.3.1.a. Project Ostrich Site: Reflectance Data

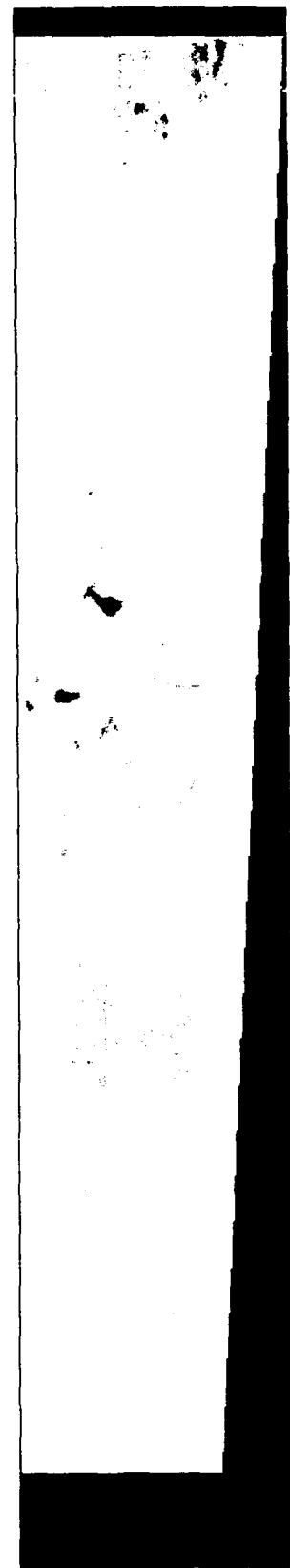
Hughes Wedge Imaging Spectrometer
Twentynine Palms, Ca. December 1992



Band 35 - 750 nm



Band 45 - 850 nm

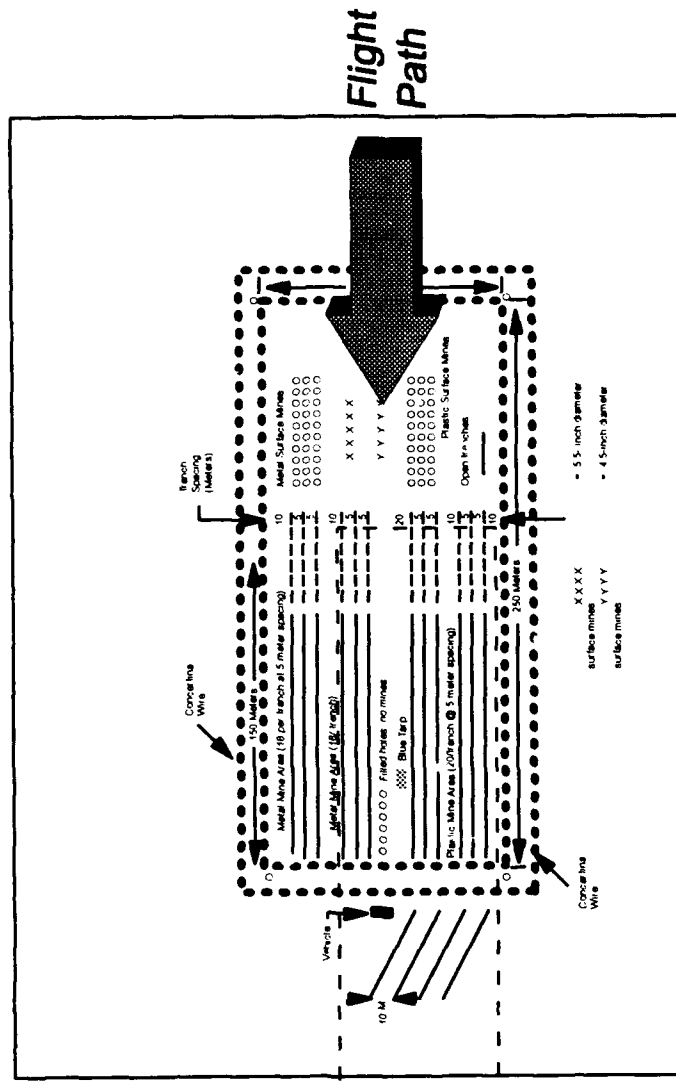


Band 58 - 980 nm

Figure 3.3.1.b. Project Ostrich Site: Reflectance Data

Project Ostrich Site: Reflectance Data
 Twentynine Palms, CA December 1992
 (Hughes Wedge Imaging Spectrometer)

Ostrich Site



Band 8 480 nm



Band 15 550 nm



Band 25 650 nm



Band 35 750 nm



Band 45 850 nm

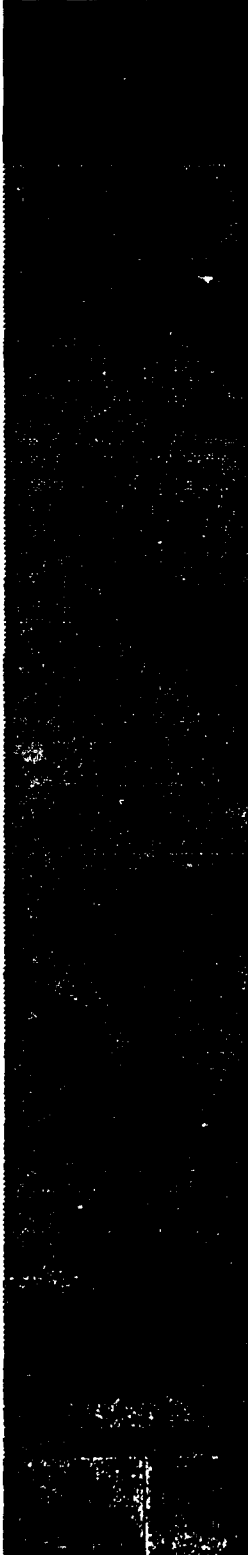


Band 58 980 nm

Figure 3.3.2. WIS Spectrometer Overflight Path

Wedge Imaging Spectrometer

Band 15



Band 25



Band 35



Band 45



Figure 3.3.3 Cleghern Pass Reflectance Data

Quick Look Analysis

The Futures Group has completed a basic examination of the Hughes WIS data for evidence that the WIS hyperspectral image can assist with the detection and delineation of minefields. Three operations (subtraction, division and spectral analysis) have been performed on a portion of the WIS data using an IBM PC computer. Processed data is shown as images with 16 shades of grey for dynamic range. When the data values for an image are read into the computer, the maximum value for an image is assigned the color white and the minimum is assigned black; other values are assigned an appropriate shade of grey. In the images shown, there is a label called "DataCutoff" below the individual greyscale images. The DataCutoff is an indication of the dynamic range of the resultant subtraction or division operation. The original data reflectance values in each band typically range from 0 (black) to around 1,400 (white). After an operation on two bands of data, the resultant image data (the subtracted or ratio image) is rescaled between black and white with every feature above the DataCutoff assigned the color white.

Subtraction operations produce an image that is the absolute value of the difference of two selected bands. Division operations (band ratios) are the ratio of two selected bands, expanded across the 16 grey shade dynamic range of the PC graphics card.

Band Subtraction (Narrowband)

Figure 3.3.4 shows the result of a set of narrowband subtraction operations performed on the WIS data recorded at the Ostrich site. The subtraction algorithm is a simple absolute value operation: $ABS(\text{band A} - \text{band B})$, equalized across 16 grey shades. Band number 32 was selected as band A, with three different bands selected as band B. The top image in Figure 3.3.4 shows (band 32 - band 35), the middle image is (band 32 - band 38), and the lower image is (band 32 - band 41). The blue tarp can be clearly seen in the lower image, indicating that the tarp reflectance differs strongly in these two bands.

Band Subtraction (20-48)

In Figure 3.3.5 showing bands 20 and 48, the jeep can be clearly seen as a white object in the upper left corner of both images. There is another prominent white feature in both band 20 and band 48 images — a line about the same length as the jeep but lower and further to the right. This may be strong reflectance from a backhoe or "cherry picker" vehicle that was in the minefield during some of the flights. The lower image (band 20 - band 48) clearly shows that the reflectance of the tarp differs between these bands, but other features (jeep, backhoe) differ less since these features appear to have reduced signatures in the subtracted image.

Band Ratios

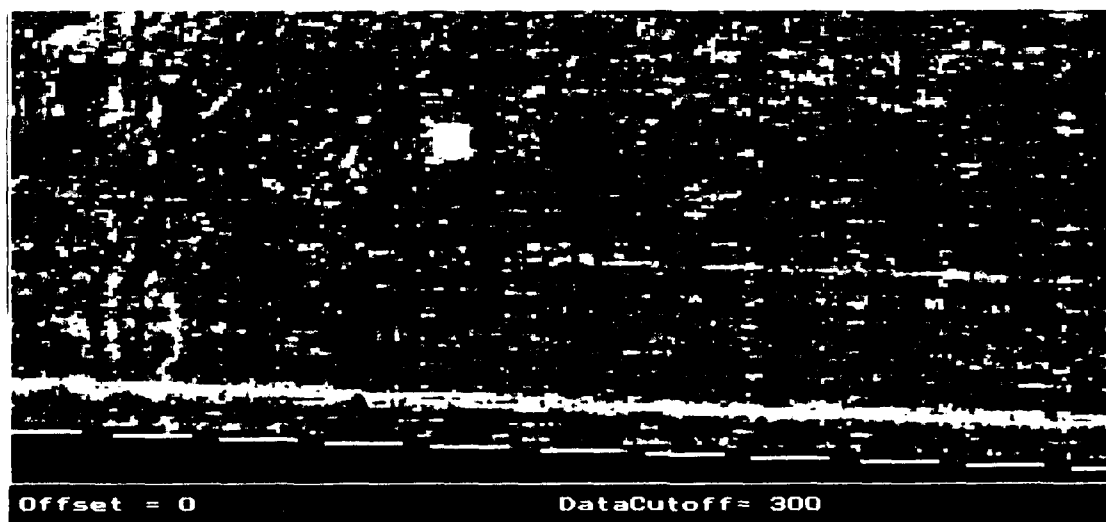
The band ratios are shown in Figure 3.3.6 for bands 18/32, 18/42, 18/52, and 18/62. The ratio dynamic range is small as shown by the DataCutoff value of 100 for these images. Features such as the tarp, jeep and the hill can be seen in the ratio images.



BAND SUBTRACTION
 Band 32-35

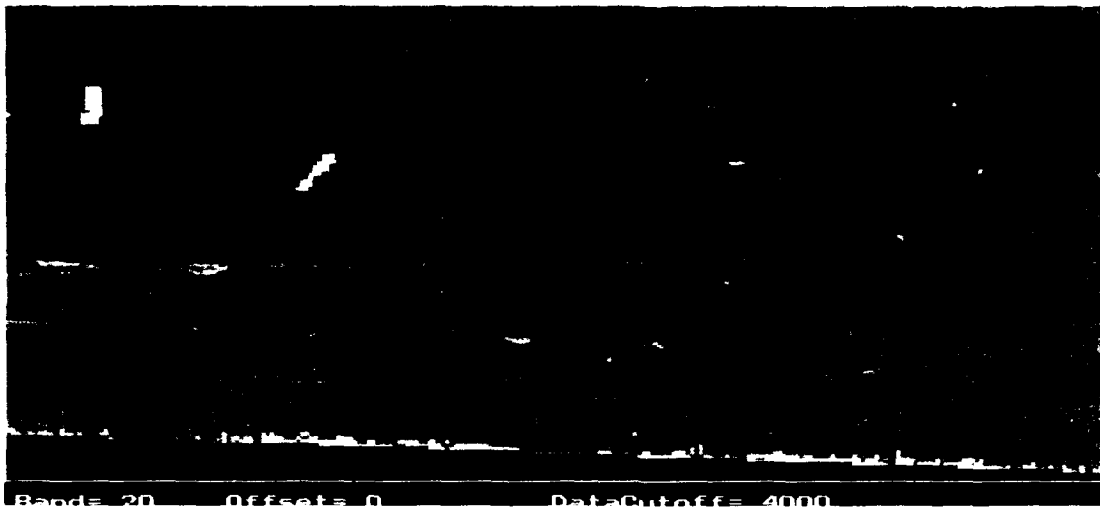


BAND SUBTRACTION
 Band 32-38



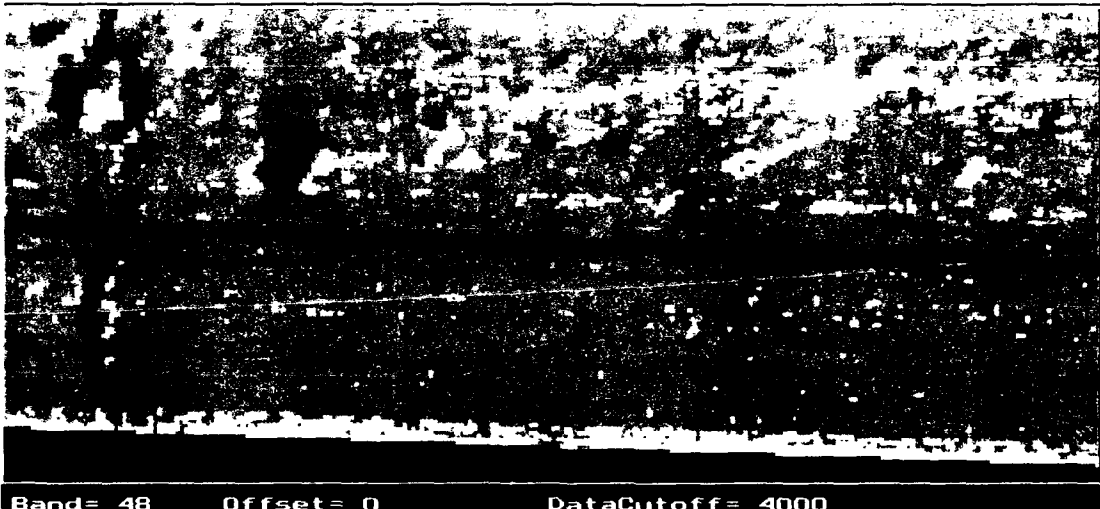
BAND SUBTRACTION
 Band 32-41

Figure 3.3.1. Narrowband Subtraction Operation for WIS Data



Band= 20 Offset= 0 DataCutoff= 4000

Band 20



Band= 48 Offset= 0 DataCutoff= 4000

Band 48



Figure 3.3.5. Wideband Subtraction Operations on WIS Data

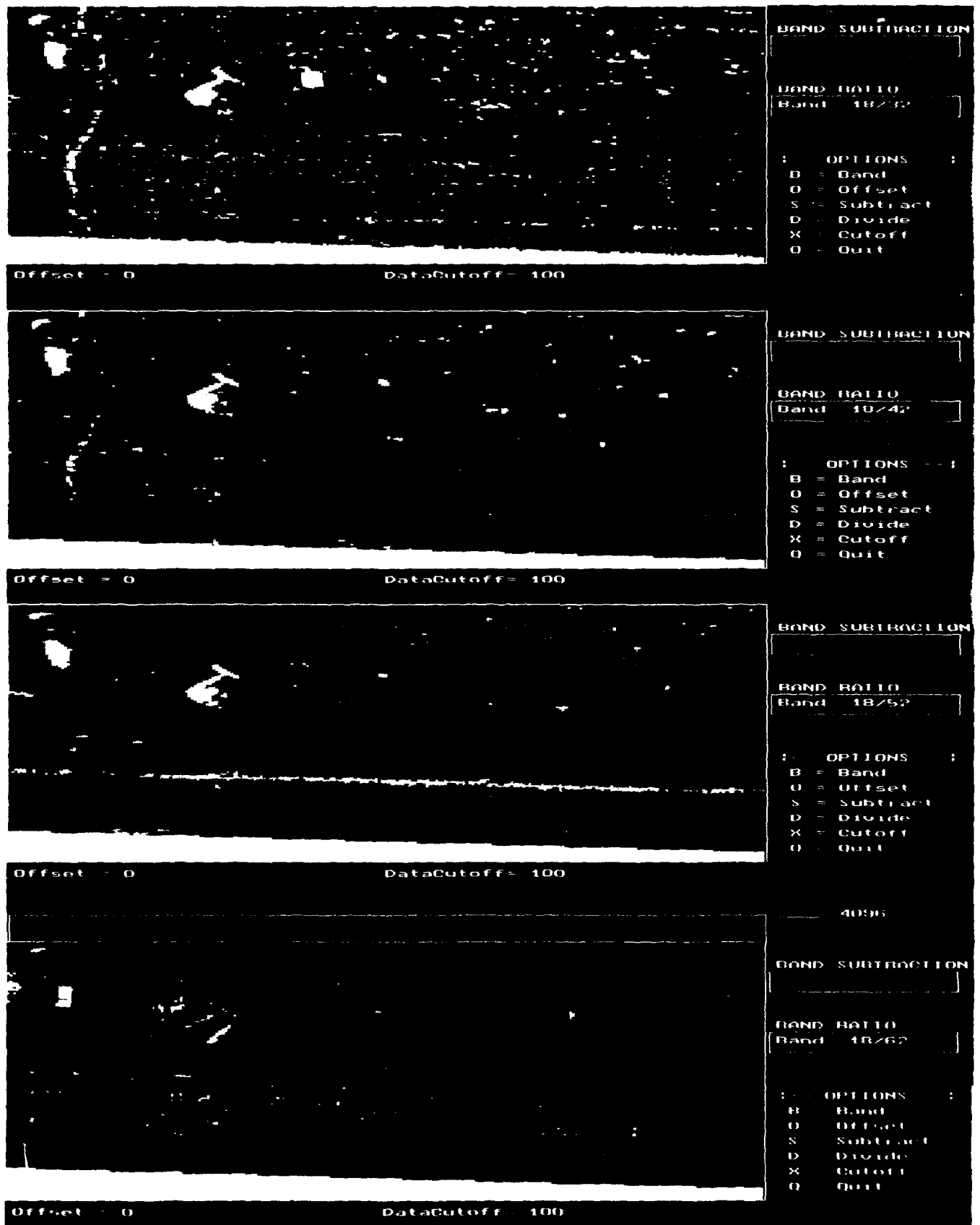


Figure 3.3.6 Band Ratios Operation on WIS Data

Feature Spectrum Analysis

The goal of the feature spectrum analysis is to identify features on the ground that exhibit changes in reflectance across the 64 bands. A simple method to detect features of the image data that have different reflectance in different bands is to compare data from a set of pixels that intersect a feature and are common to every band. A line of pixels is selected that crosses over a ground feature of interest, and the same line of pixels is plotted for every band. This feature extraction algorithm works as follows:

- Pick a feature to extract (tarp, jeep, etc.)
- Draw a focus line over the feature
- For image band = 1 to 64 DO
 - Retrieve every pixel in the image band that intersects the focus line
- Display the line of pixels for every band as a continuous image

The resultant focus-line display is 3-dimensional: the horizontal dimension is the WIS band number; the vertical dimension can be called pixel index number; and the third dimension is color, which is a translation of the 11-bit WIS data into 16 shades of grey for the computer. The accompanying feature spectrum images shows several features as they change reflectance over the 64 bands.

Feature Spectrum (Tarp and Jeep)

In the top image of Figure 3.3.7, the feature of interest is the blue tarp. A white line drawn across the tarp identifies the pixels that will be included in the resulting feature spectrum shown to the right of the image. The reflectance differences by band for the blue tarp can be seen clearly in the feature spectrum. The tarp absorbs strongly between bands 17 and 39. The tarp is not seen in bands less than 16 or greater than 41. This result agrees with the ground truth reflectance data supplied by United States Army Topographic Engineering Center (USATEC) for the blue tarp.

A similar operation on the jeep also shows a lack of contrast in the lower bands (1-14) and the high bands (58-64). The pixels of the jeep windshield can be clearly seen in the feature spectrum as dark pixels.

Figure 3.3.8 shows the correlation between WIS band number, true color, and the ground truth reflectance data supplied by the Army for the tarp and desert at the Ostrich site. The blue tarp is detectable from bands 17 through 39 because of strong absorption between 550-750 nm.

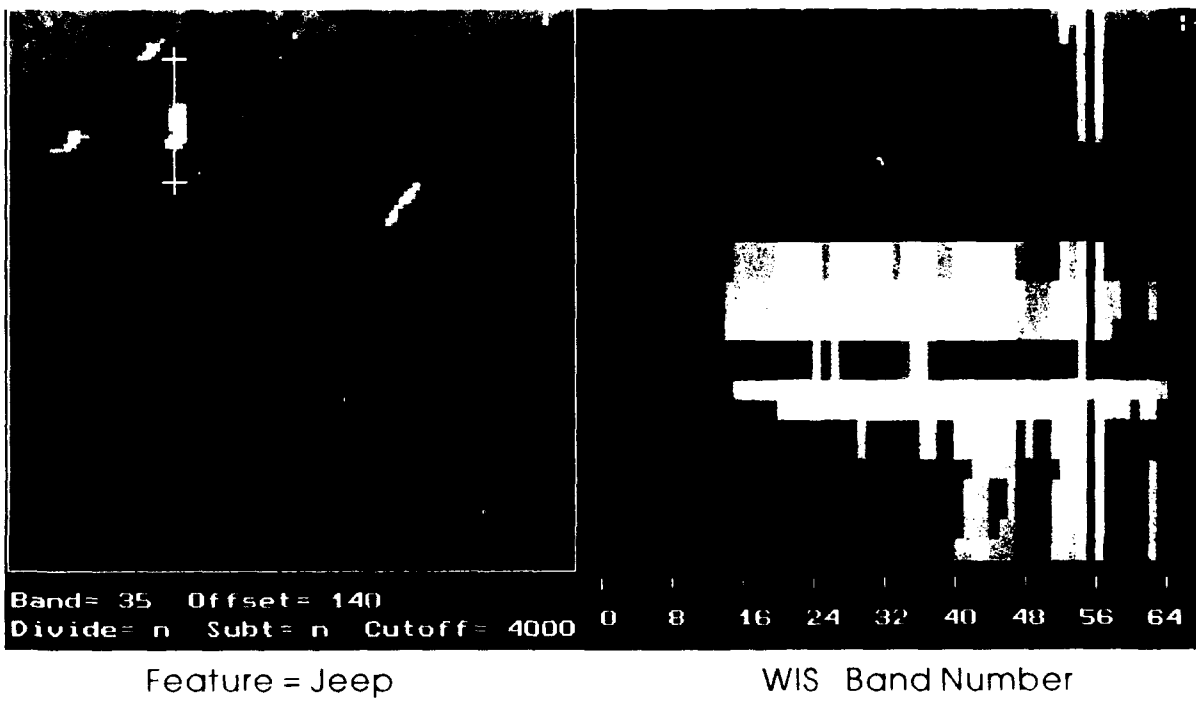
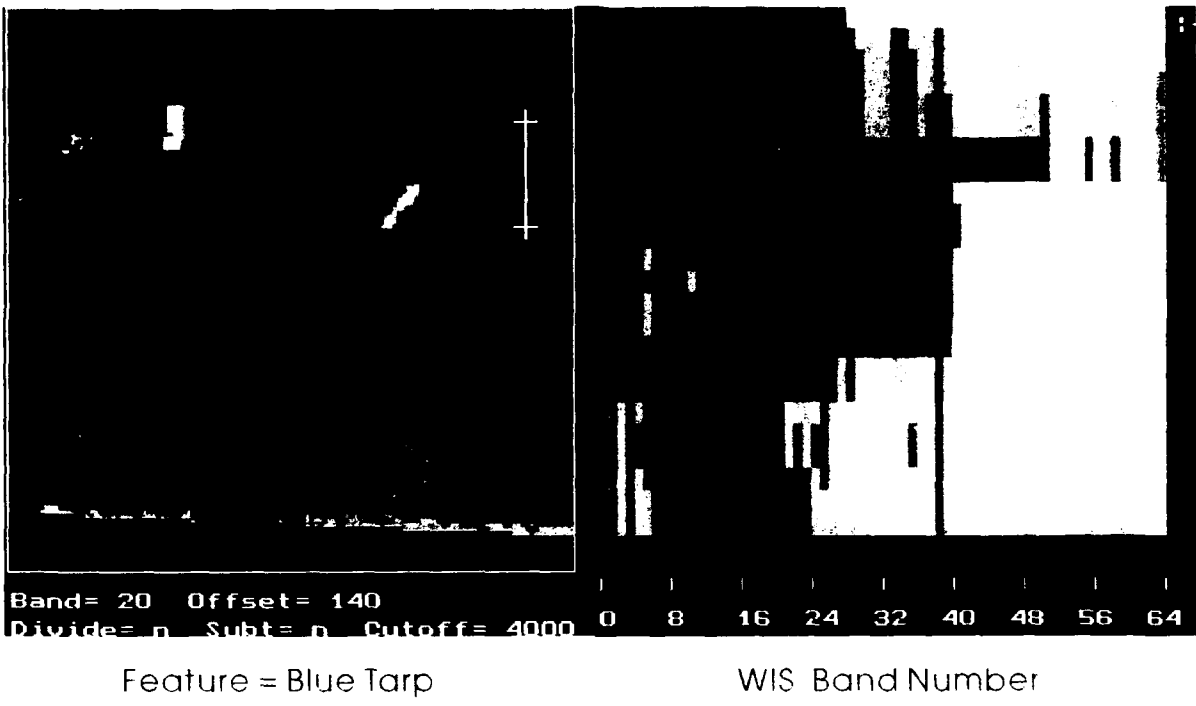


Figure 3.3.7. Feature Spectrum (Tarp and Jeep)

(Twentynine Palms Dec. 1992)

Source: U.S. Army Topographic Engineering Center.

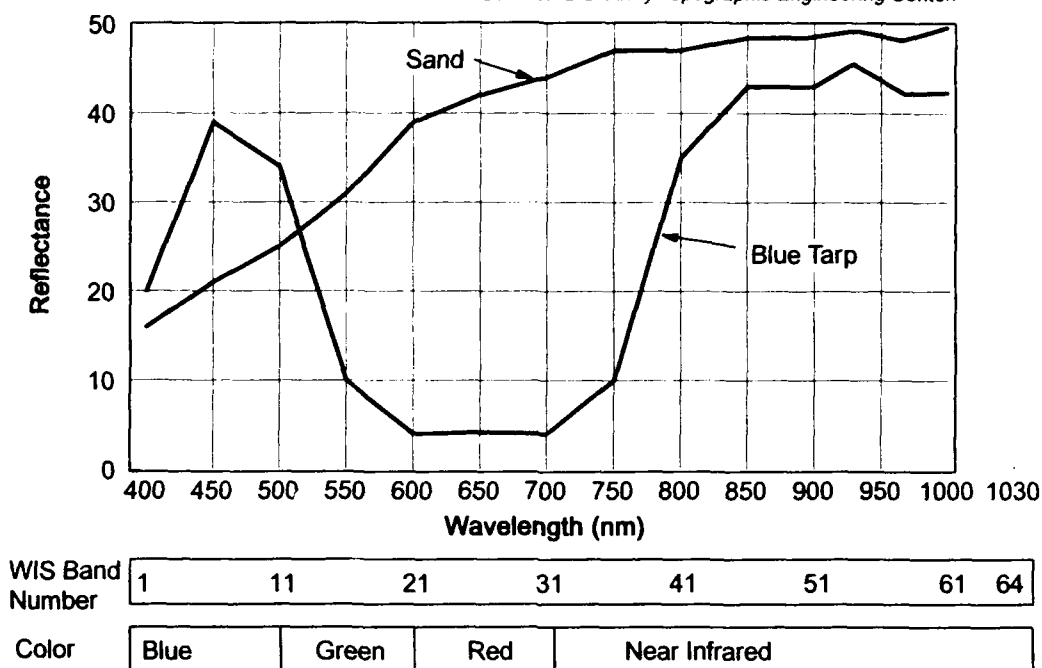
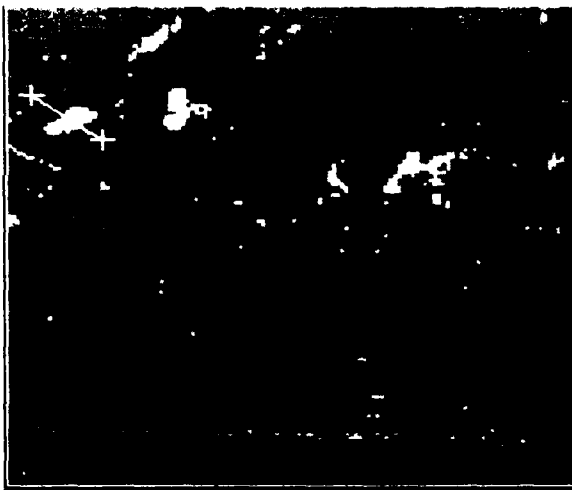


Figure 3.3.8. Ground Truth Reflectance Data

Feature Spectrum (Hill and Trench)

In the top image (band 40) of Figure 3.3.9 a line is drawn across a high reflectance feature that may be a hill or a bush. The resultant feature spectrum shows high reflectance from band 26 up to 63, with changing character throughout the spectral range.

The middle image (band 46) shows the changing reflectance across one of the open trenches that are just outside the minefield. The feature spectrum shows the trench across most bands, especially the higher bands. It is not possible to determine what aspect of the trench signature causes it to be seen in these images. The apparent trench signature may be due to shadows or preferential debris collection or other unknown characteristics. The signature is probably not due to preferential plant growth because the trenches were recently made.



Band= 40 Offset= 140
Divide= n Subt= n Cutoff= 4000

Feature = Hill or Bush?



0 8 16 24 32 40 48 56 64

WIS Band Number



Band= 46 Offset= 200
Divide= n Subt= n Cutoff= 4000

Feature = Across Open Trench



0 8 16 24 32 40 48 56 64

WIS Band Number



Band= 46 Offset= 200
Divide= n Subt= n Cutoff= 4000

Feature = Inside Open Trench



0 8 16 24 32 40 48 56 64

WIS Band Number

Figure 3-39 Feature Spectrum (Hill and Trench)

The lower image (band 46) shows the changes in reflectance along what may be the interior of the trench. The reflectance of the trench interior does not appear to change much as a function of band.

3.4 Minefield Aging Study (University of Arizona)

The University of Arizona minefield aging study was carried out during October, November and December of 1993. Measurements were taken from the roof of the OSC with a Plumbicon camera focused onto a section of desert below. The experimental setup is shown in Figure 3.4.1 and includes a curve showing the Plumbicon detector sensitivity. The complete University of Arizona Report is attached as Appendix B.

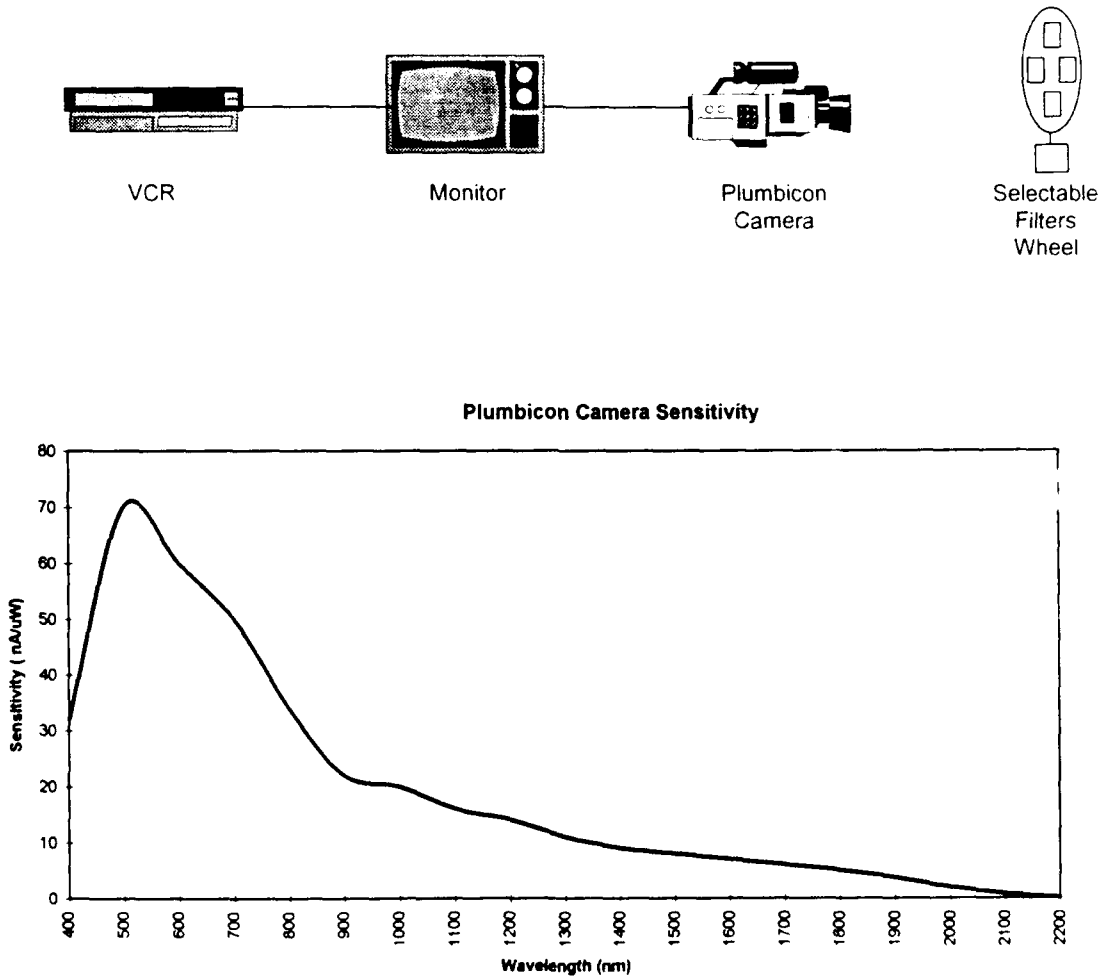


Figure 3.4.1. Arizona Test Setup and Camera Response

The camera tube spectral response bandwidth is from 400 nm to 1,900 nm, with a strong taper off beyond about 1,800 nm. All reflectance data was recorded onto VHS format videotape. Three filters were used during the tests to limit the bandwidth of the measured reflectance: the filter bandpass values are:

- Filter #1: 1,600-1,700 nm
- Filter #2: 900-1,200 nm
- Filter #3: 1,800+ nm (long pass)

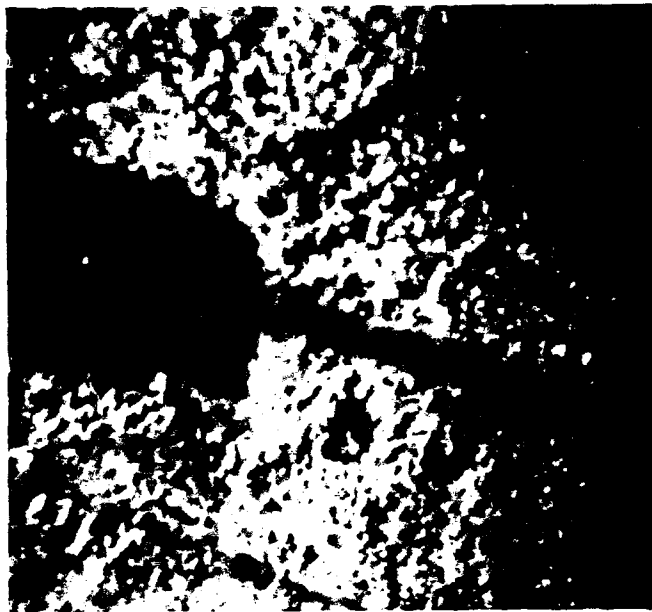
The results of the minefield aging reflectance measurements are shown on the following pages. The tests are inconclusive, due to equipment and climate effects. The camera gain and focus had been adjusted between subsequent measurements throughout the tests, and these gain adjustments preclude any meaningful reflectance comparisons from one measurement day to another. However, relative reflectance changes within an image can be indicative of signature changes over time. In any particular image, the reflectance differences between trenched and untrenched areas can be examined for changes over time. The images on the next pages show selected reflectance measurements of the trenched area over time and with the three filters. The images were obtained by capturing select images from the videotape using a *Data Translations* frame grabber board. The frame grabbed images were converted into TIFF format and imported into *CorelDraw* for manipulation and labeling.

Figure 3.4.2 shows a set of Plumbicon reflectance measurements taken on October 29, 1993. The four images show the tube response without a filter, and with filters #1, #2 and #3. The Plumbicon response with the third filter is negligible since the filter effectively cuts off all energy below 1,800 nm which is where the tube sensitivity drops off (see Figure 3.4.1).

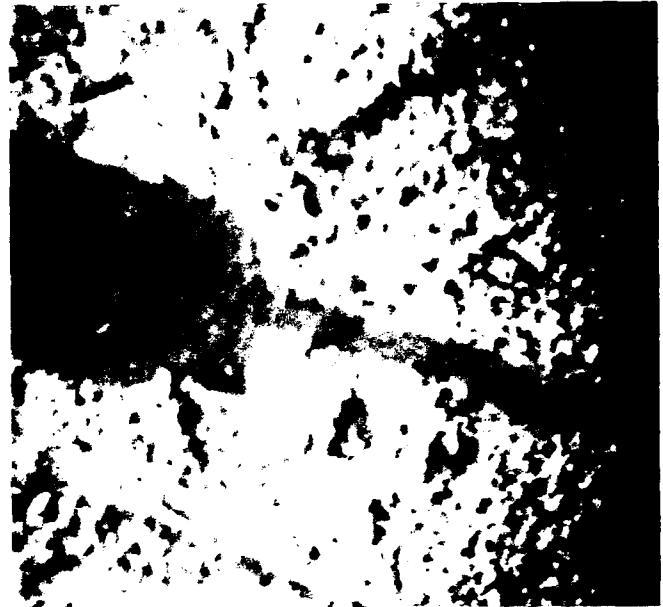
Throughout the measurement experiment, the Plumbicon camera would frequently saturate with reflectance signal, especially when filter #1 was used. The top of Figure 3.4.3 shows the camera response on December 1 with filter #1 in place. The camera detector appears to have saturated in this image. The lower image is a gradient image of the top (December 1) image and was produced at the University of Connecticut. The gradient operation converts changes in image reflectance into 3-dimensional textures. The gradient image clearly shows the camera saturation throughout the center of the image scene as an area of unchanging reflectance (no gradient). The location of the trench can be clearly seen on both the original and the gradient images, and is marked on the gradient image.

Figure 3.4.4 shows the trench reflectance for filter #1 on November 2 and December 9. Figure 3.4.5 shows the trench reflectance for filter #2 on November 2 and December 9. In both sets of data, changes in camera gain during the experiment and the saturation problems do not permit conclusions from any comparisons of these data sets over time.

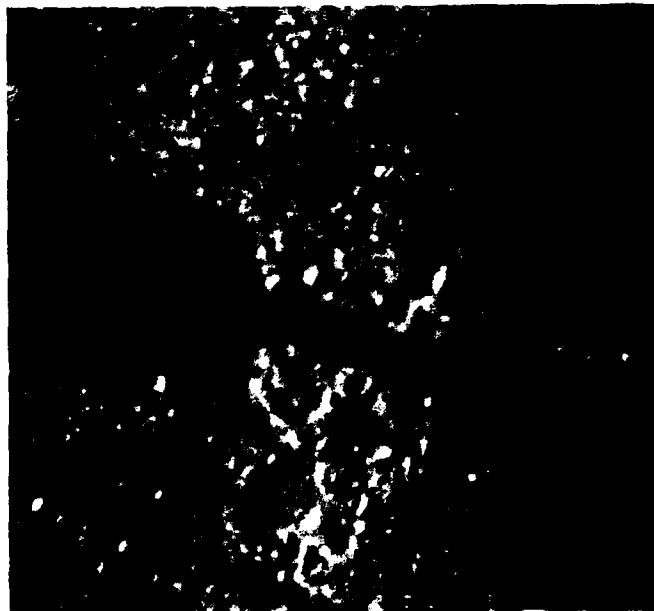
University of Arizona, Tucson



October 29 - No Filter



October 29 - Filter #1



October 29 - Filter #2

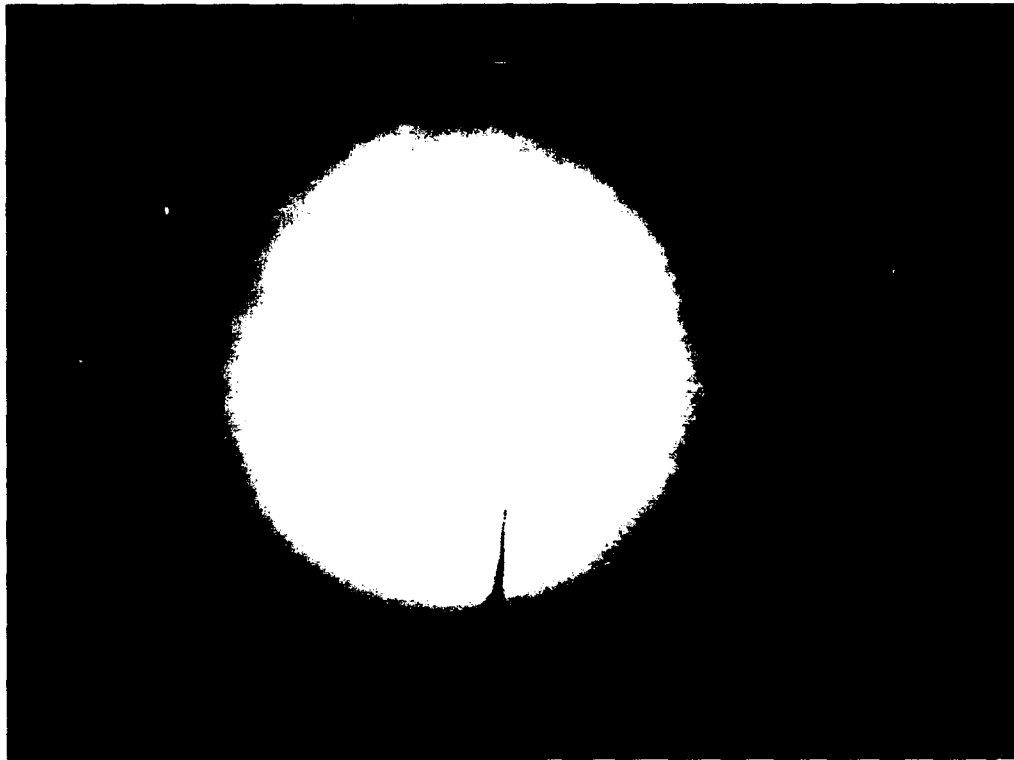


October 29 - Filter #3

Figure 3.4.2. Plumbicon Camera Reflectance Measurements

University of Arizona, Tucson

December 1 — Filter #1



Gradient Image — Saturation Indicator

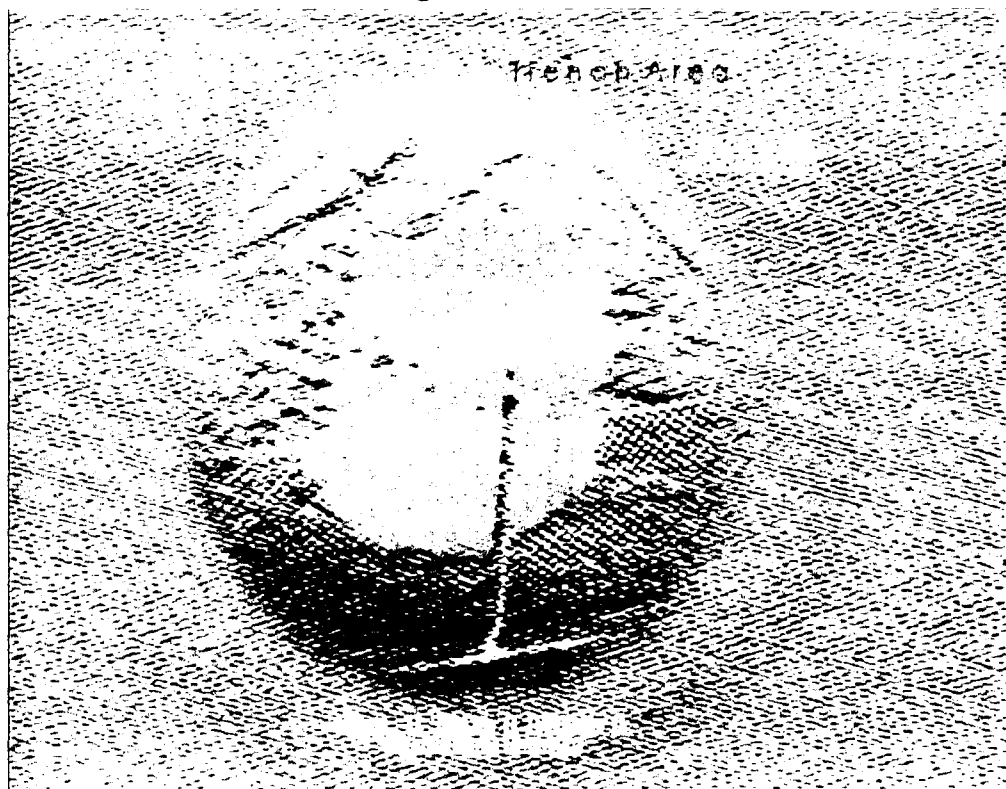


Figure 3.43 Plumbicon Camera Reflectance Measurements

University of Arizona, Tucson

November 2 --- Filter #1



December 9 — Filter #1

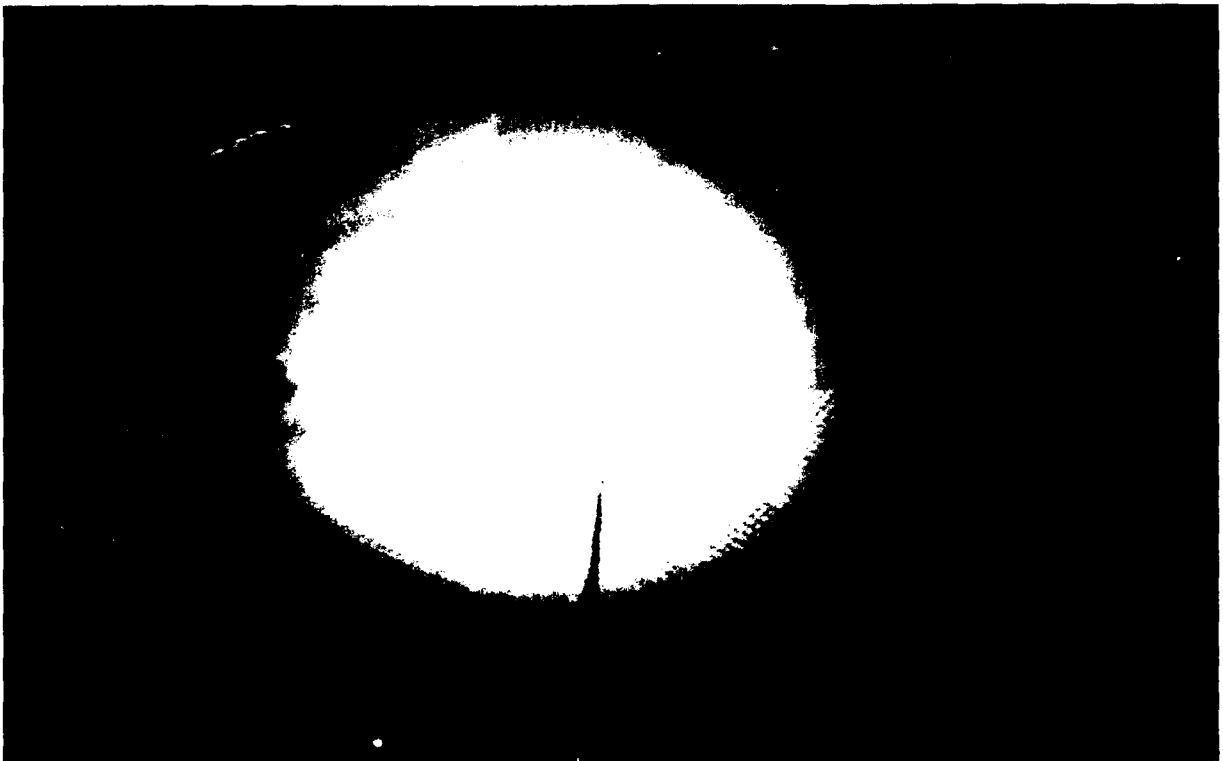
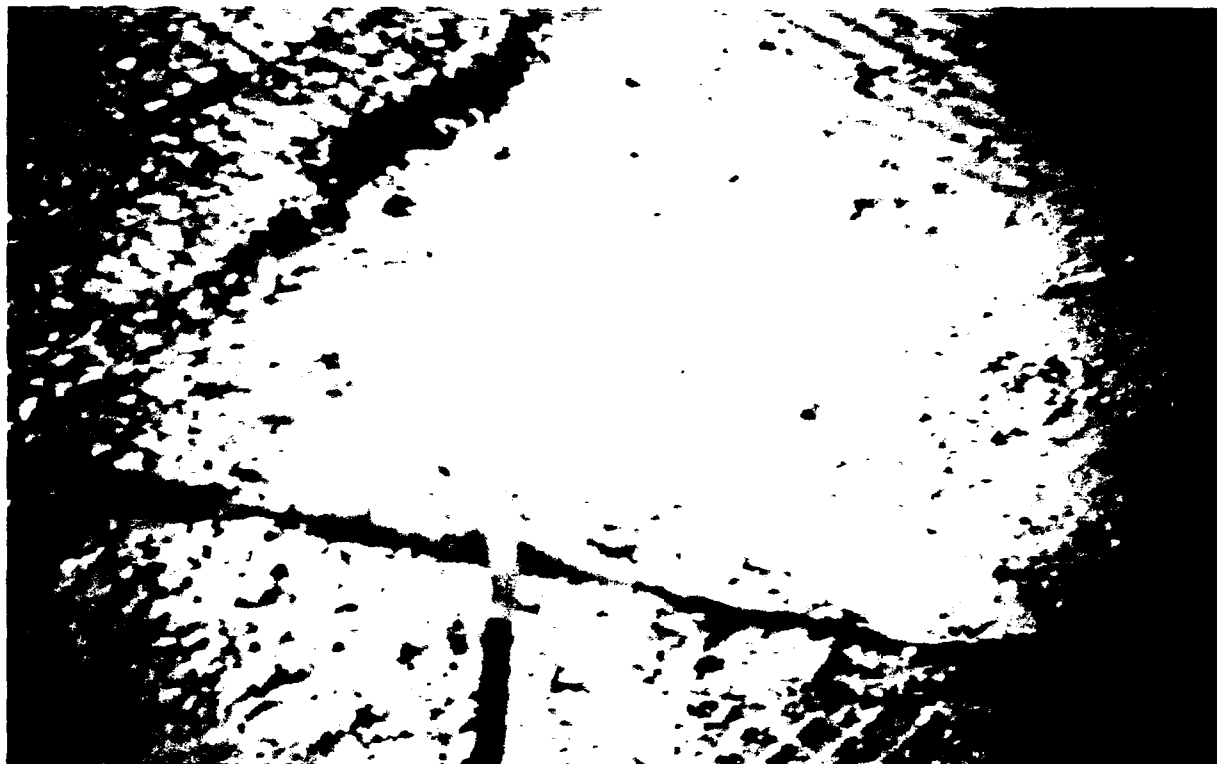


Figure 3.4.4 Plumbicon Camera Reflectance Measurements

University of Arizona, Tucson

November 2 — Filter #2



December 9 — Filter #2



Figure 3.4.5. Plumbicon Camera Reflectance Measurements

4. MINEFIELD IMAGING SATELLITE — PARAMETRIC ANALYSIS

In designing a space-based imaging sensor, design tradeoffs must be made with satellite lifetime, resolution, field of view, pixel size, pointing accuracy, data downlink opportunities, and other parameters. In this section, the satellite sensor capabilities and the tactical requirements mandated by the scenarios will be justified in a sensitivity analysis, which describes each parametric tradeoff.

4.1 Satellite Orbital Constraints

In most battlefield scenarios, including the five presented in Section 2 of this report, U.S. forces would take the necessary time to assemble the appropriate force and logistics for the planned operation. Significant military operations would not take place until this logistics support was established, over a period of several months for large-scale armored operations. Therefore, the tactical surveillance satellite sensor would require an orbital lifetime to match the typical scenario timeline — from 3 to 6 months in most cases.

An imaging satellite is constrained by orbital mechanics. In order to increase ground-based resolution, the satellite is flown at the lowest possible altitude. However, a low altitude generally means a short orbital lifetime. A compromise can be achieved by choosing an elliptical orbit with the perigee located over the target area. Another constraint imposed on an imaging satellite is the need to make a daytime pass over the target area. A way of ensuring at least one pass per day is to use a sun-synchronous orbit, which is an expensive orbit from the point of view of payload. The payload for the Pegasus launch platform decreases from 310 kg for a 28.5° inclined circular orbit at an altitude of 400 km to 225 kg for a sun-synchronous orbit (~94° inclination). General purpose imaging satellites such as SPOT and LANDSAT have revisit times of 16 days for LANDSAT 5 and 2.5 days (off nadir) for SPOT.⁵ For a tactical imaging satellite, a daily revisit time is highly desirable. For these reasons, an elliptical, sun-synchronous orbit with daily revisit times is appropriate. The orbital characteristics parametric analysis follows. A 90-minute sun-synchronous orbit (5,400 seconds) will ensure a daily revisit to the target area.

The period of an elliptical orbit can be determined from

$$P = \pi \sqrt{\frac{(r_a + r_p)^3}{2K}} \quad (1)$$

where:

K = Orbital constant = 398,600.5 km³/s²

r_a = Apogee radius

r_p = Perigee radius

⁵Ray Harris, *Satellite Remote Sensing* (London and New York: Routledge Kegan Paul, 1987), p. 51.

If a 90-minute orbit is required, $P = 5,400$ seconds, and the equation for period can be rearranged:

$$\begin{aligned}(r_a + r_p)^3 &= \left[\frac{P}{\pi} \right]^2 \cdot 2 K \\ &= \left[\frac{5,400 \text{ s}}{3.14} \right]^2 \cdot (398,600.5 \text{ km}^3 / \text{s}^2) \cdot 2 \\ &= 2.358 \times 10^{12} \text{ km}^3\end{aligned}\tag{2}$$

It is clear that a set of values of r_a and r_p can give the desired orbital period. Taking the cube root of (2)

$$(r_a + r_p) = 13,310 \text{ km}$$

These radii can be converted to altitude values for apogee and perigee by subtracting the earth's radius of 6,370 km from each.

$$h_a + h_p = 570 \text{ km}$$

Choosing a perigee pass of 185 km, yields an apogee value of

$$\begin{aligned}h_a &= 570 \text{ km} - 185 \text{ km} \\ &= 385 \text{ km}\end{aligned}$$

The orbital eccentricity is given by:

$$\begin{aligned}\epsilon &= \frac{r_a - r_p}{r_a + r_p} \\ &= \frac{6,755 - 6,555}{6,755 + 6,555} \\ &= .015\end{aligned}$$

The orbital characteristics are summarized in Table 4.1.1.

Table 4.1.1. SATELLITE ORBITAL CHARACTERISTICS

Inclination	96.60°
Perigee Altitude	185 km
Apogee Altitude	385 km
Eccentricity	0.0150
Period	5,400 sec (sun synchronous)

Given the orbital characteristics of Table 4.1.1, a computation was made to determine the amount of fuel necessary to maintain the orbit.*

The gravitational attraction between two bodies is

$$F_{m^1 m^2} = G \frac{m^1 m^2}{r^2}$$

where:

G = Universal gravitational constant

m^1 & m^2 = The masses of the two bodies

r = Distance separating the two bodies

*The calculations are based on a circular orbit due to the small eccentricity $\epsilon = 0.015$.

For a satellite orbiting the earth,

$$F_g = G \frac{m_s m_e}{r^2}$$

where:

- F_g = Gravitational force on satellite
- m_s = Mass of satellite
- m_e = Mass of earth
- r = $r_e + h$
- r_e = Radius of earth
- h = Altitude of satellite
- G = Universal gravitational constant

A stable orbit exists when the centripetal force experienced by the satellite is balanced by the gravitational force.

$$F_g - F_c = 0$$

$$F_c = m_s V^2 / r$$

$$\frac{m_s V^2}{(r_e + h)} = G \frac{m_s m_e}{(r_e + h)^2}$$

where:

- F_c = Centripetal force
- V = Velocity of satellite in orbit

$$V^2 = G m_e / (r_e + h)$$

The mass of the earth is

$$m_e = 5.98 \times 10^{24} \text{ kg}$$

$$G = 6.67 \times 10^{-11} \text{ N} \cdot \text{M}^2 / \text{kg}^2$$

$$\text{Let } K = G m_e$$

$$K = 3.99 \times 10^{14} \text{ M}^3 / \text{sec}^2 \quad (3)$$

$$\therefore V = \sqrt{\frac{K}{r}}$$

$$V = \frac{2 \pi r}{T}$$

where:

T = Orbital period

$$T = \frac{2 \pi r}{V} = \frac{2 \pi r}{\sqrt{\frac{K}{r}}} = \frac{2 \pi r^{3/2}}{\sqrt{K}} \quad (4)$$

The orbital lifetime of a satellite is influenced by atmospheric drag. The orbital drag can be determined as follows.

The potential energy of the satellite is

$$PE = \int m g dr \quad (5)$$

$$F_s = G \frac{m_s m_e}{r^2} = \frac{K m_s}{r^2}$$

$$\therefore g = \frac{K}{r^2}$$

$$PE = \int \frac{m_s K}{r^2} dr = \frac{-m_s K}{r} + C \quad (6)$$

where C = constant of integration.

The kinetic energy of the satellite is

$$KE = 1/2 m_s V^2 \quad (7)$$

$$KE = \frac{m_s K}{2 r} \quad (8)$$

The total energy E_T of the satellite is:

$$E_T = KE + PE$$

$$E_T = \frac{m_s K}{2 r} - \frac{m_s K}{r} + C$$

$$E_T = - \frac{m_s K}{2 r} + C \quad (9)$$

$$\frac{d E_T}{d r} = - \frac{m_s K}{2 r^2} \quad (10)$$

For small changes in orbital altitude

$$\frac{\Delta E_T}{\Delta r} = \frac{d E_T}{d r}$$

$$\Delta E = \Delta r \left[\frac{d E_T}{d r} \right] = \Delta r \left[-\frac{m_s K}{2 r^2} \right] \quad (11)$$

The loss in energy for one orbit is

$$\Delta E = \int F_D dx = 2 \pi r F_D \quad (12)$$

Aerodynamic drag can be expressed as

$$F_D = 1/2 \rho V^2 C_D A \quad (13)$$

where:

- ρ = Atmospheric density in kg/m³
- C_D = Drag coefficient
- A = Satellite cross-section perpendicular to the flow
- F_D = Drag force

Substituting for V^2

$$F_D = 1/2 \rho \left[\frac{K}{r} \right] C_D A \quad (14)$$

For an elliptical orbit, the density can be replaced by an equivalent density. The density of air as a function of altitude is shown in Table 4.1.2.

Table 4.1.2. DENSITY OF AIR BY ALTITUDE⁶

Altitude (km)	Density (kg/m ³)
180	5.194 x 10 ⁻¹⁰
190	3.581
200	2.541
210	1.846
220	1.367
240	7.858 x 10 ⁻¹¹
260	4.742
280	2,971
300	1.916
320	1.264
340	8.503 x 10 ⁻¹²
360	5.805
380	4.013
400	2.803

The variation in pressure with altitude from the hydrostatic equation⁷ is

$$\frac{d P}{d h} = - \rho g \quad (15)$$

where:

P = Atmospheric pressure

g = Gravitational constant

P = $\rho k T/m$

(16)

k = Universal gas constant

T = Temperature

⁶Handbook of Chemistry and Physics, 63rd ed., 1990.

⁷A. B. Cambel and B. H. Jennings, *Gas Dynamics* (New York: Dover Publications, Inc., 1958).

m = Mass of gas

$$\frac{dP}{P} = \frac{-mg}{kT} dh$$

$$\text{let } H = -\frac{kT}{mg}$$

$$= -\frac{dh}{H}$$

$$\frac{\rho}{\rho_o} = \frac{P}{P_o} = e^{\left(\frac{-h}{H}\right)} \quad (17)$$

The experimental data of Table 4.1.2 was fit to an equation of the form

$$\rho = e^{ah-b} \quad (18)$$

where constants a and b were found to be

$$a = -0.02344$$

$$b = 10.15574$$

The fit over this range yielded an R-squared = 0.990. The equivalent density was determined by

$$\bar{\rho} = \Sigma_o^n \rho_h / n \quad (19)$$

This is simply the arithmetic average density that the satellite experiences. The equivalent density was computed using a Lotus spreadsheet yielding

$$\bar{\rho} = 7.364 \times 10^{-11} \text{ kg} / \text{M}^3$$

From Equation 12 and 14

$$\Delta E = (2 \pi r) \left[1/2 \bar{\rho} \left[\frac{K}{r} \right] C_d A \right]$$

$$\Delta E = \pi \bar{\rho} K C_d A \quad (20)$$

$$\Delta E = \Delta r \left[\frac{d E_T}{d r} \right]$$

From Equation 11,

$$\Delta r = \frac{\pi \bar{\rho} K C_d A}{(d E_T / d r)}$$

From Equation 11,

$$\frac{d E_T}{d r} = -\frac{m_s K}{2 r^2}$$

$$\Delta r = \frac{2 \pi r^2 \rho C_d A}{m_s} \quad (21)$$

$$\text{Let } A_o = \pi r^2 = \text{orbital area} \quad (22)$$

$$\text{Let } \beta = m_s / C_d A = \text{ballistic coefficient} \quad (23)$$

$$\Delta r = 2 \bar{\rho} A_o / \beta \quad (24)$$

$$A_o = \pi r^2 = \pi (r_c + h)^2$$

$$r_c = 6.370 \times 10^6 \text{ M}$$

$$h = [(185 + 378) / 2] \times 10^3 \text{ M}$$

$$h = 281.5 \times 10^3 \text{ M}$$

$$A_o = 1.3899 \times 10^{14} \text{ M}^2$$

The mass of the satellite was determined from the Pegasus payload limits for polar orbit.

$$m_s = 225 \text{ kg}$$

The frontal area of the satellite was estimated to be 0.75 M^2 , yielding a ballistic coefficient of

$$\beta = m_s / C_d A = \frac{225 \text{ Kg}}{(3) (0.75)} = 100 \frac{\text{Kg}}{\text{M}^2}$$

This value is comparable to other earth observation satellites.

$$\Delta r = 2 \rho A_o / \beta$$

$$\Delta r = (2) (7.364 \times 10^{-11}) (1.3899 \times 10^{14}) / 100$$

$$\Delta r = 205 \text{ M} / \text{orbit}$$

The total number of orbits for the satellite is

$$N = 180 \text{ days} \times 16 \text{ orbits/day} = 2,800 \text{ orbits}$$

$$\frac{\Delta V}{\Delta r} = \frac{dV}{dr} \text{ for small orbital change}$$

$$\Delta V = \Delta r \left(\frac{dV}{dr} \right)$$

$$V = \sqrt{\frac{K}{r}}$$

$$\frac{dV}{dr} = \frac{V_o}{2r} \quad (25)$$

$$\Delta V = \Delta r \left[\frac{V_o}{2r} \right] \quad (26)$$

$$V_o = \frac{2\pi r}{T} \quad (27)$$

where:

$T = \text{orbital period}$

$$V_o = \frac{(2) \pi (r_e + h)}{(5,400)} = \frac{(2) (\pi) [(6,370 + 281.5) \times 10^3]}{(5,400)}$$

$$V_o = 7,739 \text{ M / s}$$

$$\Delta V = (.205) \frac{M}{\text{orbit}} \left[\frac{7,793}{(2) (6,370 + 281.5) \times 10^3} \right]$$

$$\Delta V = 0.120 \text{ M / sec / orbit}$$

$$\text{Total } \Delta V' = N \Delta V$$

$$= (2,880) (0.0120) = 346 \text{ M / sec}$$

The ΔV of a rocket is⁸

$$\Delta V = g I_s \ln \frac{1}{1 - \Lambda} \quad (28)$$

where:

I_{sp} = Specific impulse of fuel (1/sec)

Λ = Fuel mass fraction

$$\frac{1}{1 - \Lambda} = e^{\Delta V / g I_s} \quad (29)$$

⁸R. D. Heitchue, Jr., ed., *Space Systems Technology* (New York: Reinhold Book Corporation, 1968).

The specific impulse of Hydrozine/Nitrogen Tetroxide⁹ for a 300 psi chamber pressure is:

$$I_{sp} = 340 \text{ (1 / sec)}$$

$$\frac{1}{1 - \Lambda} = e^{(346) / (9.88) (340)}$$

$$\frac{1}{1 - \Lambda} = 1.108$$

$$\Lambda \approx 0.10$$

The fuel necessary for orbital maintenance is, therefore, ~ 10 percent of satellite mass. This does not account for the fuel necessary to maintain the perigee over the target area. Because of the nonsymmetry of the radius of the earth, the orbit will precess, and a small amount of fuel will be necessary to offset this effect.

4.2 Satellite Launch Vehicles

For the tactical user the ability to have imagery on short notice is crucial. There are two ways this can be accomplished; by having a constellation of tactical imaging satellites, which have been prepositioned in orbit, or by launching a satellite on demand.

A difficulty with prepositioning a galaxy of tactical imaging satellites is the tradeoff that must be made between GBR, revisit time, and cost. Another is the need to have all the satellite in polar orbits in order to enable whole earth coverage. Even with polar orbits, however, the capability for daylight imaging is severely constrained in the polar region during the winter months and enhanced during the summer.

The swath width (the distance across the satellite's axis of travel over which the camera can image) is a function of the orbital altitude and the off nadir imaging capability of the camera. For LEO satellites, the swath width is limited to approximately +/- 45 degree due to the curvature of the earth. This results in a swath width equal to approximately twice the orbital altitude. Increasing the swath width by increasing altitude comes at the expense of decreasing ground-based resolution.

If an on-demand satellite is used instead of a constellation of prepositioned satellites, daily imaging of any area on the earth is possible (this does not ensure daylight imaging of polar regions in winter). To achieve on-demand launch, both a launch vehicle and a launch site have to be available.

In the continental United States only three launch sites can be used: Cape Canaveral, Florida; Wallops Island, Virginia; and Vandenberg AFB, California. Given the present demand for launching satellites it is unlikely the United States would tie up a launch pad for an on-demand launch of a tactical satellite. There are two other ways a satellite can be launched, by aircraft or by submarine. There have been recommendations to use retired U.S. missile-launching submarines to launch

⁹Ibid.

tactical satellites. In addition to the extraordinary cost, there are severe political problems associated with launching tactical satellites from submarines.

The U.S. used an F-15 fighter to launch an anti-satellite satellite (ASAT). The OSC has pioneered the use of aircraft launch for commercial and military satellites. The OSC launch vehicle is the Pegasus rocket, a two- or three-staged launch vehicle capable of placing a 250 kg payload in polar orbit. The aircraft is a modified B-52, and launch generally takes place by flying out into the Atlantic or Pacific. It is possible, however, to launch over land, much as was done with the Tomahawks that were tested over Canada. The Pegasus provides the best near-term solution to a launch on demand.

The time necessary to have a satellite over target area depends on the priority assigned to the flight vehicle, the launch vehicle and the satellite. Under "normal circumstances," OSC expects to be able to mate the satellite to the launch vehicle and be able to launch within 5 days. If the satellite has already been mated to the launch vehicle, that time can be shortened substantially. There are no technological impediments to achieving a launch on demand for a tactical imaging satellite based on using the Pegasus launch vehicle. Figure 4.2.1 shows the altitude and payload capability of the Pegasus launch vehicle.¹⁰

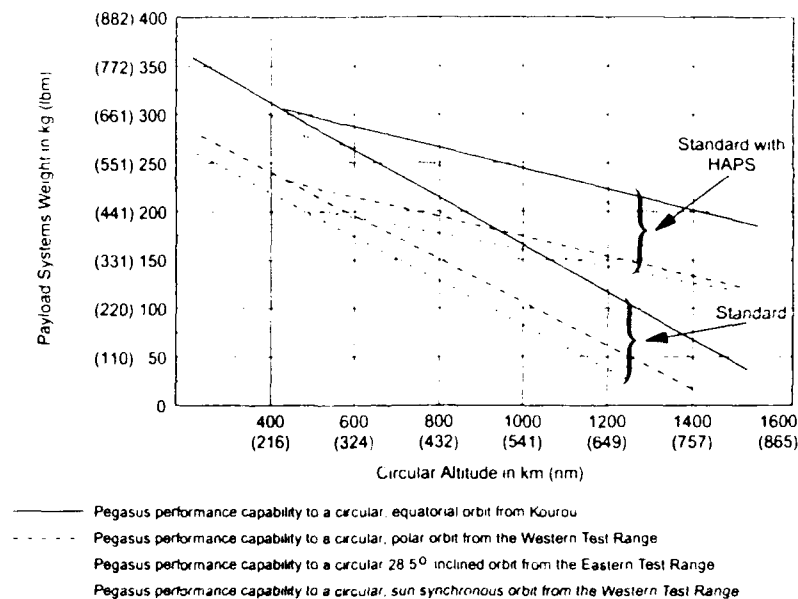


Figure 4.2.1. Pegasus Payload Capacity

4.3 Signature Bands

An object on the ground can be detected and identified using an imaging satellite if the spectral reflection and shape can be discerned. The shape is a function of the resolution of the detector and is primarily determined by the manufacturing limitations of the sensor. High spatial resolution sensors are available, but not in the whole spectral region.

¹⁰Pegasus Payload Users Guide, Orbital Sciences Corporation, May 1991.

Solar energy is reflected from the earth in the spectral band from 0.4 to 2.5 microns (see Figure 4.3.1). Below 0.4 microns the energy (ultraviolet) is strongly absorbed by the earth's atmosphere. Above ~ 2.5 microns the energy is a mix of reflected solar energy and the gray body radiation from the earth. The signature of bodies on earth, based on reflected sunlight is therefore primarily in the spectral region from 0.4 to 2.5 microns wavelength.

Unfortunately there are no usable sensors capable of sensing over this spectral range. Silicon has an excellent quantum efficiency over the range from ~ 0.4 microns to 1.0 microns (see Figure 4.3.2). In addition, it can be fabricated in large focal plane arrays with high resolution pixel sizes. Above 1 micron there are a number of sensors that have either moderate quantum efficiency in a narrow spectral region or wide spectral range but poor overall quantum efficiency.

If imagery is required over the wavelengths 0.4-2.5 microns, then a minimum of two and possibly three sensor materials is required. In addition, each sensor interval will require a different integration time.

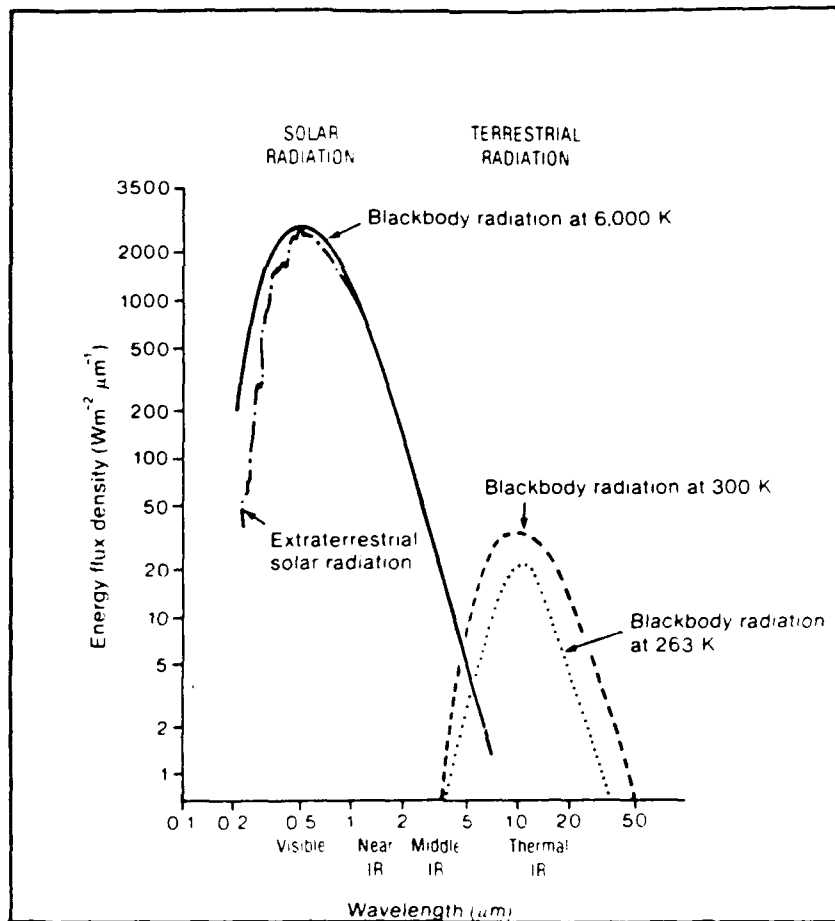


Figure 4.3.1. Solar Energy Reflected from Earth

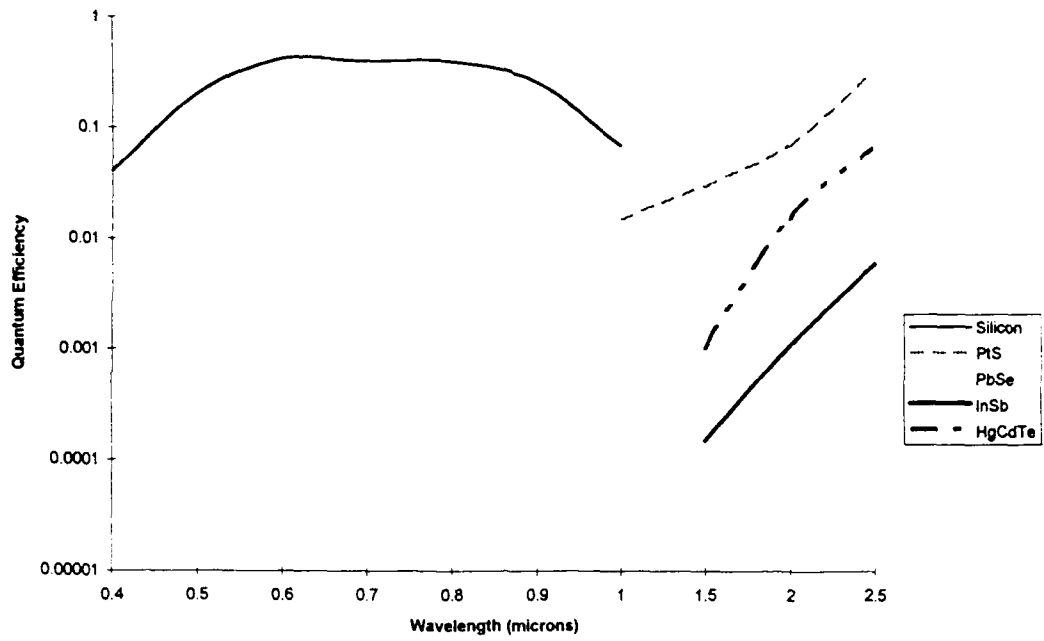


Figure 4.3.2. Quantum Efficiency of Detector Materials

4.4 Ground Resolution and Target Signature

In order to detect a target, high resolution pixels are required. However, high resolution pixels are only one of the limits on ground-based resolution for the camera. The resolution required to perform particular tasks on tactical images is shown in Table 4.4.1.

Table 4.4.1. RESOLUTION (IN METERS) REQUIRED FOR INTERPRETATION TASKS

Target	Detection ¹	General Identification ²	Precise Identification ³	Description ⁴	Analysis
Bridge	6	4.6	1.5	0.9	0.3
Communications					
Radar	3	0.9	0.3	0.15	0.04
Radio	3	1.5	0.3	0.15	0.15
Supply dump	1.5	0.6	0.3	0.03	0.03
Troop units	6	2	1.2	0.3	0.08
Airfield facilities	6	4.6	3	0.3	0.15
Rockets and artillery	0.9	0.6	0.15	0.05	0.01
Aircraft	4.6	1.5	0.9	0.15	0.03
Command and control headquarters	3	1.5	0.9	0.15	0.03
Missile sites (SSM/SAM)	3	1.5	0.6	0.3	0.08
Surface ships	7.6	4.6	0.6	0.3	0.08
Nuclear weapon components	2.4	1.5	0.3	0.03	0.01
Vehicles	1.5	0.6	0.3	0.05	0.03
Land minefields	9	6	0.9	0.03	--
Ports and harbors	30.5	15	6	3	0.3
Coasts and landing beaches	30.5	4.6	3	1.5	0.08
Railway yards and shops	30.5	15	6	1.5	0.6
Roads	9	6	1.8	0.6	0.15
Urban areas	61	30.5	3	3	0.3
Terrain	--	91	4.6	1.5	0.15
Surfaced submarines	30.5	6	1.5	0.9	0.03

Source: *Reconnaissance Handy Book*, published by McDonnell Douglas Corporation. USA, p. 125.

¹Requires location of a class of units, object or activity of military interest.

²Requires determination of general target type.

³Requires discrimination within target types of known types.

⁴Requires size/dimension, configuration/layout, components construction, count of equipment, etc.

The three fundamental limitations on ground-based resolution for the camera are:

- Aperture diameter
- Pixel size
- Focal length

Aperture Diameter

The wave nature of light limits the resolution of any optical system. "Rayleigh's criteria" for resolution is expressed as:

$$\alpha = 1.22 \lambda (f / \#)^{11}$$

α = Radius of Rayleigh disk

λ = Wavelength of light

$f / \#$ = Focal number of optical system

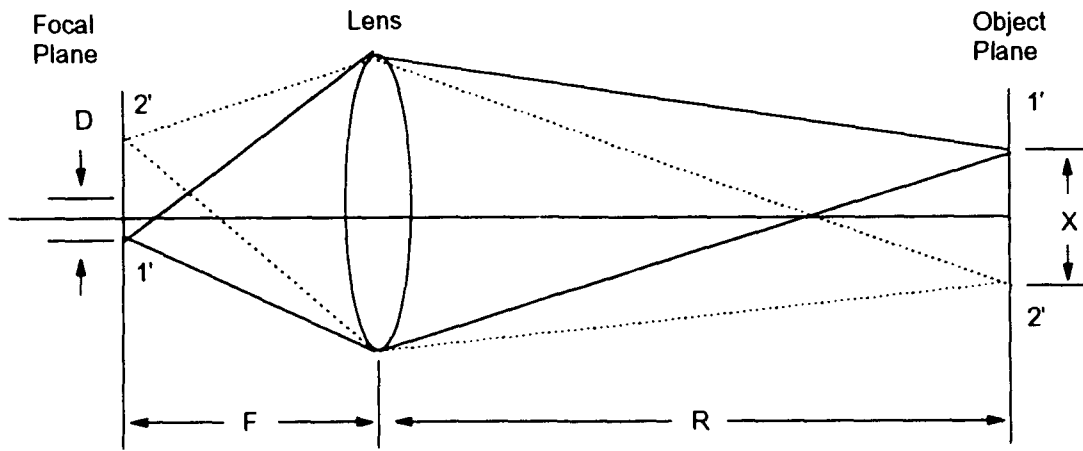
$$f / \# = \frac{F}{D}$$

F = Focal length

D = Aperture diameter

The relationship between ground-based resolution X and the airy disk is shown in Figure 4.4.1.

¹¹W. Smith, *Modern Optics/Engineering — The Design of Optical Systems*, 2nd ed. (New York: McGraw-Hill, 1990).



(a) Image formation by geometric optics

Figure 4.4.1. Aperture Diameter and Ground-Based Resolution Relationship

$$\alpha = X \frac{F}{R}$$

$$X = \frac{1.22 \lambda R}{D}$$

R = Distance from satellite to object on ground

The limitation of aperture on GBR is shown for $\lambda = 0.5$ microns and range = 185 km (see Figure 4.4.2.)

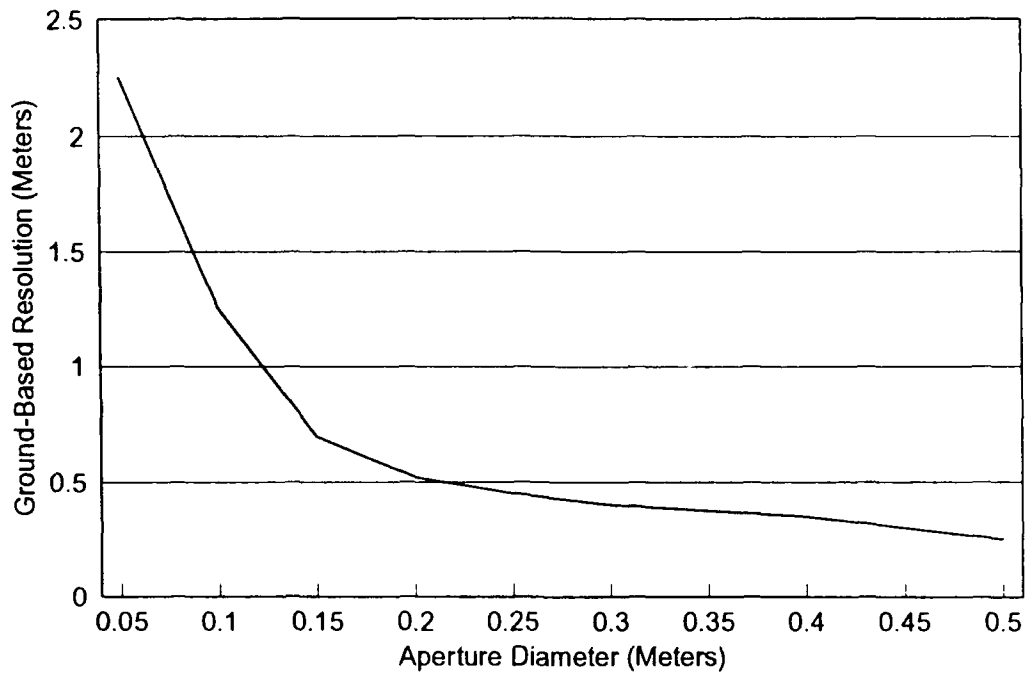


Figure 4.4.2. Aperture Diameter and Ground-Based Resolution Limitation

Based on the above, it is obvious that even a 0.1 meter ~4 in diameter aperture is capable of resolving objects on the ground that are spaced greater than 1.5 meters.

Pixel Size

The second criterion for GBR is the pixel size of the sensor. Pixel size is limited by manufacturing constraints. The "state of the art" for large linear or area focal plane arrays (FPA) in silicon is approximately 8-10 microns. The analysis is based on the Kodak KAF-6300 CCD array. This array is an imaging array of 3,074 x 2,048 pixels with each pixel 9 x 9 microns.

For an imaging sensor, the pixel size is related to GBR by

$$\frac{\alpha'}{F} = \frac{X}{R}$$

α = Imaging array pixel size

For a 9-micron pixel size with a range of 185 km, the relationship between focal length and GBR is shown in Figure 4.4.3.

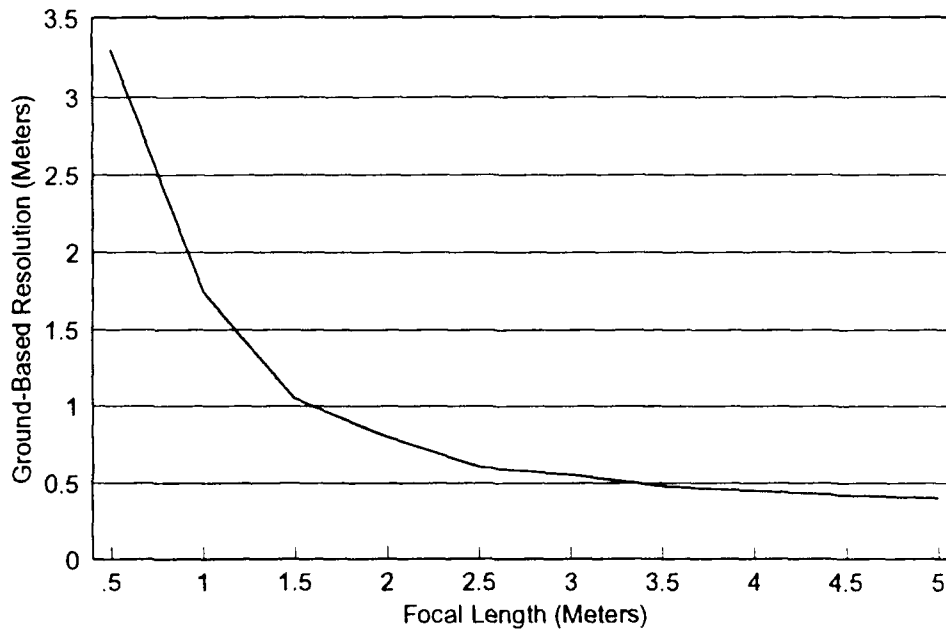


Figure 4.4.3. Focal Length and Ground-Based Resolution

At the present time large area silicon focal plane arrays are available with pixel sizes of approximately 8 microns. To achieve a 0.5 meter ground-based resolution with an 8-micron pixel size sensor and a 1.0 meter diameter aperture, the focal length of the camera would have to be 4.0 meters. Assuming a Cassegrain configuration, this still means a camera with an overall length of ~2 meters. The Pegasus launch vehicle is barely large enough to meet these requirements and would leave virtually no room for the other satellite bus needs (power, stabilization, etc.).

From a tactical point of view, there are requirements that drive satellite design, the most important of which are image area, GBR, spectral bands, and, of course, the number of images generated in a pass. Another parameter is the area of concern; however, this is more directly related to the level of command of a tactical satellite. For example, a corps commander in an operation such as Desert Storm may be concerned with an area of 600 km square, as contrasted to a brigade commander whose area of concern is probably less than 100 km square. It is probably easier to solve the area of concern problem by satellite basing (number of satellites and orbital paths) rather than use this as a criterion for design of a specific satellite.

The GBR requirement of a satellite is determined by the targets of the satellite, the target contrast, and spectral signature. For any spectral band, the minimum condition for detection is the requirement that the target pixel exhibit a signal-to-noise sufficiently high to be detected and recognized as not being part of the background scene. If the background scene exhibits a Raleigh distribution, as shown below in Figure 4.4.4, then the radiance levels below I_o and above I_m may

represent valid targets. The radiance incident on the sensor pixel is the arithmetic average of the target area multiplied by the reflectance minus path absorption.

$$I = \Sigma a_i R_i \alpha$$

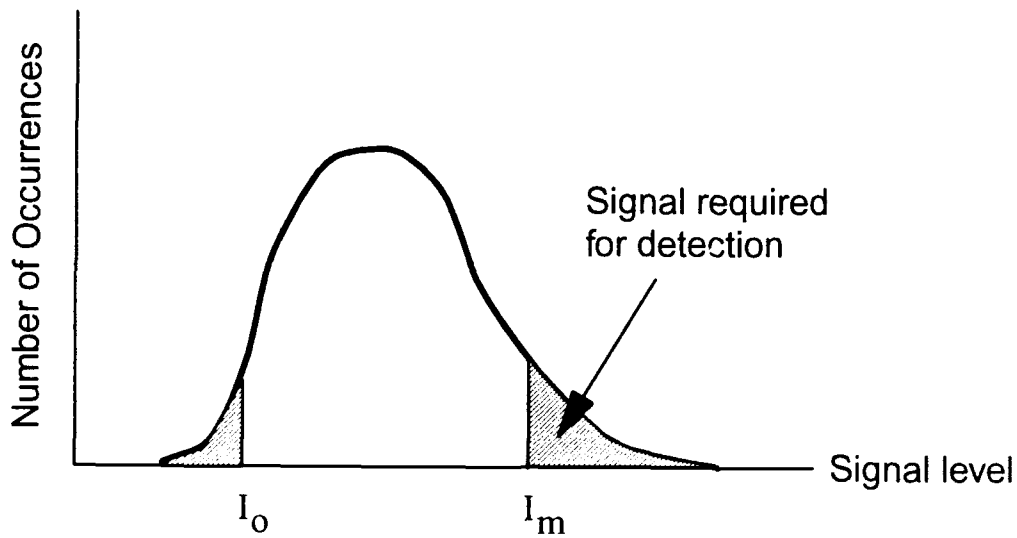


Figure 4.4.4. Rayleigh Distribution of Irradiance

where:

- a_i = Target area having reflectance R_i
- R = Reflectance
- α = Total signal absorption including atmospheric absorption and losses in the optical train

What is significant here is that, unless the target area fills the pixel, detection may require target reflectance considerably above or below the Rayleigh distribution. This is the reason the design criterion for detection usually requires the target area to at least fill the pixel.

When considering the mechanically emplaced minefield as shown below in Figure 4.4.5 consisting of three parallel trenches, spaced 5 meters apart,

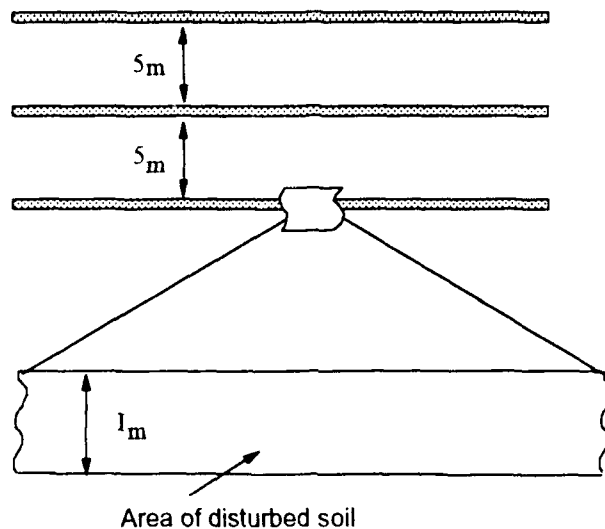


Figure 4.4.5. Minefield Trench Layout

the pixel size should equal 0.5 meters to ensure the pixel fills the target. (A 1-meter pixel might only cover one-half the minefield trench.)

If the imagery covers more than one spectral band, the probability of detection is a more complex phenomenon. Assume there are two images, one with one spectral band and one with three bands. For the single band, again, the probability of detection requires a radiance level outside of the distribution function. Either

$$I > I_m \text{ or } I < I_o$$

If there are two spectral bands, a 2-dimensional plot of the nontarget scene yields a surface resembling a hill, as shown in Figure 4.4.6.

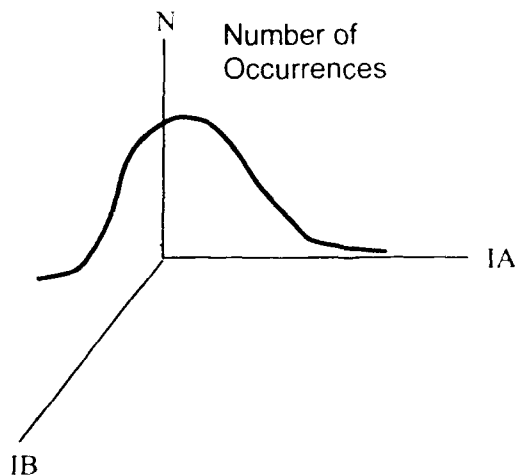


Figure 4.4.6. Multispectral Detection

What is significant here is that there may be a significantly large number of states where either band A or B is within the scene spectral distribution but not both. This is what constitutes a unique spectral signature for a target.

The presence of three or more bands simply increases the state space. If the target's spectral signature is sufficiently unique, then the probability of detection becomes high.

Moving beyond the single-pixel detection of a target to scene recognition increases the state space of scene background versus target. Assume, for example, a line segment feature in a six-pixel square array (see Figure 4.4.7).

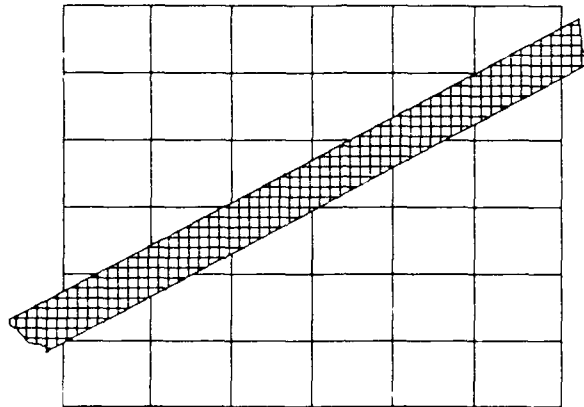


Figure 4.4.7. Linear Feature Across Pixel Array

If the target occurs along a row or column, then it is sufficient to simply compare the six rows and columns in the spectral state space. In the real world, however, the line segment may be oriented in a random way in an image; therefore, it is necessary to test at least 100 possible line segments in which the target may only fill a fraction of the pixel. Humans are vastly superior to machines in doing this, provided the scene can be reduced to a 3-dimensional plot (x and y coordinates with intensity). However, this, again, requires the target's spectral characteristics to be unique with respect to the scene spectral background. If the target, however, has a unique spectral signature, then the image can be reduced to a digital scene, and the target recognition problem made trivial.

Focal Length

To achieve a 1.5 meter ground-based resolution, a focal length of 1.11 meters is required. Using the Raleigh criteria for the aperture, the minimum dimensions are

$$FL = 1.11 \text{ M}$$

$$D = 0.075 \text{ M}$$

$$F/\# = 14.8$$

Although the aperture is adequate for resolving the separation, it is inadequate to achieve an optical gain capable of yielding reasonable signal-to-noise ratios.

Given a focal length of 1.11 meters and an aperture of 25 centimeters, the $F / \# = 4.44$.

4.5 Field of Regard, Field of View, Pointing Resolution

The field of regard of the camera is primarily a function of the orbital altitude of the satellite. The curvature of the earth limits the off-nadir imaging to approximately +/- 45 degrees. The along-track pointing is not a critical parameter due to the ability to position the satellite for image recording. The increase in the field of regard due to increased altitude is offset by the reduction in GBR.

For the situation where the satellite is in a sun-synchronous orbit, the field of regard is constant from day to day and only has to be adequate to meet the needs of the tactical user. The revisit time is automatically once per day. This is a significant advantage for the tactical user in that he can count on receiving a daily update of the area.

The field of view of the camera is determined primarily by the sensor and the required ground-based resolution. There are a number of commercially available silicon linear charge-coupled device (CCD) arrays of 6,000 to 8,000 pixels. These can be butted and linear arrays of 16, 24, or even 32,000 pixels created. If multispectral imagery is required, the arrays have to be separated into their spectral bands. If the area of interest is covered by a sensor with three spectral bands, 12 bits dynamic range and 24,000 pixels on a side, 20.7 Gbits of information is produced. If tactical needs dictate a minimum of 10 images then 207 Gbits uncompressed must be transmitted.

The tracking and data relay satellite (TDRS) downlink pipeline for a tactical imaging satellite is limited to approximately 300 Mbits/sec, taking 690 seconds to transmit the 10 images. The needs of the tactical user can more easily be met using two satellites, one with a wide field of view and one with a narrow field of view. The narrow field of view satellite would have an image size of 3.0 km x 4.5 km with a ground-based resolution of 1.5 meters, and the wide field of view satellite would have an image size of 10 km x 15 km with 5 meters ground-based resolution. Each would have a minimum of three spectral bands and 12 bits dynamic range. Each camera is now optimized for its individual tasks. Wide area searching is done with the wide field of view, and close inspection is done with the narrow field of view satellite, minimizing the demand loads on the TDRS.

The pointing resolution requirement of the satellites is determined by the accuracy of location of the intended target. If the pointing accuracy is set to 5 percent of the image field, the requirement is 150 meters (0.75 milliradians for 200 km orbit) on the ground for the narrow field of view camera. The wide field of view camera has a pointing accuracy of 500 meters on the ground (2.5 milliradians).

The camera slew rate is critical for the tactical user. A tactical G2 intelligence officer may request as many as 10 images of an area passed over in 15-20 seconds. Depending on the ground separation this could require camera slew rates of as much as 50 degrees per second. The camera must also be damped adequately so as to reduce jitter to within +/- 4 microradians in 50 to 100 milliseconds. It is ultimately the jitter of the camera and not the pointing accuracy that determines its usefulness.

Pushbroom versus Focal Plane Array

Given the availability of large area focal plane arrays it may make sense to consider a shuttered camera rather than a pushbroom sensor.

A pushbroom sensor has the advantage of using the motion of the satellite to sweep the target image. Large linear arrays are more easily constructed than large focal plane arrays. The French firm Thompson sells an 8,000 pixel silicon array that can be butted so as to enable 24,000 pixels or more on a side to be achieved. The primary disadvantage is the need to image over a time period of several seconds or more. By imaging over several seconds, atmospheric distortion is built in as noise and cannot be corrected for.

In contrast, if an image can be formed in a time commensurate with the relaxation time of the atmosphere the distortion can be minimized and is more easily compensated for using a focal plane array. The image motion compensation is also simplified by only imaging for milliseconds instead of seconds. A large focal plane array can also be used with an active system such as a laser.

4.6 Camera

The solar energy incident on the earth in the spectral region of concern is shown in Figure 4.6.1.

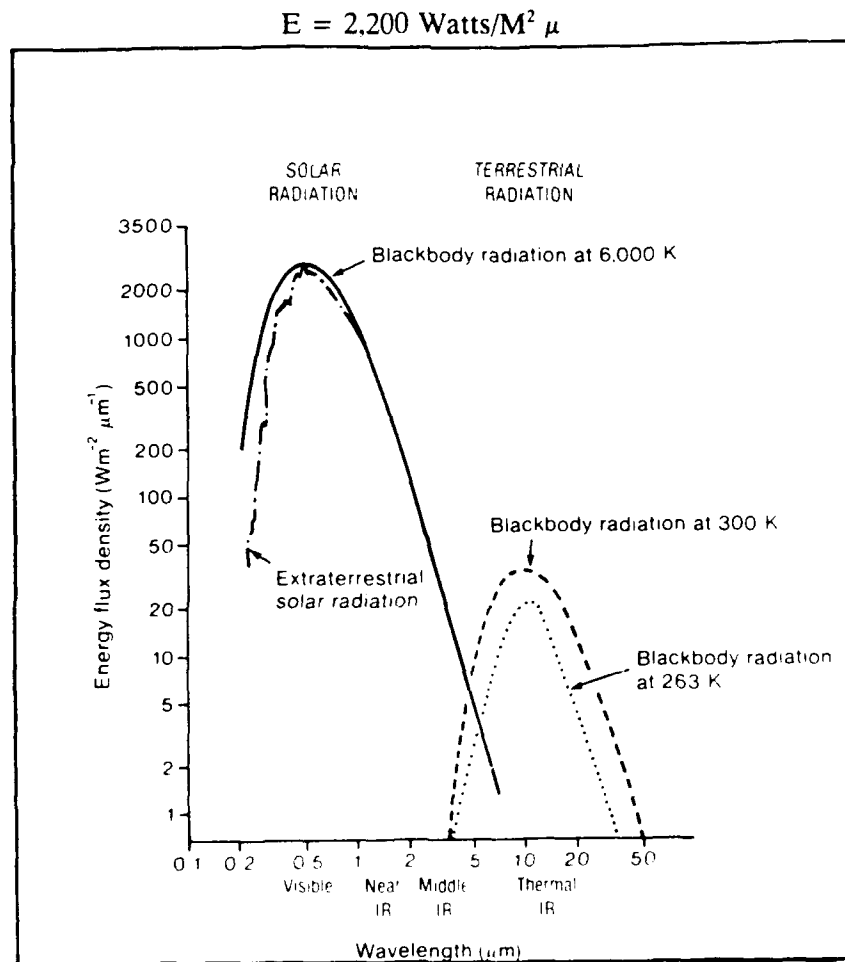


Figure 4.6.1. Solar Energy Incident on the Earth

For an area on the ground equal to the 1.5 M GBR and a 0.1 micron band pass the energy is:

$$E \lambda = 2,200 \frac{\text{watts}}{M^2 \mu} * (1.5)M^2 * 0.1 \mu = 495 \text{ watts}$$

Approximately 30 percent of this energy is reflected back to space over π steradians

$$E \lambda' = (0.30) (495) / \pi = 47.3 \text{ w} / SR$$

The reflected energy incident on the satellite's optical aperture is

$$E \lambda'' = 47.3 \frac{\text{watts}}{SR} * \frac{A_o}{R^2} = \frac{(47.3) (\pi) D^2}{(4) (185 \times 10^3)^2}$$

$$\frac{E \lambda''}{D^2} = 1.085 \times 10^{-9} \text{ watt}/M^2$$

Assume the efficiency of the optical system is 10 percent.

$$\frac{E \lambda'''}{D^2} = 1.085 \times 10^{-9} \text{ watt } M^2 * 0.1 = 1.085 \times 10^{-10} \text{ watt} / M^2$$

Each pixel occupies an area of 9 microns on a side.

$$A_o = (9 \times 10^{-6})^2 = 8.1 \times 10^{-11} M^2$$

$$\text{Let } \Phi_\lambda = \frac{E \lambda'''}{D^2 A_o}$$

$$\Phi_\lambda = 1.085 \times 10^{-10} \frac{\text{watts}}{M^2} = \frac{1}{8.1 \times 10^{-11}} M^2 * \frac{1}{D^2}$$

$$\Phi_\lambda D^2 = 1.33 \text{ watt}^5 / M^4$$

Pixel saturation for the Kodak FPA occurs.

$$\tau \Phi_{\lambda} D^2 = 0.11 \mu \text{ joules} / \text{cm}^2$$

$$\tau \Phi_{\lambda} D^2 = \frac{(0.11 \times 10^{-6}) \text{ joules}}{\text{cm}^2} \frac{(100 \text{ cm})^2}{(1 \text{ M}^2)}$$

$$\tau \Phi_{\lambda} D^2 = 1.1 \times 10^{-3} \text{ joules} / \text{M}^2$$

$$\tau D^2 = 1.1 \times 10^{-3} \frac{\text{joules}}{\text{M}^2} * \frac{1}{1.33} \frac{\text{M}^4}{\text{watts}}$$

$$\tau D^2 = 8.27 \times 10^{-4} \text{ sec} \cdot \text{M}^2$$

Figure 4.6.2. is a plot of aperture diameter as a function of saturation time for the Kodak FPA.

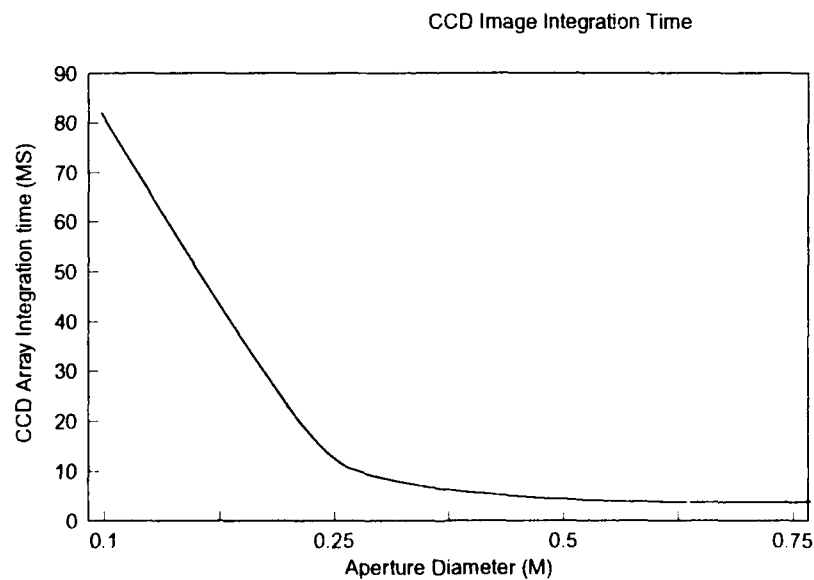


Figure 4.6.2. Kodak CCD Saturation Time

Image motion compensation is required when

$$\tau V_o = G S R / 2$$

$$V_o \approx 7.8 \times 10^3 \frac{M}{\text{sec}}$$

$$\tau = \frac{(1.5)}{(2) (7.8 \times 10^3)} = 9.65 \times 10^{-5} \sim 0.1 \text{ m sec}$$

From Figure 4.6.2, this would require an aperture of 2.87 meters, which is far in excess of the capacity of the Pegasus launch vehicle.

If a variable-speed shutter is used with an integration time of ten milliseconds, a 25 cm aperture would suffice. The actual range of shutter speeds requires a computation of the system modulation transfer function which is normally done in the design phase.

Another problem peculiar to satellites is that ground coverage is highly dependent on the orbit selected and the off-nadir imaging capability of the camera. A camera with a 45 degree off-axis capability can see an area approximately equal to twice its altitude. GBR is, however, directly related to orbital altitude; therefore, greater area coverage comes at the expense of resolution. Given that the maximum information is achieved when the pixel size is smaller than the object, the useful area that can be imaged is ultimately dependent on the size of the object and the optics of the camera.

The optics of the camera is in turn limited by the size of the orbital delivery vehicle. For a tactical satellite, the most important limit is the diameter of the fairing of the launch vehicle, which limits the aperture of the camera. Tactical satellites fielded over the next ten years will probably be based on the Pegasus or Taurus launch vehicles. The outer fairing of the Pegasus in the payload bay is 46 inches diameter. The upper limit on the aperture is therefore approximately 1 meter diameter, which is the primary constraint on the size of the optics for this satellite.

A camera with a 1.0 meter diameter aperture would have a 0.15 meters ground-based resolution at 0.5 microns wavelength and orbital altitude of 250 km. However, if the spectral signature extended out to 2.5 microns, the resulting GBR would only be 0.75 meters. If the camera were optimized for the visible region of the spectrum, it might prove totally inadequate for the near-IR.

The bottom line therefore is that the camera must be designed to the limits of the satellite bus, with the realization that the GBR is ultimately dependent on the launch platform geometry. Implicit in the above analysis is the need for a reflective system as contrasted to a refractive system.

A totally refractive system with an aperture of 1.0 meters would present a formidable task from a weight point of view and would present almost insurmountable difficulties if the spectral range extended from .4 to 2.5 microns. Chromatic aberration would severely limit resolution.

A reflective system in contrast would not be constrained by chromatic aberration but would require a light-weight mirror. To achieve adequate rigidity with a parabolic mirror, the mirror thickness is generally set equal to 1/6 of the diameter. A 1 meter diameter non-light-weight mirror would weigh approximately 325 kilograms. A similar light-weight mirror could weigh less than 50 kilograms.

There are two ways a mirror can be lightweighted: (1) by mechanically grinding it into a honeycomb shape thereby retaining the rigidity with a lighter weight structure or (2) by having a correctable lens. It may be easier to build a segmented lens with correctable elements rather than a large lightweighted lens such as on the Hubble telescope. This technology is being considered for mirrors larger than 2 meters diameter and if it proves satisfactory may be advantageous in somewhat smaller mirror diameters.

For a tactical imaging satellite it is highly unlikely that mirror size will exceed 1.0 meters diameter, and the lightweighting techniques developed for Hubble and other space mirrors should prove adequate. If a stable platform design is chosen then the same argument can be made for the optical flat.

The camera system can be based on the use of a stable platform with steering mirror or the whole camera can be moved such as is done with Hubble. The obvious advantage of using a stable platform with a steering mirror is that the energy required to move the steering mirror is less than that required to move the whole camera. Hubble was designed to image objects for time periods up to 26 hours. A tactical imaging satellite would, in contrast, require multiple images of the ground over a very short period of time.

Optical Platform

Traditionally optical platforms were built from Invar and other low coefficient of expansion metal alloys. In space platforms the metal alloys have been replaced by graphite composites. The new composites have substantially reduced the weight of the structure, but not without problems. The composites used in the Hubble telescope continued to outgas longer than expected and the resulting deformation was greater than expected. A tactical imaging satellite would not require the stability of the Hubble but care must be given the choice of structural composites.

4.7 Downlink Data Rates

A small tactical imaging satellite must minimize data downlink power requirements, while maximizing the quality and timeliness of the image data sent to the tactical commander. The complete data circuit is divided into three segments: a space segment, a user segment, and a system control segment. Two potential satellite link circuits are possible — one direct from the satellite to a mobile ground station, and one taking advantage of the NASA TDRS system that will be operational in 1996. This report addresses only the TDRS downlink because of the geometric and timeliness restrictions of a direct downlink from a LEO satellite to a mobile ground station.

Data Package Size

The problem of getting the recorded electronic image downloaded to earth is exacerbated by the potential requirement for multiple bands of image data. As an example, the Hughes Wedge Imaging Spectrometer (WIS) can collect 64 bands of image data for a 12-bit, 128-pixel image line in 3.125 milliseconds. A 128 x 128 pixel image in all 64 bands is therefore recorded in four-tenths (.04) of a second and contains over 1.5 megabytes (Mbytes) of data.

In the WIS data collection experiment at the Ostrich site, data were recorded onto tape for later analysis. In a LEO satellite operation, although temporary storage into memory may be necessary, various image compression algorithms will have to be investigated to reduce the size of the data package that is sent to an earth station. In the satellite application, the image focal plane array can be expected to be as large as 2,000 x 3,000 pixels at 12 bits per pixel, which represents 9 Mbytes per

band of data collected. In a download of 64 bands, the satellite would have to transmit 576 Mbytes of image data.

Image Compression Techniques

A number of well-known compression techniques can be employed onboard the satellite to reduce the downlink data rate requirement for transmitting image data to the earth station. Several recent studies have evaluated "lossy" (DCT [discrete cosine transform], JPEG [Joint Photographic Experts Group], Vector Quantization) and lossless (Huffman, GIF [graphics interchange format]) compression algorithms on satellite image data.^{12,13} Various compression techniques have been applied to image data and achieved compression ratios between 10:1 and 5:4 without a significant reduction in overall image quality. The truly lossless compression algorithms provide compression ratios between 4:3 and 5:4. The Defense Department National Imagery Transmission Format Standard (NITFS) for image compression includes user-selectable, JPEG, and adaptive recursive interpolated differential pulse code modulation (ARIDPCM) compression techniques with rates from 10:1 to 8:5. Using NITFS, the 9-Mbyte image from a 2,000 x 3,000 pixel array can be reduced to between 900 kilobytes (kbytes) and 7.2 Mbytes prior to storage or downlink.

Commercial image processing boards are currently available, which can compress the satellite image data at speeds that exceed the data read rate from the CCD sensor.

With a tactical imaging satellite having to serve multiple types of missions, a mission specific, user-selectable compression system is best, since the tactical user will decide the acceptable level of image degradation for the reconnaissance mission objectives. The most challenging reconnaissance requirements, such as vessel or vehicle identification, demand the highest-quality images and cannot tolerate significant losses due to image compression.

The NITF Standard

The Department of Defense has created the NITFS so that SIDS can exchange imagery and image-related data.¹⁴ The current version of the standard includes the NITFS 2.0 file format as well as standards for image compression, transmission protocol, and graphics. The Office of the Secretary of Defense for command, control, communication and intelligence (C³I) has mandated the use of NITFS for all SIDS.

Continued development responsibility for NITFS is with the Central Imagery Office (CIO), and NITFS has been incorporated into the defense standardization program under the Defense Information Security Agency (DISA).

In the NITFS concept, imagery data interchange among diverse computer-based systems is enabled by a cross-translation process. The NITFS 2.0 file format is used as the common currency of data

¹²*NITFS Military Handbook*, DISA, Joint Interoperability and Engineering Organization, June 18, 1993.

¹³"Compression of UoSAT-5 EIS Images," *Small Satellite Technology & Applications-3*, Montpetit & Prieur, Spar Aerospace Ltd., Quebec, Canada, April 1993.

¹⁴"Transmitting and Controlling Images from Small Satellites Using MPEG Image Compression," *Small Satellite Technology & Applications-3*, LeFevre & Heiberger, Cynetics Corp., April 1993.

exchange, and each system can translate NITFS files into that system's native data formats. Image files can be transmitted between systems using the TACO-2 standard message transmission protocol.

The TACO-2 protocol provides efficient message transfer across point to point or point to multipoint tactical circuits where current GOSIP protocols are unsuitable.

Four data types are supported by NITFS: images, symbols, labels, and text. A transmitted NITFS file can include any combination of these data types. Image data can be either monochrome (8 or 16 shades of grey), color-mapped, or true color. Multispectral images are currently supported by the standard up to 9 bands. NITF image size can range from 64 x 64 pixels to 65,536 x 65,536 pixels with a 2 gigabyte (Gbyte) file size limit.

Systems can be certified for several levels of NITFS compliance, including pack only, unpack only, and both pack and unpack.

Onboard Data Storage

Recent memory advances allow for the storage of multiple images onboard the satellite. Raymond Engineering, Middletown, Connecticut, manufactures a military standards (MIL-STD) PCMCIA flash memory card in a hardened case. Each PCMCIA card currently holds 40 Mbytes, weighs 2 oz, and can be configured in parallel to meet the data record rate and storage requirements for onboard storage of image files. Another flash memory unit is built by Fairchild Space and Defense Corporation with a 1 x 3.5 x 7 inch form factor. This memory unit is capable of more than 200 Mbytes storage and consumes 4 watts peak power. In small quantities these devices cost approximately \$20,000.

The primary advantage of the PCMCIA card over a space qualified hard drive is power consumption. The hard drive would consume 20-30 watts, whereas a bank of PCMCIA cards would consume several watts.

4.8 Downlink Opportunities

Geometry and Time

The geometric problem for downloading data from the satellite to a ground station is shown in Figure 4.8.1. The signal transmission opportunities from the satellite directly to the ground station are limited by the two primary factors: the transmission path between satellite and ground station, and the speed of the satellite over the earth's surface with associated pointing and tracking problems. The requirement for a daily satellite pass over the target area restricts the earth station to receive locations under the satellite path also. A direct satellite download to a mobile earth station would unnecessarily restrict the earth station receive locations to areas under the satellite path and ahead of the target zones. With 16 daily orbits, the satellite would shift relative longitude position by 22.5 degrees for each orbit.

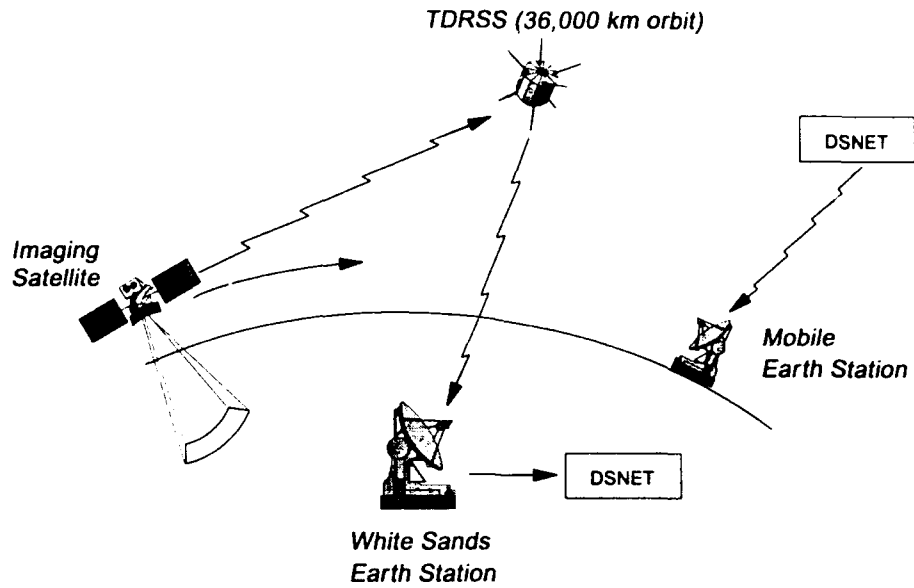


Figure 4.8.1. Data Download Geometry

For most LEO orbits under consideration, the satellite speed over the ground is approximately 7.8 km/sec (see Figure 4.8.2).

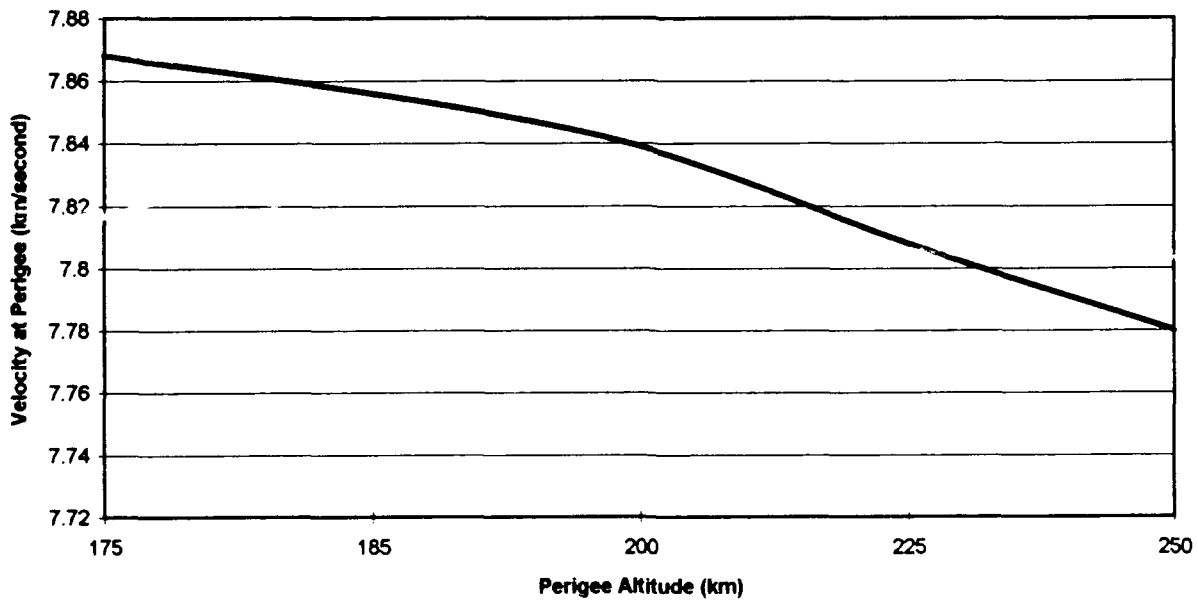


Figure 4.8.2. Velocity Over Earth at Perigee

NASA TDRS

The space network (SN) segment of the NASA TDRS satellite system can provide control, tracking and data acquisition for the satellite throughout most orbits between 200 km and 1,200 km above the earth. The TDRS system will support data rates of up to 150 megabits per second (MBps) (coded) and 300 MBps uncoded.

The inter-orbit link (IOL) provides the requirements for forwarding image data to the TDRS circuit, and will place demands on the LightSat for power and space utilization. The TDRS to VSAT downlink requirements will affect the power requirements and portability of the mobile earth station. The IOL will utilize a 15 gigahertz (GHz) carrier frequency, which is one of many ITU bands for an IOL. In hypothetical future versions possibly operating at 60 GHz, the strong 60 GHz absorption characteristic of the earth's atmosphere (20 dB/nm) will protect the link from terrestrial interference. The current two-satellite TDRS system (TDRS-East and TDRS-West) can provide both the forward service (spacecraft, command, control and housekeeping) and the return service (image data telemetry) to the LEO satellite. The TDRS system can support multiple simultaneous users during a hostile engagement, but access to the system would be expected to be prioritized for users. There are only a few restrictions on the availability of TDRS (blind spots, solar interference, and terrestrial interference), and these will be explained in a later section of this report.

TDRS Configuration

The TDRS satellites are located at 171 degrees west longitude (TDRS-West) and 41 degrees west longitude (TDRS-East) as shown in Figure 4.8.3. Each TDRS satellite offers both S-band and K-band services; the proposed imaging satellite would use the K-band service frequencies (13.775 GHz forward and 15.003 GHz return), which are designed for high data rate users as shown in Figure 4.8.4. The TDRS single access service at K-band provides up to 25 MBps forward and 300 MBps return. Each TDRS satellite can provide two simultaneous K-band forward services and two simultaneous K-band return services. The current TDRS system can be used to control the imaging spacecraft and to bring coded image data to the ground at 150 MBps per second. A choice of forward service data rates from the TDRS K-band transponder will determine the imaging spacecraft G/T figure of merit (Figure 4.8.5). On the return link, the required telemetry data rate will determine the receive power at TDRS and hence the transmit power from the imaging satellite (Figure 4.8.6).

The NASA *Space Network User's Guide*¹⁵ describes the required system approval process, and documents required before a user spacecraft can gain access to TDRS.

TDRS Link Budget

The TDRS link budget assumes that satellite command and control will be performed by large ground stations outside the battlefield area. The tactical battlefield commander will utilize current satellite earth station or land-based telecommunications resources of the Defense Department. The LEO imaging satellite will forward data to the TDRS space segment, which will supply the downlink to the NASA Earth Station at White Sands, New Mexico. From White Sands, the data can be passed into the Defense Department network DSNET. The important link budget is the space segment for the satellite-to-TDRS (interorbit link).

¹⁵*Space Network User's Guide*, NASA Goddard Space Flight Center, Greenbelt, Maryland, September 6, 1988.

The specific requirements for link budgets are driven by the anticipated telemetry data rate for satellite image data. Each of the three CCD arrays (3 bands of data) of 2,000 x 3,000 pixels (at 12 bits) will produce 9 Mbytes per band for a total of 27 Mbytes. The physical properties of the Kodak CCD focal plane array require the data to be read out from the array in less than 1 second, for an expected maximum real time data rate of 27 Mbytes per second MBps. With onboard memory in a store-and-forward architecture, the 27 MBps data rate can be regarded more as an upper limit than as a required continuous download rate. The 27 MBps data rate corresponds to a 216 MBps data rate.

Link Budget Calculations

Link budgets have been calculated for the forward service and the return service through TDRS. The tabulated budgets are shown below.

Forward Service: The forward service performance is expressed in terms of achieving a sufficient Bit Energy to Noise Spectral Density (E_b/N_0) at the imaging satellite to match the TDRS required command channel performance of $BER = 10^{-5}$. This required E_b/N_0 value will determine the spacecraft figure of merit G/T (receive antenna gain/system noise temperature).

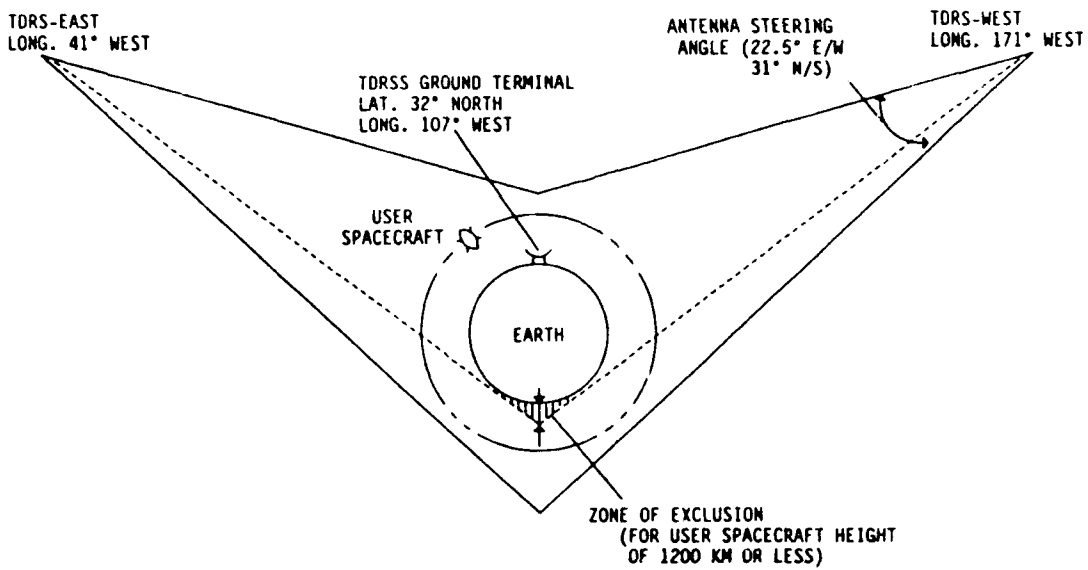


Figure 4.8.3. Tracking and Data Relay Satellite System

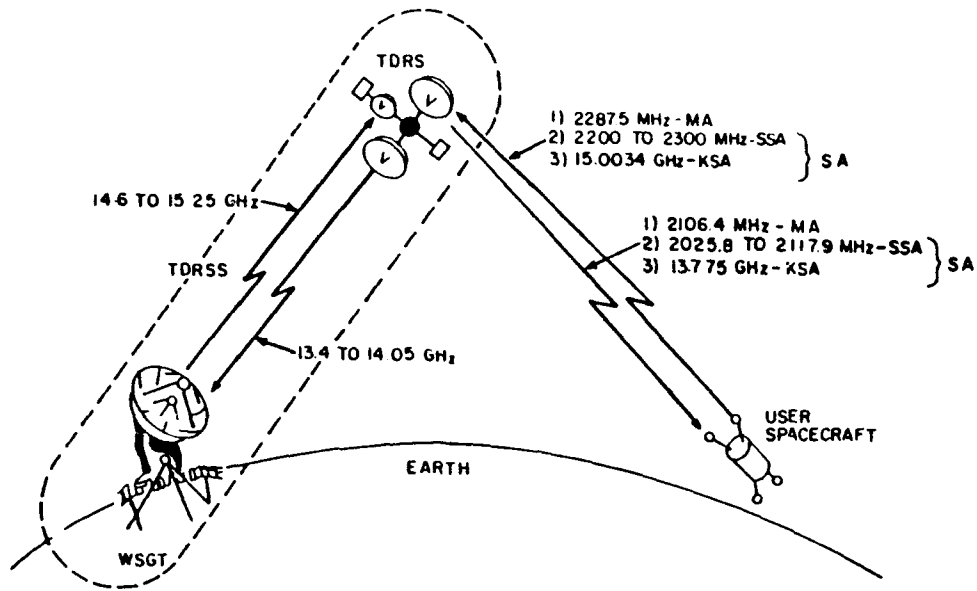


Figure 4.8.4. TDRS Forward and Return Service Frequency Plan

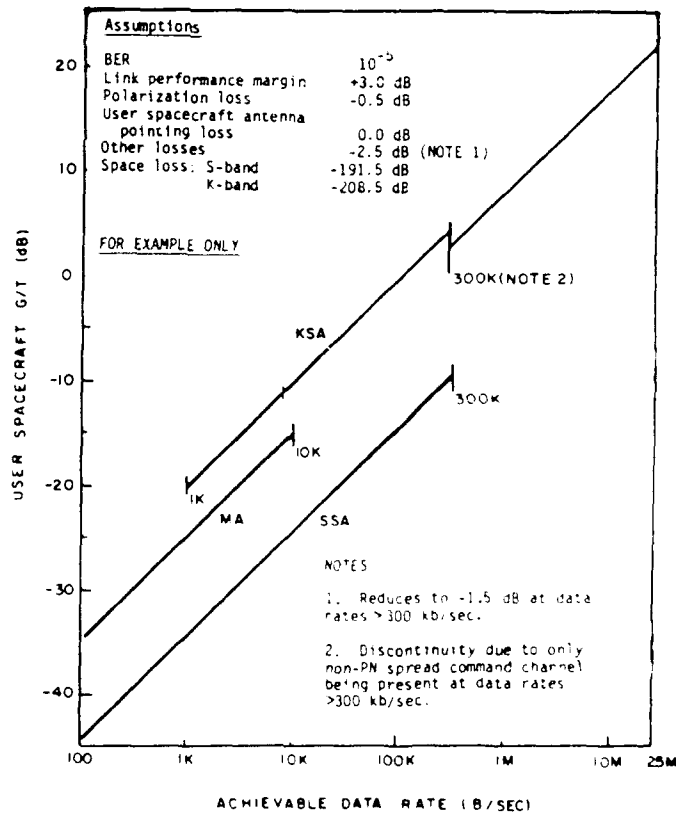


Figure 4.8.5. Typical User Spacecraft G/T Versus Achievable Data Rate Forward Services

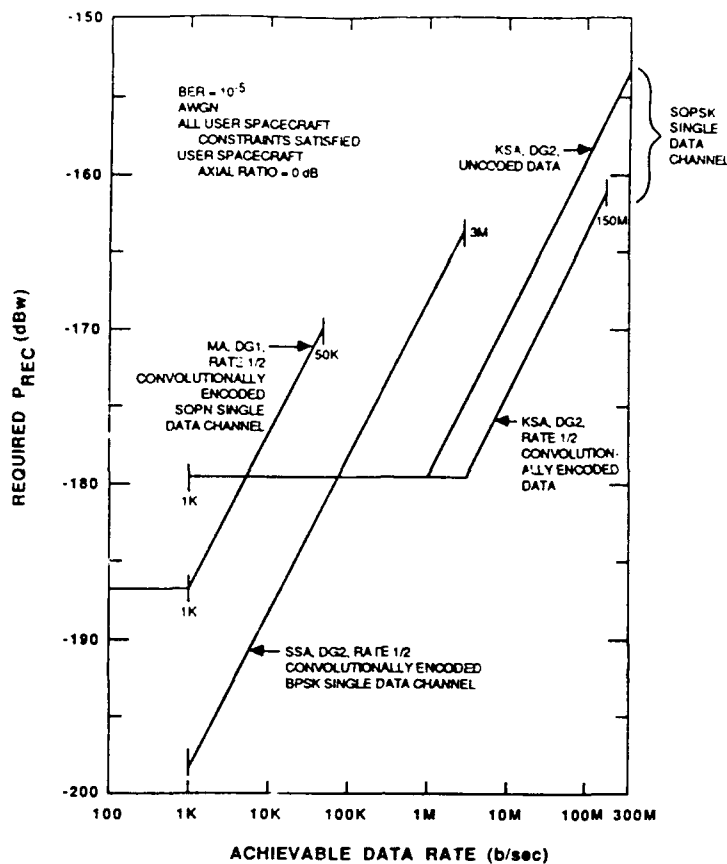


Figure 4.8.6. Required Received Power at TDRS (P_{rec}) versus ADR: Return Services

The forward link data rate will be built up from a collection of daily instructions for course correction, camera pointing, system status checks and other routine functions as shown in Table 4.8.1, Figure 4.8.7, and Table 4.8.2.

Table 4.8.1. FORWARD SERVICE DATA BUDGET

Operation	Data Rate	Items
Status Query	1,000 bps	Battery, fuel, location, time
Camera Pointing Instructions	1,000 bps	Targets, default settings
Orbital Corrections	500 bps	Thrusters
Memory Management	500 bps	Store and forward
Data Download Instructions	2,000 bps	Format, scheduling, TDRS assignment
TOTAL --->	5,000 bps	
MARGIN -->	5,000 bps	
MAX DATA RATE	10,000 bps	

- Assumptions:
- 13.775 GHz = Transmit frequency
 - 10000 bits/s = Data rate
 - 45,890 km = Inter-satellite range (worst case)
 - TDRS EIRP = 46 dBW (normal mode)
 - BPSK = Modulation
 - 209.2 dB = Free space loss
 $-(32.45 + 20 \log R + 20 \log f)$
 - 228.6 = Boltzmann constant (dBW hz-k)
 - 1 dB = Polarization mismatch loss
 - 1 dB = Antenna pointing loss
 - 3 dB = Minimum link margin
 - 9.9 dB = BPSK BER of 10^{-5}

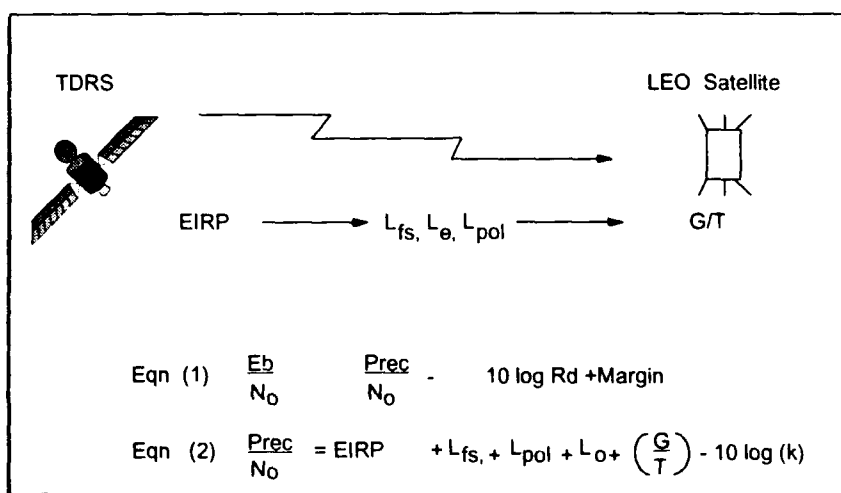


Figure 4.8.7. Forward Service Link

Table 4.8.2. FORWARD SERVICE LINK BUDGET

E_b/N_o	9.9	dB
Data Rate	40	dB
Link Margin	3	dB
Power Received/ N_o	52.9	dB
EIRP	-46	dBW
Free Space Loss	209.2	dB
Polarization Loss	1	dB
Pointing Loss	1	dB
Boltzmann Constant	-228.6	dBW (hz-k)
Satellite — Figure of Merit	-10.5	dB/K

Return Service: For the return service, the imaging spacecraft effective isotropic radiated power (EIRP) must be calculated to provide sufficient return power to the TDRS satellite receiver to achieve the required data rate at a bit-error rate (BER) of 10^{-5} (Figure 4.8.8 and Table 4.8.3).

Assumptions:	15.003 GHz	= Transmit frequency
	150 Mbits/s	= Telemetry data rate
	45,890 km	= Inter satellite range (worst case)
	-160 dBW	= Power at TDRS receive antenna (for 150 Mbps rate)
	SQPSK	= Mode "DG2" modulation
	209.2 dB	= Free space loss -(32.45 + 20 log R + 20 log f)
	-228.6	= Boltzmann constant (dBW hz-k)
	1 dB	= Polarization mismatch loss
	1 dB	= Antenna pointing loss
	3 dB	= Minimum link margin
	20%	= DC to RF amplifier efficiency

$$\frac{4 \pi A \rho}{\lambda^2} = \text{Antenna gain}$$

$$\rho = .63 \text{ antenna efficiency}$$

$$65 \lambda / d = \text{Antenna beamwidth (degree)}$$

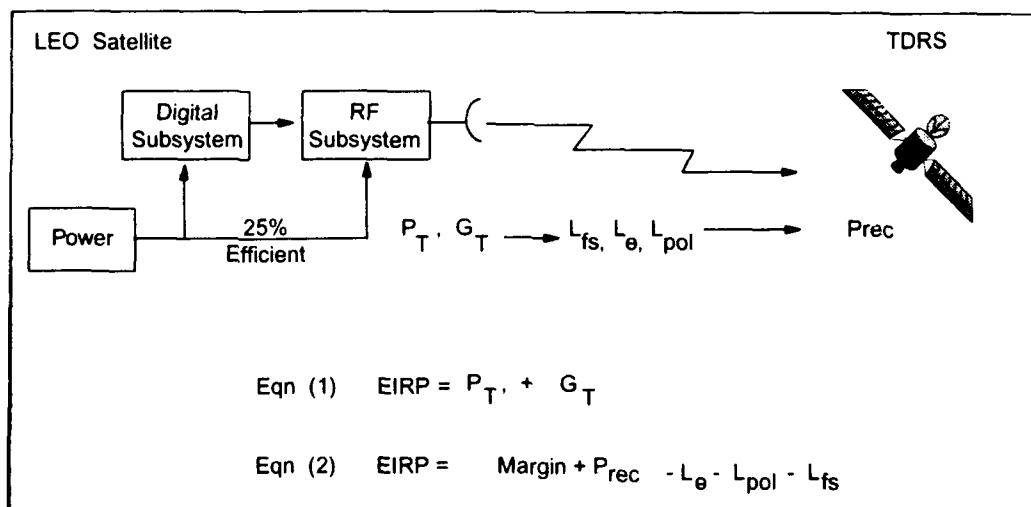


Figure 4.8.8. Return Service Link

Table 4.8.3. RETURN SERVICE LINK BUDGET

Power Received at TDRS	- 160	dBW
Free Space Loss	208.5	dB
Link Margin	3	dB
Polarization Loss	1	dB
Pointing Loss	1	dB
EIRP	53.5	dBW

A range of values of satellite transmit Antenna Gain and Transmitter Power will meet the EIRP requirement of the link calculation for any given data rate that must be supported. The K-band transmit antenna Gain and Power values for several data rates are given in Table 4.8.4.

Table 4.8.4. RETURN SERVICE K-BAND ANTENNA REQUIREMENTS

Achievable Data Rate	Power Received at TDRS	EIRP of Satellite	Tx Gain of Satellite Antenna	Diameter (D) and Beamwidth (BW)		DC Power (@ 25 % Efficiency)
				D (m)	DW (deg)	
150 MBps	-160 dBW	53.5 dBW	38 dB	.5	3 deg	142 watts
50 MBps	-166 dBW	47.5 dBW	33 dB	.2	8 deg	113 watts
10 MBps	-174 dBW	39.5 dBW	28 dB	.1	14 deg	56 watts

TDRS Limitations

There are several limitations to the availability of the TDRS system to downlink telemetry or send commands to the satellite. These limitations will affect the timeliness of imagery telemetry, but the effects will not be significant. The first limitations in TDRS availability are blind spots due to the geometric constraints of the viewing angle between TDRS and the LEO satellite (Figure 4.8.9). For a satellite between above 200 km in a near polar orbit, exclusion zones will appear only for certain parts of the orbit over the Southern Hemisphere, preventing telemetry for less than 7 percent of the orbit. The exclusion zone will prohibit satellite contact while over India and Pakistan as shown in Figure 4.8.10.

Additional coverage constraints are due to flux density restrictions on TDRS-to-satellite or satellite-to-TDRS transmission at low angles in the direction of the earth. There also are limitations due to interference effects of the sun or terrestrial transmitters. There is no forward service when the sun is within 1 degree of the TDRS boresight.

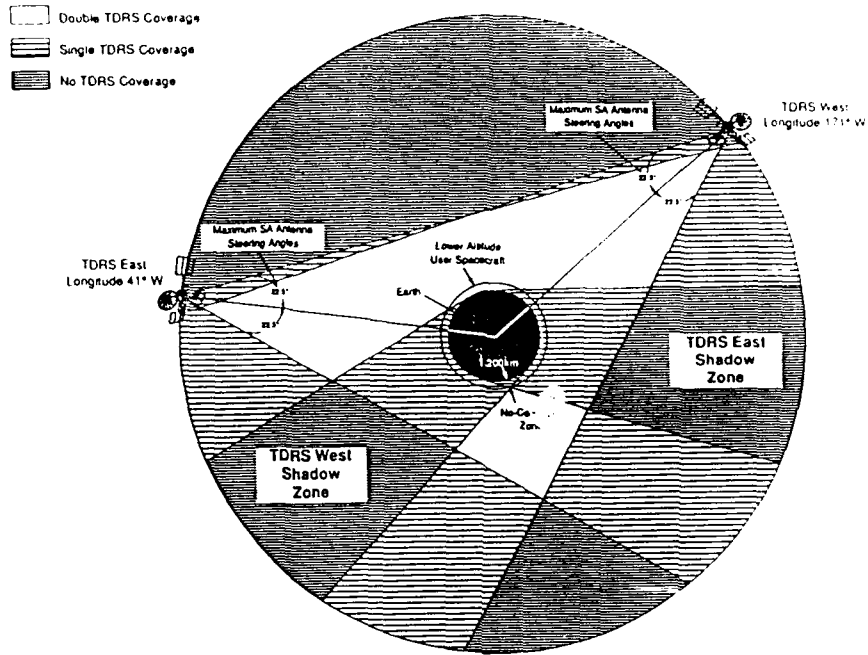


Figure 4.8.9. TDRS Lower Coverage Zone Geometry, User Spacecraft Altitudes Less Than 1200 km

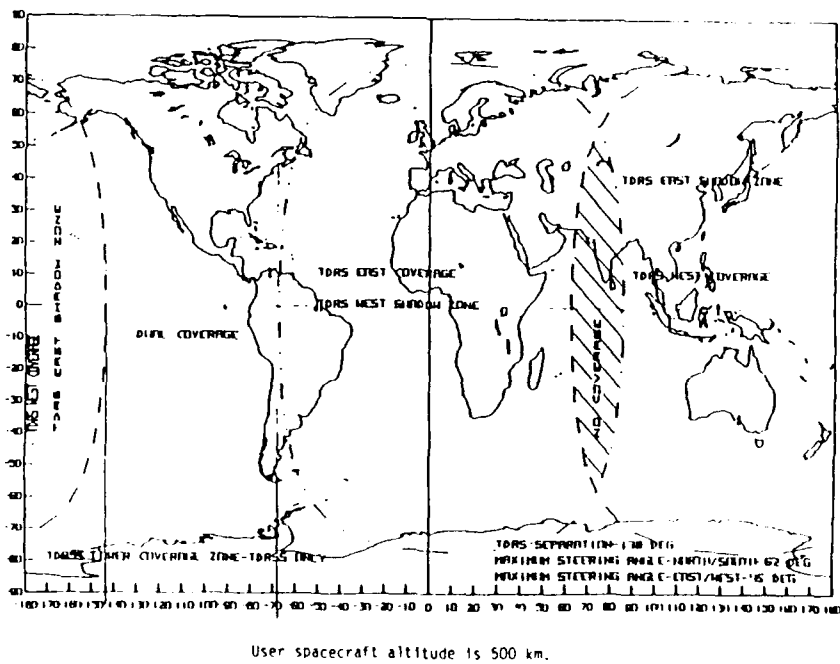


Figure 4.8.10. TDRS Lower Coverage Zone

5. SATELLITE SPECIFICATIONS AND DESIGN

5.1 Satellite Basing and Configuration

Satellite Basing

Tactical operations generally require both a wide area search and a target identification capability. If both capabilities are required on the same satellite, the design constraints are enormous. For example, tactical operations frequently require searching large areas for the presence of armed units. Identification may require ground-based resolution of 1.5 meters. A 20 km x 20 km image with 1.5 meter GBR, three spectral bands, and 12 bits dynamic range contains:

$$N = \left[\frac{20 \times 10^3}{1.5} \right]^2 * 3 \text{ spectral bands} * 12 \text{ bits}$$

$$N = 6.4 \times 10^9 \frac{\text{bits}}{\text{images}}$$

The tactical user might require as many as 20-30 images in a time period under one minute. For 25 images with a 2:1 data compression, the satellite would have to have a downlink bandwidth of:

$$B\omega = 25 \text{ images} * 6.4 \times 10^9 \frac{\text{bits}}{\text{images}} * \frac{1}{2 \text{ data compression}} * 2 \text{ Nyquist limit} * \frac{1}{60 \text{ sec}}$$

$$B\omega = 2.66 \text{ GHz}$$

Even if the data were stored and then transmitted, this is far in excess of the capabilities of tactical commanders to receive and process the information.

A more practical solution is to have two satellites, a wide area search satellite, and a moderate resolution satellite. The capabilities of the satellites would be as shown in Tables 5.1 and 5.2.

Table 5.1. WIDE AREA SEARCH TACTICAL SATELLITE

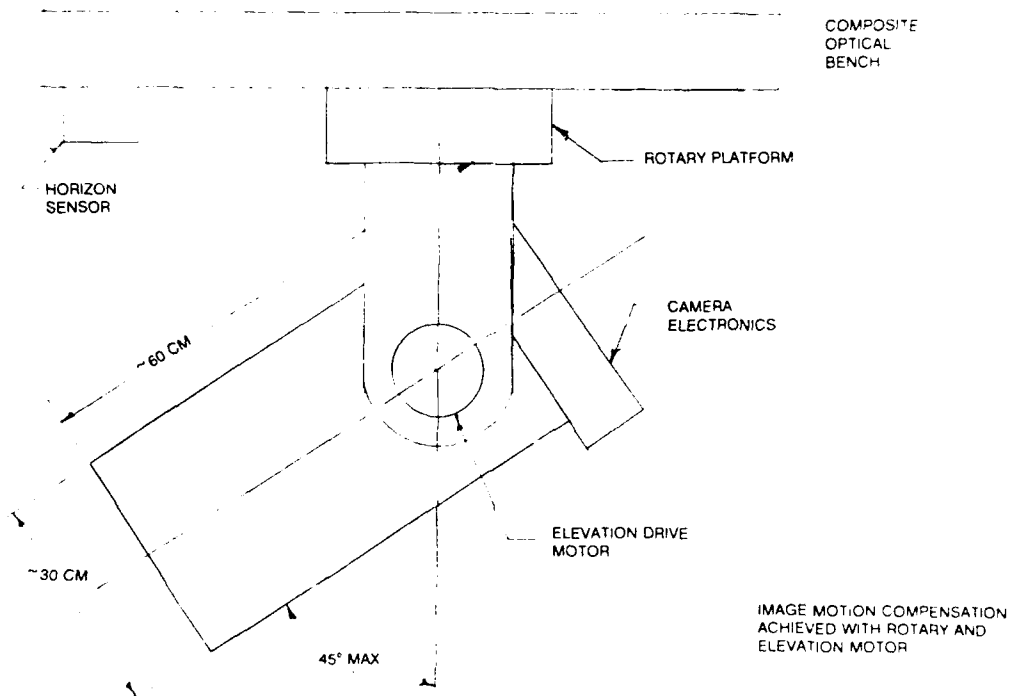
Image Size	10 km x 15 km
Ground-Based Resolution	5.0 meters
Three Spectral Bands	From 0.4 to 1.1 microns
Imaging Rate	One image every 1.5 seconds
25-50 Images Onboard Storage	
Two Passes per Day (1 night)	
Swath Width	300+ km

Table 5.2. MEDIUM RESOLUTION TACTICAL SATELLITE

Image Size	3 km x 4.5 km
Ground-Based Resolution	1.5 meters
Three Spectral Bands	0.4 to 1.1. microns
Imaging Rate	One image every 1.5 seconds
25-50 Images Onboard Storage	
Two Passes per Day (1 night)	
Swath Width	300+ km

Satellite Configuration

The proposed layout drawing (Figure 5.1) shows the telescope mounted on a rotary platform attached to the optical bench. This configuration allows the telescope optics to pivot in both azimuth and elevation. On top of the optical bench the other components are mounted as shown in Figure 5.2. These components include computer, star tracker, momentum wheel, thruster, fuel for maneuvering and the communications package.



Figures 5.1. Satellite Telescope

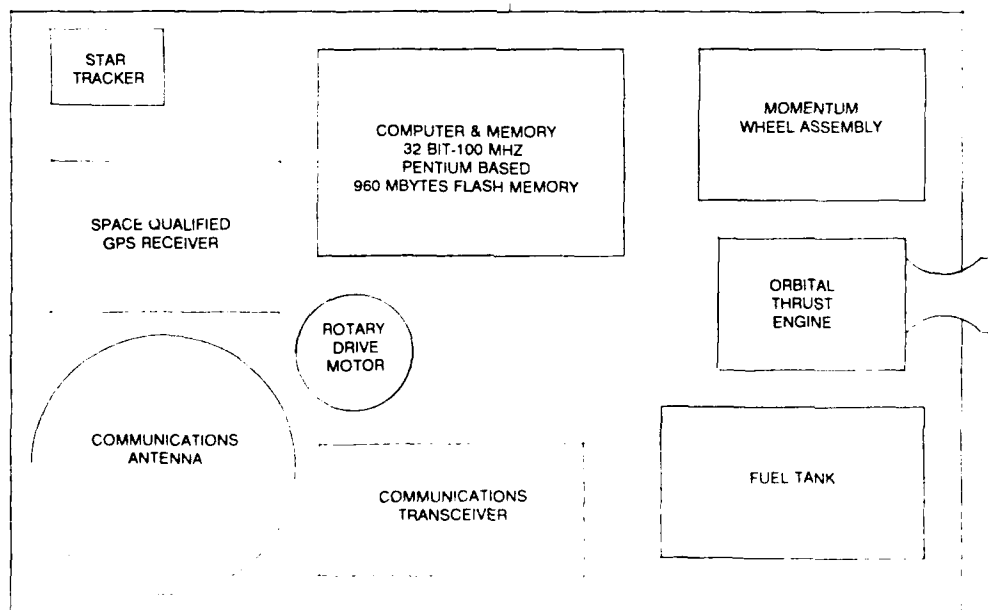


Figure 5.2. Satellite Component Layout

5.2 Telescope Configuration

The length of the camera is a function of the telescope configuration. Because of the requirement for the system to have a wide bandwidth ($0.4\text{-}1.0\ \mu$), a reflecting configuration rather than a refractor was required.

The overall length of the telescope is a function of how many reflecting surfaces can be used while still minimizing distortion. A common configuration is the Cassegrain configuration, or the Richey-Cretien. See Figure 5.2.1. It is possible to shorten the camera length even further by using a triple-folded system. See Figure 5.2.2.

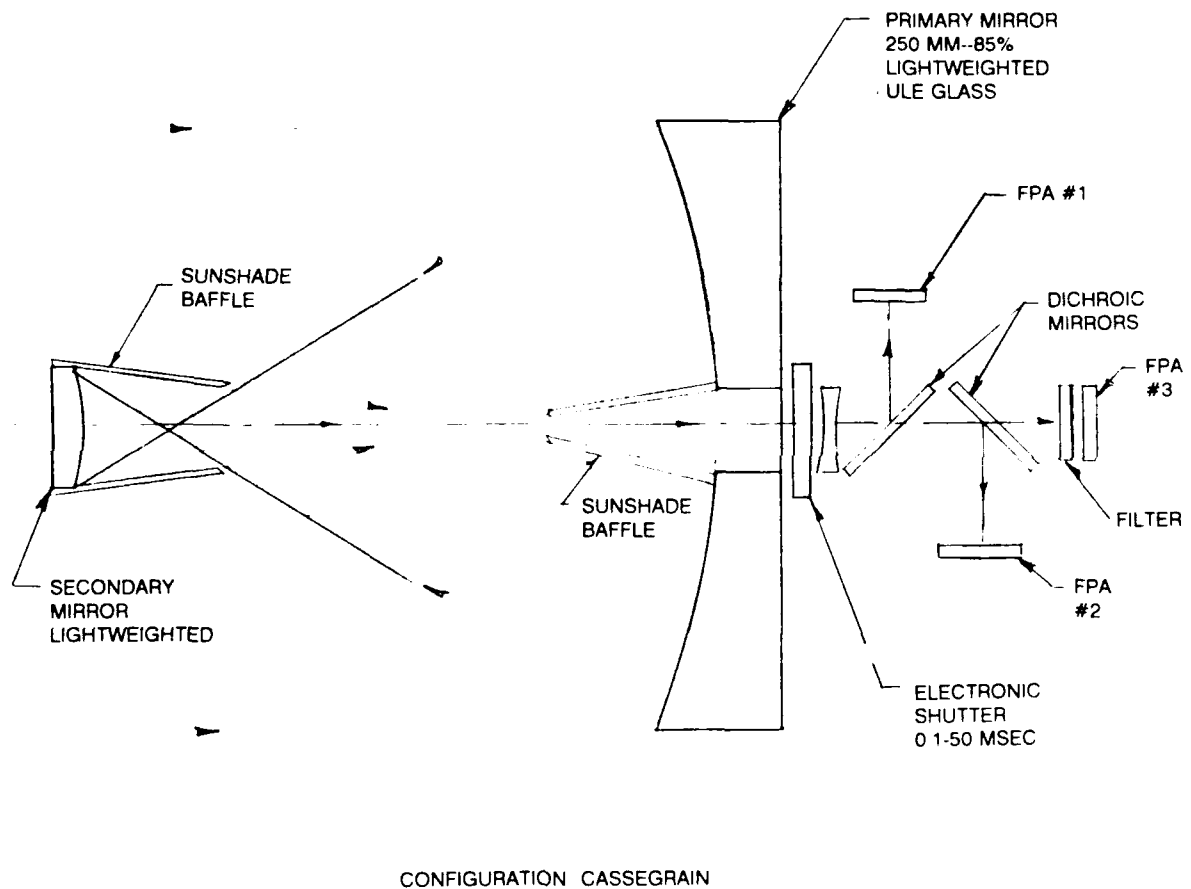


Figure 5.2.1. Cassegrain Telescope Configuration

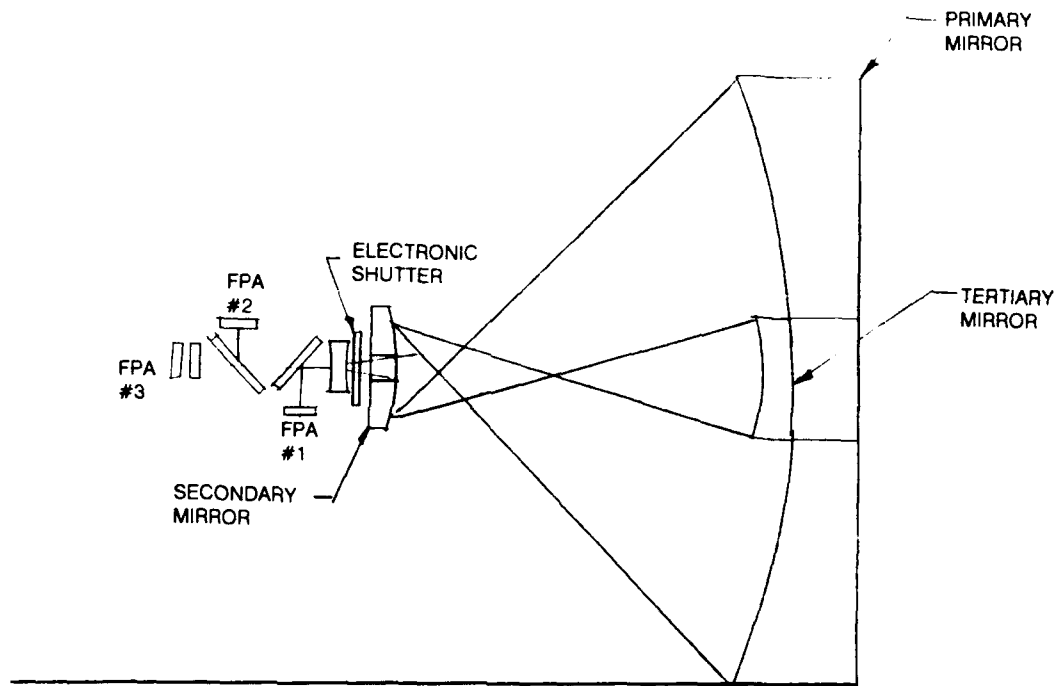


Figure 5.2.2. Triple-Folded Telescope

A Cassegrain configuration with the variable shutter located behind the primary mirror would be simple to construct, and the location of the sensors behind the primary mirror would simplify the alignment. This is especially important for multispectral imaging, where separate sensors are used for each of the optical bands.

By using two dichroic reflectors and a band pass filter a three-band multispectral image can be created. The image is formed by opening the shutter for a period of 0.1-25 ms. Depending on lighting, after the shutter is closed, each of the sensors is read out over a period of approximately 0.5-1 second. The sensors may require cooling to 250 K to minimize noise.

5.3 Optical Platform

The optical platform upon which the telescope is mounted is a critical item. All the alignment between the attitude sensors, star trackers, horizon sensors, and the camera relies on a rigid, thermally stable platform. High slew rates for the camera can only be accomplished with a very stiff platform and a superb attitude control system.

Traditional optical platforms for nonspace applications were built from Invar and other low coefficient of expansion metal alloys. For space applications, the low expansion metal alloys are being replaced by composites. However unlike most composite applications, the thermal mechanical properties are critical. The new composites have substantially reduced the weight of space structures, but not without problems. The composites used in the Hubble Telescope continued to outgas longer than expected and the resulting deformation was greater than expected.

A tactical imaging satellite does not have as critical a stability requirement as did the Hubble Telescope; however, the proper choice of materials is still important. Fortunately much of the work carried out for fabrication of light-weight mirrors can be applied to the other structural components. Wendt and Misra use a graphical technique (Figure 5.3.1) to demonstrate a figure of merit for critical optical space components.¹⁶

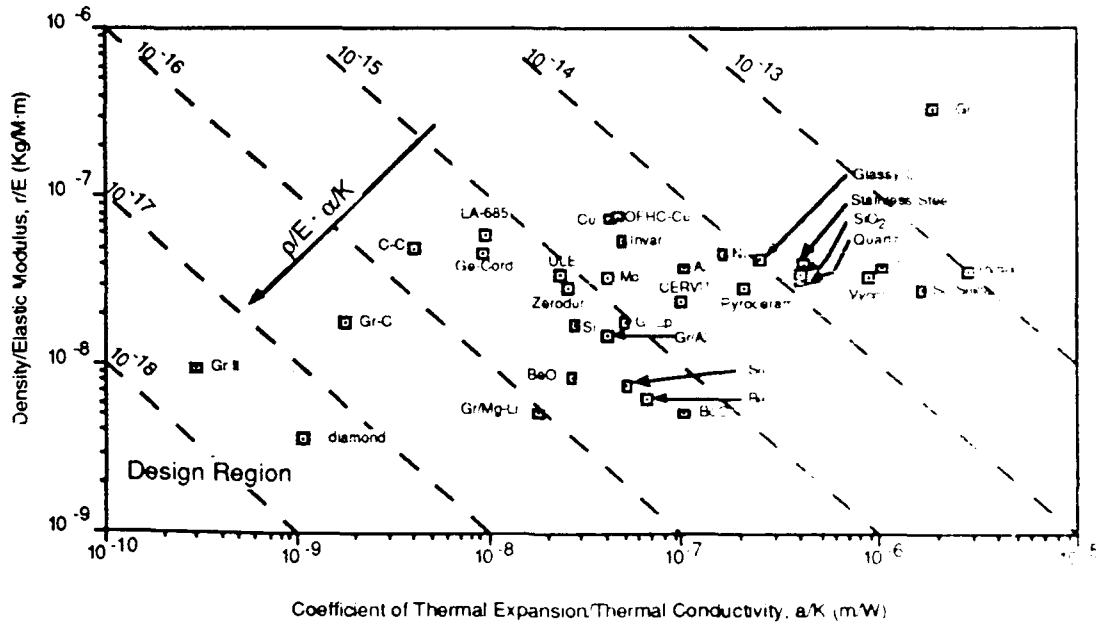


Figure 5.3.1. Figure of Merit for Optical Components

5.4 Link Budget

The available space in the Pegasus launch vehicle can probably not accommodate a half-meter diameter K-band antenna. The following calculations assume a .3 meter antenna diameter, and the antenna is used for both transmit (return service) and receive (forward service).

Command Link (Forward Service from TDRS)

As shown in section 4.8, the satellite figure of merit for the forward service must be -10.5 dB/K or more. The antenna gain from a .3 meter parabolic antenna is 37 dB at K-band and the system noise temperature is the sum of the antenna noise temperature and the effective input noise temperature of the receiver, which is primarily due to the low-noise amplifier. A typical system noise temperature easily attainable today is 250 K, giving an adequate figure of merit to provide the required BER for the forward service.

$$G/T = 37\text{dB} - 24 \text{ dB-K} = 13 \text{ dB/K}$$

¹⁶R. Wendt and M. Misra, "Fabrication of Near Net Shape Graphite/Magnesium Composites for Large Mirrors," *Advances in Optical Structure Systems*, SPIE, Vol. 1303, 1990.

Telemetry Link (Return Service to TDRS)

A range of values for transmit antenna gain and transmitter power can satisfy the EIRP requirements to achieve acceptable data rates through TDRS. The transmit antenna is assumed to have a .3 meter diameter, and a gain of 37 dB. The RF subsystems are assumed to be 25 percent efficient, so that the power ratings in Table 5.4.1 are four times the required output power at the satellite transmit antenna.

Table 5.4.1. RETURN SERVICE POWER AND GAIN REQUIREMENTS

Achievable Data Rate	Power Received at TDRS	EIRP of Satellite	Tx Gain of Satellite Antenna	DC Power (@25% efficiency)
150 MBps	-160 dBW	53.5 dBW	37 dB	178 watts
50 MBps	-166 dBW	47.5 dBW	37 dB	45 watts
10 MBps	-174 dBW	39.5 dBW	37 dB	7 watts

The power rates in the table represent the peak DC power rate that is consumed by the communication system during transmission of telemetry data. The average power consumed by the satellite transmitter will be considerably less since transmission takes place only for several minutes per day. For example, if 20 images are recorded on a pass over the target in a single day, and each image is 2,000 x 3,000 pixels @ 12-bits each = 72 Mbits per image, and 3-bands per multispectral image. The data volume is:

$$V = 20 \times 72 \times 3 = 4320 \text{ megabits per day}$$

The time required to transmit this data volume at the three telemetry rates is shown in Table 5.4.2.

Table 5.4.2. EFFECTIVE DATA TRANSMISSION TIMES

Telemetry Rate	Time to Transmit Data	Effective Duty Cycle
150 Mbps	30 seconds	.00003
50 Mbps	86 seconds	.00099
10 Mbps	432 seconds	.005

From this table it is clear that the data time-latency for a large image telemetry downlink (20 images @ 3 bands each) is 432 seconds or less than 8 minutes. The image downlink telemetry rate represents a greater demand on the satellite battery system for peak power than on the solar collectors for average power.

The IOL provides the requirements for forwarding image data to the TDRS circuit, and will place demands on the LightSat for power and space utilization. The IOL will utilize a 15 GHz carrier frequency, which is one of many international telecommunications union (ITU) bands for an IOL.

In hypothetical future versions possibly operating at 60 GHz, the strong 60 GHz absorption characteristic of the earth's atmosphere (20 dB/nm) will protect the link from terrestrial interference. The LightSat IOL transmit antenna can track the geostationary TDRS satellite using established techniques.

5.5 Earth Station

In the high data rate downlink configuration described in this report, two ground stations are part of the complete link from the imaging satellite to the tactical user in theater. The first ground station is controlled by NASA and is located at White Sands, New Mexico. The NASA White Sands ground station is the direct telemetry downlink receive system from TDRS (return link). Once the image telemetry is received at White Sands, the image data would be immediately linked into the Defense Department global network (DSNET). The tactical users in theater would have access to DSNET through communications equipment that is currently deployed. The data throughput rates to many tactical users continue to be inadequate for receiving high resolution image data.

Considering that many disadvantaged receivers on the ground may be limited to receive rates of 56 kbps, each image band may take several hours to receive. If the circuit connection time is unavailable or if the user has less than 56 kbps available for receive, the original image can be compressed or processed into an *imagery derived product*, with a lower information content and shorter transmission time. The transmission of *imagery derived products* rather than original image products will become necessary as more digital images must be transmitted to and around the battlefield with restricted receive bandwidth.

BIBLIOGRAPHY

- Cambel, A. B., and B. H. Jennings. *Gas Dynamics*. New York: Dover Publications, Inc., 1958.
- "Compression of UoSAT-5 EIS Images." *Small Satellite Technology & Applications-3*. Montpetit & Prieur, Spar Aerospace Ltd., Quebec, Canada, April 1993.
- Handbook of Chemistry and Physics*, 63rd ed., 1990.
- Harris, Ray. *Satellite Remote Sensing*. London and New York: Routledge Kegan Paul, 1987, p. 51.
- Heitchue, R.D., Jr., ed. *Space Systems Technology*. New York: Reinhold Book Corporation, 1968.
- New York Times*, March 11, 1994.
- NITFS Military Handbook*. DISA Joint Interoperability and Engineering Organization, June 18, 1993.
- Pegasus Payload Users Guide*. Orbital Sciences Corporation, May 1991.
- "Proceedings of the International Society for Optical Engineering." *Small Satellite Technology & Applications-3*. Montpetit & Prieur, Spar Aerospace Ltd., Quebec, Canada, April 1993.
- "Transmitting and Controlling Images from Small Satellites Using MPEG Image Compression." *Small Satellite Technology & Applications-3*. LeFevre & Heiberger, Cynetics Corp., April 1993.
- Scenario Gists*. TRADOC Analysis Center, Fort Leavenworth, Kansas, August 1993.
- Smith, W. *Modern Optics/Engineering — The Design of Optical Systems*. 2nd ed. New York: McGraw-Hill, 1990.
- Space Network User's Guide*. NASA Goddard Space Flight Center, Greenbelt, Maryland, September 6, 1988.
- Wendt R., and M. Misra. "Fabrication of Near Net Shape Graphite/Magnesium Composites for Large Mirrors." *Advances in Optical Structure Systems*. SPIE, Vol. 1303, 1990.

Appendix A
HUGHES SBRC REPORT



HUGHES

SANTA BARBARA RESEARCH CENTER
a subsidiary

MINE DETECTION DATA COLLECTION
SUBCONTRACT 5034-1

FINAL REPORT

15 February 1993

Prepared by the Santa Barbara Research Center
For The Future's Group
(USATEC Contract DACA76-92-C-0030)

Table Of Contents

Section 1: Summary

- MDDC Program Summary
- References

Section 2: Data Collection

- Review of Flight System
- Planning
- Parameters

Section 3: Spectral Data Processing

- Scene Selection for Rectification and Processing
- Spectral Data Processing Results
- Conclusions

Section 4: Attachments

1. Statement of Work, Subcontract 5034-1 (DACA76-92-C-0030)
2. WIS Flight System Review
3. 35 mm Photographs of Ostrich Site (3 total, one sent under separate cover, reference 5) and site sketch.
4. Aircraft Reference Video Tape of Data Collection (sent under separate cover, reference 5)
5. Photographs of Spectral Images from Display (16 total)
6. Math files of processed spectra from Image File 770 (Section 3 graphics)
7. 9-Track Digital Tape, Corrected Image File 770, Ostrich Site (1/2 m GSD)

Section 1

Mine Detection Data Collection (MDDC) Program Summary

Summary of Experiment Goals and Results:

The Futures Group of Glastonbury Connecticut contracted with SBRC for an airborne data collection experiment with the same configuration Visible and Near Infrared (VNIR) Wedge Imaging Spectrometer (WIS) instrument as was flown for both the DARPA and DNA data collections of mid 1992. The ultimate customer was the US Army Topographic Engineering Center (USATEC), Fort Belvoir VA. SBRC has successfully completed all contractually required tasks on this program within the budget and schedule as defined. Technical results of the post data collection spectral analysis indicate that the data collected is adequate to demonstrate the feasibility of utilizing a Wedge Imaging Spectrometer in this role and to satisfy the technical goals of the experiment.

The experiment had two general goals; the first was to determine if analysis of WIS generated hyperspectral images in this wavelength region (.4 - 1.05 μm) could be used to aid in the identification of a simulated minefield (Project Ostrich Site) established at the Marine Corps training center at 29 Palms, CA, during late 1990. The second goal was to determine if an airborne hyperspectral imager operating in this wavelength region could distinguish differences between the long term surface dirt and earth which was disturbed immediately prior to data collections. These two principle goals of the experiment were satisfied in that both the older periodic furrows of Ostrich Site and the newly excavated trenches located immediately adjacent to the northern site boundary were readily identifiable in the data. In addition, a clear spectral difference was identified between the typical surface sand and the fresh trench region. This difference becomes apparent between 750 and 950nm, outside the visible region.

The presence of the older furrows and the specific spectral differences identified in the data do not in themselves offer proof that periodically spaced rows and freshly disturbed earth can be detected by an automated detection algorithm, however, it is a clear indication of the feasibility of such a detection. It is SBRC's expectation that this detection would be substantially more reliable in the short wave infrared, somewhere in the 1000 - 2500nm region. This is so because the phenomenology of freshly disturbed earth, based upon detection of moisture content and minerals not yet bleached by the sun, appears much stronger in this spectral region.

References: The following references define the essentials of the program. In particular reference 1 provides the cost basis of SBRC efforts on behalf of this program, reference 2 details SBRC imposed constraints on the deliverable data, reference 3 was the authorization to proceed, reference 4 is the Technical Statement of Work which incorporates the SBRC constraints identified in reference 2 (this is included in this report as Attachment 1), and finally reference 5 identifies technical data forwarded to The Futures Group (TFG) on 2/2/93. This previously delivered technical data and supporting photographs and video tape are considered to be a part of this final report.

1. SBRC Proposal 211/PL4651/92, Mine Detection/Data Collection Study LF81, 8/21/92
2. SBRC Letter to Futures Group, 222/PL4651/92, G. Pomatto to L. Mielauskas, 9/15/92
3. Letter of Contract, L. Mielauskas to J. Burke, received 10/23/92.
4. Subcontract 5034-1 (DACA76-92-C-0030), Received from TFG, 1/27/93.
5. SBRC Memorandum 018/LF81/93, Forwarding of Technical Data, J. Burke to Ken Robinson, 2/2/93.

Section 2 Data Collection

Flight System Review:

A brief review of the WIS VNIR flight system is included in this report as Attachment 2. Also included is a graph which provides correlation of WIS band number and wavelength.

Data Collection Summary:

The MDCC Program Plan was to utilize the existing flight system without modification for a maximum of two weeks aircraft time and twelve flight hours of similar duration, profile, and overall complexity to those data collections previously cited. This specific mission was to gather data on simulated minefields located at the Marine Corps Air Ground Combat Training Center, Twentynine Palms CA. A coordination meeting was held in Tucson, Az, during October of 1992 to discuss details of the effort. The agreed upon schedule targeted 6 and 7 December as the flight dates.

The system was delivered to the aircraft and integrated during the final week of November. Detail Flight Planning was initiated at that time. TFG and USATEC coordinated program activity with the 29 Palms Range Control, identified as "Bearmat". Hughes Aeronautical Operations (HAO) performed mission specific planning and communications frequency coordination with the identified range control function.

Unfortunately, although the WIS flight system was ready, other members of the Futures Group measurement team were unable to support the missions on the originally scheduled dates. As a result the flights were scrubbed and were re-scheduled for 20 & 21 December, the next available dates at 29 Palms. A shakedown flight was conducted on 17 December. The flight crew was kept on standby Sunday the 20th, however, on-site preparations lagged such that the TFG did not authorize launch until the following day. On the 21st of December a total of 18 data runs were accomplished with positive results (Section 3).

A sketch of Ostrich site and associated Topographic map sectional is included in Attachment 3. The site was manned by 6 to ten personnel and a number of vehicles. A large square blue panel was located inside the Northern boundary of the field. Several highly reflective objects were located within the site boundaries. The newly trenched area was identifiable from the air by the system operators, however, the older furrows were not apparent to the aircrew at the speeds and altitudes of the majority of the collection passes. The older furrows do show up nicely in the reference photographs, video, and WIS hyperspectral images. The field itself was marked by 14 inch elliptical silvered balloons, filled with air and secured to mark the site boundaries. Unfortunately none of these balloons was visible from the aircraft. Attachment 3 also contains two 35mm photographs of Ostrich site taken from the aircraft. An additional photograph and an edited reference video (identified in this report as attachment 4 to the final report) were supplied to K. Robinson under a separate cover, see reference 5.

All data collection was with the 55 mm triplet lens. The required GSD was 1/2 meter for the principal data runs. At 1250 ft with the 55 mm lens, this resulted in a ground swath about 64 meters wide, less than the width of Ostrich site for a south to north run. With a maximum data file buffer storage capacity of 900 frames this corresponds to a data ground track 450 meters in length. Secondary runs were also be made at 2500 ft for a 1 meter GSD (swath of 128 meters and 900 meter track). In all cases the flight track was held down the center of the field. A secondary area (identified as Cleghorn pass) was also imaged with a 1 meter GSD. The following table outlines the specific operational data collection parameters for 1/2 and 1 meter GSD's.

Time of Day	GSD	Altitude (ft)	Ground Speed (knts)	# of frames collected	Data Swath
As Required	1/2 m GSD	1250	275	900	64X450m
	1 m GSD	2500	200	900	128X900m

Section 3 Spectral Data Processing

Scene Selection for Processing:

The data was reviewed and geometric rectification was attempted for two 1/2 meter GSD collection passes (768 and 770), one 1 meter GSD collection pass (786), and one 1 meter GSD pass over Cleghorn Pass. The principle points of interest were discussed with the Future's Group prior to extraction of the spectra. These included evaluation of the spectra associated with the surface, newly excavated trench, and blue tarpaulin (ground truth reference). Attachment 4, previously submitted under a separate cover (reference 5), provides an edited video tape reference for the data collection flights. The camera is mounted on the WIS flight structure and shares a common aperture (window) with the WIS. Video of 1/2 and 1 meter GSD data collection passes of both Ostrich site and the Cleghorn pass are included.

Attachment 5 includes a set of 16 photographs of the rectified data sets taken from a monitor display. The first 8 are from file 768, the next 6 from file 770, and the final two were one each file 786 and 774 (Cleghorn Pass). Three types of photographs are included and in all cases these photographs represent subsets of the complete data sets. The long image stripes (93-1-288, 289, 290, 291, and 301) are complete spatial files of selected spectral bands (this attachment also contains the information necessary to correlate wedge filter band number with actual wavelength). For example figure 93-1-289 depicts only 4 of the 64 total bands collected and contained in data file 770. In this case every 10th band (at $\approx 10\text{nm}$ per band) starting with band 20 at the top ($\approx 600\text{nm}$) and ending with band 50 at the bottom ($\approx 900\text{nm}$). The second type of photograph (93-1-286 and 287) provide six "snapshots" (every 5th band, 25 - 45) of a specific spatial location within the indicated data files. The final variety is single band details of specific locations within given data files.

Spectral processing was accomplished utilizing file #770, the most promising data file with respect to the identified customer interests. This data set had the least amount of virtual motion in the image due to variations in aircraft roll during the period of data collection. Aircraft roll degrades the ability of the current generation of geometrical correction software to successfully rectify the 64 separate spectral images collected by the WIS. Data file 770 was collected under partly cloudy conditions around 1: 28 PM on the 21st of December with a 1/2 meter Ground Sample Distance (GSD). This file contains a particularly good look at both the freshly excavated trenches as well as the blue tarpaulin reference.

Spectral Processing Results:

The experiment had two general goals; the first was to determine if analysis of WIS generated hyperspectral images in this wavelength region (.4 - 1.05 μm) could be used to aid in the identification of a simulated minefield (Project Ostrich Site) established late in 1990 at the USMC training center at 29 Palms, CA. The second goal was to determine if an airborne hyperspectral imager operating in this wavelength region could distinguish differences between the long term surface soil and earth which was disturbed immediately prior to data collections. These two goals were satisfied in that both the older periodic furrows of Ostrich Site and the newly excavated trenches located immediately adjacent to the northern site boundary were readily identifiable in the data. In addition, a clear spectral difference was identified between the typical surface sand and the fresh trench region. This difference becomes apparent between 750 and 950nm, outside the visible region.

The following graphs and text summarize the spectral analysis of file 770. A soft copy (IBM format) of all of these data files is provided as attachment 6. The plots (with the exception of figure 1) were all created in MathCAD Version 3.1 on a MAG 386 PC running under Windows 3.1; this MathCAD worksheet could also be run under MathCAD for the Macintosh. Attachment 7 is a 9 track tape of data file 770 (corrected for offset, gain, and solar).

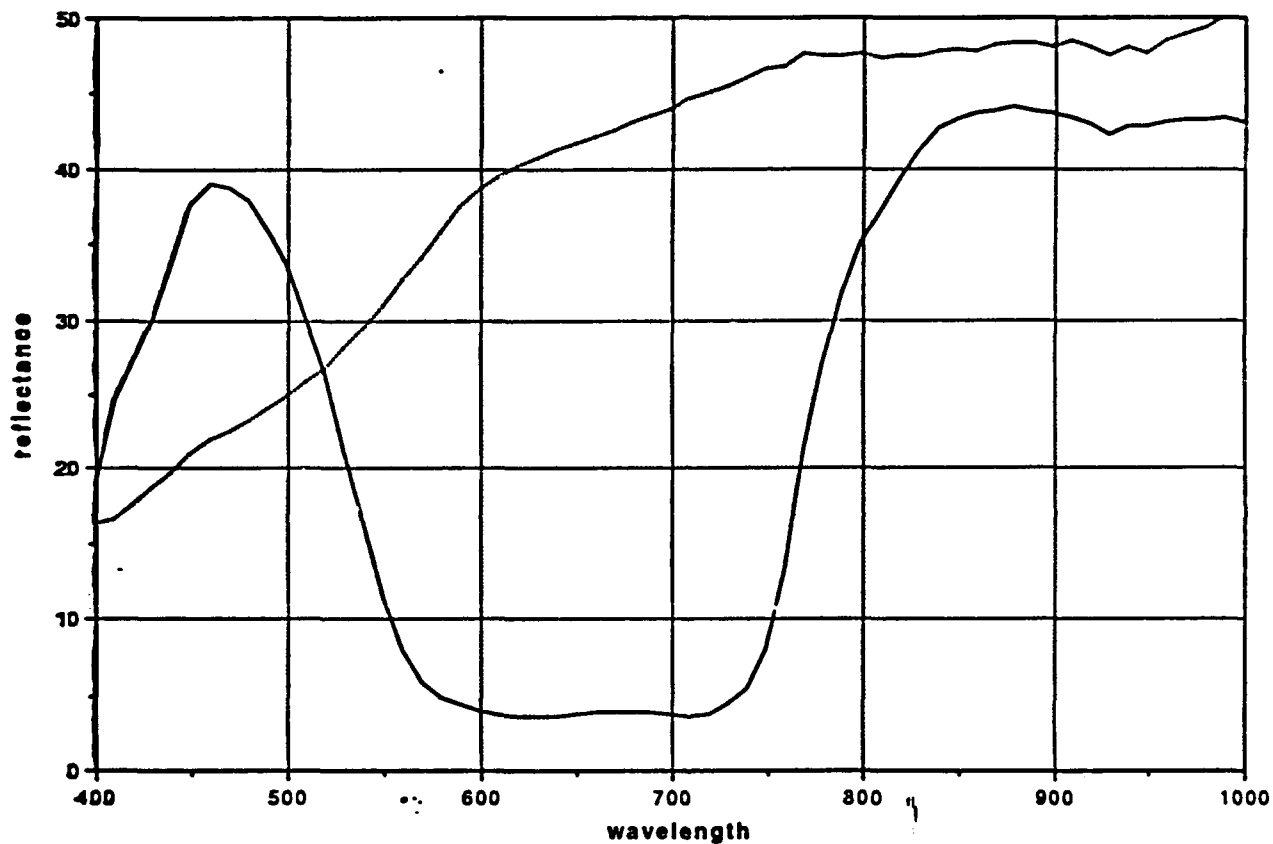


Figure 1: "Ground Truth" Data as supplied by USATEC

This plot shows a slightly smoothed version of the data supplied by the Topographic Engineering Center as the measured ground truth from the Twentynine Palms site on 21 Dec 92. The solid curve is the Blue Tarpaulin (K-Mart special), and the dotted curve is of nearby sand. These curves were created by scanning the original plots supplied by USATEC into a Macintosh, and digitizing with FlexiTrace, and then recreating them with Cricket Graph on the Macintosh.

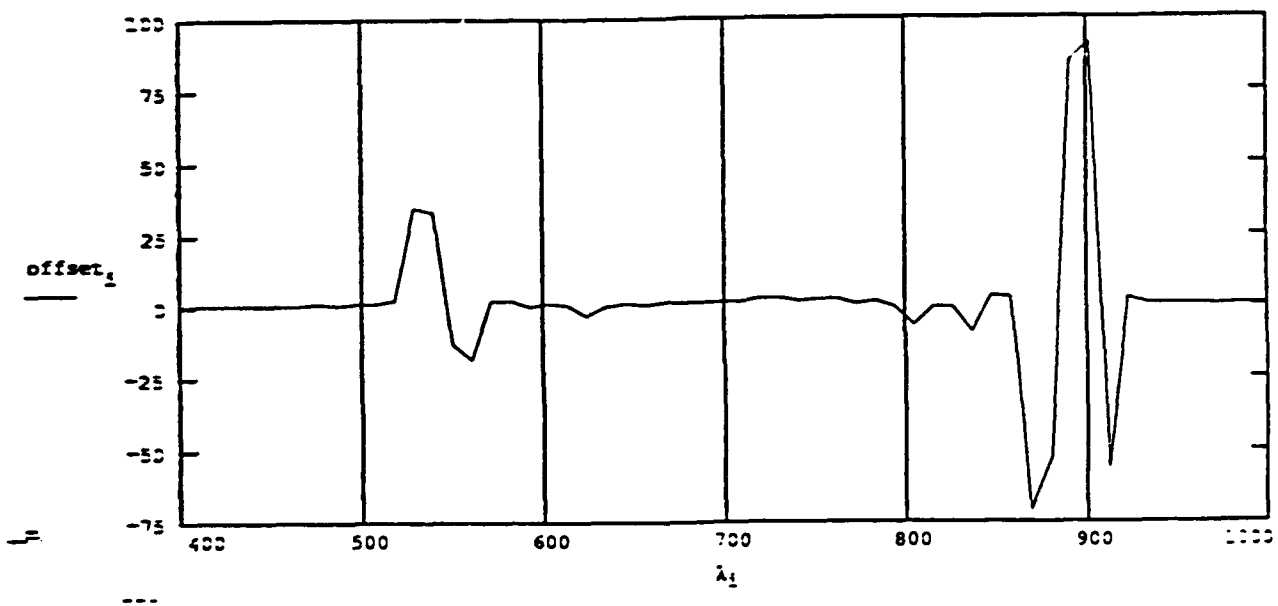


Figure 2: Offset Correction Curve (from page 1 of F770SPCT.mcd)

This plot shows the offset correction versus wavelength. It is derived from "dark" data set F796 (collected with the aperture covered) by offset correcting each frame by row 129 (which is covered with aluminum to provide a dark offset signal), and then averaging all frames (99 for F796) to derive a single offset for each column (each band). The detail seen in the plotted offset correction curve is due to the interference of two clocks which occur during the readout of row 129.

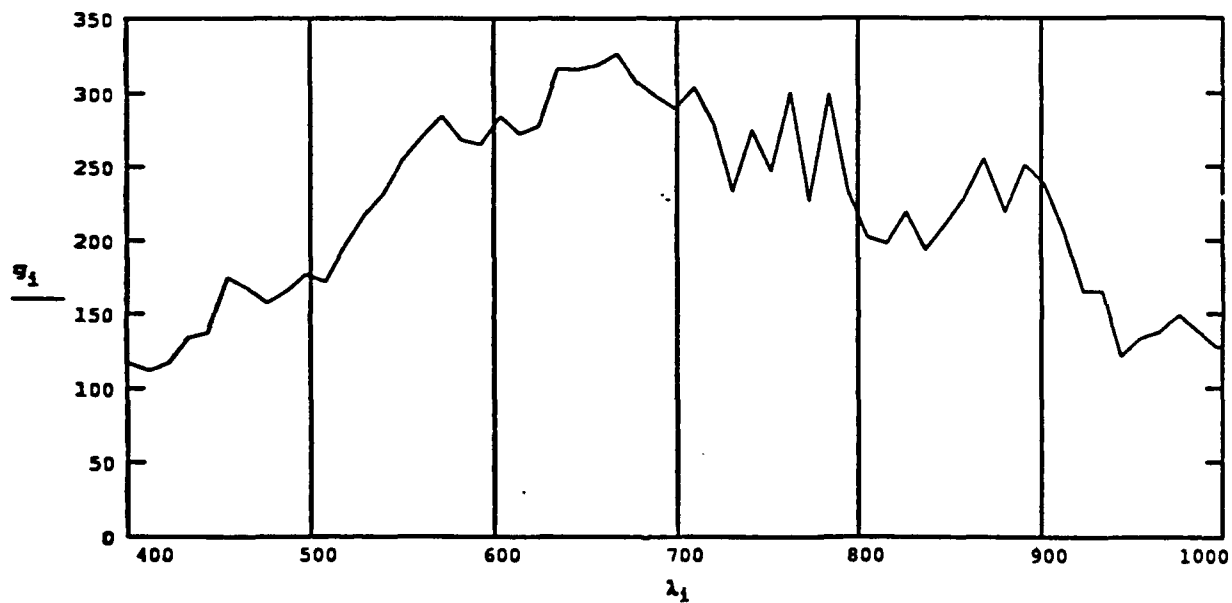


Figure 3: Gain Correction Curve (from page 1 of F770SPCT.mcd)

This plot shows the gain correction versus wavelength. It is derived from "bright" data set F795 (collected by viewing a very overcast sky -- no shadows -- off a BaSO₄ target) by offset correcting each frame by row 129, then offset correcting the result by the offset correction curve shown previously, and finally averaging all frames (99 for F795) to derive a single value for each column (each band). This curve basically shows the instrument response function versus wavelength for these collection conditions.

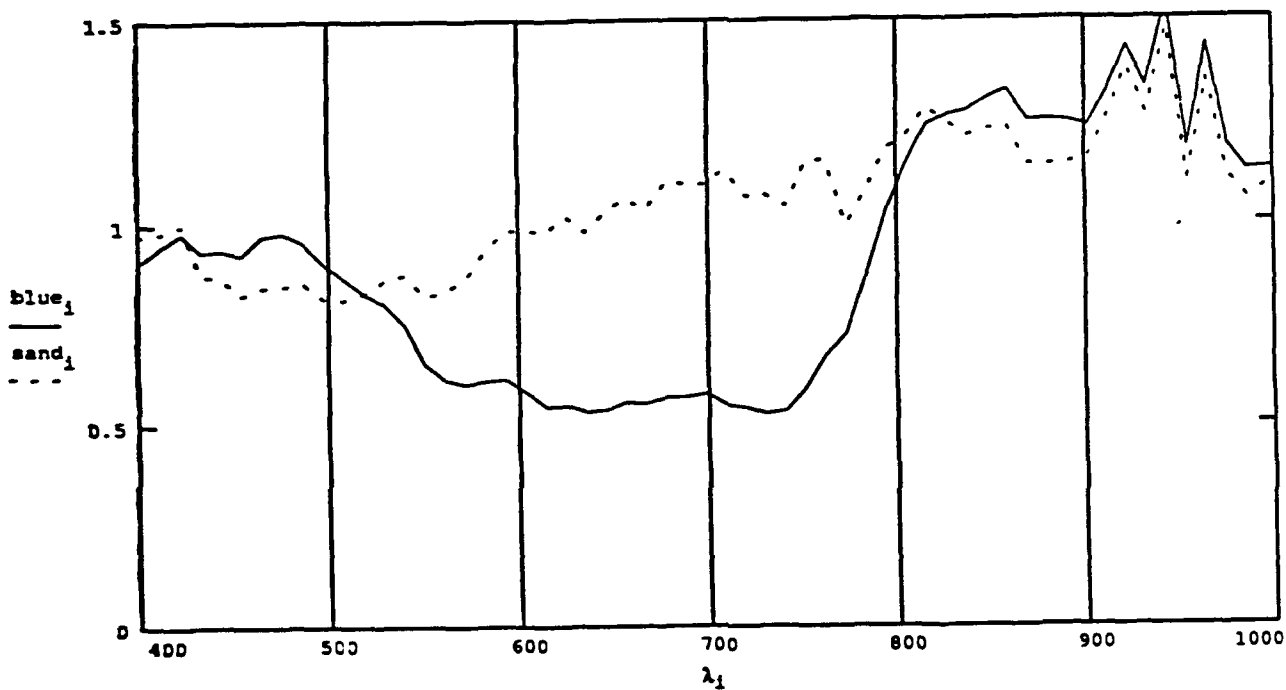


Figure 4: Blue Tarpaulin and Sand Spectra (from page 2 of F770SPCT.med)

This plot shows the spectra for the blue tarpaulin and a region of sand in image data set F770 (all of the remaining plots are from data set F770). The blue tarpaulin spectrum is an average of a 5x6 area within the tarpaulin (covering virtually all of the tarpaulin); while the sand spectrum is an average of a 7x9 area in an apparently uniform region just below the tarpaulin. For this data set (F770), we were not able to obtain reliable correction coefficients for bands above about 900nm, and the low instrument response below about 450nm precludes reliable correction in that region. Nevertheless, the spectra in this plot clearly show a strong resemblance to those in the "ground truth" data. Also, they show additional spectral detail in the sand spectrum, particularly around 750-800nm. This feature, while not present in the "ground truth" data, is extremely consistent in all spectra of natural items (sand, dead bushes, etc.) from this data set.

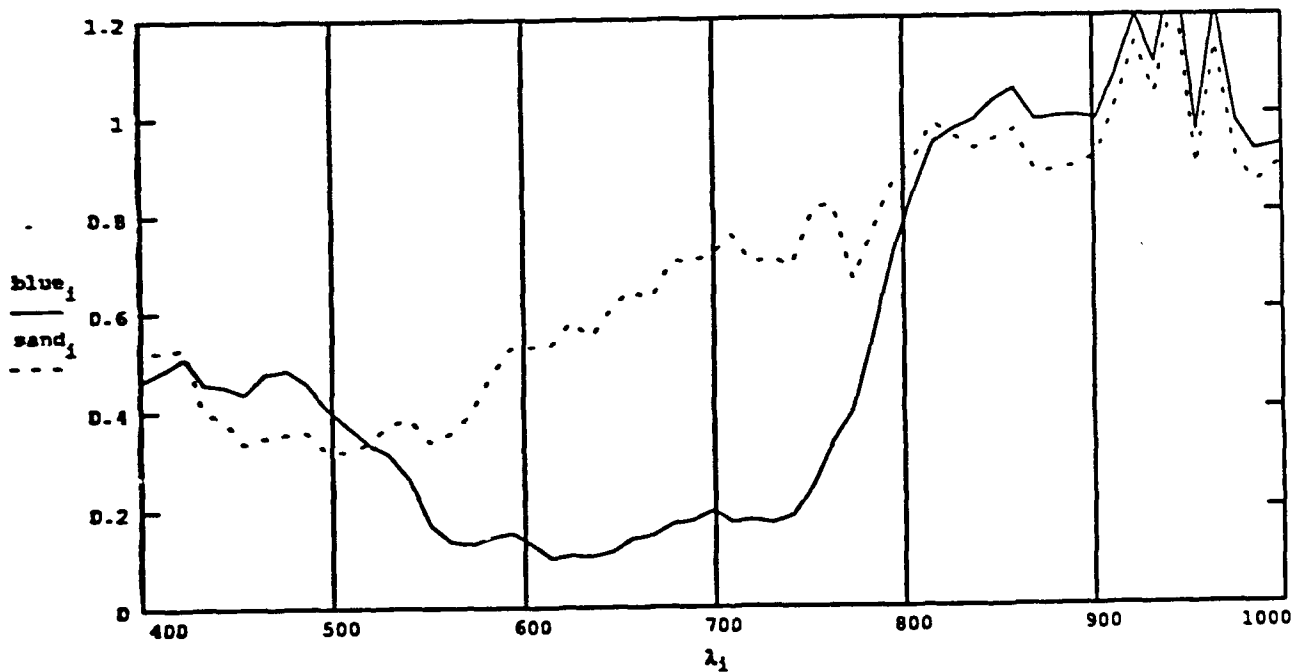


Figure 5: Blue Tarpaulin and Sand Spectra (from page 2 of F770SPCT.mcd)

This plot is the same as Figure 4, except a small amount of solar-colored signal has been subtracted to remove what appears to be contamination by specular solar reflection in Figure 4. The amount subtracted was selected empirically to force the result to more closely match the shapes of the "ground truth" data in Figure 1 (particularly the relatively flat-bottomed shape of the blue tarpaulin absorption over 550-750nm).

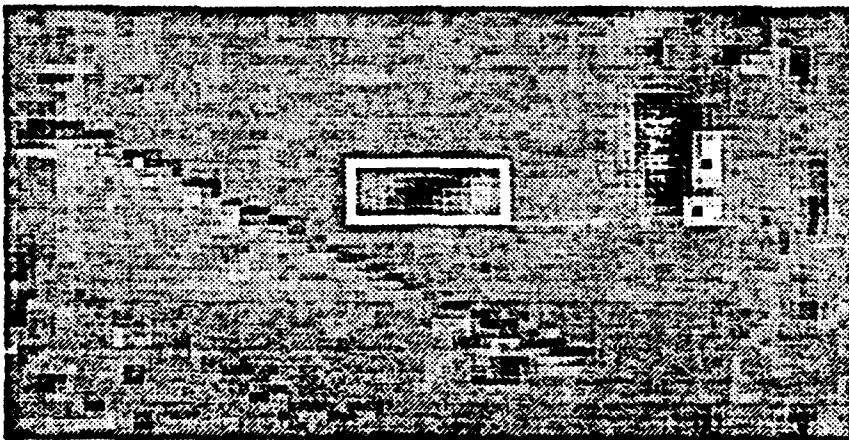
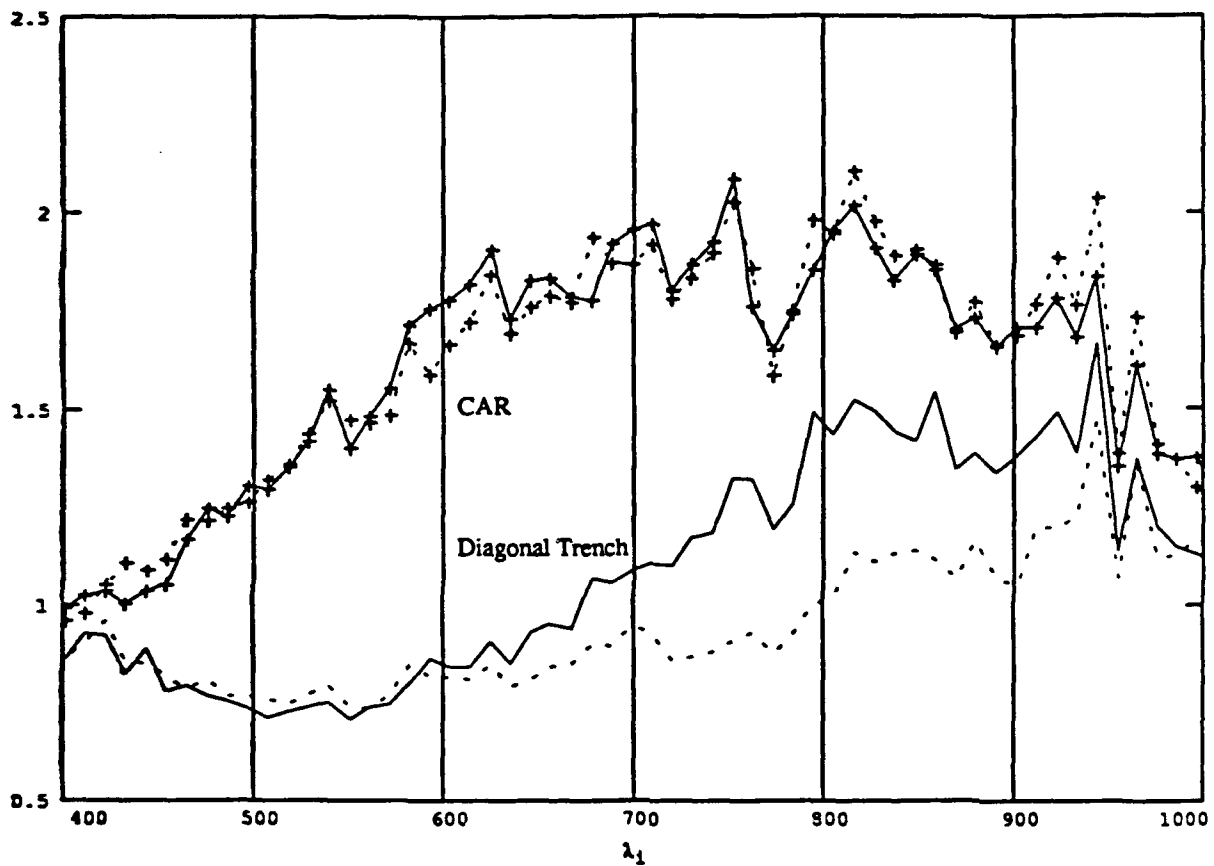
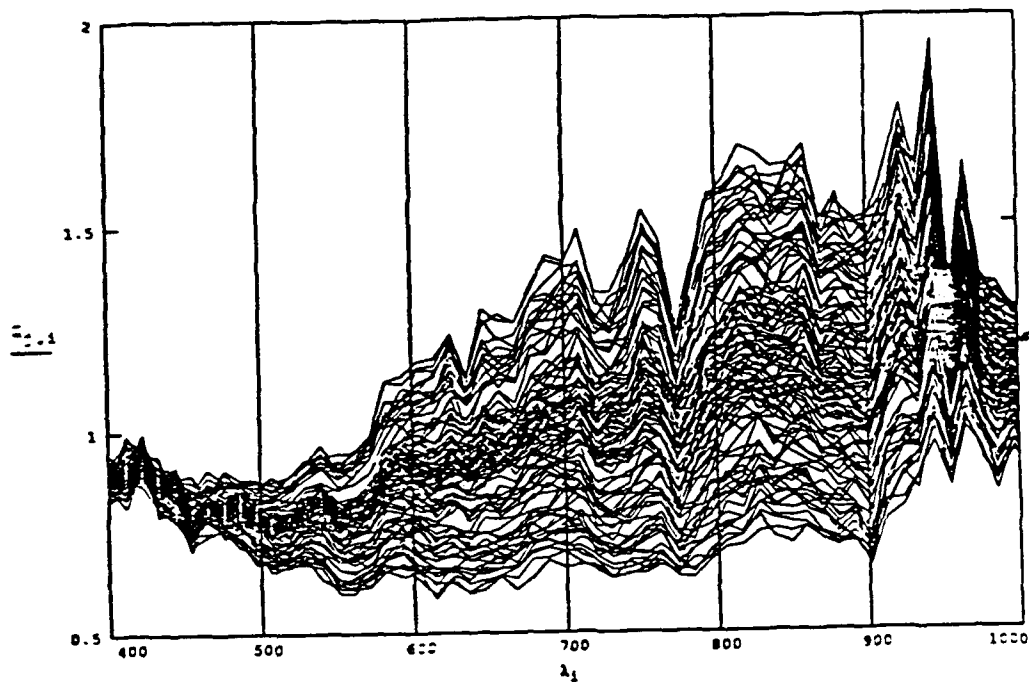


Figure 6: Car and Trench Spectra (from page 3 of F770SPCT.med)

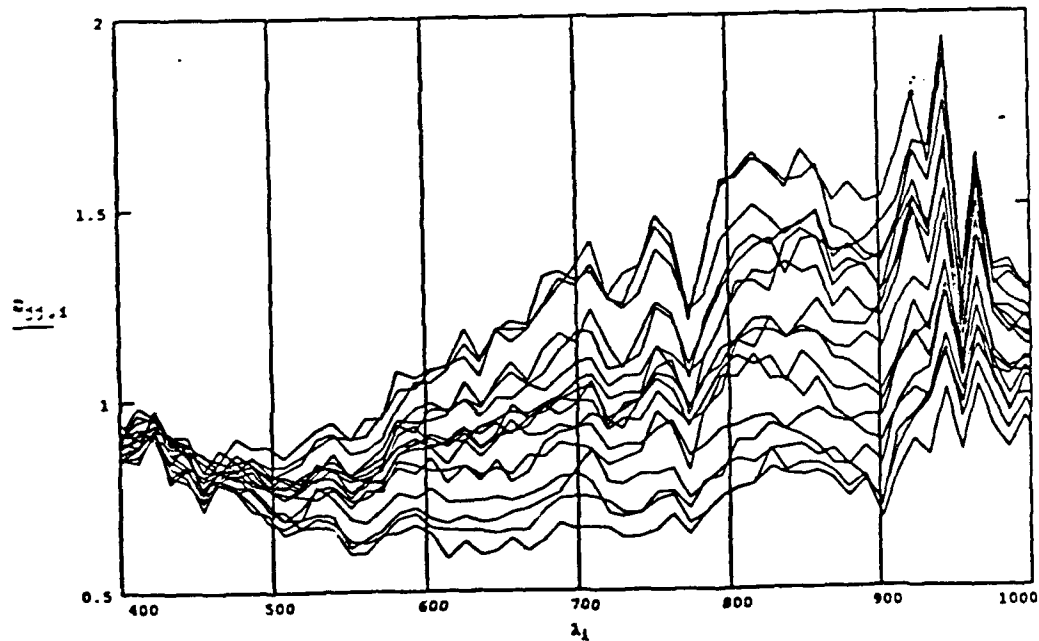
This plot shows the spectra for two points on the car (one on the roof and one on the hood) and two points in the top-most (deepest) diagonal trench (one on the bright side and one on the darker side). The car is apparently white, and both points from the car have similar spectral shapes. The two spectra from the trench are very similar spectrally, with the darker point just dimmer in magnitude compared to the brighter point. This is consistent with the collection conditions: since these data were collected at mid-winter, the sun angle is quite low, even near noon (F770 was collected at about 1:30 pm). Therefore, we would expect that the dominant characteristic of trenches is determined by shadows -- the bright side is the rising side of the trench well illuminated by the sun, while the darker side is in shadow. The image below this plot indicates the points selected for the spectra in the plot, along with the region used for the next plots (page 4).



Set of spectra through horizontal middle of box:

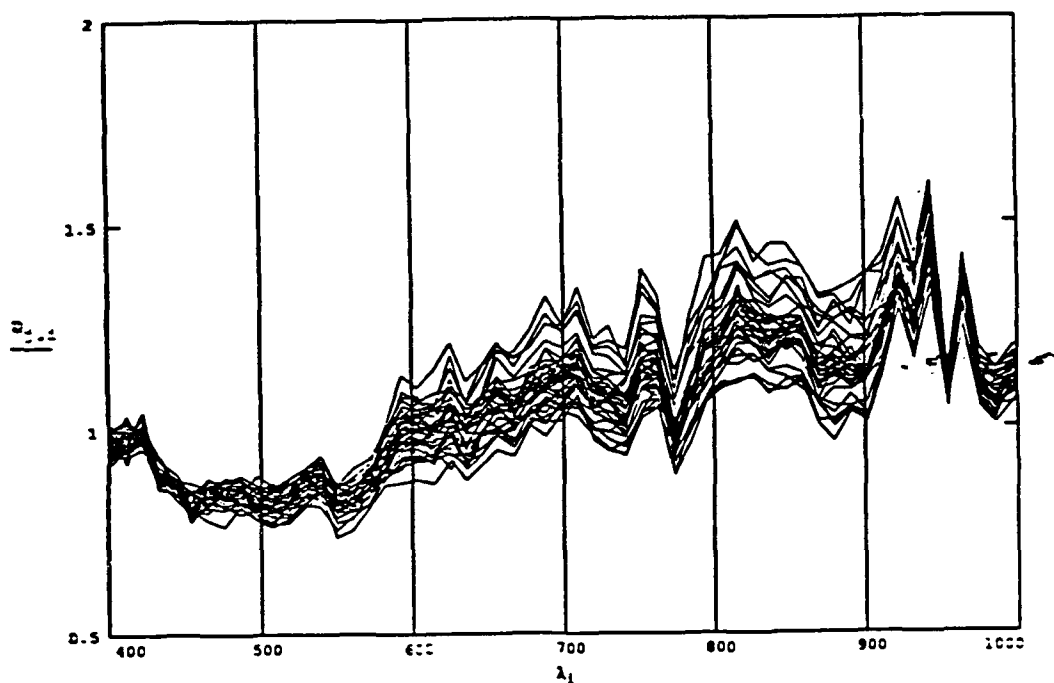
$$j,j = 2, 2 + 5 \dots 2 + 5 \cdot 16$$

$$Q_{j,j,i} = (X_{i,j,j} - \text{offset}_j) \cdot \text{gain}_j$$



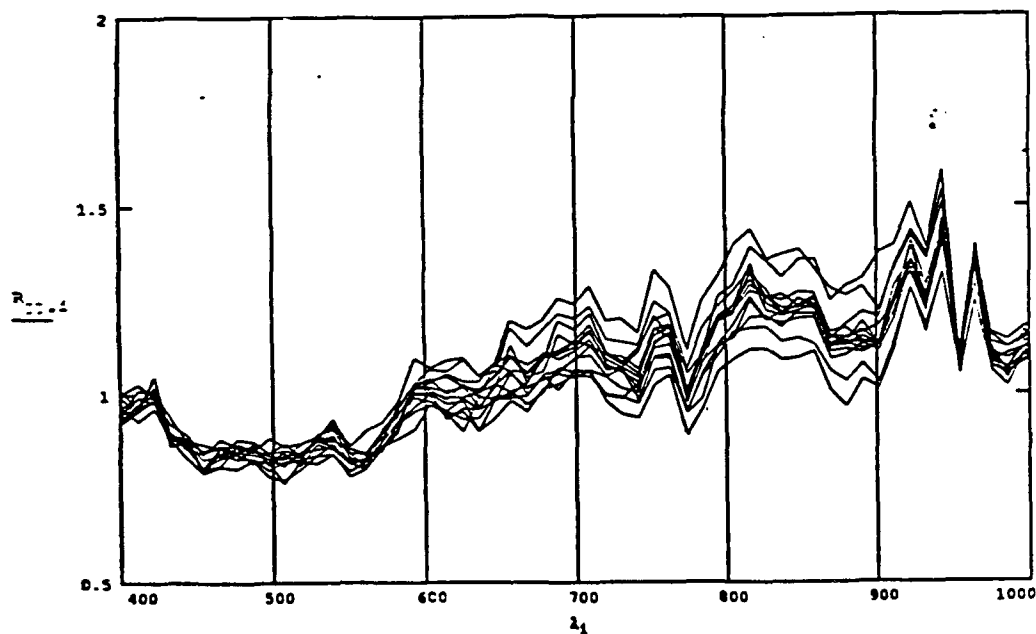
Figures 7 and 8: Bush on left of Car (from page 4 of F770SPCT.mcd)

These plots show the collection of spectra for a 17x7 region surrounding the large bump (bush? sand hillock?) to the immediate left of the white car (see the image on the preceding page). The first plot shows all 119 spectra, while the second plot just shows the 17 spectra through the horizontal middle of the region. The spectral shapes are quite similar, with just amplitude differences predominating, probably due to shading (illumination) differences.



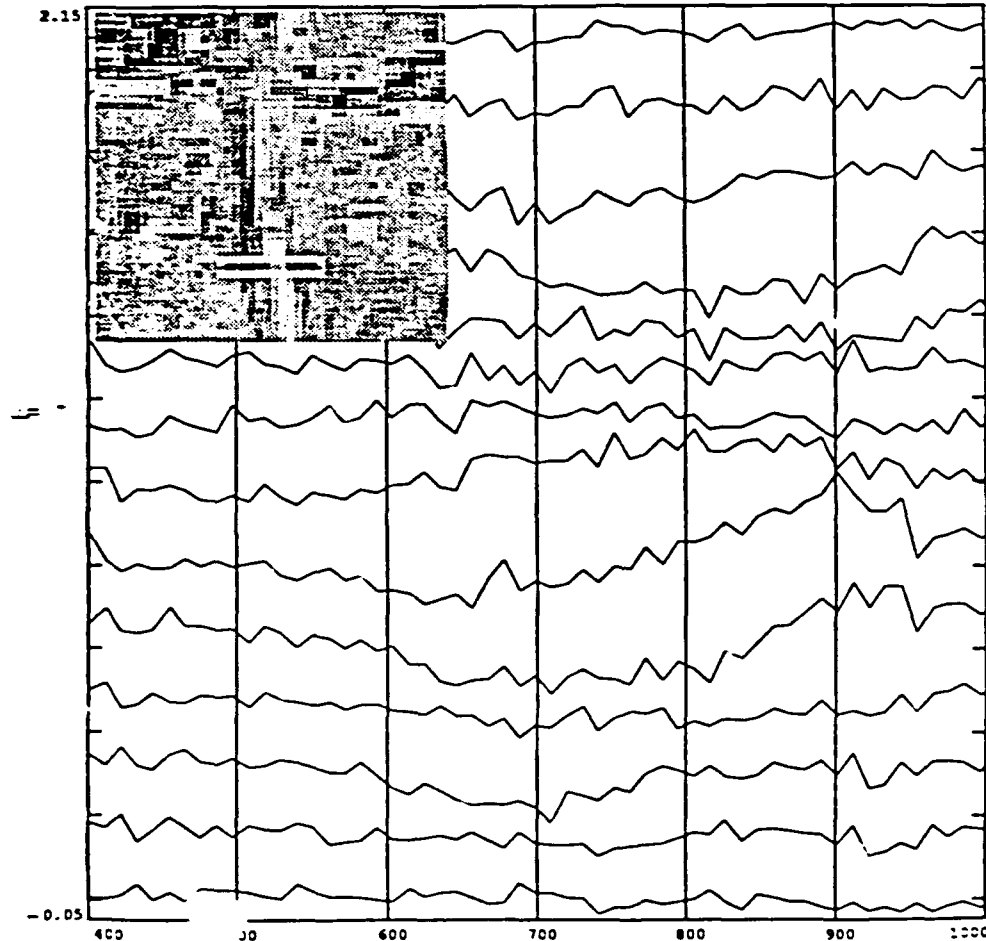
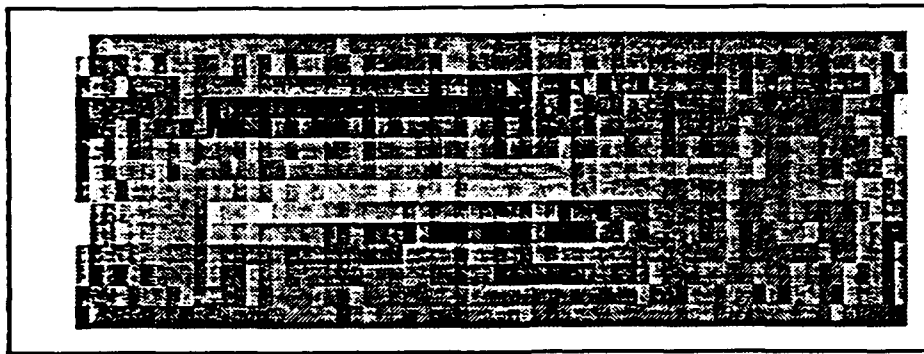
Set of spectra through horizontal middle of box:

$$jj = 0 \dots 13 \quad R_{jj,\lambda_1} = (X_{\lambda_1, jj+1} - \text{offset}_{\lambda_1}) \cdot \text{gain}_{\lambda_1}$$



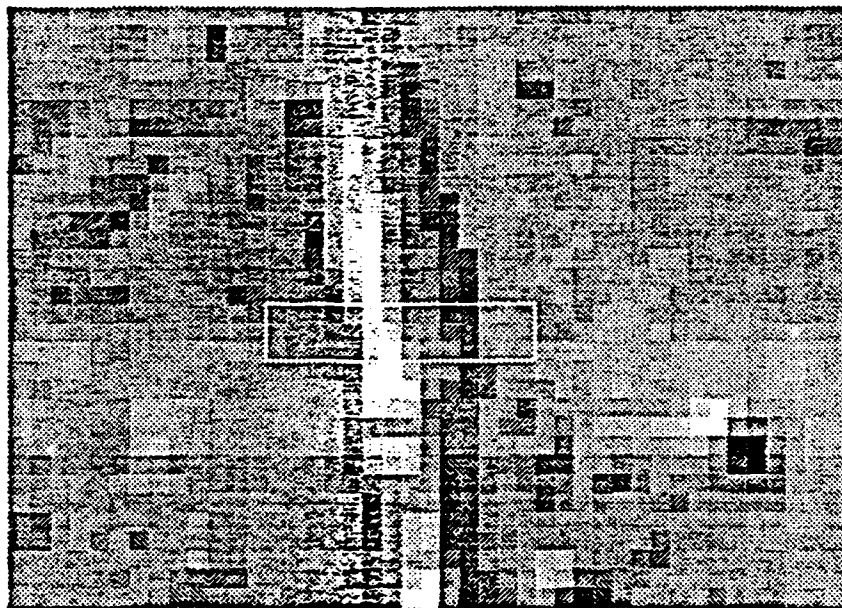
Figures 9 and 10: Lower Arm of Trenched Cross (from page 5 of F770SPCT.mcd)

These plots show the collection of spectra for a 14x3 region crossing the lower arm of the large cross-shaped trench (images appear on the next two pages); the first is all 42 spectra, while the second is the 14 spectra through the horizontal center of the box (ie, perpendicular to the arm). Once again, the dominant difference appears to be due to shading (illumination); however, the succeeding plots address the possibility of spectral differences due to the freshly turned earth.



Figures 11 and 12: Lower Arm of Trenched Cross (from page 6 of F770SPCT.mcd)

These plots show the 14 spectra perpendicular to the arm in more detail. In these cases, the spectra from the two end points (the left-most and right-most spectra) were averaged and then subtracted from all 14 spectra; the intent was to remove the expected background (normal sand) in order to magnify differences. In both the grey-shaded surface plot (Figure 11) and the spectral sequence plot (Figure 12), there is a clear spectral difference between the typical sand and the fresh trench region which appears between about 750 and 950nm. This is not proof that freshly dug trenches (ie, freshly disturbed earth) can be detected, but it is a clear indication of potential feasibility for such a detection. Note that this region is outside the normal visible range (usually cited as about 400-750nm). Our expectation is that this detection would be substantially more reliable in the shortwave infrared (somewhere in the 1000-2500nm region), since the phenomenology of freshly disturbed earth (based upon detection of moisture content and minerals not yet bleached by the sun) appears much stronger in this spectral region.



Figures 13: Enlarged Lower Arm of Trenched Cross (from page 6 of F770SPCT.mcd

Conclusions:

The presence of the older furrows and the specific spectral differences identified in the data do not in themselves offer proof that periodically spaced rows and freshly disturbed earth can be detected by an automated detection algorithm, however, it is a clear indication of the feasibility of such a detection. It is SBRC's expectation that this detection would be substantially more reliable in the short wave infrared, somewhere in the 1000 - 2500nm region. This is so because the phenomenology of freshly disturbed earth, based upon detection of moisture content and minerals not yet bleached by the sun, appears much stronger in this spectral region.

A review of the requirements of the Statement of Work indicate that with the submission of this final report SBRC has successfully completed all contractually required tasks and data deliveries on this program, within the budget and schedule as defined. Technical results of the post data collection spectral analysis indicate that the data collected is adequate to demonstrate the feasibility of utilizing a Wedge Imaging Spectrometer in this role and to satisfy the technical goals of the experiment.

Attachment 1
MDDC SOW

Task 1. Planning and Setup

SBRC shall participate in the planning of data collection flights. SBRC shall define the collection procedures and the processing to be performed on the data. SBRC shall ensure that the collection equipment is installed in the aircraft and tested prior to the scheduled data collection flights.

Task 2. Data Collection

SBRC shall manage and operate the system during the data collection flights. SBRC shall provide operations staffing for these flights. Flights shall be carried out by Hughes Aeronautical Operation (HAO). Data collection flights will nominally be flown over a designated area near Twentynine Palms, California. The flights, originating from Burbank, California, shall occur over a two-week period. A nominal estimate of 12 flight hours has been utilized.

Task 3. Data Rectification and Processing

The collected data shall be processed by SBRC to remove data collection flight artifacts and correct for sensor optical geometry. Spectral analysis algorithms shall be executed against a subset of the data to demonstrate any unique characteristics of special interest areas within the collected data. Display of spectra and imagery shall be provided in softcopy form. Any hardcopy multicolor display will be provided via photographs of the display screen.

Period of Performance

Normal period of performance shall be assumed to start on or about 01 October 1992 for Task 1. Data collection flights of Task 2 are assumed to occur after the aircraft installation contract (with DARPA/NRAD) has completed final integration. For planning purposes, this is assumed to be in the November 1992 time frame. Final report of activity is assumed to be deliverable at the end of January 1993.

Deliverables

It is assumed that a 1 to 3 page summary progress report shall be delivered each month by the 15th of each succeeding month. This monthly report shall include a brief summary of monthly activities and a high-level summary of contract funds expended. A final report, in SBRC format, shall be delivered at the end of the contract. The report will describe the activities during the contract and final results of the program. It would nominally comprise about 30 pages of text and diagrams. Processed imagery from a subset of the data will be made available in both digital and hardcopy format.

Travel

It is assumed that one two-person trip to Glastonbury, Connecticut, for coordination during the contract will be required. In addition, any Southern California TDY support costs for SBRC personnel during data collection activities not to exceed one person-week are also included.

Attachment 2
WIS Flight System Review

WIS DATA COLLECTION FLIGHTS FLOWN IN HAO SABERLINER

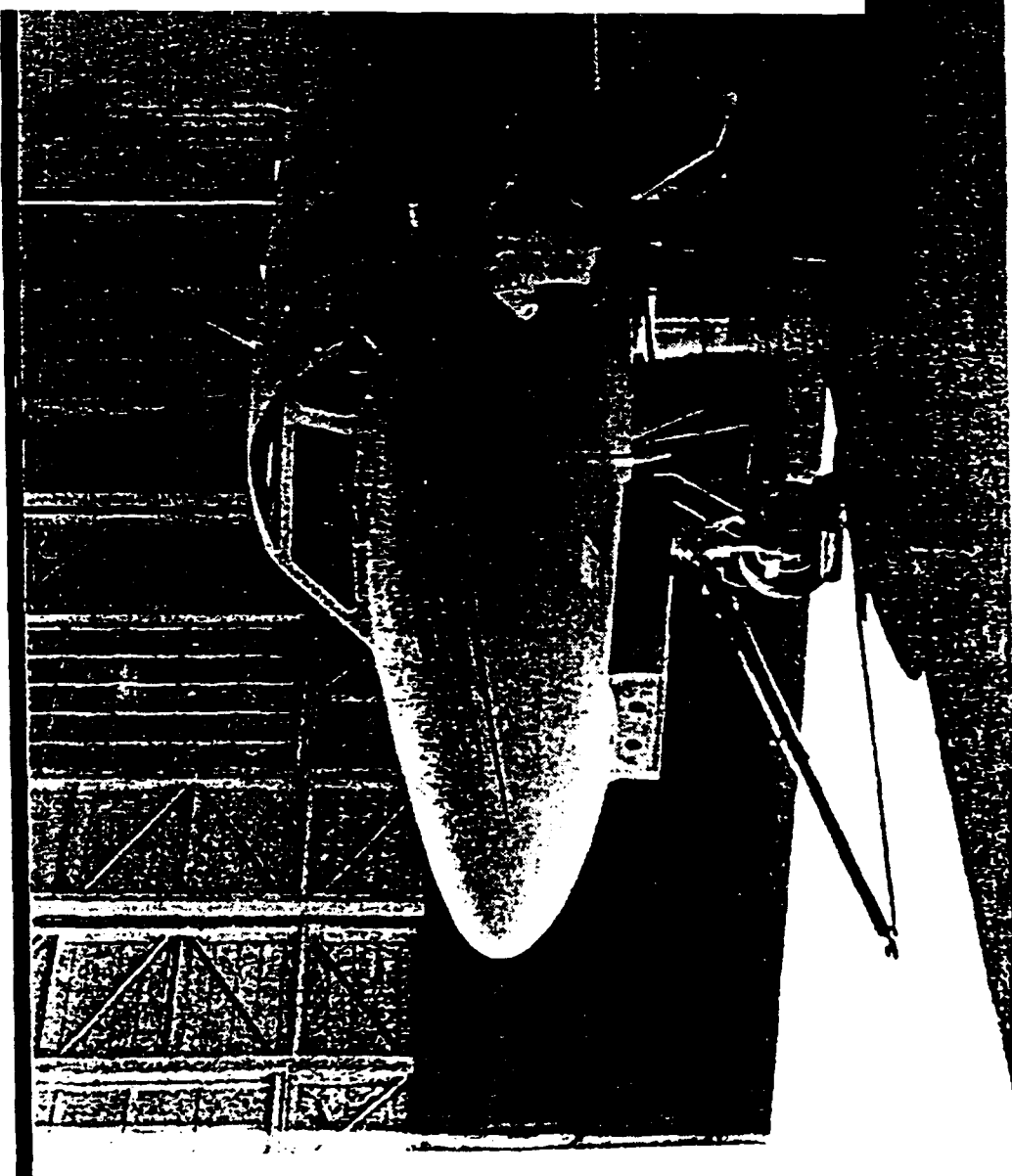
92-7-97 (#11)

HUGHES

SANTA BARBARA RESEARCH CENTER
a subsidiary



**WIS DATA COLLECTION FLIGHTS
FLOWN IN HAO SABERLINER ⁹**



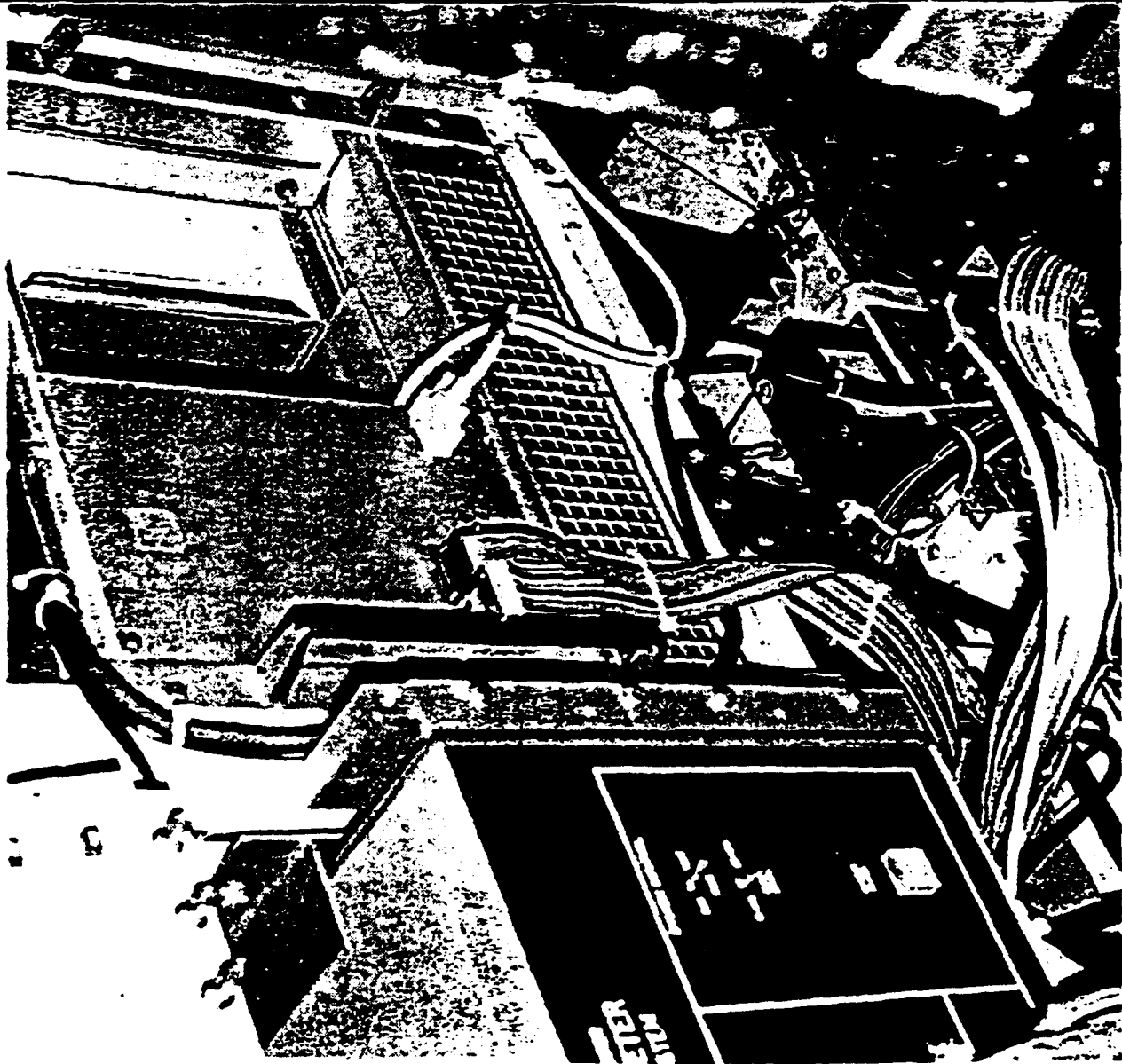
1

HUGHES

SANTA BARBARA RESEARCH CENTER
a subsidiary

92-7-97 (#5)

WIS REQUIRES MINIMAL SUPPORT ELECTRONICS

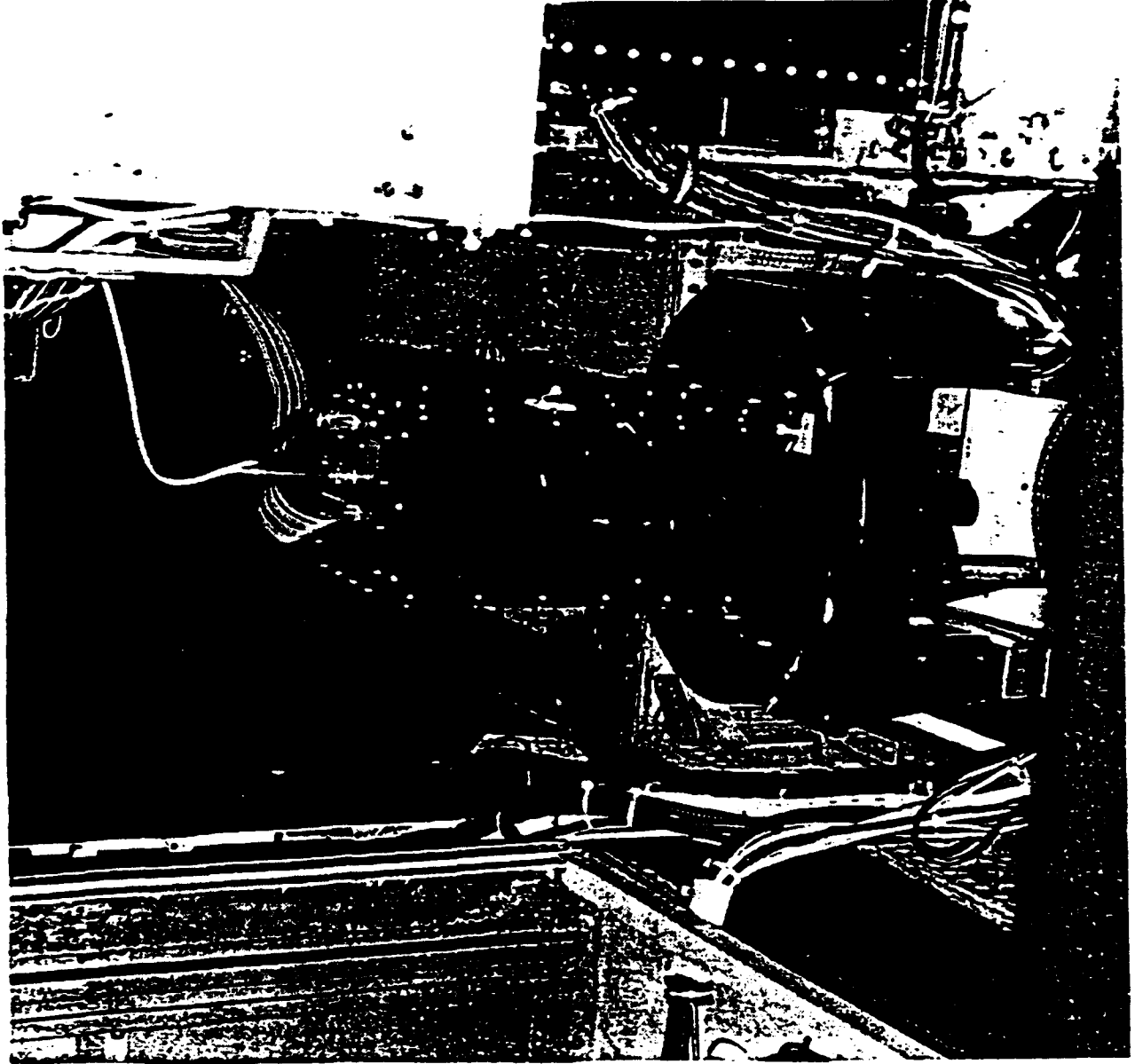


HUGHES

SANTA BARBARA RESEARCH CENTER
a subsidiary

92-7-97 (#2)

WIS SENSOR HEAD MOUNTED INTERNALLY ON HATCH

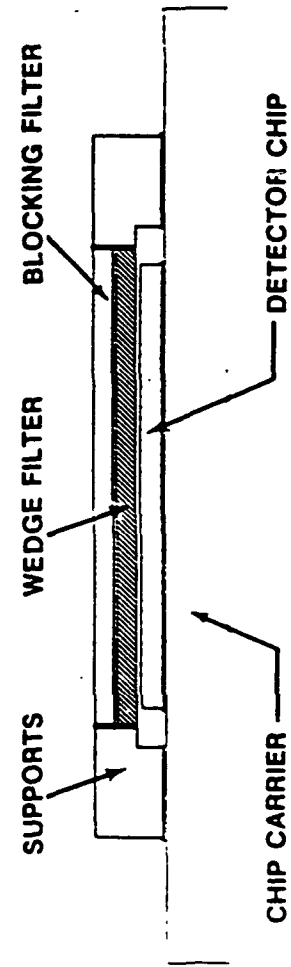
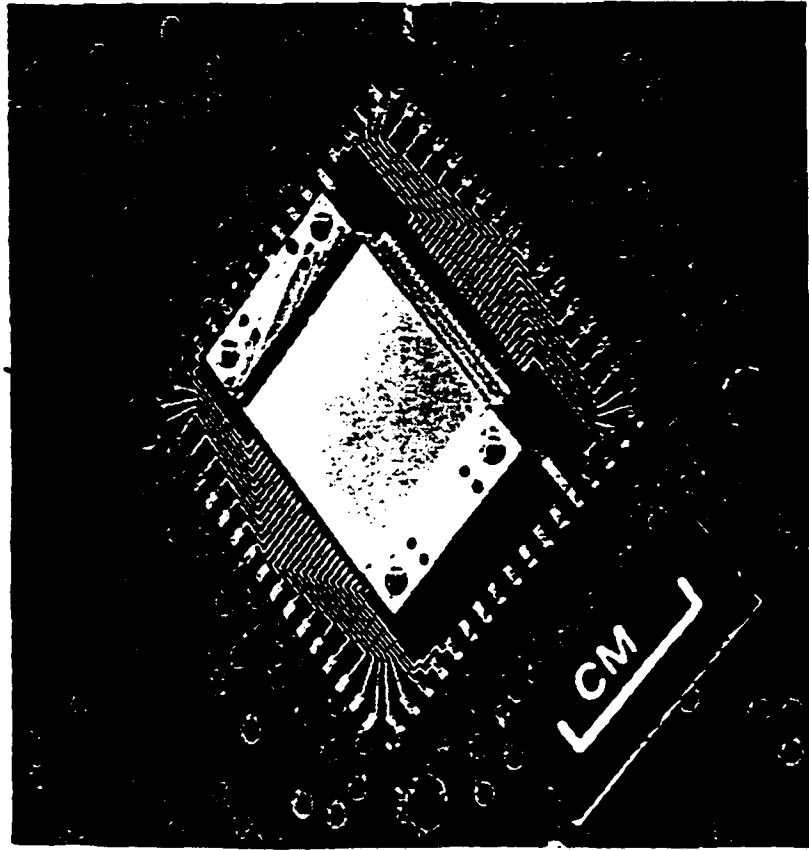




SANTA BARBARA RESEARCH CENTER
of Lockheed

89-8-5

WEDGE FOCAL PLANE ASSEMBLY

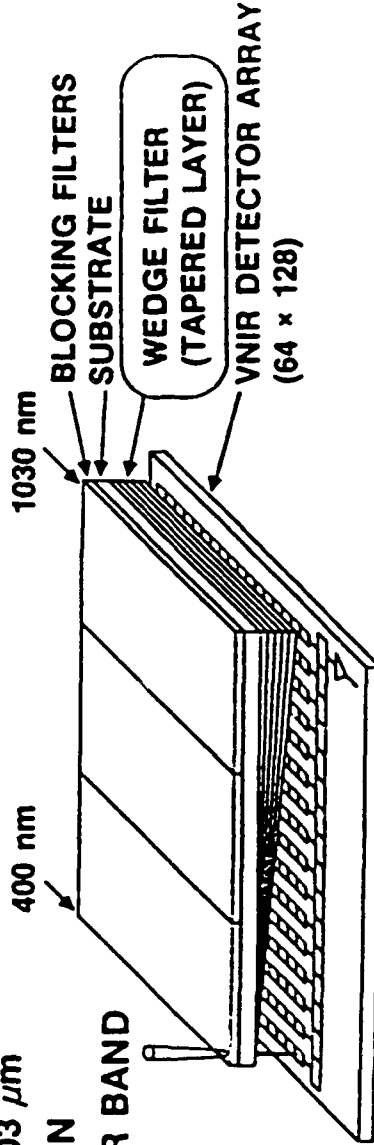


WEDGE FOCAL-PLANE CONCEPT IS THE HEART OF WSD

HUGHES

SANTA BARBARA RESEARCH CENTER
a subsidiary

- EXAMPLE DESIGN
 - 64 x 128 ELEMENT VNIR DETECTOR ARRAY
 - 64 BANDS OVER 0.4 TO 1.03 μm
 - 1% SPECTRAL RESOLUTION
 - 128 SPATIAL SAMPLES PER BAND



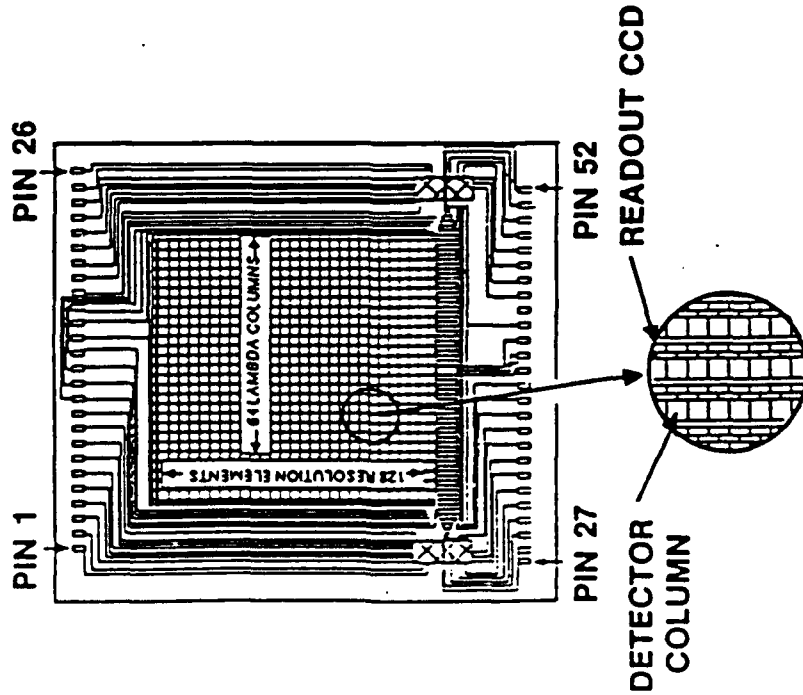
- ADVANTAGES OF WEDGE FPA:
 - COMPACT SOLID AFT OPTICS (1 cm x 1 cm x 0.3 cm)
 - THERMALLY STABLE SPECTRAL CHARACTERISTICS
 - SPECTRAL BAND SPACING AND BANDWIDTH INDEPENDENTLY SET BY FILTER DEPOSITION PARAMETERS

12/01
91-0950-1

CUSTOMIZED VNIR DETECTOR ARRAY HAS BEEN DEVELOPED

HUGHES

SANTA BARBARA RESEARCH CENTER II
a subsidiary



DETECTORS ARE $75 \times 75 \mu\text{m}$
ON $150 \times 75 \mu\text{m}$ CENTERS

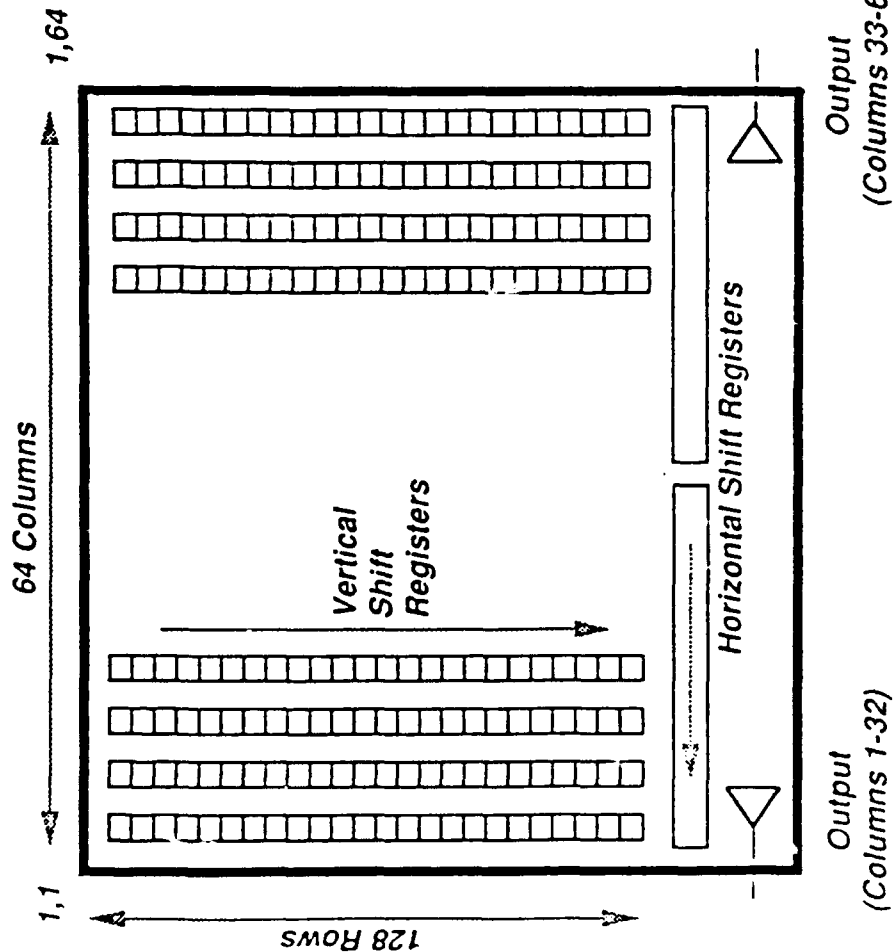
- TRIPLE-POLY, DOUBLE-METAL BURIED-CHANNEL CCD
- UNIT CELL HAS POLYSILICON WINDOWS TO ENHANCE BLUE RESPONSE
- SPLIT HORIZONTAL READOUT REGISTER MINIMIZES CLOCK RATE TO IMPROVE CHARGE TRANSFER EFFICIENCY
- DUAL OUTPUT AMPLIFIERS FOR SIMULTANEOUS LOW NOISE (SMALL SIGNAL) AND HIGH DYNAMIC RANGE (LARGE SIGNAL) OUTPUTS
- DETECTOR GEOMETRY MEETS REQUIREMENTS
- DETECTOR ARRAY IS $1 \text{ cm} \times 1 \text{ cm}$
- REQUIRED PROCESS WAS SUCCESSFULLY DEVELOPED AT FOUNDRY IN 1987

7/89
90008-0

WIS CCD is Custom SBRC Device

HUGHES

SANTA BARBARA RESEARCH CENTER
a subsidiary



69 μm X 69 μm Photosites on 75 μm Pitch

Saturation Charge of 4.5 Million Electrons

Noise Performance Supports 12 Bit Quantization

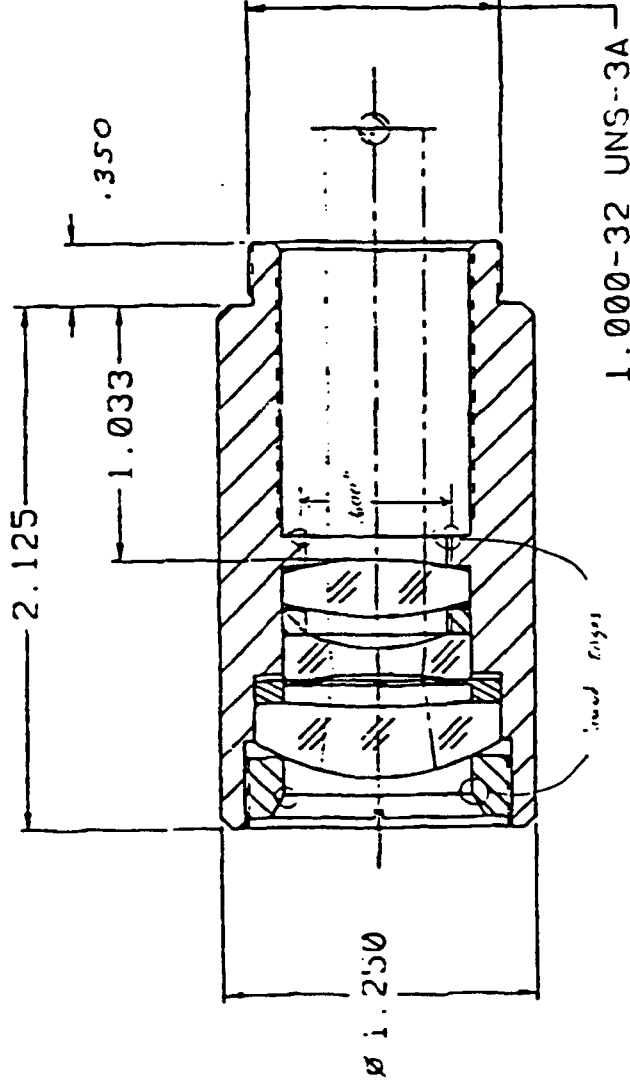
WIS Integration Time of 3.125 ms

Readout Rate of 1.4 MHz per Output

55 mm Lens Design Completed

HUGHES

SANTA BARBARA RESEARCH CENTER
a subsidiary



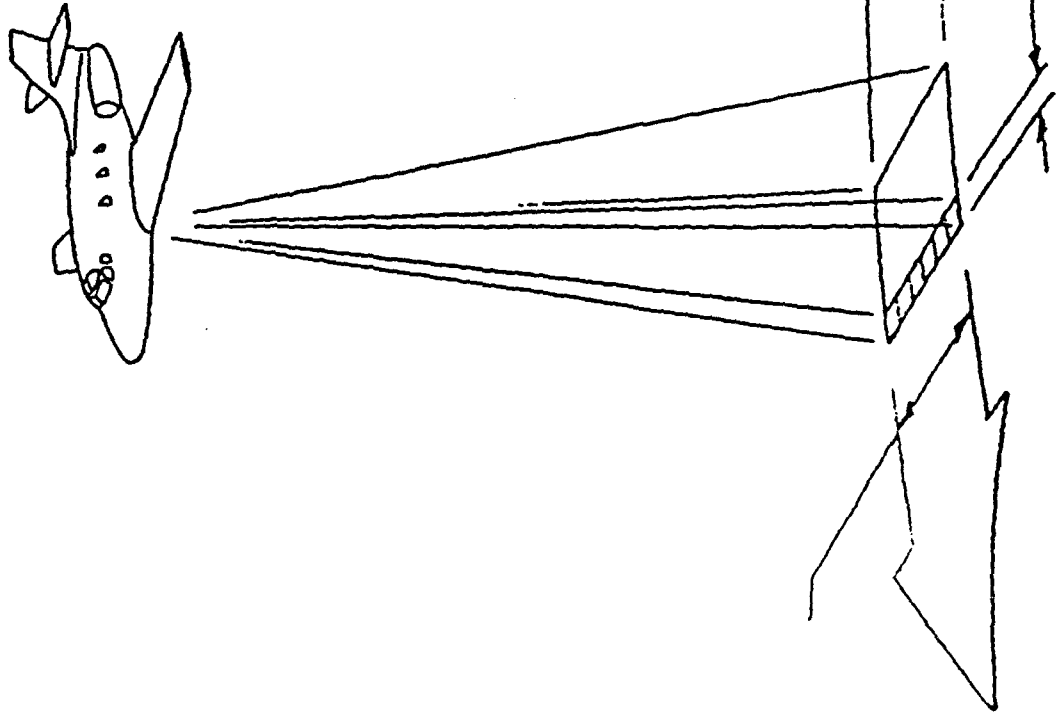
Optical Elements and Housing Assembly Being Fabricated by
Optical Instruments Corporation

Scheduled Delivery Date 4/30/92

LENS SELECTION AND SUBSAMPLING KEEP FLIGHT OPERATIONS REASONABLE

HUGHES

SANTA BARBARA RESEARCH CENTER
a subsidiary



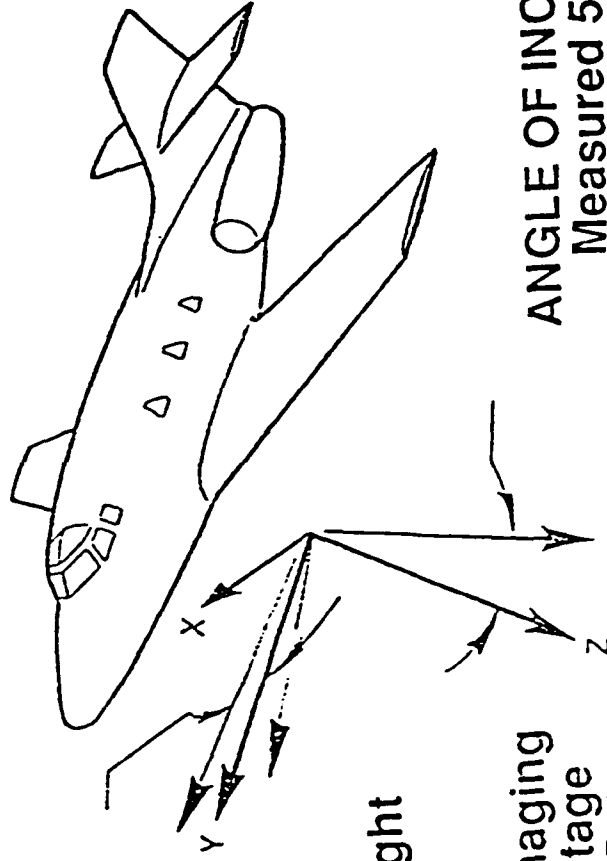
Ground Sample Distance

	<u>0.5 m</u>	<u>1.0 m</u>	<u>2.5 m</u>	<u>5.0 m</u>
Lens	110 mm	55 mm	110 mm	55 mm
Altitude (ft)	2500	2500	12000	12000
Velocity (kt)	160	215	245	258
Subsample	2	3	10	12

Saberliner Flight Attitudes Accommodated by WIS Sensor



SANTA BARBARA RESEARCH CENTER
a subsidiary



CRAB ANGLE
 $\pm 15^\circ$ Based upon Flight
Conditions

Correct Along-Track Imaging
Provided by Rotary Stage
Autopilot using Flux Gate
Compass

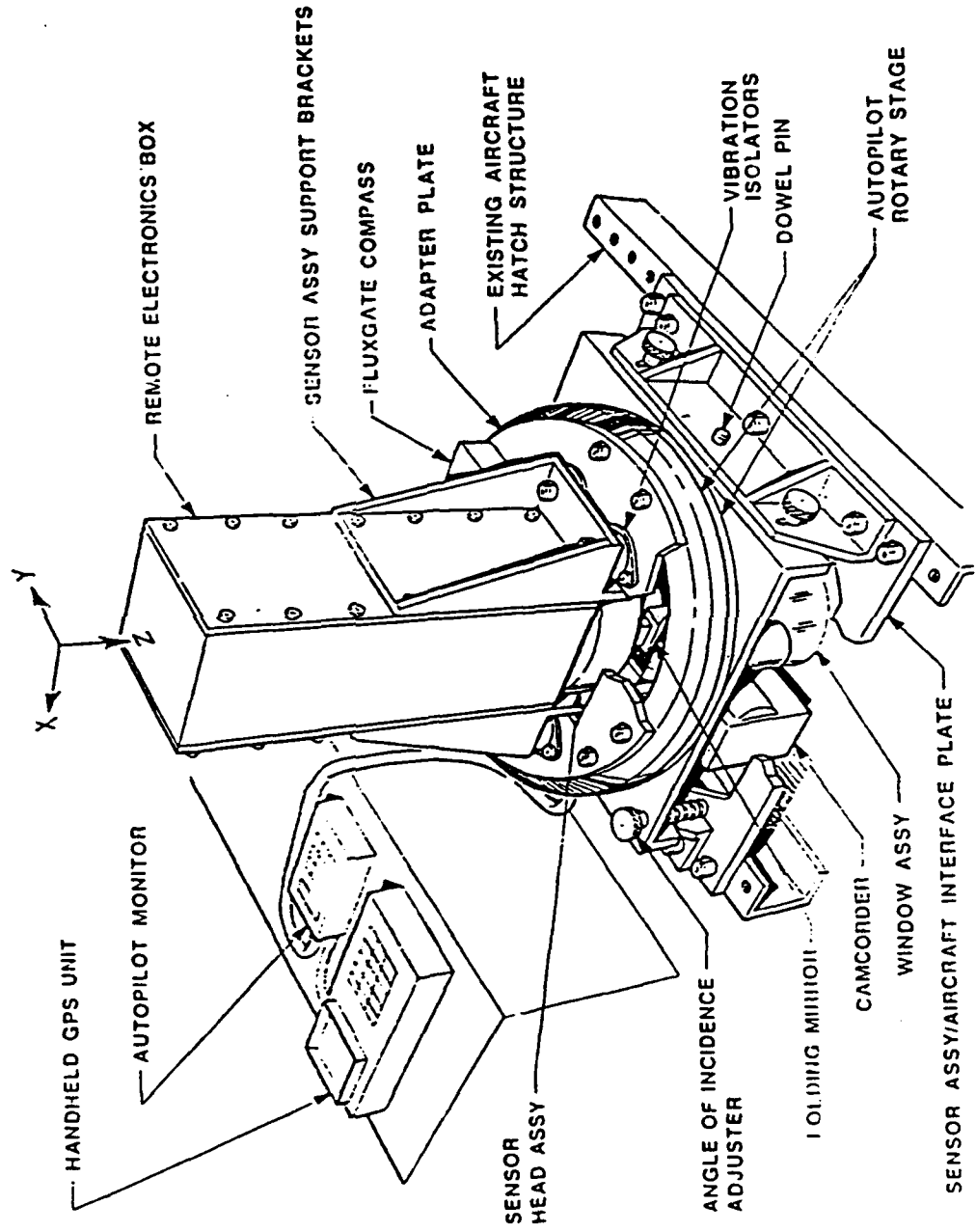
ANGLE OF INCIDENCE
Measured $5^\circ \pm 2^\circ$

Sensor Head Design Will
Incorporate Adjustable Pitch
Control

Conceptual Design of Flight Sensor Head Assembly

HUGHES

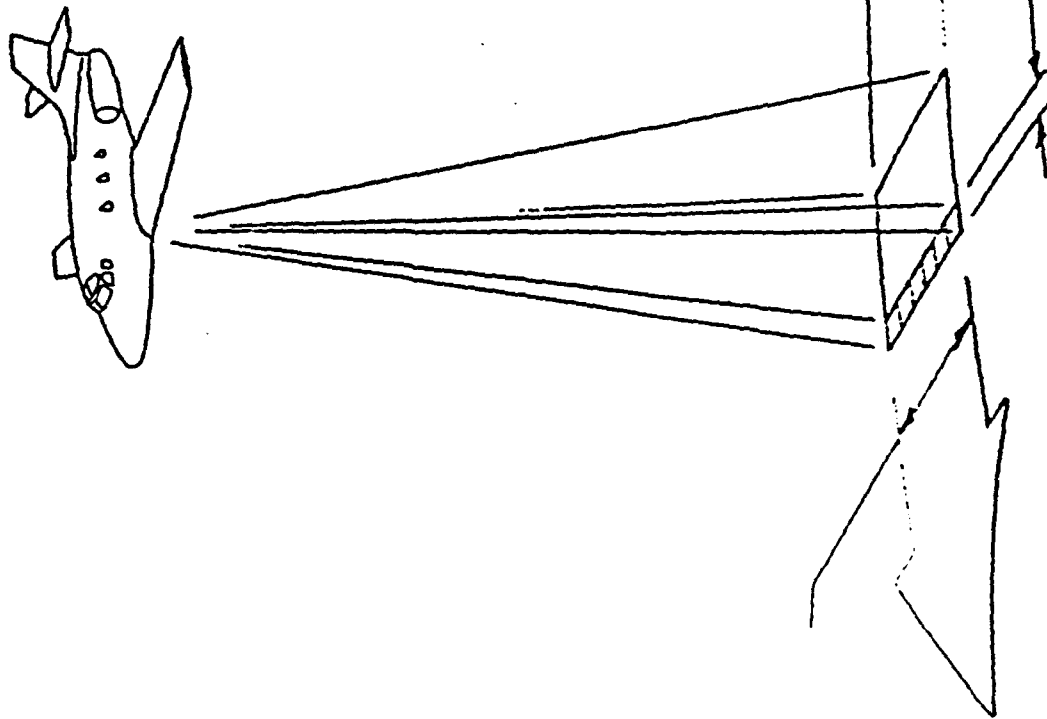
SANTA BARBARA RESEARCH CENTER
a subsidiary



LENS SELECTION AND SUBSAMPLING KEEP FLIGHT OPERATIONS REASONABLE

HUGHES

SANTA BARBARA RESEARCH CENTER
a subsidiary



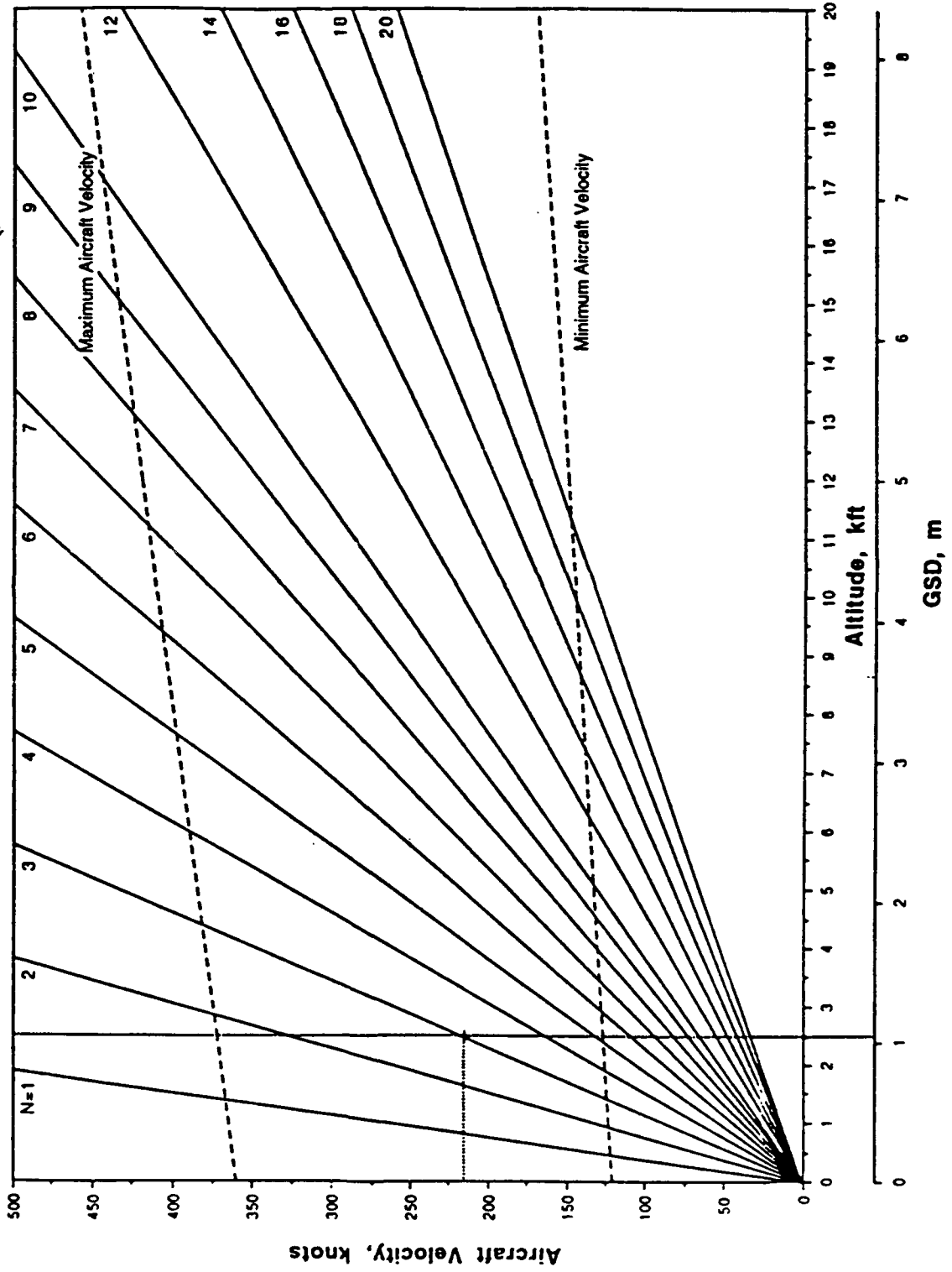
Ground Sample Distance

	<u>0.5 m</u>	<u>1.0 m</u>	<u>2.5 m</u>	<u>5.0 m</u>
Lens	110 mm	55 mm	110 mm	55 mm
Altitude (ft)	2500	2500	12000	12000
Velocity (kt)	160	215	245	258
Subsample	2	3	10	12

AIRCRAFT ALTITUDE AND VELOCITY DETERMINE GSD AND SAMPLE RATE

HUGHES

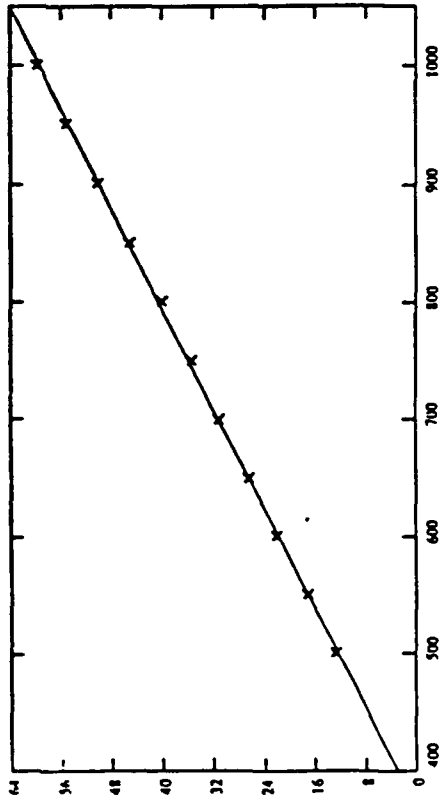
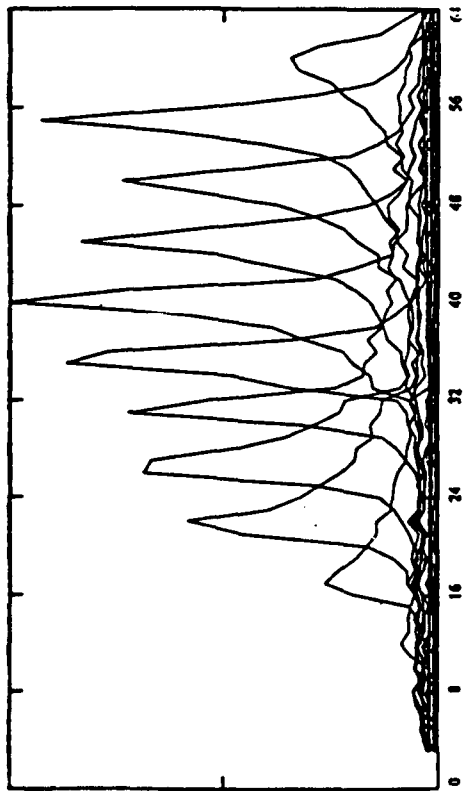
SANTA BARBARA RESEARCH CENTER
a subsidiary



HUGHES

SANTA BARBARA RESEARCH CENTER
a subsidiary

SPECTRAL CALIBRATION SHOWS LINEARITY OF DISPERSION



**SLOPE = 10.63 nm per band
BAND #1 = 380.0 nm**

Attachment 3
Ostrich Site Sketch and Photographs





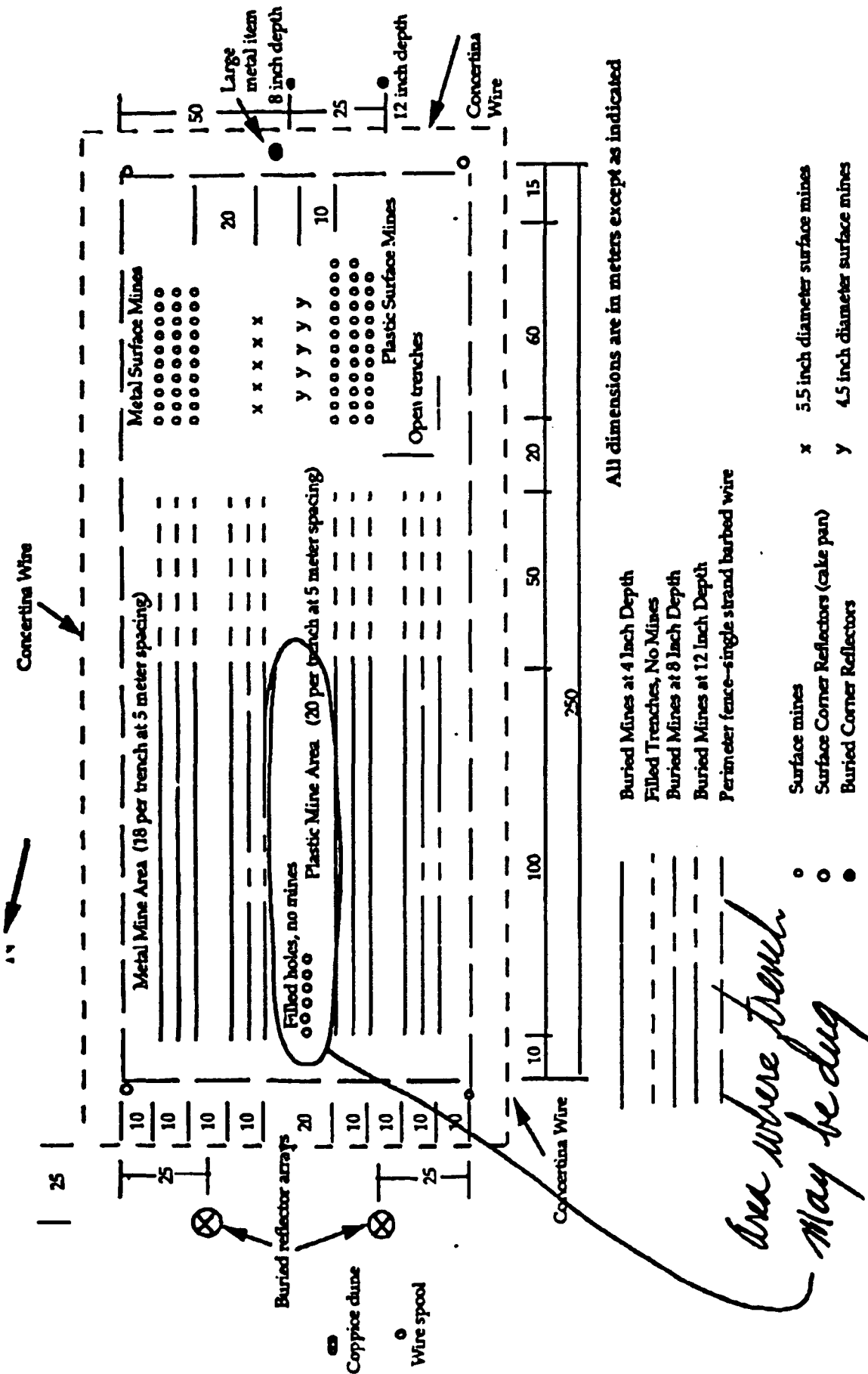
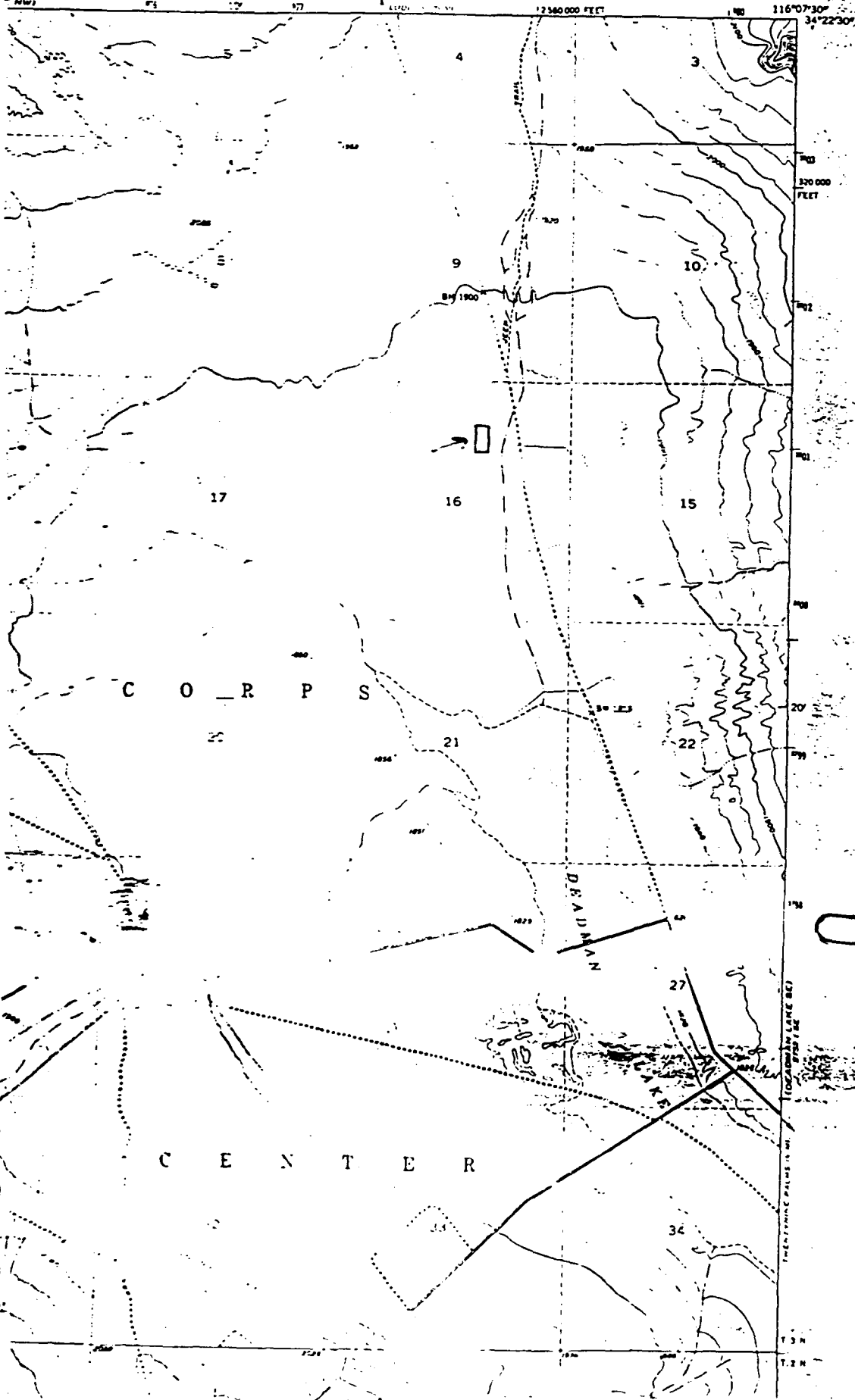


Figure 4. Phase II Test Site Layout

SITE LOCATION
 ~ 34 20 20
 ~ 116 08 47

RNIA
VERNOR
F PUBLIC WORKS
ENGINEER

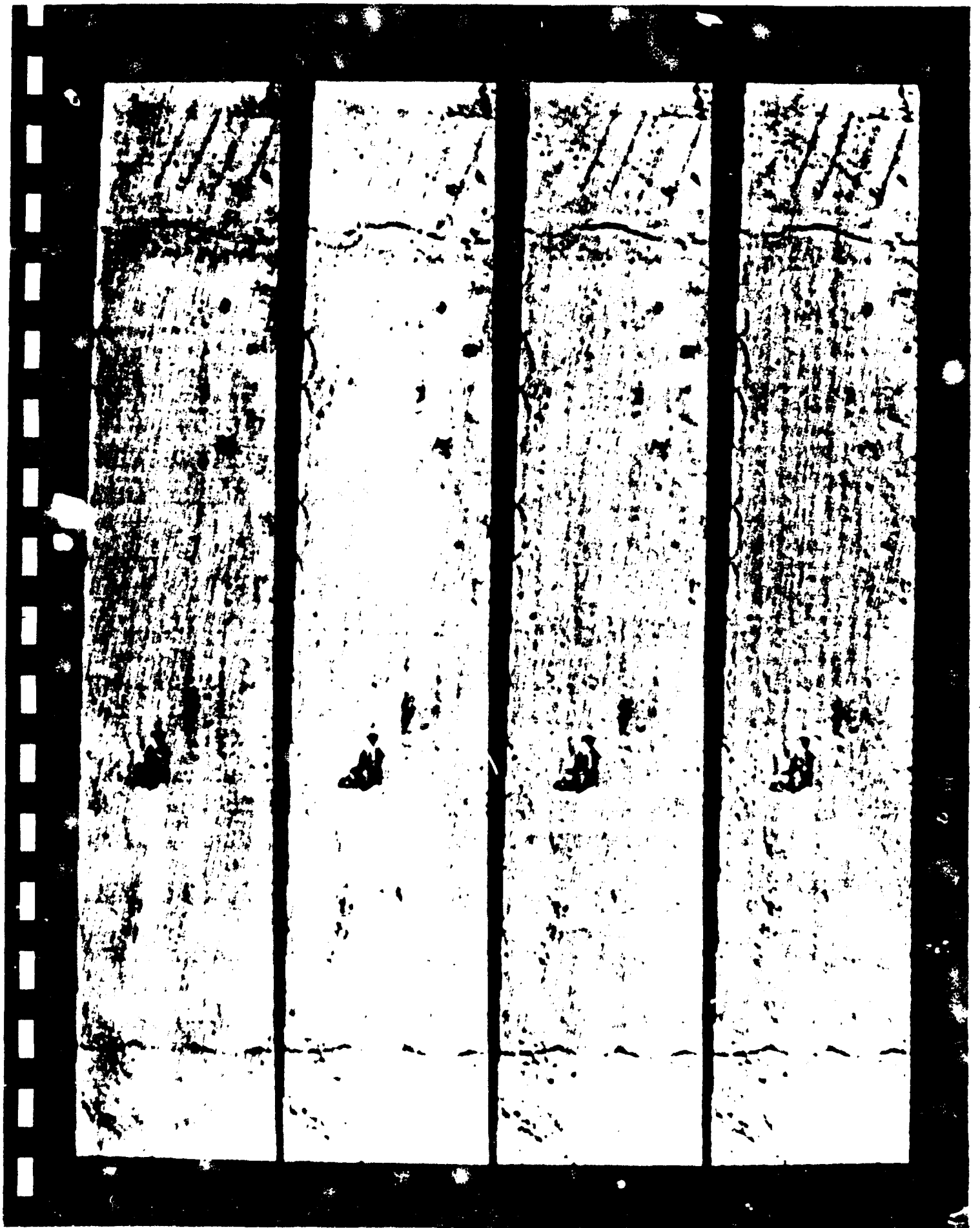
DEADMAN LAKE SW QUADRANGLE
CALIFORNIA—SAN BERNARDINO CO.
7.5 MINUTE SERIES (TOPOGRAPHIC)



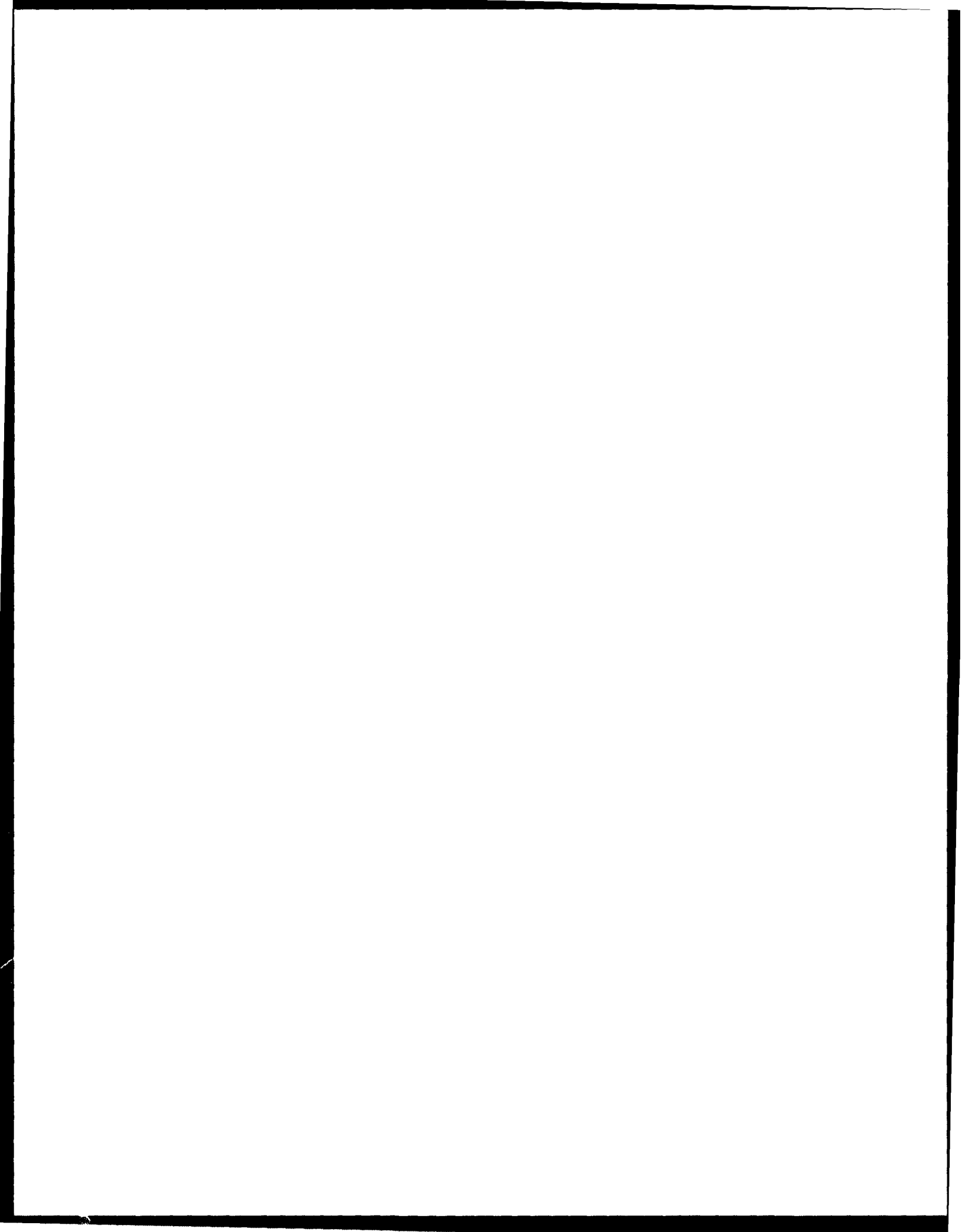
DEADMAN LAKE
116°07'30"
34°22'30"

T.3N
T.2N

Attachment 5
WIS Display Image Photographs
(16 Photographs, 93-1-286 through 93-1-301)

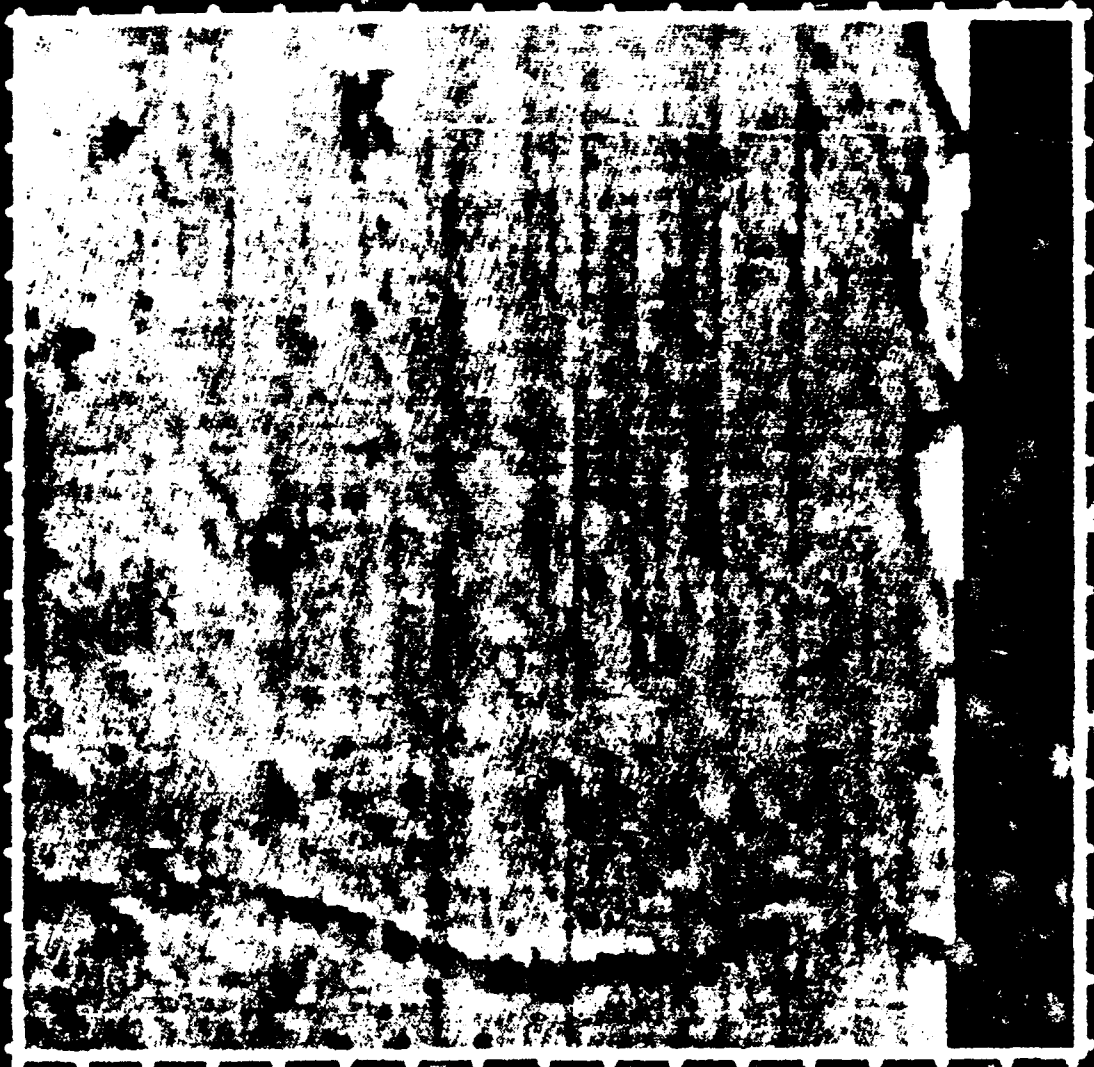




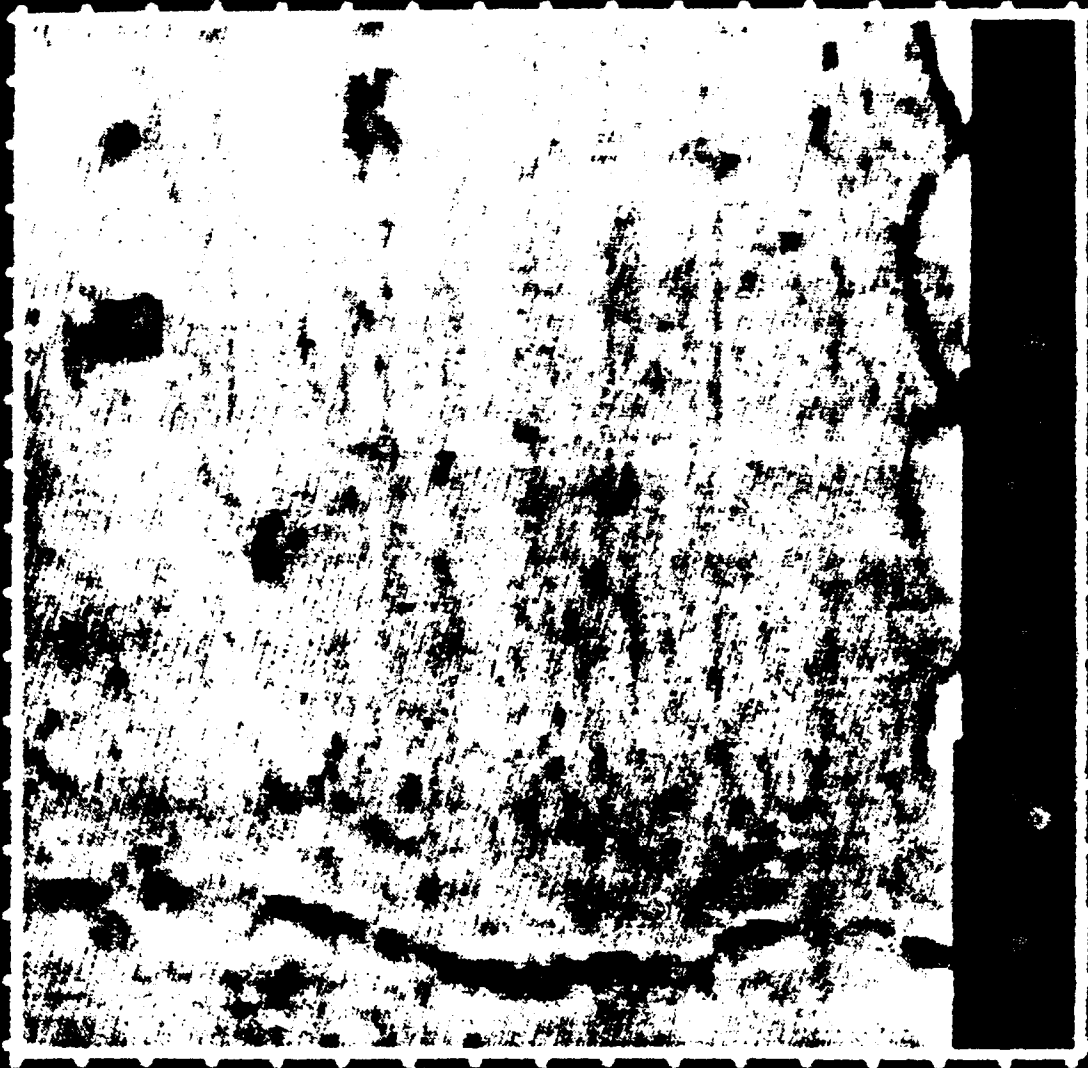




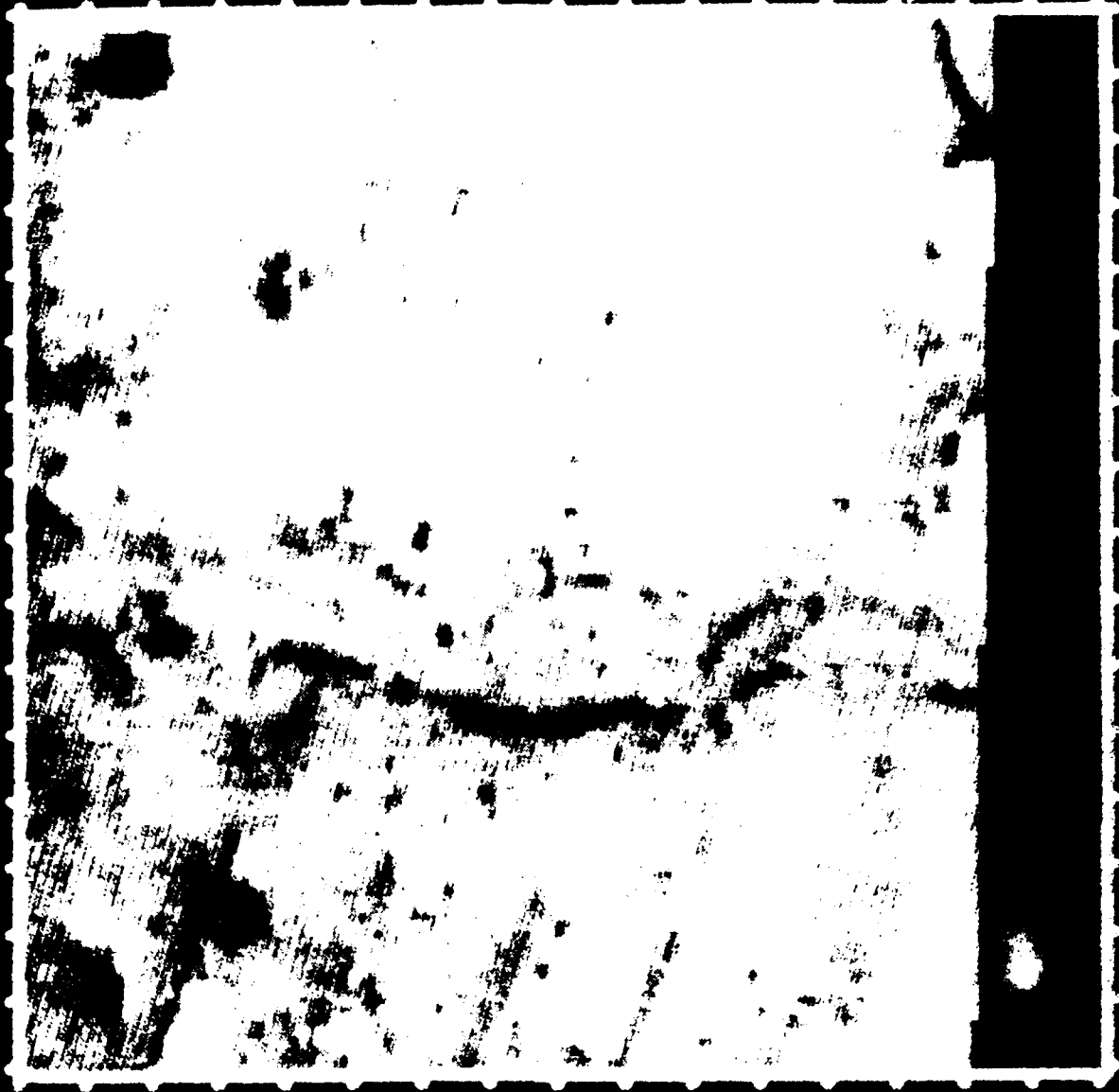
FRCTFY2.768
band 20
offset 475



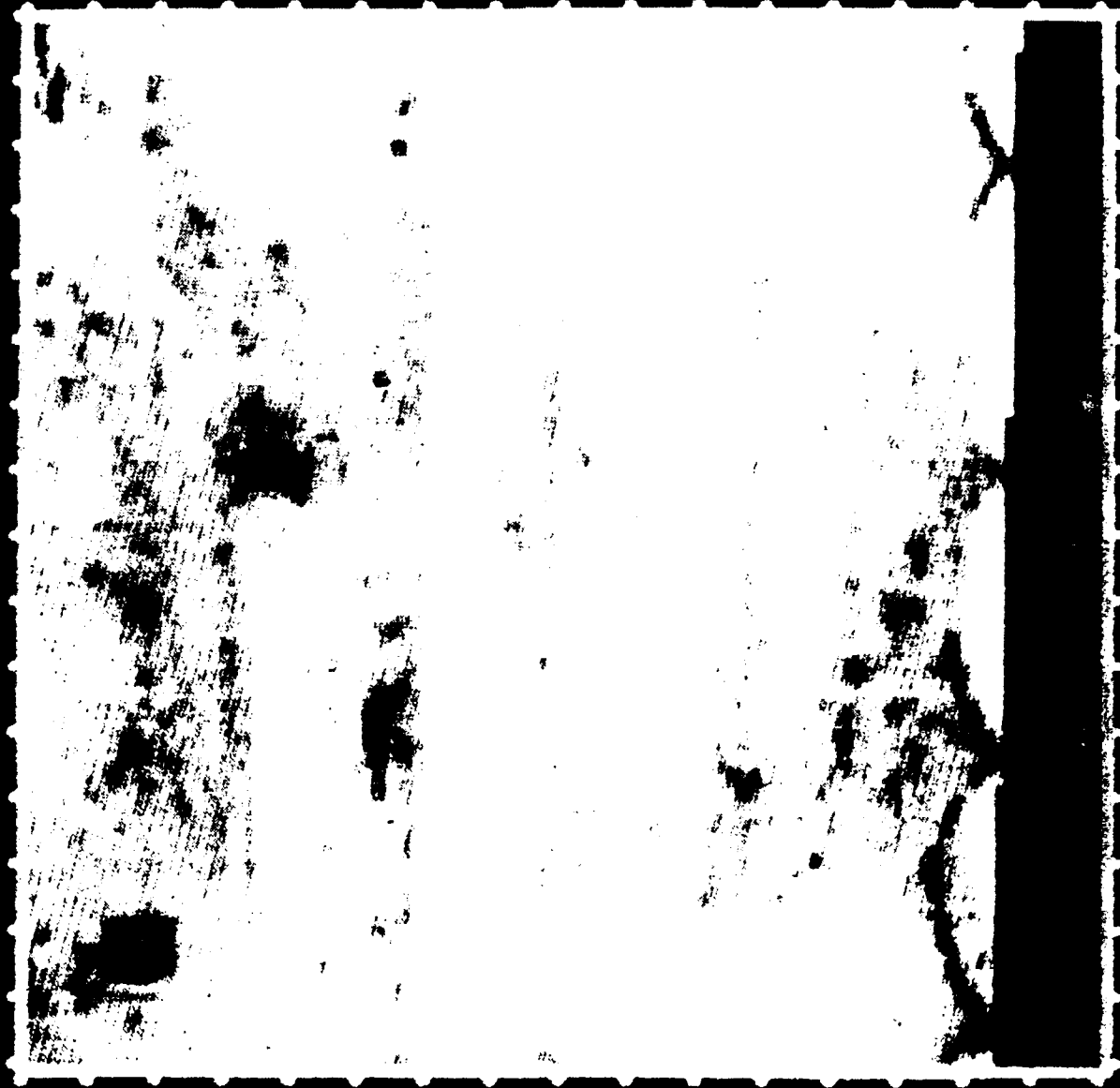
FRCTFY2.768
band 30
offset 475



FRCTFY2.768
band 40
offset 508



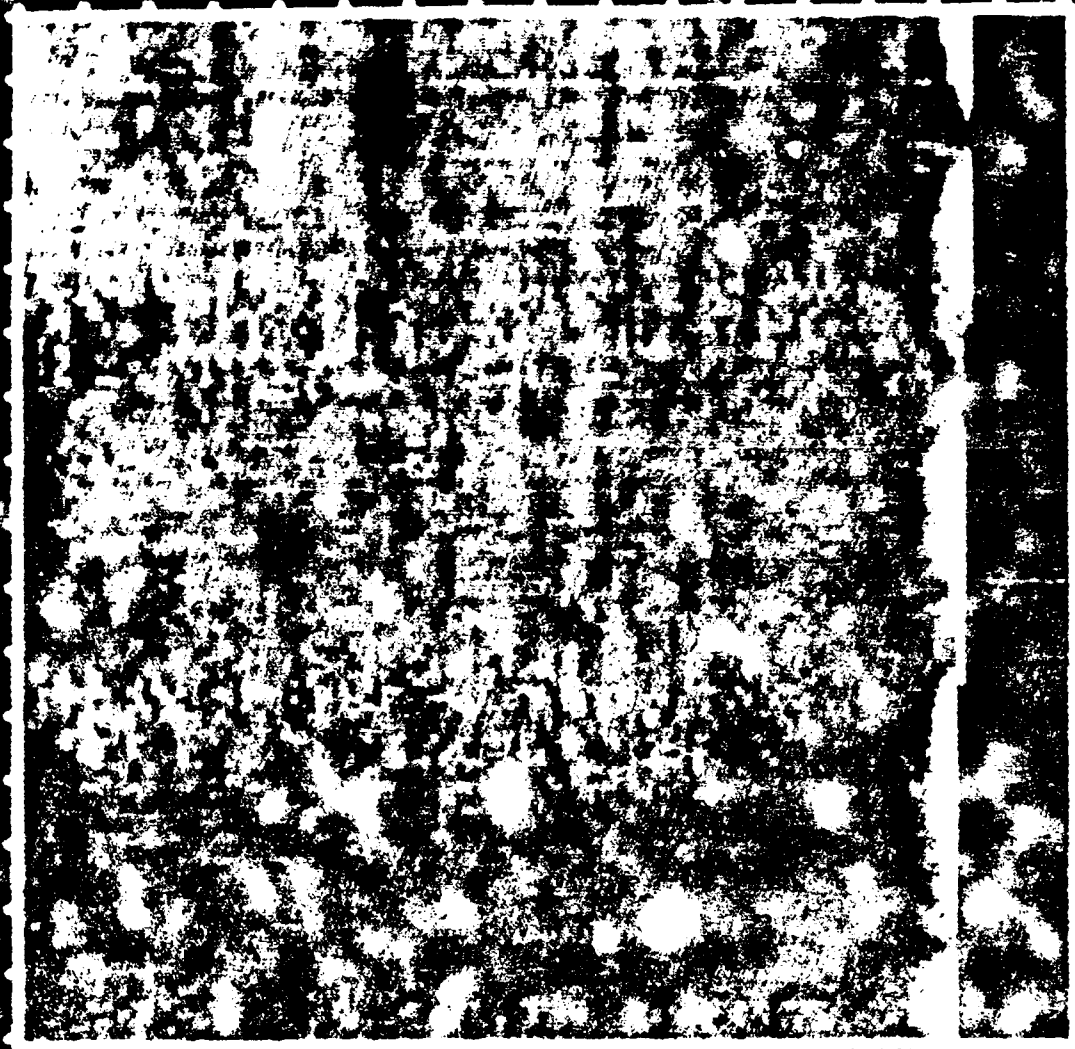
FRCTFY2.768
band 40
offset 400







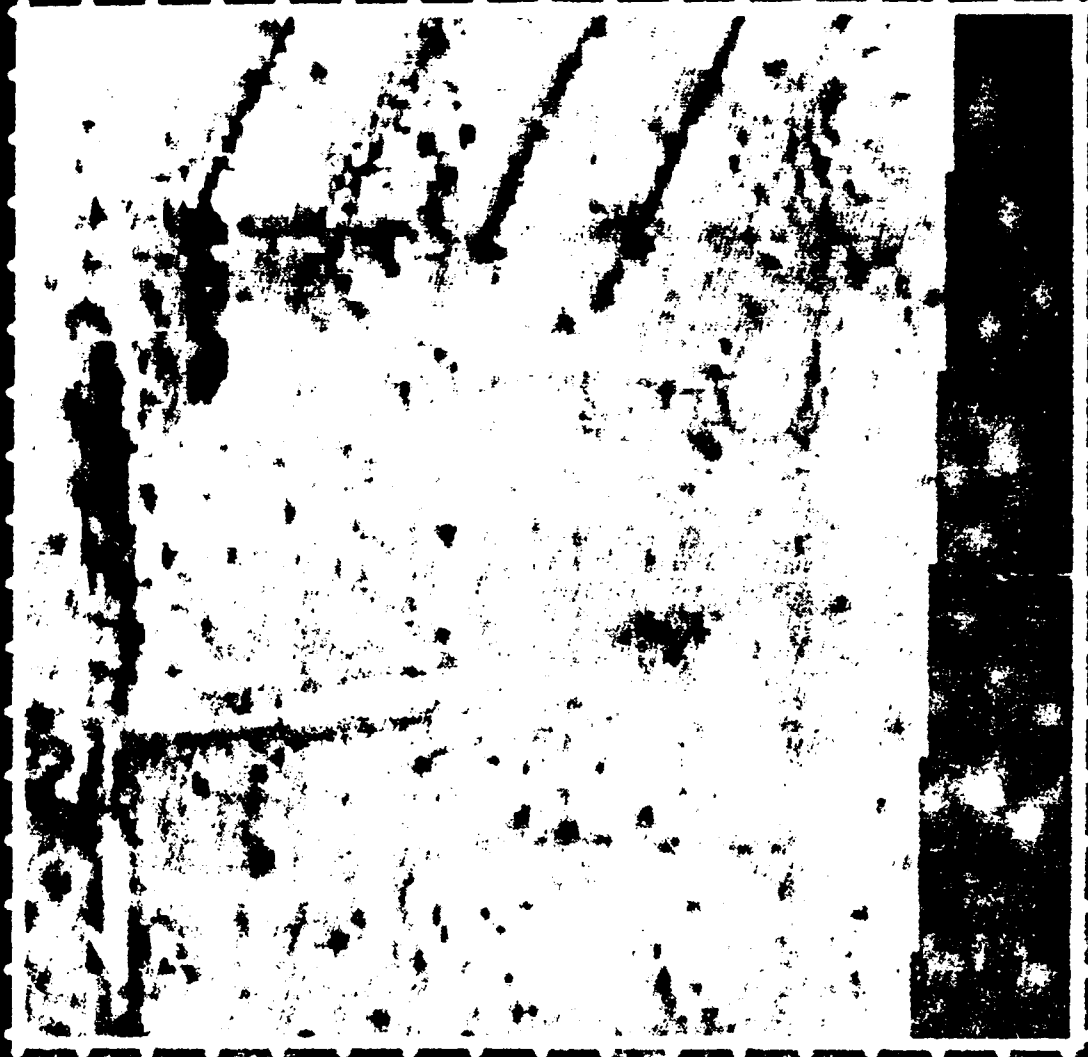
FRONTY 2.768
band 50
offset 475



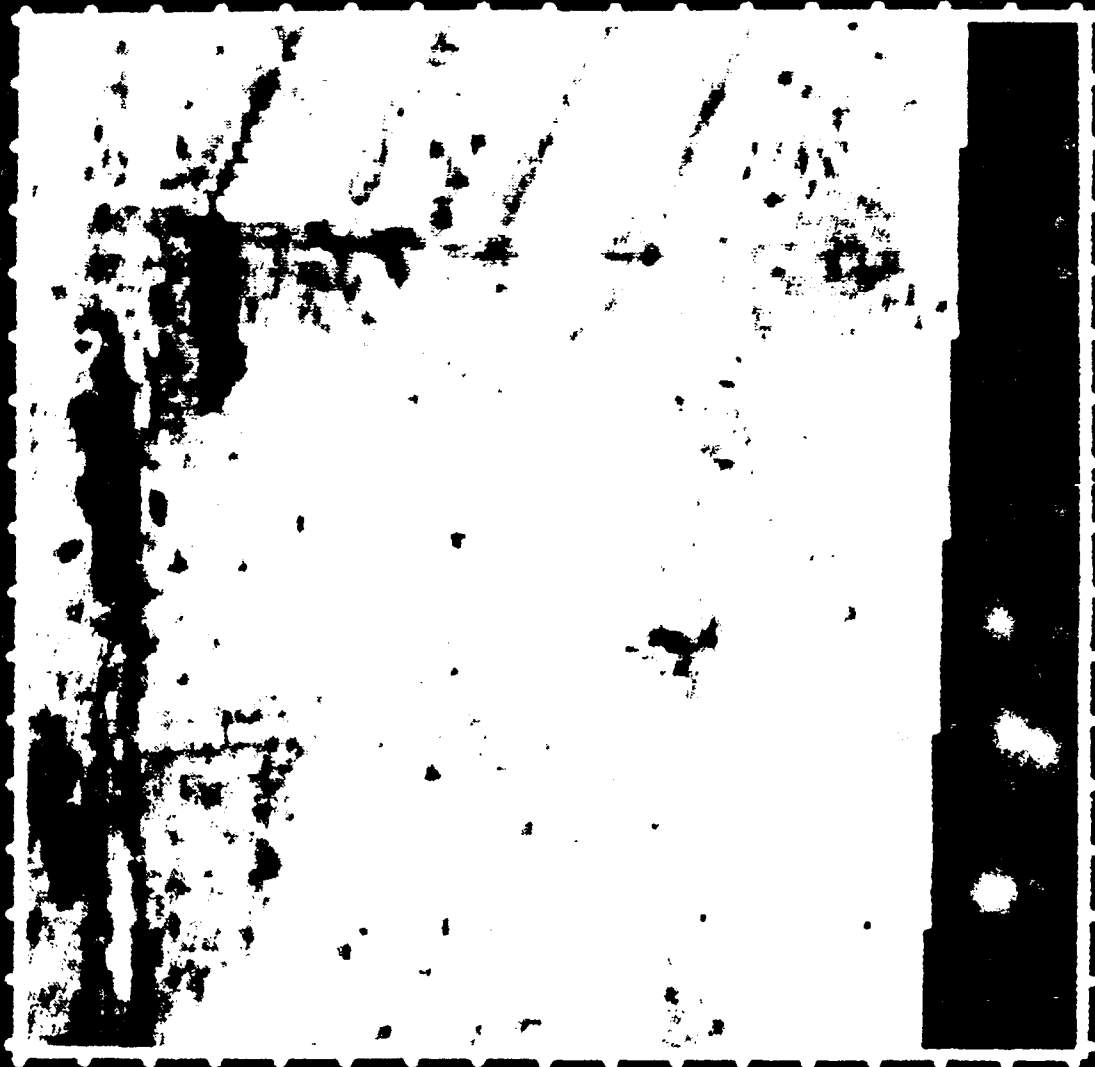
FRCTFY2.770
band 20
offset 275



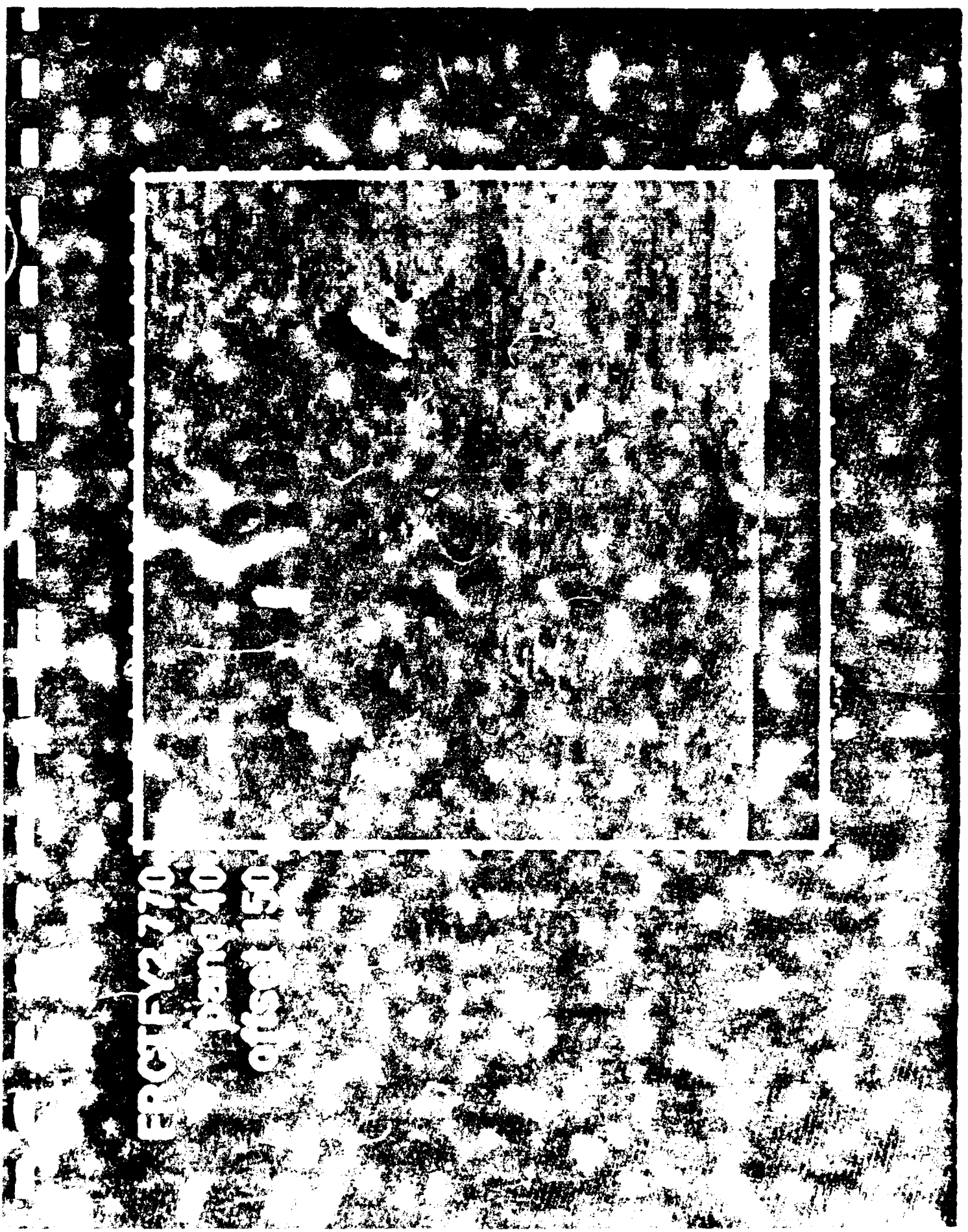
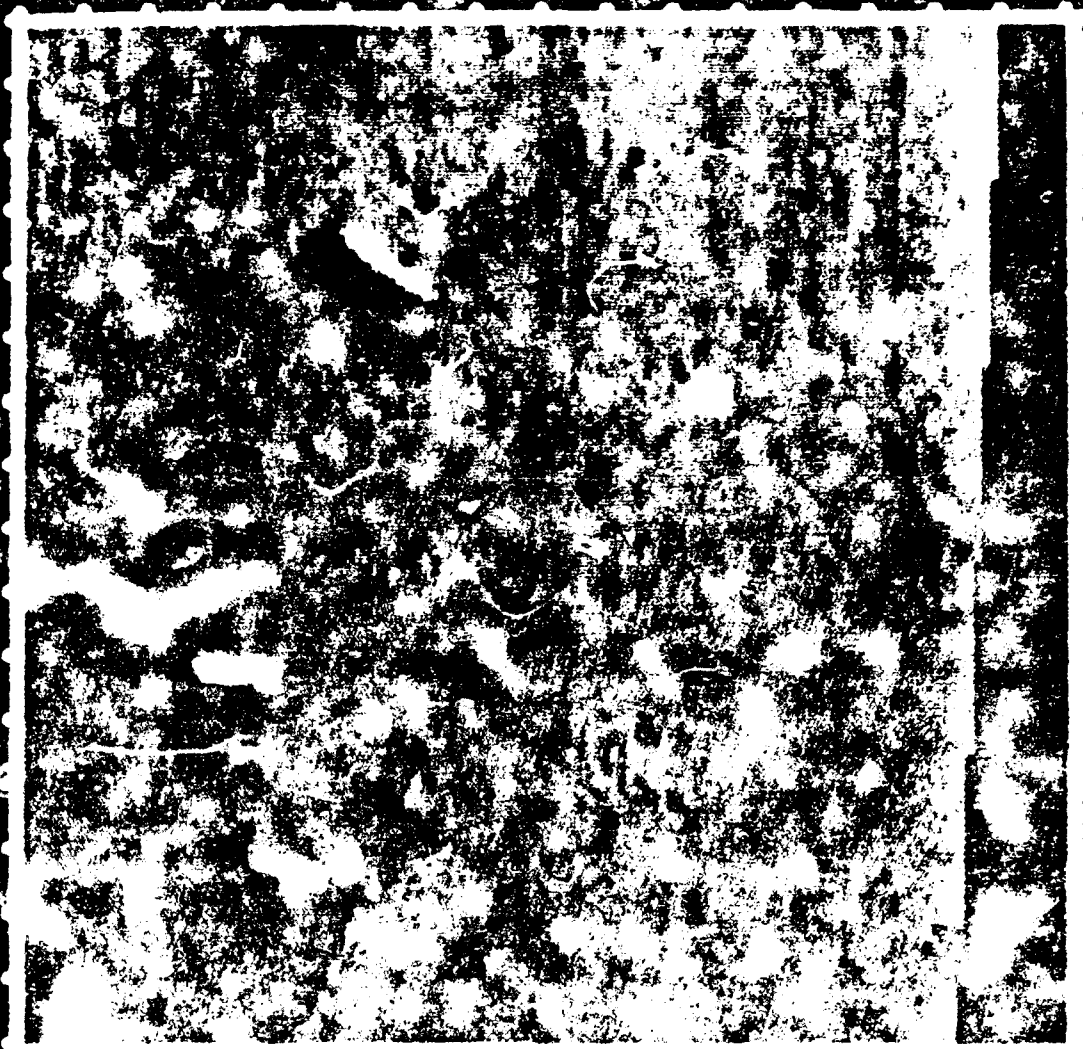
FRCI FY2.770
band 30
offset 275

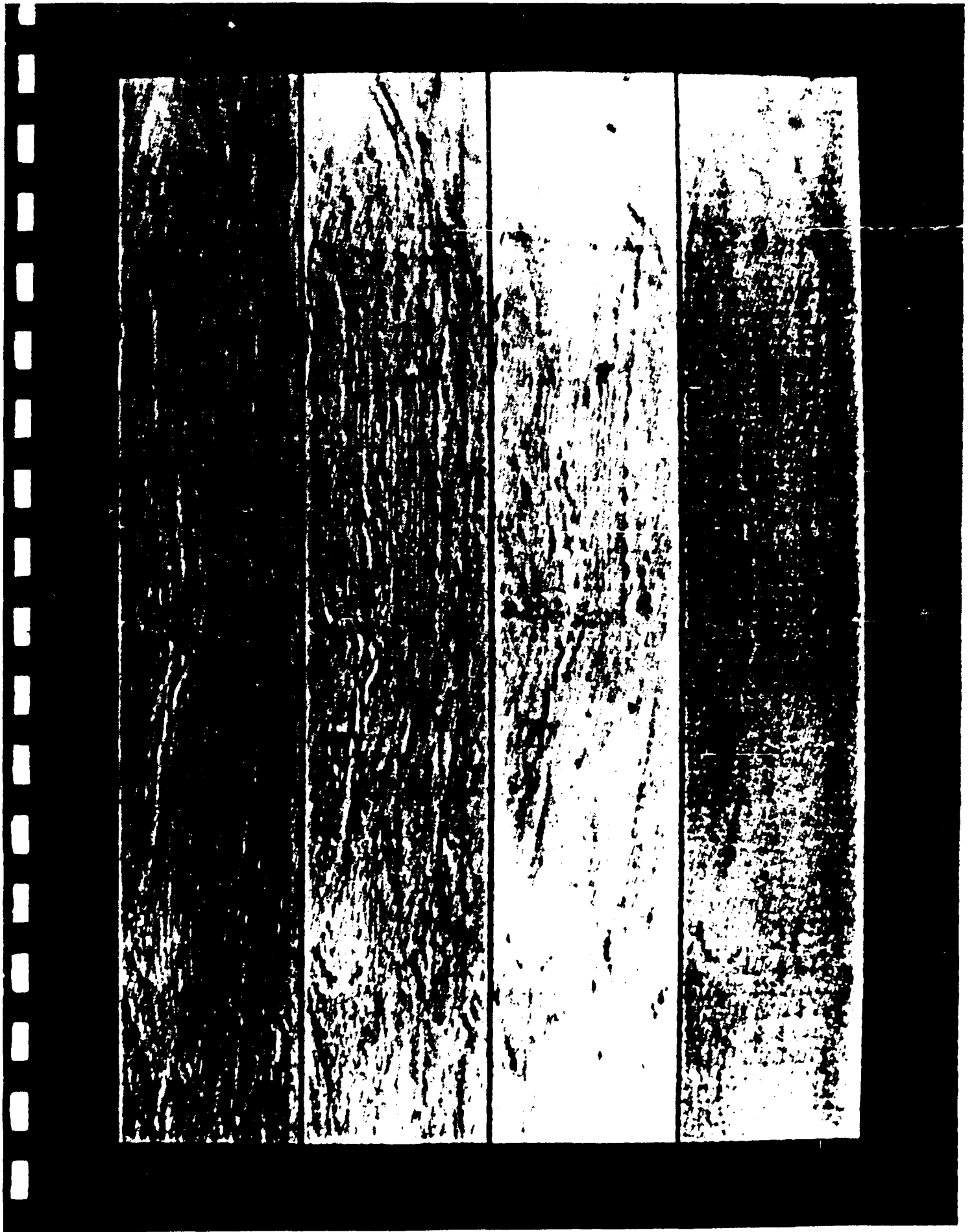


FRCTFY2.770
band 40
offset 275



ERCTFY2770
pamq10
qfscq150







Attachment 7
9 Track Digital Image of Data File 770
Ostrich Site, 12/21/92, 1/2 meter GSD
(File 770 as used for Section 3 spectral processing;
· Corrected for offset, gain, and solar)

Appendix B

UNIVERSITY OF ARIZONA REPORT

Futures - Final Report

Introduction

The University of Arizona contracted to make measurements of the signatures of mine fields. The plan called for measurements in Twenty-Nine Palms, CA and from a local area with an appropriate spectral imager.

Twenty-Nine Palms, CA

Considerable logistical difficulties were encountered. The first set of tests were scheduled within weeks of the contract start date. The equipment was not ready, and subsequent tests never materialized. Although we prepared the equipment and all the required logistics, these tests just never came to fruition.

Local Area Tests

We replanned with technical representatives and the Future Group. It was mutually agreed that we would carry out measurements from our rooftop with a Plumbicon Camera and a selected area of desert terrain. The area was prepared, a zoom lens and filters were purchased for the camera and the measurements were started. Several videotapes of data have been sent to Futures reporting these results.

Three filters were used which passed from 1.6 to 1.7 μm and 0.9 to 1.2 μm and a 1.8 long pass. The area of observation was a section of the campus area that had been in place and undisturbed for three years. It was completely barren and consisted of sand and gravel. A trench about a foot deep and wide was dug and filled by a backhoe. It was then observed every other day at one hour intervals from approximately from 8:00 am until noon. The tube cutoff was at about 1.9 μm although the field of view of the camera was not as large as we wanted, we obtained good imagery that showed the contrast.



The imagery of the wide-open tube was showed a definite contrast between the trough and the surround. This could also be seen easily by eye. The first two filters showed the same information with about the same visual contrast. The third filter apparently cut off too much light.

Although the trough is clearly visible, it seem to be as a result of texture and has little apparent spectral variation the area experienced several rainstorms during the tests. They seemed to have no affect on the visual appearance. The difference in texture just seemed to become permanent - it caked.

Conclusion

Visible sensing of troughs seem to be entirely possible based on textural differences of the ground - given enough resolution. There seems to be little spectral variation from the visible to the near infrared. The results are based on limited data.

Tuesday, Nov. 23, '93		... Thanksgiving, Nov. 24 - 28, '93...	
Time	10:00 AM	11:00 AM	12:20 PM
Weather	Cloudy	Cloudy	Mostly Cloudy
Sky	61°	64°	66°
Temperature	48%	46%	45%
Humidity	Calm	Calm	Calm
Wind (miles)	45	45	45
Visibility (miles)	00:00:01 - 00:12:34		
Tape Counter			

Monday, Nov. 29, '93		Tuesday, Nov. 30, '93		Wednesday, Dec. 1, '93					
Time	9:00 AM	10:00 AM	11:30 AM	9:00 AM	10:00 AM	11:00 AM	7:30 AM	8:30 AM	9:30 AM
Weather	P/C	P/C	P/C	M/C	M/C	M/C	P/C	P/C	P/C
Sky	50°	52°	59°	54°	58°	63°	39°	45°	51°
Temperature	37%	27%	25%	31%	27%	25%	68%	65%	58%
Humidity	E 9	SE 10	S 8	SE 12	SE 9	S 10	N 6	SE 3	SE 5
Wind (miles)	50	50	50	50	50	50	50	50	50
Visibility (miles)	00:12:35 - 00:24:46		00:24:47 - 037:01		00:37:02 - 00:47:10				
Tape Counter									

Thursday, Dec. 2, '93		Friday, Dec. 3, '93		Monday, Dec. 6, '93		
Time	9:00 AM	10:00 AM	11:00 AM	9:00 AM	10:00 AM	11:00 AM
Weather	Clear	Clear	Clear	Clear	Clear	Clear
Sky	42°	49°	55°	43°	50°	55°
Temperature	75%	56%	41%	57%	36%	30%
Humidity	S 7	NW 5	Light	SE 9	Light	Calm
Wind (miles)	35	40	45	50	50	50
Visibility (miles)	00:49:11 - 01:01:19		01:01:20 - 01:13:19		01:13:20 - 01:25:25	
Tape Counter						

		Tuesday, Dec. 7, '93		Wednesday, Dec. 8, '93		Thursday, Dec. 9, '93	
Time		9:00 AM	10:00 AM	9:00 AM	10:00 AM	9:00 AM	10:00 AM
Weather		P/C	Cloudy	Cloudy	Cloudy	Cloudy	Clear
Sky		43°	57°	50°	57°	60°	51°
Temperature		60%	42%	32%	37%	35%	38%
Humidity		SE 12	Light	SE 12	S 9	SE 10	SE 5
Wind (miles)		50	50	50	50	50	50
Visibility (miles)							
Tape Counter		01:25:26 - 01:37:26		01:37:27 - 01:49:29		01:49:30 - 02:01:35	

Tape Counters for Days and Takes			
Day	Take I	Take II	Take III
Tuesday, Nov. 23, '93	00:00:01 - 00:04:27	00:04:28 - 00:08:29	00:08:30 - 00:12:34
Monday, Nov. 29, '93	00:12:35 - 00:16:37	00:16:38 - 00:20:41	00:20:42 - 00:24:46
Tuesday, Nov. 30, '93	00:24:47 - 00:28:50	00:28:51 - 00:32:58	00:32:59 - 00:37:01
Wednesday, Dec. 1, '93	00:37:02 - 00:41:05	00:41:06 - 00:45:07	00:45:08 - 00:49:10
Thursday, Dec. 2, '93	00:49:11 - 00:53:12	00:53:13 - 00:57:15	00:57:16 - 01:01:19
Friday, Dec. 3, '93	01:01:20 - 01:05:21	01:05:22 - 01:09:22	01:09:23 - 01:13:19
Monday, Dec. 6, '93	01:13:20 - 01:17:20	01:17:21 - 01:21:24	01:21:25 - 01:25:25
Tuesday, Dec. 7, '93	01:25:26 - 01:29:24	01:29:25 - 01:33:26	01:33:27 - 01:37:26
Wednesday, Dec. 8, '93	01:37:27 - 01:41:25	01:41:26 - 01:45:29	01:45:30 - 01:49:28
Thursday, Dec. 9, '93	01:49:30 - 01:53:30	01:53:31 - 01:57:32	01:57:33 - 02:01:35

Tape Counters for Days and Takes				
Day	Take I	Take II	Take III	Tape Counter
Tuesday, Nov. 23, '93	00:00:01 - 00:04:27	00:04:28 - 00:08:29	00:08:30 - 00:12:34	00:00:01 - 00:12:34
Monday, Nov. 29, '93	00:12:35 - 00:16:37	00:16:38 - 00:20:41	00:20:42 - 00:24:46	00:12:35 - 00:24:46
Tuesday, Nov. 30, '93	00:24:47 - 00:28:50	00:28:51 - 00:32:58	00:32:59 - 00:37:01	00:24:47 - 00:37:01
Wednesday, Dec. 1, '93	00:37:02 - 00:41:05	00:41:06 - 00:45:07	00:45:08 - 00:49:10	00:37:02 - 00:49:10
Thursday, Dec. 2, '93	00:49:11 - 00:53:12	00:53:13 - 00:57:15	00:57:16 - 01:01:19	00:49:11 - 01:01:19
Friday, Dec. 3, '93	01:01:20 - 01:05:21	01:05:22 - 01:09:22	01:09:23 - 01:13:19	01:01:20 - 01:13:19
Monday, Dec. 6, '93	01:13:20 - 01:17:20	01:17:21 - 01:21:24	01:21:25 - 01:25:25	01:13:20 - 01:25:25
Tuesday, Dec. 7, '93	01:25:26 - 01:29:24	01:29:25 - 01:33:26	01:33:27 - 01:37:26	01:25:26 - 01:37:26
Wednesday, Dec. 8, '93	01:37:27 - 01:41:25	01:41:26 - 01:45:29	01:45:30 - 01:49:28	01:37:27 - 01:49:29
Thursday, Dec. 9, '93	01:49:30 - 01:53:30	01:53:31 - 01:57:32	01:57:33 - 02:01:35	01:49:30 - 02:01:35